Novel biomarkers in two gastrointestinal malignancies - the potential of early detection and identification of new therapies

By

Vandana Mridhu Sagar

MRCP (UK) (Gastroenterology), MBChB

A thesis submitted to the University of Birmingham for the degree of

DOCTOR OF MEDICINE

Centre for Liver and Gastroenterology Research

Institute of Immunology and Immunotherapy

College of Medical and Dental Sciences

University of Birmingham

May 2019

Abstract

Currently, there are no sufficient biomarkers that can be utilised in hepatocellular cancer (HCC) and neuroendocrine tumours (NETs) that can help in making an early diagnosis, or recognise serious complications that can be associated with the tumour. HCC is usually diagnosed at an advanced stage when curative treatment options are limited. There is no recommended biomarker to use in clinical practice to diagnose early HCC at present. NETs can occur in different sites, but the gastroenteropancreatic NETs are the commonest sites of origin. Serious complications can be associated with this cancer due to the underlying gastrointestinal and cardiac valve fibrosis, including intestinal obstruction and ischaemia, and carcinoid heart disease (CHD).

Within this thesis the suitability of prothrombin induced by vitamin K absence-II (PIVKA-II) as a biomarker in HCC will be presented. The aims of this study are to compare PIVKA-II to the traditional marker alpha-fetoprotein (AFP) in diagnosing early HCC, as well as a combination of both biomarkers, assess PIVKA-II levels in patients undergoing ablation therapy, and assess if levels of PIVKA-II increase with disease progression of HCC. The second project in this thesis describes the suitability of vascular adhesion-protein 1 (VAP-1) as a biomarker in NETs and CHD. The aims of this project are to compare the levels of soluble VAP-1 (sVAP-1) in different NET cohorts and healthy volunteers and compare levels of sVAP-1 pre- and post-treatment in midgut NETs. I also aim to study the tissue expression of VAP-1 in midgut NET tissue and CHD.

AFP has been the traditional marker used in HCC surveillance. PIVKA-II was not found to be a superior marker to AFP in diagnosing early HCC, and the combination of both markers was only slightly better compared to AFP alone. However, on explant histology, pre-transplant serum PIVKA-II levels were found to be significantly higher in the presence of microvascular invasion and also in moderately- or poorly- differentiated HCC. This was not seen with AFP. In the longitudinal data analysis, PIVKA-II shows a promising role in the surveillance of recurrent HCC post-ablation.

Tissue expression of VAP-1 was present in midgut NETs and in the CHD valves, associated with the presence of a dense stromal and collagen network. Significantly higher % area of tissue expression of VAP-1 was seen in CHD valves compared to control valves. Across the healthy controls, midgut NETs and CHD groups, significantly higher levels of circulating sVAP-1 was seen with highest levels found in CHD. The longitudinal data analysis did not show any significant change in the sVAP-1 levels between the pre- and post-treatment samples, similar to the markers currently used in clinical practice (chromogranin A, 24 hour urinary 5-hydroxyindole acetic acid and N-terminal pro b-type natriuretic peptide).

PIVKA-II could therefore be a prognostic marker in HCC and may support patient stratification for therapy. Despite a small number in the longitudinal data analysis, PIVKA-II shows a promising role in the surveillance of recurrent HCC post-ablation therapy. The VAP-1 study identifies the presence of VAP-1, both in a circulating form and tissue expression in midgut NETs and in CHD, and therefore could be a potential biomarker and treatment target in NETs.

Table of Contents

Dedication

This thesis is dedicated to my father, Dr Gian Sagar, who is not here with me today but I know is always watching over me and I hope I will always make him proud, and to my mum, Anu Sagar, who has taken on the role of two parents, and is and always will be my rock and best friend.

Acknowledgements

My research work presented in this thesis would not have been possible without the support and help of the following people.

I would first like to start by thanking my supervisors, Dr Tahir Shah and Dr Shishir Shetty. Their support, enthusiasm and encouragement have never ceased to amaze me and their guidance throughout my research has been most appreciated. I have learnt so much from both of them which will remain with me throughout the rest of my career.

I would also like to express my gratitude to Dr Christopher Weston who has also been a wonderful supervisor and provided me with constant support, and invaluable scientific experience and knowledge. Huge thanks also go to Professor Gideon Hirschfield and Dr Yuk Ting Ma for their support and guidance.

I would like to especially thank Dr Desley Neil for the amount of time and help she has given me with the histopathological analysis for all the carcinoid heart disease valves. Thanks also go to Dr Mona El-Shafie and Dr Owen Cain for their advice and expertise in histopathology. I would also like to thank Dr Rick Steeds for all his advice and help he has given me for the carcinoid heart disease analysis. Thanks to Dr Boyang Liu who has greatly helped me with the quantitative analysis of my staining work.

A special thanks goes to James Hodson, for all of his expert help and teaching me statistics, as well as his valuable input with all of my statistical analysis.

Abbreviations

^{18}FDG	18-fluoro-deoxy-glucose
^{68}Ga	Gallium-68
^{123}I-MIBG	Radioiodinated metaiodobenzylguanidine
5-HIAA	5-hydroxyindole acetic acid
5-HT	Serotonin
4-MUP	4-methylumbelliferyl phosphate
α-SMA	Alpha-smooth muscle actin
aVICs	Activated valve interstitial cells
AASLD	American Association for the Study of Liver Diseases
Ab	Antibody
AFP	Alpha-fetoprotein
AFP-L3	*Lens-culinaris* agglutinin-reactive alpha-fetoprotein
ALD	Alcohol-related liver disease
ALT	Alanine transaminase
ANOVA	Analysis of variance
AUC	Area under the curve
AUROC	Area under the receiver operating characteristic curve
BALAD-2	Bilirubin, albumin, AFP-L3, AFP, and DCP
BCLC	Barcelona Clinic Liver Cancer
BMI	Body mass index
c-MET	Cellular mesenchymal-epithelial transition factor
CAFs	Cancer-associated fibroblasts
CECT	Contrast enhanced computed tomography

CgA	Chromogranin A
CgB	Chromogranin B
CHD	Carcinoid heart disease
CI	Confidence interval
CLD	Chronic liver disease
CPG	Clinical practice guidelines
CS	Carcinoid syndrome
CT	Computed tomography
DAB	3,3'-diaminobenzidine
DC	Dendritic cell
DCP	Des γ- carboxy-prothrombin
EASL	European Association for the Study of the Liver
ECM	Extracellular matrix
EGFR	Epidermal growth factor receptor
ELISA	Enzyme-linked immunosorbent assay
EMT	Endothelial to mesenchymal transformation
EPC	Endothelial progenitor cell
ERK	Extracellular signal-regulated kinase
ENETS	European Neuroendocrine Tumour Society
EORTC	European Organisation for Research and Treatment of Cancer
FGF	Fibroblast growth factor
G	Grade
GALAD	Gender, age, AFP-L3, AFP, and DCP
GEP	Gastroenteropancreatic

GI	Gastrointestinal
GP73	Golgi-protein-73
GPC3	Glypican-3
HBRC	Human Biomaterials Resource Centre
HBV	Hepatitis B virus
HCC	Hepatocellular carcinoma
HCV	Hepatitis C virus
HGF	Hepatocyte growth factor
HR	Hazard ratio
HSCs	Hepatic stellate cells
IHC	Immunohistochemical
IMC	Isotype matched control
INR	International normalised ratio
IQR	Interquartile range
JAK-1	Janus kinase 1
kDa	Kilodalton
KDR	Kinase insert domain receptor
L	Litre
LN	Lymph node
LT	Liver transplantation
μl	Microlitres
μg	Micrograms
mAU	Milli arbitrary unit
mg	Milligrams

miRNAs	MicroRNAs
mL	Millilitres
mm	Millimetres
MAPK	Mitogen activated protein kinase
MC	Milan criteria
MELD	Model for end-stage liver disease
MEN	Multiple Endocrine Neoplasia
MMP	Matrix metalloproteinase
mTOR	Mechanistic target of rapamycin
MRI	Magnetic resonance imaging
MVI	Microvascular invasion
ng	Nanograms
NAFLD	Non-alcoholic fatty liver disease
NECs	Neuroendocrine carcinomas
NENs	Neuroendocrine neoplasms
NET	Neuroendocrine tumour
NETs	Neuroendocrine tumours
NFκB	Nuclear factor kappa light chain enhancer of activated B cells
NRES	National Research Ethics Service
NT-proBNP	N-terminal pro b-type natriuretic peptide
obVICs	Osteoblastic valve interstitial cells
OPN	Osteopontin
OS	Overall survival
pVICs	Progenitor valve interstitial cells

PBST	Phosphate-buffered saline with tween
PET	Positron emission tomography
PFS	Progression free-survival
PIVKA-II	Prothrombin induced by vitamin K absence-II
PLC-γ	Phospholipase C-gamma
PP	Pancreatic polypeptide
PPI	Proton pump inhibitor
PRRT	Peptide receptor radionuclide therapy
PS	Performance status
PSC	Primary sclerosing cholangitis
PVT	Portal vein thrombosis
qVICs	Quiescent valve interstitial cells
ROC	Receiver operating characteristic
siRNA	Small interfering RNA
sVAP-1	Soluble vascular adhesion protein-1
SD	Standard deviation
SPECT	Single-photon emission computed tomography
SRS	Somatostatin receptor scintigraphy
SSA	Somatostatin analogue
SSAs	Somatostatin analogues
SSAO	Semicarbazide-sensitive amine oxidase
SST	Somatostatin
SSTR	Somatostatin receptor
STAT3	Signal transducer and activator of transcription 3

TACE	Transarterial chemoembolisation
TBST	Tris buffered saline with tween
TGF-β	Transforming growth factor β
TPQ	Topoquinone
TR	Tricuspid regurgitation
umol/L	Micromole/litre
U	Units
UK	United Kingdom
US	Ultrasound
USS	Ultrasound scan
VAP-1	Vascular adhesion protein-1
VEGF	Vascular endothelial growth factor
VHL	Von Hippel Lindau
VICs	Valve interstitial cells
VIP	Vasoactive intestinal peptide
WHO	World Health Organisation
ZES	Zollinger-Ellison syndrome

List of Tables

Chapter 5

Chapter 6

List of Figures

Chapter 5

Chapter 6

CHAPTER 1:
INTRODUCTION

1. Introduction

Increasing knowledge on the biology of cancer, in addition to a greater understanding in the pathophysiology of the disease, has led to a significant interest in the use of biomarkers.(1) A biomarker is defined by the National Cancer Institute as *'a biological molecule found in blood, other body fluids, or tissues that is a sign of a normal or abnormal process, or of a condition or disease.'*(2)

Biomarkers can help diagnose cancer at an early stage allowing curative treatment options to be considered, as well as being implemented as a surveillance and treatment response marker. Biomarkers can also be used to help detect complications early when treatment can then be offered.

In this thesis two markers will be discussed, one in hepatocellular carcinoma (HCC) and one in neuroendocrine tumours (NETs), where there are unmet needs in both these cancers, with an overall aim of diagnosing cancer or detecting complications early to allow the initiation of treatment. The markers that will be discussed in this thesis are prothrombin induced by vitamin K absence-II (PIVKA-II) in HCC and vascular adhesion protein-1 (VAP-1) in NETs.

1.1 Epidemiology, aetiology and pathogenesis of hepatocellular carcinoma

Incidence of HCC varies according to geographic regions, with high incidence of disease found in Asian countries including China, Southeast Asia, and Sub-Saharan Western and Eastern Africa.(3) In 2016, a total of 5933 cases of HCC were diagnosed in the United Kingdom (UK). The age-standardised incidence rate for males in 2016 in the UK was 14.1 per 100,000 population, and 6.1 per 100,000 population for females.(4) A variety of risk factors for HCC exist, with viral infections showing a strong association with HCC development worldwide. Other common risk factors that can cause HCC include alcohol, smoking, non-alcoholic fatty liver disease and hereditary haemochromatosis.(3) Around 90% of cases occur in the presence of underlying liver cirrhosis.(5, 6) In addition to the extrinsic risk factors, genetic mutations also can lead to the development of HCC.(3)

Chronic liver inflammation and fibrosis are present in the background liver occurring as a result of continuous liver insult and injury to common causes including alcohol and viral infections. These hepatotoxic agents target the hepatocytes which leads to the release of reactive oxygen species (ROS) and cytokines (including platelet derived growth factor, transforming growth factor β, TGF-β, tumour necrosis factor-α, interleukins and interferons), and activation of hepatic stellate cells resulting in the onset of fibrosis and extracellular matrix (ECM) production. The presence of chronic inflammation and fibrosis influences certain changes to take place in the microenvironment, including hepatocyte proliferation and chromosomal instability (by telomere shortening), thereby

predisposing to HCC development.(7) Alterations in genomes have been found to drive HCC progression including mutations affecting telomere maintenance, activation of Wnt/β-catenin, mechanistic target of rapamycin (mTOR) and ROS pathways, inactivation of p53, and activation of the Ras signalling pathway.(8) Another change in the microenvironment is hypoxia-induced reactive nitrogen species production, and upregulation of angiogenic factors such as vascular endothelial growth factor (VEGF), leading to tumour angiogenesis and growth.(9) Gut microbiota and lipopolysachharides are also a driver to HCC development, by promoting inflammatory reactions in the hepatic microenvironment and activating Kupffer cells and endothelial cells to trigger the release of pro-inflammatory chemokines leading to liver inflammation and fibrosis.(10) Additionally, changes in the innate and adaptive immune system influences tumour progression by causing the immune system to become tolerant to cancer.(7)

1.2 Background of hepatocellular carcinoma

Worldwide, HCC is the fifth most common cause of cancer, and is the second leading cause of deaths related to cancer.(11) The American Cancer Society has recently shown that the overall 5-year relative survival rate in all cancers combined has improved, and the overall cancer mortality rate has also reduced. A large reduction in the mortality associated with the 4 major cancers (lung, breast, prostate and colorectal) has also been witnessed, largely because of an improvement in early diagnosis and effective treatments being offered.(12) However, in contrast to the reduced mortality observed in these cancers, HCC

has shown an increase in mortality rate.(12) Liver cancer mortality rates have increased by approximately 55% over the last decade, and between 2014 and 2035, mortality rates are estimated to rise by 58% in the UK.(4) The 5-year survival without treatment for patients with HCC is 10 – 12%.(13) However, with early detection and diagnosis of the cancer, the 5-year survival rate improves markedly to >70%.(11) This therefore highlights the importance of developing markers that will contribute towards an earlier diagnosis of cancer, to enable more effective and potentially curative treatment to be provided.

1.3 Biomarkers in hepatocellular carcinoma

The presence of liver inflammation and cirrhosis may complicate the early diagnosis of HCC.(11) Hence, the use of biomarkers is increasingly being required to assist in making the diagnosis. If HCC is diagnosed at an early stage, curative treatment options including liver resection, ablative techniques and liver transplantation can be offered, thereby improving the overall morbidity and mortality associated with this cancer.

Three biomarkers used in clinical practice in Japan include alpha-fetoprotein (AFP), *Lens-culinaris* agglutinin-reactive alpha-fetoprotein (AFP-L3) and des γ-carboxy-prothrombin (DCP).(14) The diagnostic accuracy of the combination of these three biomarkers has been shown to be greater in diagnosing both HCC and early HCC compared to each marker alone.(15) AFP is used in combination with ultrasound (US) imaging in high-risk patients in Asia, but a high level of uncertainty in the clinical effectiveness of this marker does remain.(14)

However, in Western Countries, including the United Kingdom (UK), guidelines do not include the utilisation of this marker.(16, 17)

An ideal biomarker is one that is non-invasive, is tumour-specific, can be used as a screening marker in asymptomatic patients, has a high sensitivity and specificity (≥ 90%), and finally is cost-effective.(11)

1.3.1 Alpha-fetoprotein in hepatocellular carcinoma

Traditionally, AFP has been used as the main biomarker in detecting the presence of HCC. However, a number of investigations looking at the diagnostic utility of this marker have been undertaken.(18)

A meta-analysis showed a combined sensitivity of 66% and specificity of 95% for AFP.(19) One study showed a relationship between high serum AFP with the presence of important HCC features, including a larger tumour size, bilobar involvement, and evidence of portal vein thrombosis (PVT). However, there was no correlation identified between an increased AFP level and other tumour characteristics including degree of tumour differentiation or the presence of extrahepatic metastasis.(20) Another study conducted in a Sicilian population, showed a sensitivity of 65% and a specificity of 89% with an AFP cut-off value of 30 nanograms/millilitres (ng/mL) to differentiate HCC from liver cirrhosis.(21) Marrero et al found the optimal cut-off value for AFP to be 10.9 ng/mL in diagnosing early HCC in a cohort of patients with cirrhosis, yielding a sensitivity of 66%.(22) A Chinese group reported that AFP is an independent risk predictor

in tumour differentiation, size and survival.(23) These results therefore show varying results on the suitability of AFP as an ideal biomarker in diagnosing HCC.

The European Association for the Study of the Liver - European Organisation for Research and Treatment of Cancer clinical practice guidelines (EASL-EORTC CPG) has provided guidance in the surveillance of HCC, advising that surveillance should involve using 6-monthly abdominal ultrasound imaging in all at-risk groups without the measurement of the traditional tumour marker, AFP.(17) Interestingly, a recent meta-analysis showed that the addition of AFP to US imaging significantly increased the sensitivity in diagnosing early HCC. US alone diagnosed early stage HCC with a sensitivity of 45% compared to a sensitivity of 63% with the addition of AFP (P=0.002).(24)

Table 1 shows the sensitivities and specificities associated with AFP in diagnosing HCC in different clinical scenarios found in various studies. Regarding AFP, the optimal cut-off value ranged from 10.9 ng/mL to 200 ng/mL. The sensitivity and specificity ranged from 40% to 95.2%, and 47.1% to 100%, respectively.

Study	Clinical scenario	AFP Cut-off value	Sensitivity	Specificity
Taketa et al(25)	HCC from cirrhosis	30 ng/mL	65%	89%
Taketa at al(25)	HCC	200 ng/mL	70%	100%
Marrero et al(22)	Early-stage HCC	10.9 ng/mL	65%	82%
Sung et al(26)	HCC among cirrhosis	20 ng/mL	55%	90%
Hippo et al (27)	HCC from non-malignant liver diseases	20 ng/mL	73%	77%
Marrero et al (28)	HCC from chronic cirrhosis	13.6 ng/mL	95.2%	47.1%
Muramatsu(29)	HCC	20 ng/mL	51.9%	86.3%
Muramatsu(29)	Early stage HCC	20 ng/mL	40%	NA
Zhu et al (30)	HCC	20 ng/mL	62.5%	53.3%
Zhu et al (30)	Early stage HCC	20 ng/mL	40%	NA
Fouad et al(31)	HCC from cirrhosis	20 ng/mL	53%	93%
Fouad et al(31)	Early stage HCC from cirrhosis	20 ng/mL	46%	93%
Zhang et al(32)	HCC	14.88 ng/mL	63.4%	79.7%
Zhang et al(32)	Early stage HCC	15.64 ng/mL	55%	81.3%
Mao et al (33)	HCC	35 ng/mL	58%	85%
Giannelli et al (34)	HCC	18.8 ng/mL	41%	94%
Hussein et al (35)	HCC	7.7 ng/mL	90%	93%

Table 1: Sensitivities and specificities of the biomarker, AFP, in various clinical applications. AFP, alpha-fetoprotein. HCC, hepatocellular carcinoma. (Adapted from Lou et al. (18) and Witjes et al. (36)).

In addition to AFP and PIVKA-II, there are various biomarkers currently being assessed and used in diagnosing early HCC, including AFP-L3, glypican-3 (GPC3), osteopontin (OPN), golgi-protein-73 (GP73), nucleic acids and microRNAs (miRNAs).(11)

AFP-L3 is a glycoform of AFP and is increased specifically in HCC with AFP-L3 levels correlating with AFP levels.(11) A multicentre study showed that AFP-L3 had a sensitivity of 28% and a specificity of 97% in diagnosing early HCC.(22) When total AFP levels are <20 ng/mL, AFP-L3 is not usually detected, and therefore AFP-L3 cannot be used as a biomarker for HCC when total AFP concentrations are <20 ng/mL. The sensitivity of AFP-L3 is therefore limited by overall AFP levels.(11)

GPC3 is a member of the glypican family and binds to the cell surface membrane. It is involved in cellular proliferation and survival, as well as tumour suppression, and is usually not present in healthy and non-cancerous hepatocytes.(11) GP73 has been found to be upregulated in HCC.(26) A meta-analysis showed the pooled sensitivity and specificity of serum GPC3 in the early diagnosis of HCC was 55.1% and 97% respectively, compared to 34.7% and 87.6% respectively for AFP.(37)

OPN is an integrin-binding glycophosphoprotein that is overexpressed in various malignancies and is involved in tumour growth, progression and metastasis.(11, 38) Increased expression of serum OPN has been seen in HCC

compared to normal liver / chronic hepatitis / cirrhosis patients.(39, 40) One study showed that OPN had a sensitivity and specificity for early HCC of 75% and 62% respectively compared to 46% and 93% respectively for AFP.(39)

GP73 is a type II golgi-specific membrane protein usually expressed in epithelial cells of different human tissue types excluding hepatocytes. However, serum GP73 is found in patients with liver disease especially in HCC.(11, 41) One study showed a higher sensitivity of serum GP73 in diagnosing early HCC compared to AFP.(42) Another study showed GP73 had a significantly higher sensitivity for diagnosing early HCC compared to AFP, 62% and 25% respectively.(28)

Molecular biomarkers for disease diagnosis by probing nucleic acids using microarray technology is an alternative method of detecting disease.(43) Three separate genes have been found associated with HCC by Shi et al and showed that the combination of all three gene markers increased the accuracy in detecting early HCC compared to individual gene markers, with a sensitivity of 72% and specificity of 95%. The study also showed that the addition of AFP improved the accuracy and sensitivity in detecting early HCC.(44)

MicroRNAs have been found to play a role both as oncogenes as well as tumour suppressor genes in human cancer.(45) Serum miR-15b and miR-130b are found to be upregulated in HCC.(46) Both miRNA markers have a high sensitivity in early HCC which may be beneficial when AFP levels are low.(46)

1.4 GALAD and BALAD-2 Score

The gender, age, AFP-L3, AFP, and DCP (GALAD) score and bilirubin, albumin, AFP-L3, AFP, and DCP (BALAD-2) score are two validated models in diagnosing HCC and predicting patient survival respectively in international patient cohorts.(47) The BALAD-2 score is very similar to the BALAD score that was originally developed in Japan, but has been shown to have a slightly better performance incorporating a more detailed statistical analysis.(48, 49)The GALAD score was found to have a superior area under the receiver operating characteristic curve (AUROC) in diagnosing HCC in the UK, German and Japan cohorts compared to each individual marker, as well in diagnosing early HCC in the UK and Japan cohorts. The BALAD-2 score reflects both the severity of liver dysfunction by incorporating the bilirubin and albumin levels into the score, as well as tumour associated factors by including the AFP-L3, AFP and DCP. The score showed a clear differentiation in the four different score categories in the median survival in the UK, German, Japan and Hong Kong cohorts, irrespective of tumour size and liver disease aetiology.(47, 48) The GALAD score was also shown to significantly improve the detection of early HCC according to the BCLC staging, with a sensitivity of 85.6% and a specificity of 93.3%.(50) Given that these scores were applied to various international cohorts, they have the ability to be utilised in an international setting.(47)

1.5 Radiological diagnosis of hepatocellular carcinoma

It is thought that early diagnosis of HCC is possible in 30-60% of cases in developed countries, therefore enabling curative interventions to be applied.(17) Liver biopsy remained the standard test to be performed to diagnose HCC until 2000. However, improvements in radiological investigations and technique meant that diagnosis could be based on imaging alone. EASL and American Association for the Study of Liver Diseases (AASLD) adopted a specific HCC radiological feature: evidence of contrast uptake in the arterial phase (arterial hypervascularity) with washout in the venous/late phase.(17)

Patients who should be entered into the surveillance programme to screen for liver lesions include patients with underlying liver cirrhosis, non-cirrhotic hepatitis B virus (HBV) carriers with active hepatitis or have a family history of HCC, and non-cirrhotic patients with chronic hepatitis C virus (HCV) and advanced liver fibrosis.(17) There is variation in the surveillance interval. Japanese guidelines propose a three to four month interval for patients falling in the extremely high risk category (cirrhosis secondary to viral hepatitis).(14, 51) However one study did not show any difference between three-monthly and six-monthly interval scans.(52) A meta-analysis of prospective studies showed the combined sensitivity of US based surveillance falls from 70% with the six-month programme to 50% with the twelve-month programme.(53) Cost-effectiveness studies have in fact shown that six-monthly surveillance scans do improve quality-adjusted life expectancy at an acceptable cost.(54) Therefore in view of this, EASL-EORTC CPG recommend six-monthly US surveillance scans.(17)

The diagnostic pathway for HCC using radiology is in accordance to the size of the mass identified on the surveillance ultrasound scan (USS), and this is explained below, with **Figure 1** summarising this pathway.

1.5.1 Lesions <1cm in diameter

Lesions <1cm in size have a low risk of being malignant; however, there is a high probability that small liver nodules may turn cancerous over time. Therefore, close surveillance of these lesions needs to be undertaken.(55) A repeat USS should be performed after 4 months: if this is stable, then repeat imaging every 4 months should be done. However, if the lesion is growing or the appearance is changing, further investigation should then be carried out according to the size.(17)

1.5.2 Lesions 1-2cm in diameter

Lesions within this size group have a high likelihood of being HCC.(55) Following the detection of a lesion between 1-2cm in size on USS, a 4-phase computed tomography (CT) or dynamic contrast enhanced magnetic resonance imaging (MRI) scan should then be performed. Both techniques should be undertaken in this group of patients, and only a one imaging technique is recommended in centres of excellence with advanced radiological equipment. If HCC radiological hallmarks are present then a diagnosis of HCC can be made. However, if there are no definite HCC radiological hallmarks present then a liver biopsy is recommended.(17)

1.5.3 Lesions >2cm in diameter

Identification of a hepatic mass >2cm in size is highly suspicious of HCC.(55) Following detection of this lesion, imaging using 4-phase CT or dynamic contrast enhanced MRI scan should be done. For this group, only one imaging technique is required for diagnosis. A diagnosis is made if radiological hallmarks for HCC are seen; a liver biopsy is required if radiological hallmarks are not identified.(17)
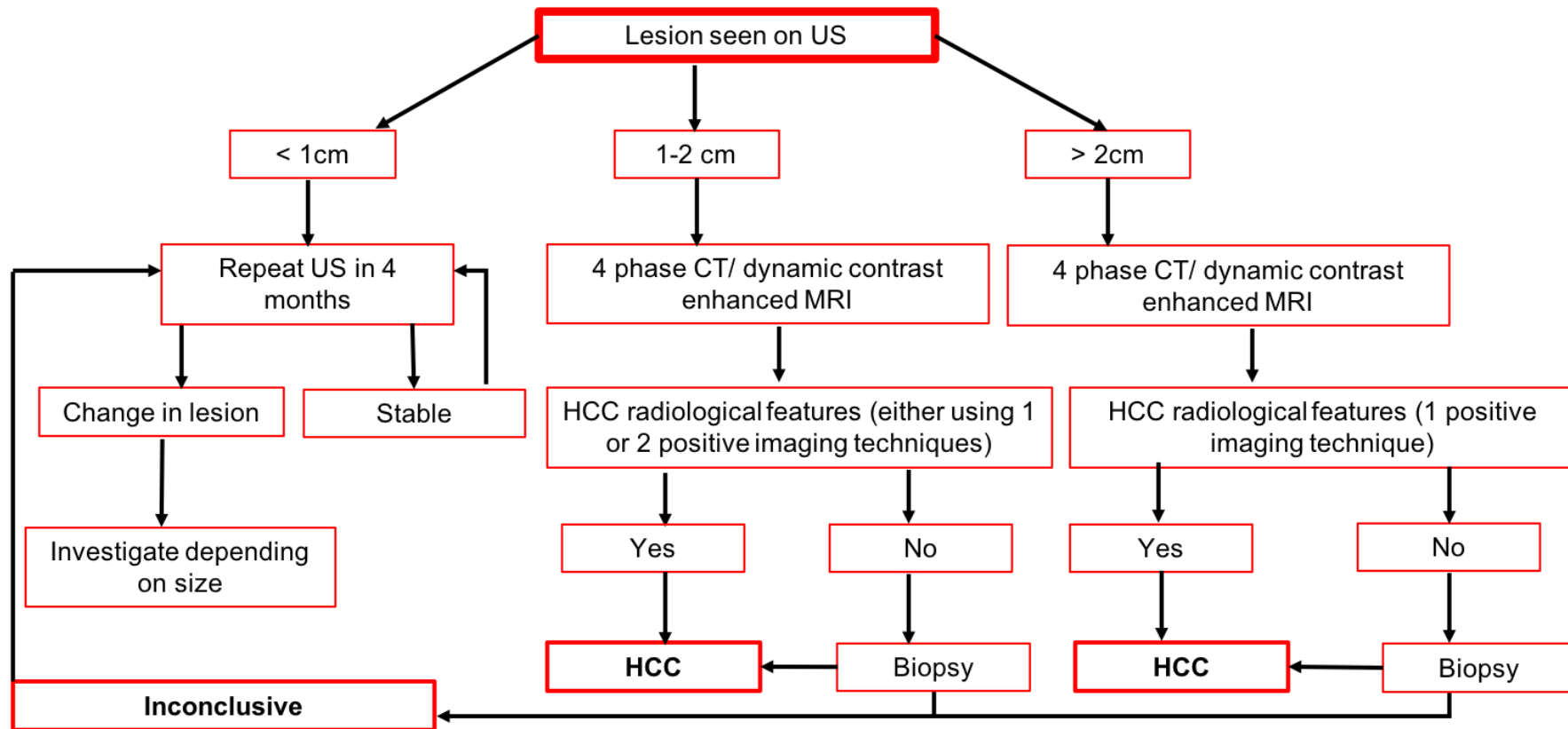
Figure 1: Radiological pathway following liver lesion identification on US imaging. (Adapted from EASL-EORTC CPG, (17)). US, ultrasound. CT, computed tomography. MRI, magnetic resonance imaging.

1.6 Pathological diagnosis of hepatocellular carcinoma

The sensitivity of liver biopsy ranges from 70-90% across all tumour size groups, and is dependent on a number of factors including location and size of the tumour, and operator expertise. For lesions between 1-2cm in size, pathological diagnosis remains challenging.(17, 56) One study reported a positive first liver biopsy for HCC in 70% of tumours 2cm or less in size.(57) Therefore, a positive liver biopsy is clinically useful in identifying HCC cases, but a negative biopsy does not rule out the diagnosis.(17) There is a 2.7% risk of needle tract tumour seeding after a median time of 17 months from the time of biopsy to the presence of seeding, and therefore patients undergoing liver biopsy need to be appropriately selected.(58)

Differentiating high-grade dysplastic nodules from early HCC by solely using the classical morphological criteria can be difficult, particularly because the most important pathological hallmark of stromal invasion seen in HCC is frequently found to be absent or difficult to identify in biopsy specimens.(17, 56) Therefore, additional markers used in staining methods have been validated for their use in diagnosing early HCC on molecular profiling. These include GPC3, heat shock protein 70 and glutamine synthetase.(56) The combination of these three markers showed good sensitivity and specificity in diagnosing HCC (72% and 100% respectively with two positive markers) and have also been validated in two large series.(59-62)

Significant poor prognostic factors on histological diagnosis of HCC include the presence of microvascular invasion (MVI) and nuclear grade 3, with the combination of these parameters providing good prognostic stratification.(63) Other prognostic factors of HCC include tumour size and number.(64)

1.7 Staging of hepatocellular carcinoma

Staging systems are used in cancer aids in predicting prognosis and allocating treatment appropriately. Additionally, they enable exchange of information in the research environment and clinical trials to be developed with comparable criteria.(17) Prognostic assessments are further complicated in HCC, as two independent variables can both result in death: cancer and liver function associated with cirrhosis.(65, 66)

The staging of HCC commonly follows the Barcelona Clinic Liver Cancer (BCLC) staging system that stages the cancer (Stage 0, A, B, C and D) after taking into account several factors including the tumour status, the patient's performance status (PS) and assessment of liver function (Child-Pugh's score). This staging system allows appropriate treatment allocation in accordance to cancer stage.(17)

BCLC stage 0 represents the very early cancer where there is a single lesion <2cm in diameter with no evidence of vascular invasion or satellite lesions in patients who have a PS of 0 and preserved liver function (Child-Pugh A), or if there is carcinoma in situ.(17) Data has shown that resection and liver

transplantation provide a five-year survival of around 70-90% and 70% with liver ablation.(67-69)

BCLC stage A represents the early HCC where there is a single nodule between 2-5cm in size or if there are 3 nodules ≤3cm in diameter, in patients who have a PS of 0 and Child-Pugh A or B.(17) Median survival with early HCC at five years after resection, liver transplantation or ablation reaches 50-70%.(17)

Curative treatment options are possible for stage 0 and A, which includes hepatic resection, ablation therapies and liver transplantation.(17)

BCLC stage B represents the intermediate stage where there is multinodular disease, PS 0 and Child-Pugh A or B. Transarterial chemoembolisation (TACE) treatment is possible for this stage with a median overall survival (OS) of 20 months.(17) TACE has also been shown to improve the two year survival of patients.(17, 70)

BCLC stage C represents the advanced stage where there is now evidence of macrovascular invasion (portal invasion), lymph node involvement or metastases, PS 1-2 and Child-Pugh A or B. Treatment with Sorafenib can be considered for this stage of disease and has a median OS of 11 months.(17, 71)

BCLC stage D represents the terminal stage where the PS is >2 and evidence of poor liver function (Child-Pugh C). Best supportive care is the management plan for this group of patients with a median OS of <3 months.(17, 72) **Figure 2** summarises the BCLC staging system.
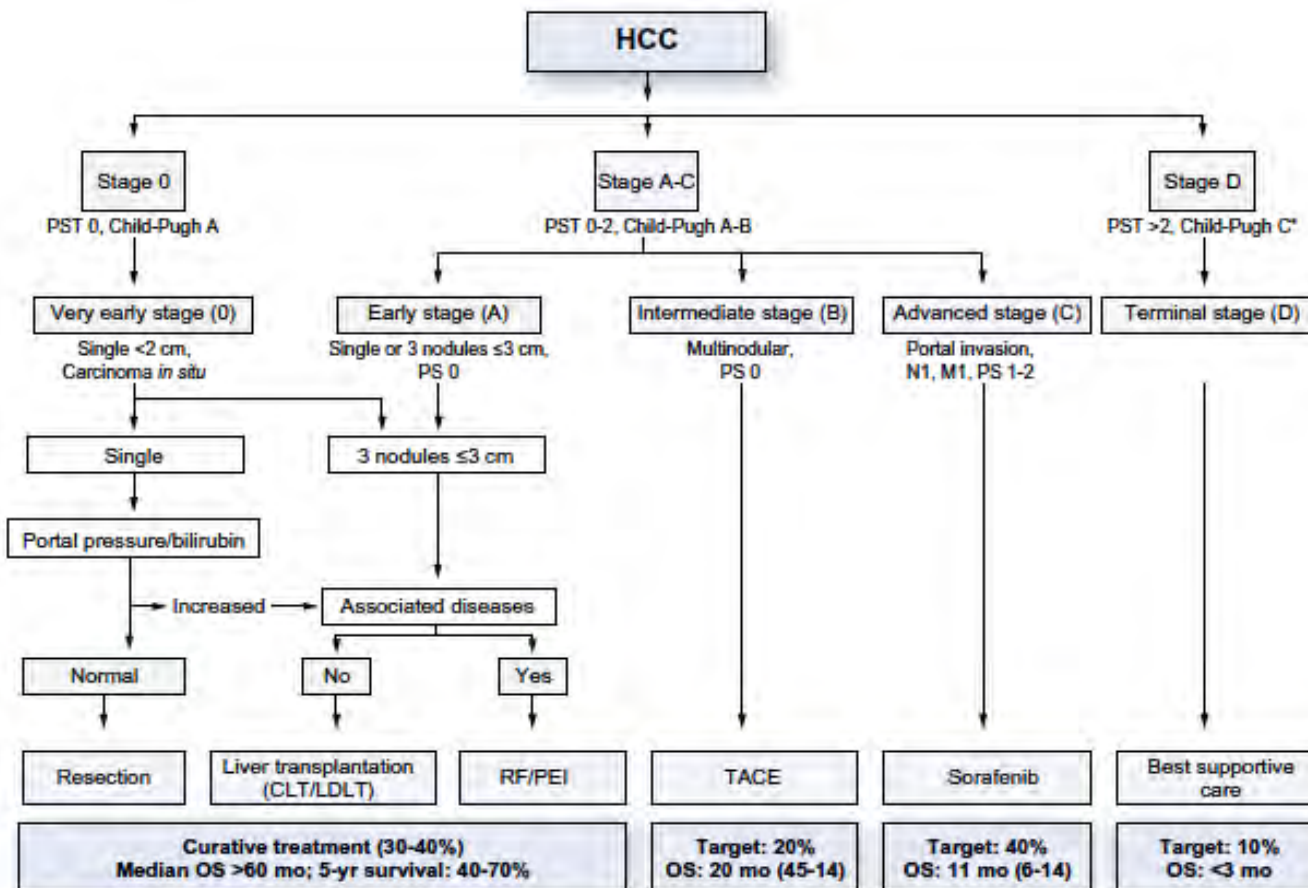
Figure 2: Barcelona Clinic Liver Cancer staging system in HCC. (Taken from EASL-EORTC CPG, (17)).

1.8 Milan criteria

The Milan criteria (MC) was introduced in 1996 by Mazzaferro et al who showed the overall four-year survival for patients transplanted for HCC was 75% with a recurrence free survival of 83%.(73) This was found to be highly promising given the three-year survival for small untreated HCCs occurring on a background of liver cirrhosis is only 21%.(74) The four-year survival reported by Mazzaferro et al was found to be similar to patients transplanted without HCC.(73) The defined MC is a single hepatic lesion ≤5cm, or up to 3 lesions each ≤3cm, without evidence of tumour vascular invasion or extra-hepatic metastases.(73, 75)

The principal aim for performing liver transplantation (LT) in HCC, is to provide a similar rate of disease-free survival to those transplanted for benign liver disease. Therefore, it is imperative that an agreed set of criteria is followed to ensure appropriate patients are selected for LT. Agreed criteria also allow prioritisation of accepted candidates on the waiting list, and to set out clear indications for bridging and downstaging therapy to be offered with the goal of reducing the risk of disease progression and allowing continued activation on the waiting list.(13, 76)

The MC has been adopted worldwide for selecting patients with HCC for LT. Fifteen years following the introduction of the MC good outcomes following LT is still being seen with a 5-year survival of at least 70% when the criteria are met.(77)

Current UK selection criteria for patients with HCC to undergo LT represent a modification of the MC.(78) The Liver Advisory Group state that an AFP >1000 ng/mL is a contraindication to LT, given that a higher risk of recurrence was seen when the AFP was found to be higher than this.(79) A solitary lesion measuring between 5-7cm may also be an indication for LT if this has not grown >20% over a period of 6 months.(78, 80)

1.9 Downstaging hepatocellular carcinoma

For patients who are outside the MC for liver transplantation, downstaging can assist in bringing this group within criteria for possible transplantation.(81) One large study showed that around a third of patients with HCC were within MC.(82) In the UK, despite the expansion of selection criteria for LT, less than 10% of patients with HCC met this criteria.(83) Downstaging is achieved by performing liver-targeted therapy, such as liver ablation, TACE and stereotactic ablative radiotherapy (SABR). The response to these downstaging treatments is defined radiologically as per the modified Response Evaluation Criteria in Solid Tumours (mRECIST).(84)

The Duvoux criteria are used in listing for HCC following downstaging treatment.(79) This takes into account the largest diameter of the HCC, number of nodules and the AFP. A score of ≤ 2 is required for eligibility to be assessed for liver transplantation. An interval of ≥ 6 months following downstaging treatment to imaging, or an interval of ≥ 3 months after the first imaging has demonstrated the patient is within selection criteria, is required.(85)

The five-year survival rate in those transplanted following successful downstaging of HCC is comparable to patients transplanted within the MC.(86)

1.10 Introduction to prothrombin induced by vitamin K absence-II

PIVKA-II (also known as des-γ-carboxyprothrombin, DCP) was first detected in 1984 by Liebman et al as an independent serum biomarker for primary HCC.[87, 88]

Abnormal prothrombin was first purified in 1972 and compared to normal prothrombin production.[89, 90] Both prothrombins were seen to have the same structure of amino acids and carbohydrates; however, the abnormal prothrombin was unable to bind calcium ions and the functional prothrombin activity was absent. Two years later, it was found that the normal prothrombin contained residues of carboxylated glutamic acid, γ-carboxyglutamic acid, and further studies showed the presence of 10 γ-carboxyglutamic acid residues in normal prothrombin that were absent in abnormal prothrombin. The carboxylated glutamic acid is required for the high affinity binding of calcium ions, leading to the activation and functioning of prothrombin.[91-93] PIVKA-II is therefore an abnormal form of the coagulation prothrombin protein, found to be raised in the sera of HCC patients.

1.10.1 Production of PIVKA-II

Vitamin K is a fat-soluble vitamin and an important co-factor in the carboxylation reaction of glutamic acid residues (Glu) to form γ-carboxyglutamic (Gla) acid residues.[94, 95] The vitamin K-dependent carboxylase enzyme, γ-glutamylcarboxylase uses vitamin K hydroxyquinone as the energy source for the carboxylation, which is oxidised to vitamin K, 2-3 epoxide.[96] In normal

prothrombin production, the vitamin K-dependent carboxylase enzyme catalyses the conversion of 10 Glu residues present in the Gla domain at positions 6, 7, 14, 16, 19, 20, 25, 26, 29 and 32 to Gla residues.(97) The vitamin K-dependent carboxylase responsible for the post-translational carboxylation of prothrombin is impaired in many HCC cells, and an abnormal prothrombin with all or some of unconverted glutamic acid is secreted.(98-101) Another factor involved in the production of PIVKA-II is vitamin K deficiency given that the activity of the carboxylase enzyme is dependent on the presence of vitamin K as a co-factor.(88) One study showed that vitamin K levels were significantly lower in cancerous tissue in patients with HCC compared to non-malignant tissue.(102) Naraki et al identified that the abnormal prothombin contained less than 4 Gla residues in HCC, but chronic liver disease including cirrhosis contained PIVKA-II with more than 5 Gla residues.(97)

Therefore, this non-carboxylated form (PIVKA-II) could be considered a HCC biomarker, and a summary of PIVKA-II production is shown in **Figure 3**.
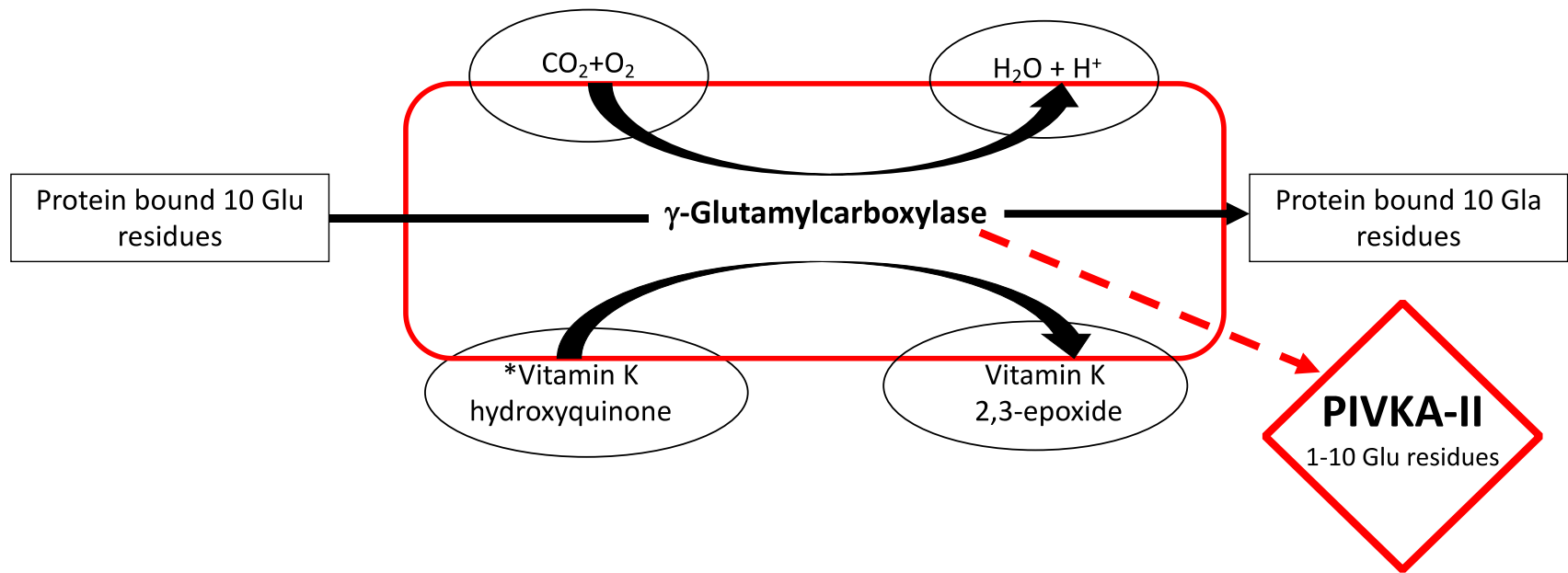
Figure 3: Schematic representation summarising PIVKA-II production. PIVKA-II, prothrombin induced by vitamin K absence-II. Glu, glutamic acid. Gla , γ-carboxyglutamic.

1.10.2 PIVKA-II signaling pathways

A number of studies have looked at the role and mechanism of PIVKA-II/ DCP in tumour survival, growth and metastasis.

It has been shown that PIVKA-II binds to a membrane spanning tyrosine kinase receptor, cellular mesenchymal-epithelium transition factor (c-Met), leading to Met autophosphorylation of tyrosines 1234 and 1235 of the tyrosine kinase domain and tyrosine 1349 and 1356 of the multifunctional docking site.(103-105) Hepatocyte growth factor (HGF) is the ligand for c-Met and is known to have a significant role in tumour growth, including in HCC.(106, 107) DCP was found to phosphorylate only tyrosine 1234 and 1235, whereas HGF phosphorylated all residues in both sites.(108) The difference in phosphorylation may lead to alternative biological effect on cellular proliferation.(108) Following the binding of DCP to c-Met, this then led to downstream activation of the Janus kinase 1 / Signal transducer and activator of transcription 3 (JAK-1/STAT3) signaling pathway, resulting in cell proliferation and tumour growth.(108, 109) STAT3 and c-Met small interfering RNA (siRNA), as well as functional inhibition of c-MET by the c-Met inhibitor SU11274, suppressed the PIVKA-II induced HCC cell growth.(108, 110) It has been noted that high levels of PIVKA-II are a risk factor for extrahepatic HCC metastasis.(111) Another study showed that PIVKA-II increased the expression and secretion of matrix metalloproteinase (MMP) 2 and 9 (MMP-2 and MMP-9) following c-Met binding and subsequent activation of the epidermal growth factor receptor (EGFR). This then stimulated activation of the extracellular signal-regulated kinase/mitogen activated protein kinase (ERK 1/2

MAPK) pathway, leading to MMP-2 and MMP-9 secretion and promotion of HCC growth and metastasis. Blocking this pathway with an ERK 1/2 inhibitor, PD98059, removed the DCP induced MMP-2 and MMP-9 activity.(112) PIVKA-II is also associated with the onset of angiogenesis in HCC, and angiogenesis is an important process in tumour growth given that HCC is a highly hypervascular tumour.(113) Tumour cells release angiogenic factors that stimulate vascular endothelial cells and infiltrating cells. These angiogenic factors including VEGF, fibroblast growth factor (FGF) and MMPs, stimulate the migration and proliferation of vascular endothelial cells which lead to a dense vascular network in the stromal space.(114-116) DCP was found to bind directly with the kinase domain receptor (KDR), a VEGF receptor 2, leading to activation of the phospholipase C-gamma-mitogen activated protein kinase (PLC-γ-MAPK) pathway and promoting angiogenesis in HCC.(117) Exposing vascular endothelial cells to KDR siRNA, KDR kinase inhibitor or MAPK inhibitor stops the DCP-induced angiogenesis from taking place.(115)

Figure 4 outlines the pathways involved by PIVKA-II in HCC growth, metastasis and angiogenesis.
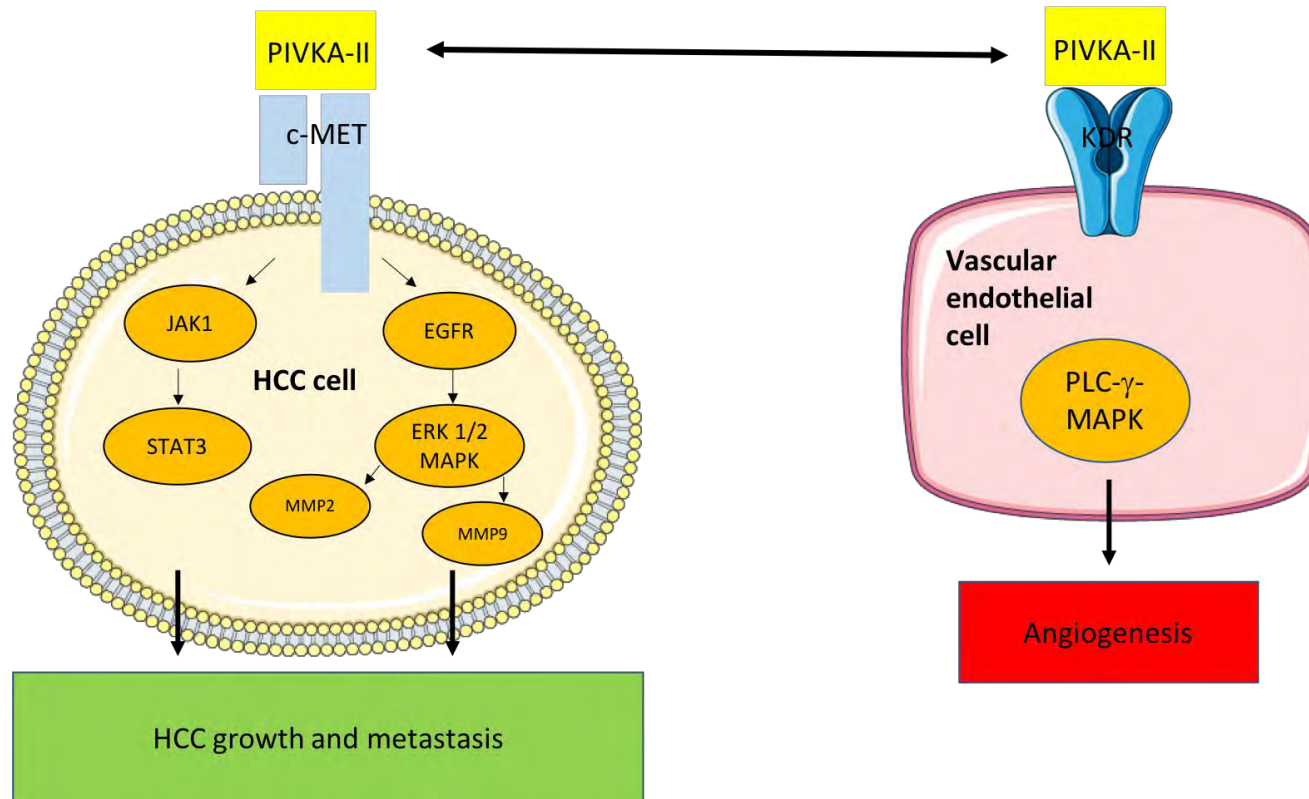
Figure 4: Schematic diagram of the various signaling pathways involved by PIVKA-II in promoting HCC growth, metastasis and angiogenesis. Some components of this diagram were obtained from Servier (118). JAK1 STAT3, Janus kinase 1 / Signal transducer and activator of transcription 3. MMP, matrix metalloproteinase. EGFR, epidermal growth factor receptor. ERK 1/2 MAPK, extracellular signal-regulated kinase/mitogen activated protein kinase. KDR, kinase domain receptor. PLC-γ, phospholipase C-gamma.

1.10.3 What is already known of prothrombin induced by vitamin K absence-II and hepatocellular carcinoma

PIVKA-II is mainly used in Asia as a diagnostic and surveillance marker for HCC, and has also been shown to be a predictor of MVI, an important prognostic factor in HCC. However, there is limited experience in Europe with PIVKA-II.(11, 119) The majority of studies looking into PIVKA-II have taken place in Asia, where the patient cohort differs from the UK. There have been no studies conducted in the UK comparing AFP with PIVKA-II and PIVKA-II's association with prognosis, nor the response of PIVKA-II with ablation treatment.

Studies have shown variable results in the efficacy of PIVKA-II in HCC both as a single biomarker and also as a combination with AFP. In addition to this, a high proportion of studies looking at the role of PIVKA-II in HCC, have involved patients with viral hepatitis being the main aetiology of underlying liver disease.

A recent study conducted in China has shown that PIVKA-II is superior to AFP in diagnosing early HCC versus liver cirrhosis with an area under the curve (AUC) of 0.73 (95% CI 0.70 – 0.85) and 0.62 (95% CI 0.60 – 0.77) respectively. Comparing HCC as a whole versus liver cirrhosis, PIVKA-II performed better than AFP, AUC 0.78 (95% CI 0.64 – 0.81) and 0.67 (95% CI 0.68 – 0.80) respectively. In early stage AFP-positive HCC, AFP-L3 was found to be a superior diagnostic marker compared to PIVKA-II, whereas PIVKA-II was the better marker compared to AFP-L3 in early stage AFP-negative HCC. The combination of AFP and PIVKA-II showed a better diagnostic performance

compared to either marker alone in diagnosing early HCC versus liver cirrhosis (AUC 0.75, 95% CI 0.71 – 0.87). (120)

One European study showed that a high percentage of non-alcoholic steatohepatitis had positive PIVKA-II tumours, and the combination of both AFP and PIVKA-II increases the overall sensitivity of diagnosing HCC, even in the early stages.(121) Previous studies in Egypt and France have shown a higher sensitivity and specificity of PIVKA-II in comparison with AFP.(98, 119) Zakhary et al showed a sensitivity of 44% and specificity of 73% using the best cut-off value of >28 for AFP and 100% sensitivity and specificity with cut-off value of >53.7 for PIVKA-II, in detecting and diagnosing HCC at an earlier stage when curative treatment options are possible. The plasma level of PIVKA-II also showed a significant gradual rise correlating with progressive tumour burden.(98) Poté et al showed the AUC for PIVKA-II was better for diagnosing early HCC compared to AFP (0.81 vs 0.582). For very early HCC, PIVKA-II was found to be a better marker than AFP (AUC 0.716 vs 0.5 for PIVKA-II and AFP respectively). The PIVKA-II serum level was found to be significantly higher in tumours >2cm, in moderately / poorly differentiated HCC and in HCC with MVI. The AFP serum level was significantly higher only in tumours >2cm. The combination of AFP and PIVKA-II did not improve the diagnostic performance for overall or very early HCC. A slight improved performance of early HCC diagnosis was found when combining the two markers (AUC 0.826).(119)

A Chinese group showed that between the different BCLC stages (excluding between BCLC stage B and C), PIVKA-II levels significantly increased (p<0.05)

whereas AFP showed no difference. PIVKA-II levels >40 milli arbitrary unit (mAU)/mL independently predicted the presence of MVI, similar to another study showing that high serum PIVKA-II levels was an independent risk factor for MVI.(122, 123) Another group in China showed that PIVKA-II correlates with tumour size, tumour differentiation and BCLC staging but had a negative correlation with serum hepatitis B viral load.(124) A recent study performed in Italy showed that PIVKA-II has a higher accuracy than AFP in differentiating HCC from patients with benign chronic liver disease (CLD).(125) A recent meta-analysis conducted by Caviglia et al summarised the performance of both markers across three different groups: HCC, liver cirrhosis and CLD. Viral hepatitis, in particular chronic hepatitis B, accounted for the vast majority of the underlying liver disease aetiology. The weighted summary AUC of PIVKA-II was 0.791 in diagnosing HCC compared to 0.767 for AFP, and this showed no significant difference (p=0.524). The combination of AFP and PIVKA-II however was seen to be significantly better and had a weighted summary AUC of 0.859, (p<0.001).(126)

In a study in South Korea, the AUC for diagnosing HCC was slightly better with AFP compared to PIVKA-II (0.879 vs 0.801 respectively). In the multivariate analysis, PIVKA-II correlated with laboratory tests including aspartate aminotransferase, bilirubin, platelets and albumin levels.(127) Marrero et al also showed that AFP had a better sensitivity than PIVKA-II for diagnosing very early and early HCC.(22) Park et al compared the diagnostic accuracy of AFP, AFP-L3 and PIVKA-II in HCC and found that AFP had the best diagnostic

performance in diagnosing HCC as a single biomarker.(128) A Korean study recently showed that AFP and AFP-L3 started to show an increase in levels 6 months prior to HCC diagnosis (very early stage) (p<0.05). AFP was superior to AFP-L3 and PIVKA-II at HCC diagnosis with AUROCs of 0.77, 0.73 and 0.71 respectively. The sensitivity of US alone at HCC diagnosis was 48.6% and improved to 88.6% with the addition of AFP and 94.3% with both AFP and AFP-L3.(129) A group in America recruited patients with viral hepatitis and showed that PIVKA-II was the superior marker compared to either AFP and AFP-L3 in diagnosing HCC, had a direct correlation with tumour size and was not elevated in non-HCC patients.(130)

Yu et al have recently shown that liver cirrhosis accounted for the largest part of the PIVKA-II positive non-HCC group. They showed that PIVKA-II had a better diagnostic effectiveness in differentiating HCC from non-HCC cases, with an improved AUC when both markers are combined in differentiating HCC from cirrhosis, and HCC from cirrhosis and hepatitis. Both AFP and PIVKA-II could barely differentiate early HCC from cirrhosis, with AFP having a better (non-significant) AUC compared with PIVKA-II (0.635 vs 0.607 respectively). The study also showed an increase in PIVKA-II levels with HCC progression.(131)

Table 2 shows the differences between AFP, PIVKA-II and the combination of both markers in diagnosing HCC in different clinical scenarios found in various studies.

However, results from previous studies do not necessarily apply to UK patients as the patient cohorts are different in some studies compared to the UK, with hepatitis B or C viral hepatitis being the cause of liver cirrhosis. In the UK the commonest causes of cirrhosis are alcohol, hepatitis C and obesity. Since demographics and causes of liver disease differ significantly between geographical regions it is important to assess the relevance of potential biomarkers in specific populations.

Study	Clinical scenario	AFP AUC (95% CI)	PIVKA-II AUC (95% CI)	AFP and PIVKA-II combination AUC (95% CI)	Cut-off PIVKA-II	Cut-off AFP	Combination of AFP and PIVKA-II sensitivity	Combination of AFP and PIVKA-II specificity	AFP Sensitivity	AFP Specificity	PIVKA-II Sensitivity	PIVKA-II Specificity
Chen H et al (110)	Early HCC from cirrhosis	0.62 (0.60 – 0.77)	0.73 (0.70 – 0.85)	0.75 (0.71 – 0.87)	NR	NR	52.6%	90%	30.6%	90%	48.3%	90%
Chen H et al (110)	HCC from cirrhosis	0.67 (0.68 – 0.80)	0.78 (0.64 – 0.81)	0.83 (0.68 – 0.84)	NR	NR	64.2%	90%	40.1%	90%	57.2%	90%
Ertle JM et al (111)	HCC from controls*	0.88	0.87	0.91	5 ng/mL	10 ng/mL	78%	89.3%	54.9%	94.5%	63.4%	94.5%
Ertle JM et al (111)	Early HCC from controls*	0.84	0.81	0.87	5 ng/mL	10 ng/mL	58.3%	89.3%	38.9%	94.5%	45.8%	94.5%
Pote et al (109)	Early HCC from cirrhosis	0.582 (0.443 – 0.722)	0.81 (0.697 – 0.924)	0.826 (0.722 – 0.929)	42 mAU/mL	5.5 ng/mL	NR	NR	61%	50%	77%	82%
Wang X et al (113)	HCC from chronic hepatitis B	0.781	0.756	0.868	32.1 mAU/mL	17.6 ng/mL	NR	NR	64.6%	73.3%	52.2%	81.5%
Caviglia GP et al (116)	HCC from CLD or cirrhosis	0.767	0.791	0.859	NR	NR	NR	NR	NR	NR	NR	NR
Choi JY et al (117)	HCC from CLD	0.879	0.801	NR	40 AU/mL	10 ng/mL	NR	NR	78.9%	84.6%	62.2%	94.9%
Marrero JA et al (22)	Early HCC from cirrhosis	0.80 (0.77 – 0.84)	0.72 (0.68 – 0.81)	0.83 (0.8 – 0.87)	150 mAU/mL	20 ng/mL	78%	62%	53%	90%	61%	70%
Choi JY et all (119)	Early or very early HCC from cirrhosis +/or CHB	0.77 (0.68 – 0.86)	0.71 (0.61 – 0.80)	0.77 (0.67 – 0.87)	20 mAU/mL	5 ng/mL	62%	78%	62%	87%	48%	86%

Park SJ et al (118)	HCC from cirrhosis	0.751 (0.683 – 0.818)	0.705 (0.633 – 0.777)	0.765 (0.708 – 0.823)	40 mAU/mL	10 ng/mL	55.7%	97.4%	68.4%	81.8%	70.9%	70.1%
Yu R et al (121)	Early HCC from cirrhosis	0.635 (0.595 – 0.674)	0.607 (0.566 – 0.646)	0.641 (0.601 – 0.679)	NR	NR	NR	NR	NR	NR	NR	NR

Table 2: Comparisons between AFP, PIVKA-II and as a combination of both markers, in diagnosing HCC in various clinical applications. AUC, area under the curve. CLD, chronic liver disease. NR, not reported, CHB, chronic hepatitis B. *Controls were patients with chronic liver disease, cirrhosis, or viral hepatitis

Previous studies have also looked at immunohistochemical staining of PIVKA-II in HCC. Poté et al assessed PIVKA-II tissue expression in HCC cases and showed that high PIVKA-II expression ($\geq$50% stained cells) was significantly associated with moderately/poorly differentiated HCC (p=0.03) and in the presence of MVI (p=0.001). They also showed that early HCC cases had low PIVKA-II expression. In non-HCC tissue, PIVKA-II expression was negative in 76% of cases (53/70), weakly positive in 20% of cases (14/70) and strongly positive in 4% of cases (3/70). The combination of serum PIVKA-II levels with the PIVKA-II staining improved the sensitivity and specificity of diagnosing MVI.(119) These findings are in keeping with previous studies showing that positive PIVKA-II tumour expression influences prognosis.(132-134) It has also been shown that PIVKA-II expression is present in small-sized and well-differentiated HCCs but is not present in premalignant nodules (adenomatous hyperplasia).(135)

1.10.4 PIVKA-II and treatment with ablation

Approximately a fifth of all patients who develop HCC are suitable candidates for liver resection, though cancer recurrence can still occur following resection.(136) The demand for organ donors continues to rise with increasing number of patients requiring a liver transplant. Therefore, non-surgical treatments to cure small HCCs are increasingly being used where appropriate.(137, 138) Controversy remains in the prognostic value of PIVKA-II in HCC patients treated with ablation.

A meta-analysis published in 2018 showed that high PIVKA-II levels were significantly associated with a poorer OS (Hazard ratio, (HR) 1.59, p<0.001) and recurrence-free survival (HR 1.76, p<0.001) in patients with HCC treated with ablation.(139) Another study showed that in addition to PIVKA-II, AFP-L3 was also significantly related to survival, but that PIVKA-II was the sole factor associated with local tumour progression. Both serum PIVKA-II and serum AFP were significantly related to distant recurrence.(140) A Japanese group showed that the cumulative survival rate, recurrence-free survival rates and staying within the MC for liver transplantation was significantly lower in patients who had a PIVKA-II ≥100 mAU/mL compared with a PIVKA-II <100 mAU/mL, and therefore concluded that PIVKA-II is the optimal prognostic predictor following curative ablation treatment.(141)

Again, no studies in the UK have looked at the role of PIVKA-II in patients with HCC undergoing ablative treatment, and therefore it is important to assess the suitability of this marker in different cohorts of patients and see if current known results and findings can be extrapolated to patients in different countries diagnosed with early HCC undergoing treatment with ablation.

1.11 Aetiology, genetics and biology of neuroendocrine tumours

NETs originate from cells containing neuroendocrine properties (known as enterochromaffin or Kulchitsky cells) and are slow growing cancers.(142, 143) Certain proteins are expressed by these cells, including neuron-specific enolase and synaptophysin, classically seen in neural cells. They are stimulated by the autonomic nervous system and produce amines and peptide hormones such as serotonin (5-HT), substance P, vasoactive intestinal peptide (VIP) and somatostatin.(143, 144) Historically, NETs were classified according to their embryological origin: foregut (includes NETs originating in the bronchi, stomach, pancreas, gallbladder and duodenum), midgut (originating in jejunum, ileum, appendix and right side of colon) and hindgut (left side of colon and rectum).(145)

NETs usually arise sporadically, but a small group of patients will have an inheritable condition leading to the development of a NET.(142) They may be associated with familial endocrine cancer syndromes including multiple endocrine neoplasia (MEN)1, MEN2, Von Hippel Lindau (VHL) and neurofibrotosis type 1.(146-148) The incidence of MEN1 varies between different Gastroenteropancreatic (GEP) NETs from nearly 0% in gastrointestinal (GI) NETs, to 5% in insulinomas and up to 25-30% in gastrinomas.(149) Mutations in the succinate-ubiquinone oxidoreductase subunit D (SDHD) gene has been identified in some patients with midgut NETs, which is commonly associated with paraganglionomas and phaeochromocytomas.(150) It is therefore imperative to take a detailed family history and examination to identify

patients who may have an underlying genetic association so genetic screening can then be performed in the patient as well as genetic testing in relatives.

Early discoveries in the biology of NETs involve somatostatin (SST) and this peptide's G-protein-coupled membrane somatostatin receptors (SSTR) subtypes 1-5.(151-153) SST regulates endocrine function with largely inhibitory effects by inhibiting secretion of most GI hormones and growth hormone, reducing motility in the GI tract and gallbladder contraction and a reduced GI tract blood flow.(151, 154, 155) SSTR subtypes 2 and 5 are mainly found in NETs, with SSTR2 being the predominant subtype seen.(156, 157)

There have been some studies looking at the molecular biology of NETs. One study looked at sporadic pancreatic NETs and found the most common mutated genes were MEN-1 (44%), DAXX/ATRX (43%) and genes in the mTOR pathway (14%). A study of small intestine NETs did not find any significant somatic mutations, suggesting this group of NETs are mutationally inactive. However, several recurrent somatic copy number alterations were identified in cancer-related pathways including PI3K/Akt/mTOR signalling, TGF-β (via alteration in the SMAD gene) and the SRC proto-oncogene.(158) Another study involving small intestine NETs identified repeated somatic mutations and deletions in CDKN1B, which is a cyclin-dependent kinase inhibitor gene, encoding p27.(159) A different study performed whole-genome sequencing of pancreatic NETs and found that there was a deficiency in G:C > T:A base excision repair. This was due to inactivation of MUTYH gene which encodes a DNA glycosylase. Sporadic

pancreatic NETs were seen to contain more germline mutations than anticipated in addition to mutations in the DNA repair genes MUTYH, BRCA2 and CHEK2. The combination of these mutations, with the mutations seen in MEN1 and VHL, were seen in 17% of patients. The study found that somatic mutations (including both gene fusions and point mutations) occurred in genes involved in four pathways: DNA damage repair, chromatin remodelling, mTOR signalling activation and telomere maintenance. The group also showed a subgroup of pancreatic NETs associated with hypoxia-inducible factor signalling and hypoxia.(160)

1.12 Epidemiology of neuroendocrine tumours

The incidence of NETs in the UK is rising. Public Health England recorded a total of 8,726 neuroendocrine neoplasms (NENs), of which 3,978 were low grade NETs, between 2013 and 2014 , yielding an overall incidence rate of 8 per 100,000 persons. Approximately 75% of lower GI NENs are NETs compared to upper GI and lung neoplasms (48% and 36% respectively), **Figure 5**. There is an almost equal distribution of disease between males and females and little variation in ethnicity. (161) Public Health England showed that the one-year NET survival for patients with either grade 1 (G1) or grade 2 (G2) disease is better even in the advanced stage groups (at least 80% in the most advanced stage) compared to neuroendocrine carcinomas (NECs) and other subtypes which have a poorer one-year survival with survival determined by the stage of disease (as low as 20%), **Figure 6**.(161) The GI tract and pancreas are the commonest sites of NET origin, with the lung being the next commonest site.

Rarer sites of NET origin include the ovaries, breast, renal tract, head and neck, and skin.(162) The primary site of origin is unknown in around 8.7% of cases.(161)

Early diagnosis of NETs allows possible curative treatment by surgical resection.(163) More than 50% of NETs are unresectable at the time of diagnosis, given the presence of non-specific symptoms and delay in diagnosis when the tumour is then diagnosed at an advanced stage.(164)
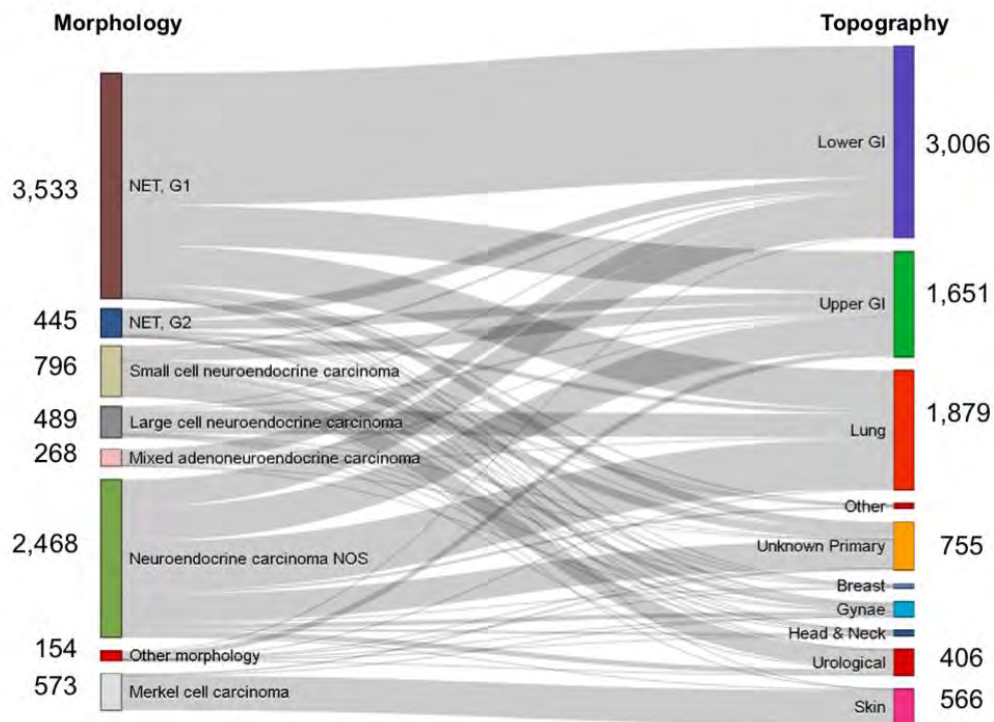
Figure 5: Morphological and topological distribution of neuroendocrine neoplasms diagnosed between 2013 and 2014 in England. (Taken from Public Health England, (161)).
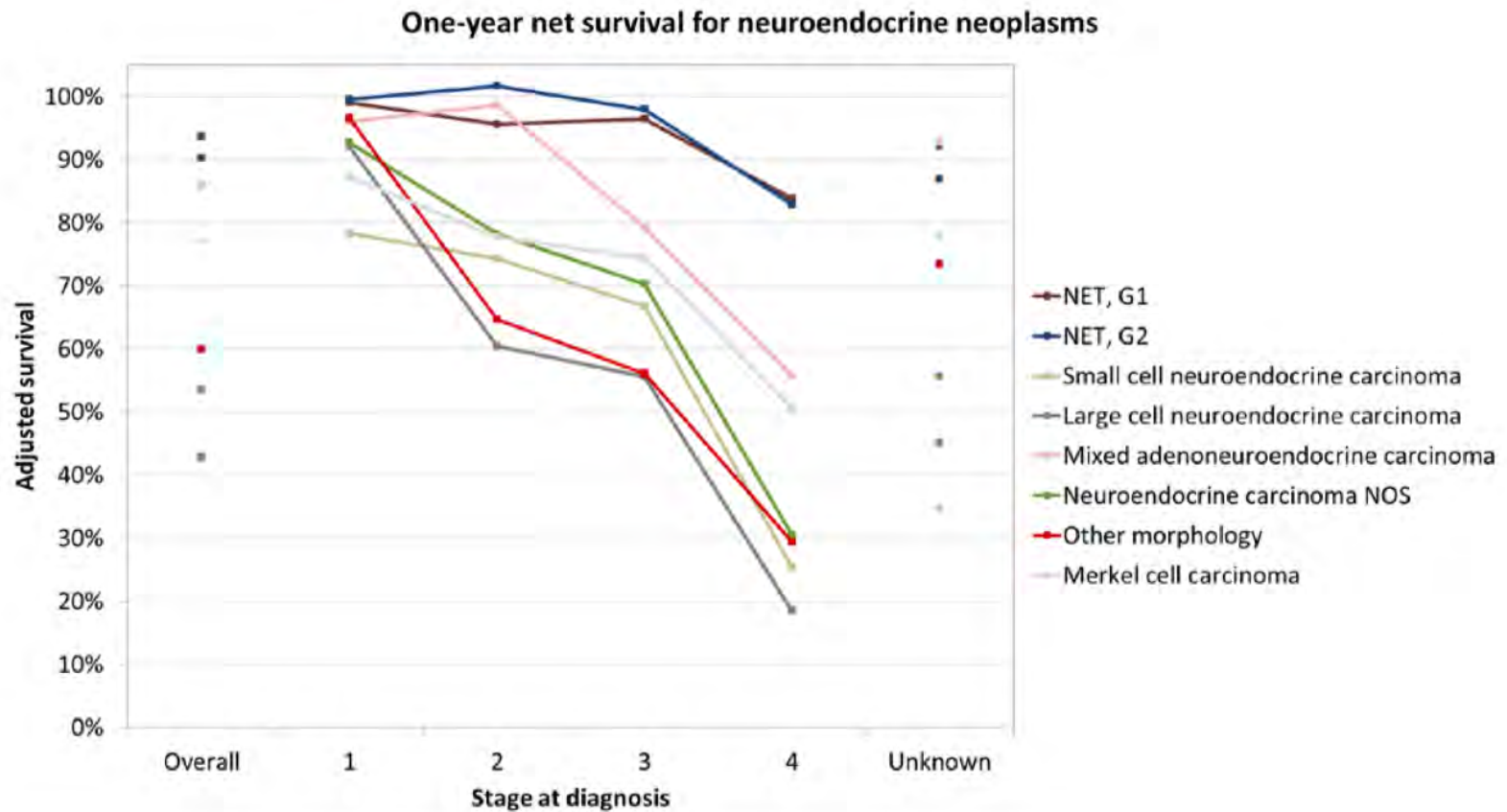
Figure 6: One year net survival for the different neuroendocrine neoplasm groups diagnosed in England between 2013 and 2014. (Taken from Public Health England, (161)).

1.13 Classification of neuroendocrine tumours

In 2007, the European Neuroendocrine Tumour Society (ENETS) introduced the classification of NENs into well-differentiated NETs and poorly-differentiated NECs based on two indexes, with the classification positively correlating with prognosis.(165) Diagnosis of NETs takes into account both characteristic histologic features as well as particular immunoprofiles.(166)

NETs arising in the GI tract follow the World Health Organisation (WHO) 2010 classification and are graded from G1-3, based on their cellular proliferation rate (i.e. Ki-67 index) and the mitotic count.(144, 167) G1 and G2 are well-differentiated NETs and G3 represents the poorly-differentiated NECs. In 2017, a revised WHO classification for pancreatic NENs recognised that the G3 tumours display heterogeneity in their morphology, and includes both well-differentiated G3 NETs and poorly-differentiated G3 NECs.(168) Treatments do differ significantly between the G3 NETs and G3 NECs, and it is therefore important to distinguish between the two subtypes.

Pulmonary NETs have a separate classification terminology to the non-pulmonary NETs. They are classified as typical carcinoid, atypical carcinoid, small-cell lung carcinoma and large-cell neuroendocrine carcinoma.(169) The typical and atypical pulmonary carcinoids are well differentiated NETs and include low and intermediate grade malignant tumours respectively. The small-cell lung carcinoma and large-cell neuroendocrine carcinoma correspond to the poorly-differentiated NECs.(170)

Table 3 summarises the classification system for the pulmonary and GEP

NENs.

Classification	Grade	Differentiation	Pulmonary NENs	Mitotic index	Ki-67 index
WHO 2010					
	Low grade, G1 NET	Well differentiated	Typical carcinoid	<2/10 HPF	≤2%
	Intermediate grade, G2 NET	Well differentiated	Atypical carcinoid	<2-20/10 HPF	3-20%
	High grade, G3 NEC	Poorly differentiated	Small cell lung carcinoma; Large cell neuroendocrine carcinoma	>20/10 HPF	>20%
*WHO 2017					
	Low grade, G1 NET	Well differentiated		<2/10 HPF	≤2%
	Intermediate grade, G2 NET	Well differentiated		<2-20/10 HPF	3-20%
	High grade, G3 NET	Well differentiated		>20/10 HPF	>20%
	High grade, G3 NEC	Poorly differentiated		>20/10 HPF	>20%

Table 3: Classification of pulmonary and gastroenteropancreatic NENs.
*World Health Organisation 2017 classification: Pancreatic NENs. HPF: High
power fields, NENs, neuroendocrine neoplasms. G, grade. NET,
neuroendocrine tumour.

1.14 Clinical features of neuroendocrine tumours

A large proportion of NETs are diagnosed incidentally, for example gastric NETs and rectal NETs diagnosed on endoscopy and GI NETs including appendiceal NETs diagnosed on histology of the resected specimen. Given the increasing number of investigations being performed, in particular the 2 week wait for upper and lower GI endoscopies, the number of referrals to our centre continues to rise.

NETs can be asymptomatic or non-functioning, or functional resulting in hormone secretion (commonly bradykinin and 5-HT) which can cause syndromic symptoms.(171)

NETs are associated with various hypersecretory syndromes through hormones secreted, determined by the cell of origin.(172) The clinical features and functioning syndromes of GEP NETs will be discussed below.

Carcinoid syndrome

Small intestine NETs account for 75-90% of all carcinoid syndrome (CS) cases.(173) All NETs commonly metastasise to the liver. In addition, small bowel NETs usually involve the mesenteric lymph nodes. Classical CS results from direct release of hormones, in particular 5-HT, into the systemic circulation. Hormones released by GI NETs are usually inactivated by liver enzymes thereby preventing their release into the systemic circulation. Therefore, patients with GI NETs usually only develop CS if they have significant liver metastases.(174, 175) Presence of metastases at certain anatomical sites, such as the retroperitoneum,

bone, distant nodal disease, as well as lung and ovary primaries, also allows direct access to the systemic circulation.(176) This can therefore lead to CS in the absence of liver involvement. CS is associated with carcinoid heart disease.(142, 143) It has been reported that CS occurs in around 10-15% of patients with midgut NETs.(177)

Serotonin was initially identified in 1954 and was seen to be associated with flushing, diarrhoea and right-sided heart failure in patients with small intestine NETs and secretion of this hormone was believed to be a possible cause of this syndrome.(178, 179) The typical symptoms of facial flushing, diarrhoea, abdominal pain, weight loss and bronchospasm associated with CS is made clinically indicating increased levels of circulating serotonin.

Treatment with a somatostatin analogue (SSA) injection is the commonest medical therapy in treating carcinoid symptoms and achieving disease control.(180) The first synthetic SSA, Octreotide, was produced in the 1980s.(154) Two long acting synthetic analogues of somatostatin that we use frequently in clinical practice include Sandostatin LAR and Lanreotide Autogel. Studies first looking at the role of SSAs in NETs found a significant reduction in carcinoid symptoms due to reduction in the secretion of serotonin.(181)

Randomised controlled trials then followed assessing the effectiveness of SSAs in these tumours. The PROMID trial showed a significant increase in median progression free-survival (PFS) from 6 months to 14.3 months in patients with metastatic midgut NETs treated with Octreotide LAR compared to placebo and

36% of the group had CS at baseline.(182) The CLARINET trial showed that Lanreotide Autogel significantly prolonged PFS in patients with either G1 or G2 (Ki-67 <10%) metastatic enteropancreatic NETs (not reached versus 18 months in the placebo group). At 24 months, the estimated rate of PFS was 65.1% in the treated group compared to 33% in the placebo group.(183) The PROMID trial was predominately composed of patients with G1 NETs with generally lower hepatic tumour burden compared to the CLARINET trial.(183) Telotristat ethyl, an inhibitor of tryptophan hydroxylase (an enzyme involved in the synthesis on serotonin), has shown promising results in the management of patients with CS refractory to SSAs, showing significant reduction in daily bowel movements.(184)

Other treatments offered include peptide receptor radionuclide therapy (PRRT) and Everolimus. PRRT uses radiolabelled somatostatin analogues that binds to the SSTR on the tumour cell membrane resulting in internalisation of the radiopeptide/SSTR complex and delivery of the radioactivity straight into the intracellular area of the tumour cell.(185, 186) Everolimus is an oral mTOR inhibitor.(187) The mTOR pathway is a key regulator of cellular proliferation, growth, protein synthesis, autophagy and metabolism. Everolimus therefore blocks the activity of the mTOR pathway.(188, 189) The NETTER-1 trial revealed an improved PFS in patients with metastatic midgut NETs. 65.2% of patients treated with PRRT (^{177}Lu-Dotatate) plus normal dose Sandostatin LAR were without disease progression compared to 10.8% in the control group where doubled dose Sandostatin LAR was given.(186) The RADIANT-2 trial showed that Everolimus plus octreotide LAR improved PFS compared to placebo plus

octreotide LAR in patients with advanced NETs associated with CS (16.4 months versus 11.3 months respectively).(187) The RADIANT-4 trial recruited patients with advanced, non-functioning NETs of lung or GI origin and showed that the median PFS was 11 months in the Everolimus treated group versus 3.9 months in the placebo group. Everolimus was associated with a 52% reduction in the estimated risk of progression or death.(188)

Gastric and duodenal NETs

There are three types of gastric NETs: types 1,2 and 3. Type 1 is the commonest, representing 70-80% of all gastric NETs and is associated with atrophic gastritis and chronic hypergastrinaemia. Type 2 occurs due to raised gastrin from a gastrinoma and is associated with Zollinger-Ellison Syndrome (ZES) and MEN1. Type 1 is usually asymptomatic, and both type 1 and 2 are commonly diagnosed early following symptoms of reflux, diarrhoea and abdominal discomfort. Type 3 does not present with symptoms until metastases have occurred. Metastases are present in 50-100%, 10-30% and 2-5% of type 3, 2 and 1 respectively.(190, 191) Duodenal NETs are mostly sporadic but may also be associated with MEN1. They are usually non-functioning but are a frequent cause of ZES.(192)

Pancreatic NETs

NETs arising in the pancreas secrete various hormones. **Table 4** summarises the hormones and clinical features associated with the different types of functioning pancreatic NETs.

Type of pancreatic NET	Hormone secreted	Clinical features
Insulinoma	Insulin	Hypoglycaemic symptoms: • Confusion • LOC • Sweating • Dizziness • Improvement with eating
Gastrinoma	Gastrin	Severe peptic ulcer disease: ZES Diarrhoea
Glucagonoma	Glucagon	Diabetes mellitus Typical skin lesion: necrolytic migratory erythema Weight loss Glossitis
Vasoactive intestinal peptide-secreting tumour (VIPoma)	Vasoactive intestinal peptide	Verner-Morrison syndrome: Severe diarrhoea, hypokalaemia and metabolic acidosis
Somatostatinoma	Somatostatin	Cholelithiasis Diabetes mellitus Diarrhoea Steatorrhoea

Table 4: Types of functioning pancreatic NETs with hormones secreted and associated clinical features. (Adapted from Ramage JK et al and Zandee WT et al, (142, 171)). LOC, loss of consciousness. ZES, Zollinger-Ellison syndrome.

Despite the relatively slow progression of NETs, they can cause significant GI and cardiac pathology related to fibrosis due to desmoplastic reactions. Intestinal fibrosis can lead to strictures that can cause further complications including chronic abdominal pain, small bowel bacterial overgrowth and bowel obstruction. Carcinoid heart disease (CHD) is characterised by fibrous thickening of the endocardial surface and cardiac valvulopathy, that can result in heart failure.(175, 193-195) GI complications can occur due to the tumour itself or secondary to treatments given for NETs including SSAs and as a consequence of surgery.(195)

These complications can be very troublesome for patients, and are associated with a significant morbidity and mortality, therefore impairing the patient's quality of life. At present, there are no effective therapies to prevent these complications, and patients often require major surgery and intense input from the dieticians and nutrition team including the requirement for parenteral nutrition. It is still poorly understood why some patients develop severe fibrotic complications and what factors drives this process. Therefore, by gaining a better understanding in the molecules involved in the fibrosis associated with NETs, therapies to target these molecules can be identified with the aim of curing or preventing these complications.

1.15   Fibrosis in neuroendocrine tumours

Local desmoplasia or distal fibrotic reactions can be associated with NETs. The commonly encountered fibrotic reactions that can occur are mesenteric fibrosis in small bowel NETs and CHD. Mesenteric fibrosis can occur in up to 50% of cases and is usually diagnosed radiologically. Complications that can be associated with mesenteric fibrosis include the development of intestinal ischaemia (in around 10% of cases) and bowel obstruction. Mesenteric vasculature involvement can lead to the onset of ascites, and extensive infiltration can make surgical resection very challenging or not possible. The presence of mesenteric fibrosis is associated with significant morbidity and mortality.(196-198)

CHD occurs due to fibrosis of the cardiac valves, and usually affects the right-sided heart valves. This fibrotic complication can progress to the development of

heart failure and is a major cause of mortality and morbidity in NETs.(196, 199)

CHD is discussed in more detail later on in this chapter.

1.16 Diagnosis of neuroendocrine tumours

NETs are usually diagnosed incidentally on imaging or endoscopies performed, or on histology. The histological diagnosis and classification of NETs has been discussed above. Various transcription factors on histological staining may help point towards a primary site of origin when patients present with metastatic disease, although individual factors are not 100% sensitive or specific.(200) For example, thyroid transcription factor-1 is a good marker to indicate a pulmonary site of origin, and CDX2 indicates a small bowel primary site. Pancreatic NETs may be positive for Isl1 and PAX8, but these two stains may also label rectal NETs.(201)

Certain biochemical markers and/or radiological features can all aid in making the diagnosis of a NET alongside a detailed history.

Biochemical assessment

Current biomarkers used in NETs are primarily for monitoring the progress of cancer, response to treatment and help determine the overall prognosis. However, at present there are no markers used in clinical practice to identify the onset of fibrosis occurring in NETs. Common biomarkers used currently in NETs include chromogranin A (CgA), chromogranin B (CgB), 24 hour urinary 5-hydroxyindoleacetic acid (5-HIAA), N-terminal pro b-type natriuretic peptide (NT-proBNP) and pancreatic polypeptide (PP).

Biochemical assessments commonly used in clinical practice to help in diagnosing MEN1 include measuring the calcium level, parathyroid hormone and prolactin level in addition to taking a thorough family history.

CgA is a secretory protein found in the neuroendocrine secretory granules and is the sole pan marker for all types of NETs, with high levels correlating with tumour bulk.(142, 202, 203) CgA can be secreted in both functioning and non-functioning NETs.(204) One study of a mixed cohort of 128 patients showed that elevated levels of CgA were seen in 30% and 67% of patients with limited or metastatic disease respectively.(205) The level of CgA can be raised in other conditions such as renal impairment and protein pump inhibitor (PPI) use, yielding a sensitivity of 60-90% with a specificity of less than 50%.(206) Markedly raised CgA levels are very rarely seen in non-NET cases, but this may be seen in patients on gastric acid secretory blockers, in particular PPIs, or in the presence of hypergastrinaemia.(207) CgB is also a member of the granin family and may be elevated even when CgA is within normal range.(142, 208) The endocrine pancreas usually secretes PP, and is also found in high concentrations in GEP NETs: 50-80% of pancreatic NETs and >30% of GI NETs. This can therefore be a useful marker in certain cases, particularly when CgA and CgB are within their reference ranges.(142)

5-HIAA is a breakdown product of serotonin which can be measured in a 24 hour collection of urine. This has been the most useful marker in NET diagnosis and follow-up of patients with CS.(209) In the setting of CS, the overall sensitivity and specificity of the 24 hour urinary 5-HIAA is 70% and 90% respectively.(210, 211)

Midgut NETs are most likely to be associated with the presence of CS and an elevated 5-HIAA, thereby resulting in the high specificity of this marker. Foregut and hindgut NETs secrete less serotonin than midgut NETs.(210) In patients with midgut NETs without CS, the sensitivity of the 24 hour urinary 5-HIAA is lower. Levels of this test may also be dependent on tumour load, and therefore may be normal in patients with non-metastatic disease. Urinary 5-HIAA may even be normal in those with CS, particularly in patients who do not have diarrhoea, although this is unusual.(209, 212) The 24 hour urinary collection to measure 5-HIAA does however require a strict adherence to specific dietary restrictions.(142, 202) Some medications may also result in both increased 5-HIAA levels (such as acetaminophen and diazepam) as well as false negative results (including aspirin and levodopa).(213) Some centres are validating the role of plasma 5-HIAA measurement which may take over the 24 hour urinary 5-HIAA in the near future, and a study has shown that plasma 5-HIAA is proportional to urinary 5-HIAA and yielded identical correlation as urinary 5-HIAA with other biomarkers.(214)

NT-proBNP is a useful marker to suggest the presence of left ventricular dysfunction.(215) NT-proBNP is used to screen for CHD, and has been shown to have both diagnostic and prognostic significance.(216) However, other factors including renal, pulmonary and central nervous system diseases, may also influence the NT-proBNP level.(217) Elevated levels of NT-proBNP prompt an echocardiogram to be performed and referral to cardiology if necessary. A study has shown that NT-proBNP is an excellent biomarker for CHD with a sensitivity of 0.92 and specificity of 0.91 with a cut-off level of 260 pg/mL. Additionally, to

diagnose one case of CHD, the number of patients screened reduced from 5.1 to 1.4.(218)

Radiological assessment

The radiological assessment of NETs can be categorised as 'anatomic imaging' and 'functional imaging'. Anatomic imaging modalities, including CT, US and MRI, provide important information on the staging and extent of disease. Functional imaging, including somatostatin receptor scintigraphy (SRS), positron emission tomography (PET)/CT imaging, and tracers that mark NET metabolism, give information related to the biological behaviour of the tumour in addition to medical treatments that can be appropriately initiated.(142, 219). Usually, a number of imaging modalities are required to reliably detect and diagnose lesions, in particular the smaller lesions, adequately stage the disease and finally to assess treatment response.

Anatomic imaging

The main anatomic imaging used in NETs, including the surveillance scans, is CT. On biphasic and triphasic contrast enhanced CT imaging (CECT), avid early enhancement of lesions, especially with pancreatic NETs, can be seen. An isodense lesion with calcification on unenhanced scans can be seen in approximately 20% of pancreatic NETs, which is different to pancreatic adenocarcinomas that display no calcification.(219) CECT is the gold standard in detecting pulmonary NETs, although more than 40% of this group can be identified on chest x-ray alone. Pulmonary NETs are highly vascular tumours and

show enhancement following intravenous contrast enhancement.(170) Small bowel NETs are frequently associated with mesenteric nodules and fibrosis resulting from desmoplastic reactions leading to stranding, tethering and fat changes on CT. Signs of bowel ischaemia can also be seen radiologically, occurring as a result of venous congestion due to encasement by nodal metastases. The presence of liver metastases can be seen on the hepatic arterial phase of a CT scan, although MRI imaging is superior to CT for identifying liver metastases as well as assessing response to liver-targeted treatment.(219) MRI has a high sensitivity (94%) in diagnosing pancreatic lesions, but there is a lower sensitivity in extra-pancreatic lesions.(220, 221) The benefit of MRI imaging over CT imaging, in particular with the surveillance scans, is the reduced risk of ionising radiation exposure.

Functional imaging

As explained earlier, NETs highly express SSTRs, in particular the SSTR2 and SSTR5 subtypes. An improvement in the sensitivity and specificity of SSTRs is seen with the use of anatomic imaging: single-photon emission computed tomography (SPECT) or with SPECT-CT imaging. The abundance of SSTRs on the cell surface of NET cells make them an ideal target for both imaging as well as treatment.(222)

There are two main types of SRS imaging used in NETs. The first one is octreotide imaging which uses the SSTR specific ligand ^{111}In-DPTA-D-Phe-1-octreotide that binds primarily to SSTR subtypes 2 and 5.(223) The octreotide scan image is

combined with the SPECT/CT images and therefore improves the anatomic localisation and overall diagnostic accuracy of this imaging modality.(224-226) This improvement in combining the anatomic imaging to the planar images acquired by octreotide imaging has been shown to alter the management in 14% of patients.(227) The sensitivity of octreotide imaging is limited by tumour size.(228) Octreotide scans are useful at detecting liver metastases and extrahepatic sites of metastases and are better at detecting liver metastases compared to primary tumour detection.(229, 230) Given that octreotide scan is a type of functional imaging and requires the presence of SSTR expression to be positive, it can identify lesions that have been missed on anatomic imaging such as CT or MRI scans performed alone.(225) One study showed that octreotide scanning detected new lesions in 28% of patients.(229) Studies concentrating on the identification of NET metastases have shown that octreotide imaging picked up new lesions in 50% of patients that were missed by CT. However, MRI was found to be superior to octreotide scans in detecting hepatic metastases.(228, 231) The octreotide images are usually obtained 24 hours following ligand administration, but may also be acquired at 4 hour and 48 hours post ligand injection.(232)

The more recent and improved diagnostic accuracy of SSR imaging is the application of DOTA PET/CT which uses the positron-emitting radionuclide gallium-68 (^{68}Ga) to label various somatostatin analogues, including ^{68}Ga-DOTATOC (DOTA Octreotide), ^{68}Ga-DOTANOC (DOTA-Nal-Octreotide) and ^{68}Ga-DOTATATE (DOTA Octreotate). All of these ligands bind with high affinity

to SSTR2 and SSTR5, and ^{68}Ga-DOTANOC also binds to SSTR3.(142) One study showed the sensitivity and specificity of ^{68}Ga-DOTATOC to be 96% and 92% respectively for the identification of unknown primary, initial disease staging and follow up post-treatment and was superior to SRS SPECT or CT imaging. Bone metastases and other sites of metastatic disease were also detected by ^{68}Ga-DOTATOC.(233) The improved anatomic resolution of this modality is achieved by the combination of PET and CT imaging.(234, 235) ^{68}Ga-DOTANOC PET/CT imaging has been stated to change either tumour staging or management in 55.5% of cases assessed.(236) ^{68}Ga-DOTATATE has been found to be superior with a higher sensitivity and specificity compared to ^{111}In-octreotide scintigraphy.(219) DOTA PET/CT images are obtained just once, 60 minutes following radiotracer administration.(235) The major disadvantage of ^{68}Ga-peptide PET/CT imaging is the limited availability in the UK.

Radioiodinated metaiodobenzylguanidine (^{123}I-MIBG) has a norepinephrine analogue and is used to image catecholamine-secreting tumours such as phaeochromocytomas and paragangliomas.(237) ^{123}I-MIBG as a high sensitivity of 90% with a positive predictive value of 100% in those with functional phaeochromocytomas or paragangliomas.(238, 239) However, there is limited uptake of ^{123}I-MIBG in GEP NETs, with a positive scan being seen in 49.1% of GI NETs versus 91.2% seen with octreotide scan use.(240) PRRT has largely replaced ^{123}I-MIBG, and ^{123}I-MIBG is mainly used in locating the catecholamine-secreting NETs.

18-fluoro-deoxy-glucose (^{18}FDG) PET/CT imaging use in NETs is limited given that the vast majority of NETs are metabolically inactive and do not take up the tracer much, particularly in GEP NETs.(241) High grade NETs are more likely to show ^{18}FDG uptake and therefore a positive scan can indicate a more aggressive tumour.(242) This scan is used in pulmonary NETs as part of a standard workup following detection of a bronchial lesion. In well-differentiated bronchial NETs, however, it is usually negative, but if positive again can suggest a poorer prognosis with a less favourable phenotype.(162)

1.17 Carcinoid heart disease

Management of patients with metastatic NETs has developed over recent years, with an improvement in quality of life and survival seen.(213, 243) However, CHD does remain the major cause of morbidity and mortality in patients with CS. Previously, CHD was seen to be present in 50% of patients with CS, but recent studies now report that CHD can affect around 20% of patients with carcinoid syndrome.(244-247) This fall in CHD prevalence could be a result of the wider use of SSA therapy in patients.(243) Progressive heart failure secondary to cardiac valvulopathy is the usual cause of death in patients with CHD.(248) The tricuspid and pulmonary valves are commonly involved.(213) In >50% of patients, progression of valve disease and clinical deterioration can occur rapidly.(249) The survival rate for patients with CHD seen in a three year mortality data was 31%, whereas patients with NETs without cardiac involvement have around twice this survival rate.(245) CHD is diagnosed approximately 17 months following the diagnosis of CS.(250) An improvement in

the prognosis of CHD has been seen more recently likely owing to advances in cardiac investigations, and medical and surgical management.(251) A retrospective analysis of 200 patients showed that in patients with CS and CHD the median survival has greatly improved from 1.5 years in the 1980s to 4.4 years in the late 1990s, as a result of increased valve replacement procedures.(250)

The exact pathogenesis in CHD is not fully understood and involves a complex process. Before covering the pathophysiology, I will outline the main anatomical components of cardiac valves.

1.18 Valve interstitial cells

Valve interstitial cells (VICs) are the most abundant cells found in the heart valve that maintain the valve's structural integrity, and are found dispersed throughout the three valve layers: the fibrosa, spongiosa and ventricular/atrial layers. In both normal and diseased states, VICs play an important role.(252, 253) The three layers have different compositions: the fibrosa layer is rich in collagen, the spongiosa layer is rich in proteoglycans and the ventricular/atrial layer is dense in elastin.(254) The valve structure is covered by valve endothelial cells, **Figure 7**.(255) Studies have shown that an accumulation of VICs associated with inflammatory cells, neovascularisation, increased matrix production and eventually fibrosis and calcification, occurs in response to valvular injury.(253) In diseased valves, VICs become activated to regulate repair and valve remodelling.(256)
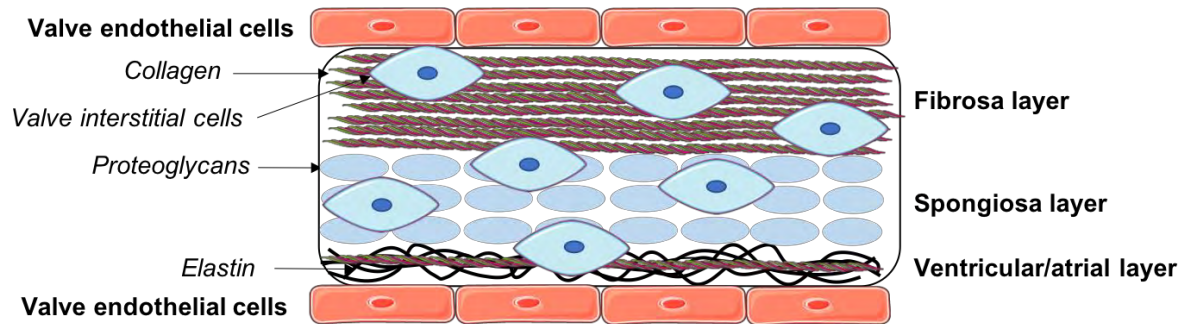
Figure 7: Schematic diagram illustrating the valve layers. Some components of this diagram were obtained from Servier (118).

There are five different phenotypes in the VIC group: embryonic progenitor endothelial / mesenchymal cells, quiescent VICs (qVICs), activated VICs (aVICs), progenitor VICs (pVICs) and osteoblastic VICs (obVICs).(253)

The embryonic progenitor endothelial / mesenchymal cells undergo endothelial to mesenchymal transformation (EMT). Individual endothelial cells then migrate into the endocardial cushion resulting in the transformation of endothelial cells into mesenchymal cells, and matrix remodelling occurs in the cushion to develop into mature heart valves.(253, 257, 258) It is thought that the EMT process also occurs after post-natal development in adult valves following injury and valve disease. The endothelial cells on the cushion surface contain properties of the valve progenitor cells and may result in VICs formation which then participate in valve repair.(259)

The qVICs are located in the heart valve leaflet, and maintain the valve structure and function, and generally keep the valve avascular by inhibiting angiogenesis.

In response to valve injury, qVICs become activated and also give rise to aVICs to enable valve repair and remodelling to take place.(253)

The pVICs are valvular stem cells derived from various origins, and are found in the bone marrow, circulation, and heart valve leaflet. They consist of two cell types: endothelial progenitor cell (EPC) and dendritic cell (DC).(253) EPC is identified by the stem cell markers CD133 and CD34, are highly proliferative and are able to form new blood vessels.(253, 260) DC is identified by the intracellular calcium binding protein, S100.(253) In response to injury, pVICs including the circulating cells, bone marrow derived cells and the resident valvular progenitor cells are another source of aVICs.(253)

The aVICs responding to valve injury and disease take on characteristics of myofibroblasts but are not smooth muscles as they have incomplete basement membranes.(253, 261) These cells are located in the heart valve leaflet. The aVICs are positive for alpha-smooth muscle actin (α-SMA) and lead to increased ECM production and degradation, MMP expression and tissue inhibitors of MMP expression, as well as increased proliferation and migration. These are all important factors in the repair process. These VICs also increase the secretion of cytokines, particularly TGF-β.(253) The majority of aVICs are then discarded by apoptosis after remodelling has occurred.(262) When this process is dysregulated, aVICs survive resulting in abnormal extracellular matrix production and remodelling, pathological fibrosis, angiogenesis and neovascularisation and calcification, eventually leading to valve disease.(253, 262)

The obVICs are also located in the heart valve leaflet too and may be derived from pVICs. They actively participate in the calcification process, and also cause chondrogenesis and osteogenesis in the heart valve.(253)

1.19 Pathophysiology of CHD

NETs secrete a range of vasoactive substances, including 5-HT, prostaglandins, bradykinin, histamine, and substances containing fibroblast proliferative properties (such as substance P) or TGF-β, that are thought to be involved in the pathogenesis.(176) 5-HT receptors play a major role in the development of CHD which are present in the heart, with subtype 5-HT$_{2B}$ receptor found most on the valves.(263) Activation of these receptors results in mitogenesis of fibroblasts and smooth muscles cells, cytokine recruitment, and up-regulation of TGF-β. Another factor involved in the pathogenesis of this disease is deficiency of the 5-HT transporter which is involved in uptake of 5-HT and inactivation in the lungs.(213, 264) This complex process results in the deposition of endocardial plaques, plaques in the chordae, papillary muscles and heart chambers, and occasionally within vasculature intima, including the pulmonary arteries and aorta.(176) These plaque deposits are comprised of myofibroblasts, smooth muscle cells, extracellular matrix components including collagen, elastin and myxoid matrix, and an endocardial cell layer.(176, 213, 265) These plaques classically involve the right side of the heart (around 90% of cases), likely due to pulmonary inactivation of the vasoactive substances, resulting in right heart failure.(245) In left valvular pathology, occurring in 5-10% of cases, a bronchial

NET, extensive liver metastases or a patent foramen ovale should be suspected.(245, 266)

Screening biomarkers currently used

Currently in clinical practice, the most useful marker that is measured is NT-proBNP, which has been shown to have both diagnostic and prognostic influences in CHD.(216) CgA and urinary 5-HIAA are also used in clinical assessment.

Bhattacharyya et al showed that NT-proBNP was significantly higher in patients with CHD (median 1,149 pg/mL) compared to those without CHD (median 101 pg/mL). A cut-off NT-proBNP level of 260 pg/mL is used as a screening tool in CHD, and this showed a sensitivity of 92% and specificity of 91%.(218) The paired combination of NT-proBNP with CgA has been studied by Korse et al, and levels were independently associated with the presence of CHD and mortality. Five-year survival was shown to be 81% in patients with a normal CgA, 44% in patients with a raised CgA but normal urinary 5-HIAA, and 16% when both markers were elevated.(216)

CgA has been shown to be a sensitive marker in CHD, with a sensitivity of around 100% but a low specificity of 30% to predict severe CHD. CgA is therefore not used as a screening marker in CHD.(213)

Both plasma and urinary 5-HIAA levels have been seen to be significantly higher in patients with CHD compared to those without this complication.(267, 268) A retrospective study showed that a higher peak level of 5-HIAA significantly predicted progressive CHD and was also raised in patients who had severe symptoms requiring valve surgery.(269) Bhattacharyya et al showed that 24 hour urinary 5-HIAA $\geq$300 μmol/24 hours and $\geq$3 episodes of facial flushing a day are predictors for the development or progression of CHD.(270)

Valve surgery is the only definitive treatment for these patients with severe right-sided heart failure, if the patient is a suitable candidate. It has been noted that operating at an early stage or at a time close to the onset of symptoms is preferable, to reduce the risk of worsening right heart failure and reduce the risk of surgery.(245) However, some patients may be asymptomatic and therefore a delay in diagnosis can occur when treatment options are then limited. The benefit of diagnosing fibrosis at an early stage by use of sensitive and specific markers can be seen in this group of patients, so cardiac surgery can be offered early to reduce the risk of worsening right ventricular failure occurring, and therefore improve symptoms and overall survival.

1.20 Vascular adhesion protein-1

VAP-1 is a 170-kilodalton (kDa) homodimeric transmembrane sialoglycoprotein.(271) It has a short (4 amino acid) N-terminal cytoplasmic tail, a single transmembrane segment and a large extracellular domain.(272) VAP-1 is heavily glycosylated and the adhesive function of VAP-1 is dependent on the

terminal sialic acid groups of the glycans.(273) A VAP-1 monomer consists of potentially 6 N-linked glycosylation sites and 3 O-linked glycosylation sites, **Figure 8**. VAP-1 consists of two monomers and each monomer contains one copper atom.(274)
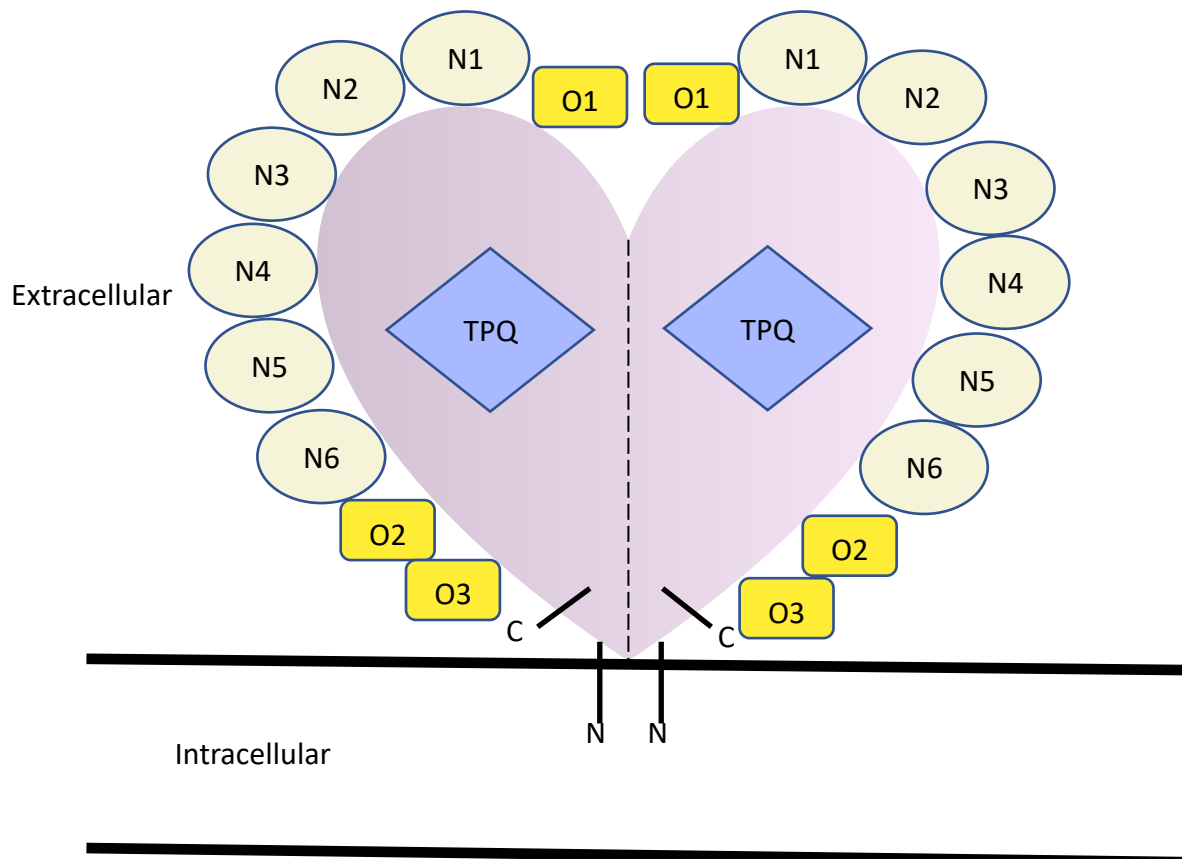
Figure 8: Structure of vascular adhesion protein-1. The positions of the potential glycosylation sites are for illustration purposes only. N1-6, N-linked glycosylation sites. O1-3, O-linked glycosylation sites. C, C-terminus. N, N-terminus. The dotted line represents the outline of the two monomers.

VAP-1 has two main functions: firstly, it is an endothelial cell adhesion molecule that regulates lymphocyte binding to the endothelium under certain conditions.(275, 276) Secondly, VAP-1 is a copper-dependent semicarbazide-sensitive amine oxidase (SSAO) known as amine oxidase copper-containing 3.(277) The enzymatic activity of VAP-1 catalyses the oxidative de-amination of

both endogenous and exogenous primary amines leading to the production of ammonia, aldehyde and hydrogen peroxide (H_2O_2).(277) These resulting products then activate nuclear factor kappa light chain enhancer of activated B cells (NFκB) pathway leading to chemokine secretion and upregulation of leucocyte adhesion.(278, 279) The active site of SSAOs contains an important topoquinone (TPQ) co-factor, modified from a tyrosine residue in a copper dependent reaction. Following reduction of the primary amine, the formation of a transient Schiff base occurs via the TPQ with the generation of aldehyde. The reduced TPQ is then hydrolysed with oxygen leading to the release of H_2O_2 and ammonia.(280) This reaction plays an essential role in the rolling and transmigration steps during leucocyte extravasation.(281, 282) The exact lymphocyte ligand is currently unknown. It has been proposed that Siglec 9 and 10 may be the lymphocyte ligands for VAP-1, with Siglec 10 serving as a direct substrate to VAP-1 and therefore is dependent on the enzymatic function of VAP-1. Siglec 9, however, binds additionally to another site present in the enzymatic groove.(283, 284) Maula et al showed that the 6 N-linked glycosylation sites located on the extracellular 'cap' of VAP-1 contributes to the adhesive and enzymatic functions of this molecule.(285) VAP-1 has also been found to be expressed highly on endothelial cells, adipocytes, smooth muscle cells, pericytes, follicular DCs and hepatic stromal cells.(277, 280, 286) VAP-1 is expressed on hepatic endothelium both in normal conditions and in an inflammatory environment.(277, 278, 287) VAP-1 has also been shown to play a vital role in promoting the onset of liver fibrosis in models of chronic liver injury.(277, 288) Weston et al showed several mechanisms by which VAP-1

promotes fibrosis in liver disease. Firstly, they showed that VAP-1 is expressed by stromal cells and drives amine-oxidase-dependent leucocyte migration. VAP-1 was shown to link inflammation and fibrosis following liver injury and response to exposure of carbon tetrachloride (CCl_4). In the absence of VAP-1 or having an antibody to VAP-1, there was evidence of reduced fibrosis and a fast recovery following liver insult to CCl_4. There was a substantial reduction in the absolute numbers of both lymphoid and myeloid cells recruitment when VAP-1 was absent in the mice models. The group also showed that rendering the catalytic site of VAP-1 inactive and using an antibody to VAP-1 led to a reduction in lymphocyte transmigration and expression of fibrotic genes. VAP-1 was also found to regulate the transcription of profibrotic factors, including collagen I and lysyl oxidase-like protein 2 (an amine oxidase that has been shown to be associated with fibrosis development) and increased expression of platelet-derived growth factor receptor beta which is characteristic of activated hepatic stellate cells, therefore promoting the fibrotic response in CLD.(277)

VAP-1 also exists in a soluble form (sVAP-1) and represents nearly all of the circulating amine oxidase activity in humans.(276, 289, 290) Levels of sVAP-1 have been found to be significantly raised in chronic liver inflammatory conditions, but not in rheumatoid arthritis nor in inflammatory bowel disease.(276, 277, 288) A recent study conducted by our Birmingham group involving a cohort of patients with primary sclerosing cholangitis (PSC) has shown that elevated sVAP-1 levels are associated with a poorer transplant-free survival and an increased risk of liver-related death.(291) VAP-1 is released

from adipose tissue and from the hepatic vasculature and levels of VAP-1 measured in the portal and hepatic veins imply that the liver is a major source of sVAP-1.(277) The exact mechanism for the release of VAP-1 by adipocytes is currently unknown, but it has been shown that VAP-1 release induced by TNF-alpha may be dependent on MMP activity, and inhibiting MMP resulted in a large reduction of VAP-1 release.(289) In patients with non-insulin and insulin-dependent diabetes, obesity, congestive heart failure and atherosclerosis, raised sVAP-1 levels have also been found.(292-295)

Hsia et al showed the association of VAP-1 with myofibroblast expression in cancerous tissue.(296) Our Birmingham group have shown that levels of sVAP-1 are reduced in colorectal cancer patients. The molecular basis for the reduced detection of sVAP-1 levels in colorectal cancer is not yet known, but the cancer may activate a mechanism that prevents the recruitment of anti-tumour immune cells and the cancer may also have systemic effects in reducing expression of VAP-1.(297)

1.21 Preliminary data of vascular adhesion protein-1 in neuroendocrine tumours

Preliminary data (unpublished data) from our laboratory suggested that VAP-1 may also contribute to the fibrotic complications in patients with NETs with our data showing increased expression of VAP-1 and fibroblast associated proteins in NETs. The data has also shown high VAP-1 expression in carcinoid heart disease valves compared to valves with no evidence of carcinoid heart disease. Significantly elevated sVAP-1 levels have been found in patients with NETs (median 562.5, interquartile range (IQR) 438.8 – 697.3 ng/mL; mean 586.0 ± standard deviation (SD)166.2ng/mL) compared to the control group (median 256.0, IQR 212.0 – 308.0 ng/mL; mean ±SD 265.0±79.3 ng/mL), ($p < 0.0001$), and even higher sVAP-1 levels in in those with CHD (median 691.0, IQR 684 – 854 ng/mL; mean ±SD 744.4±136.6 ng/mL) compared to patients with NETs and no CHD (median 511, IQR 411.3 – 583.8 ng/mL; mean ±SD 514.7±128.6 ng/mL) ($p < 0.01$). However, the numbers included in this preliminary data were small, both for the serum and the staining analysis, and therefore no conclusions could be firmly drawn. The preliminary data was very interesting and therefore further work was undertaken to explore the role of VAP-1 in NETs.

We therefore believe that VAP-1 may be a therapeutic target for fibrosis in NET patients. This will be the first study assessing the role of VAP-1 in NETs and also in CHD. Understanding the role of VAP-1 in driving tissue fibrosis in NETs could allow patient stratification for therapy, potentially lead to novel therapies

which reduce morbidity and mortality in patients with NETs, and significantly improve their quality of life.

1.22 Hypotheses of my research studies presented in this thesis

The need for accurate biomarkers to diagnose cancer can be appreciated. This will improve the overall median survival of HCC patients by the ability to offer curative treatments at an appropriate stage when there is early stage disease and patients are physically fit enough to undergo treatment. At present there are no such biomarkers that clinicians in the UK can use in their clinical practice. Particularly in Asia, PIVKA-II has been shown to be a promising marker to aid in the diagnosis of early HCC in at-risk groups, and is incorporated into the Japanese HCC surveillance guidelines for high-risk patients. With patient cohorts differing between the UK and Asia, assessment of PIVKA-II is required to see if this marker can be utilised worldwide.

My hypothesis for the role of PIVKA-II in early HCC includes:

a) PIVKA-II is a potential biomarker in the diagnosis of early HCC. The combination of PIVKA-II and AFP markers will yield a greater predictive accuracy in diagnosing early HCC. As PIVKA-II is thought to be expressed by hepatocytes, I hypothesise that serum levels of PIVKA-II will be normal in non-HCC cancers.

b) PIVKA-II serum levels correspond to disease activity following ablation treatment and can therefore be used as a post treatment surveillance marker. Therefore, I hypothesise that following treatment and imaging

showing no evidence of cancer, PIVKA-II levels will fall, and levels will rise with disease recurrence.

c) Pre-transplant PIVKA-II serum levels can be utilised for the prediction of poor prognostic outcomes, with higher levels being associated with the presence of MVI and moderately / poorly differentiated HCC.

Serious complications associated with certain cancers can manifest at various stages of disease and can present at an advanced stage when treatment options are limited. NETs are associated with desmoplasia, with cardiac involvement and CHD being the most serious complication related to this disease. The current marker used in practice to help in the diagnosis of CHD is NT-proBNP. However, this marker may be within normal values despite the presence of CHD and therefore levels do not always correlate with disease status and so a delay in diagnosis can result. For valve surgery to be considered in patients with CHD, this complication needs to be diagnosed at an early stage, so there can be close monitoring under a specialist and a timely referral for surgery. Additionally, a proportion of patients are not fit enough for valve surgery, and there are no other treatments that can be offered to treat this disease. Therefore, the evaluation of VAP-1 in NETs could be a significant finding, with this marker being used in both diagnosis as well as a target for future treatment.

My hypothesis for assessing the value of VAP-1 in NETs includes:

a) Serum VAP-1 levels will be increased in patients with NETs compared to healthy controls, with levels highest in fibrotic complications associated

with NETs (i.e. CHD) compared to the absence of these complications in NETs. Serum VAP-1 levels will fall following treatment.

b) VAP-1 tissue expression will be increased in tissue from midgut NETs and in CHD valves.

Figure 9 shows summary flow charts of the patient groups recruited into each study.

Figure 9a

Total number of patients
N=99

Healthy controls	Pancreatic NET	Midgut NET	CHD
N=12	N=20	N=50	N=17
Median sVAP-1: 740.4 ng/mL	Median sVAP-1: 979.4 ng/mL	Median sVAP-1: 1005 ng/mL	Median sVAP-1: 1280 ng/mL
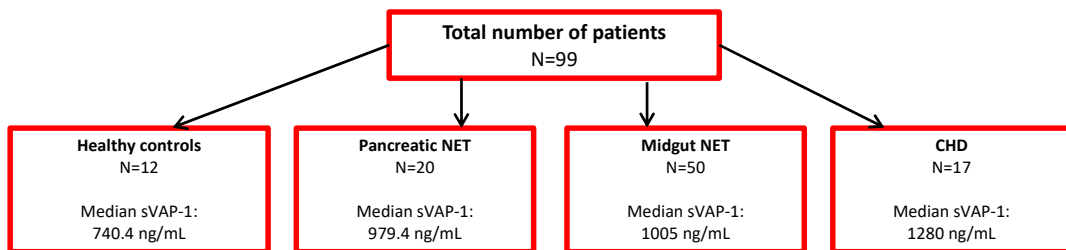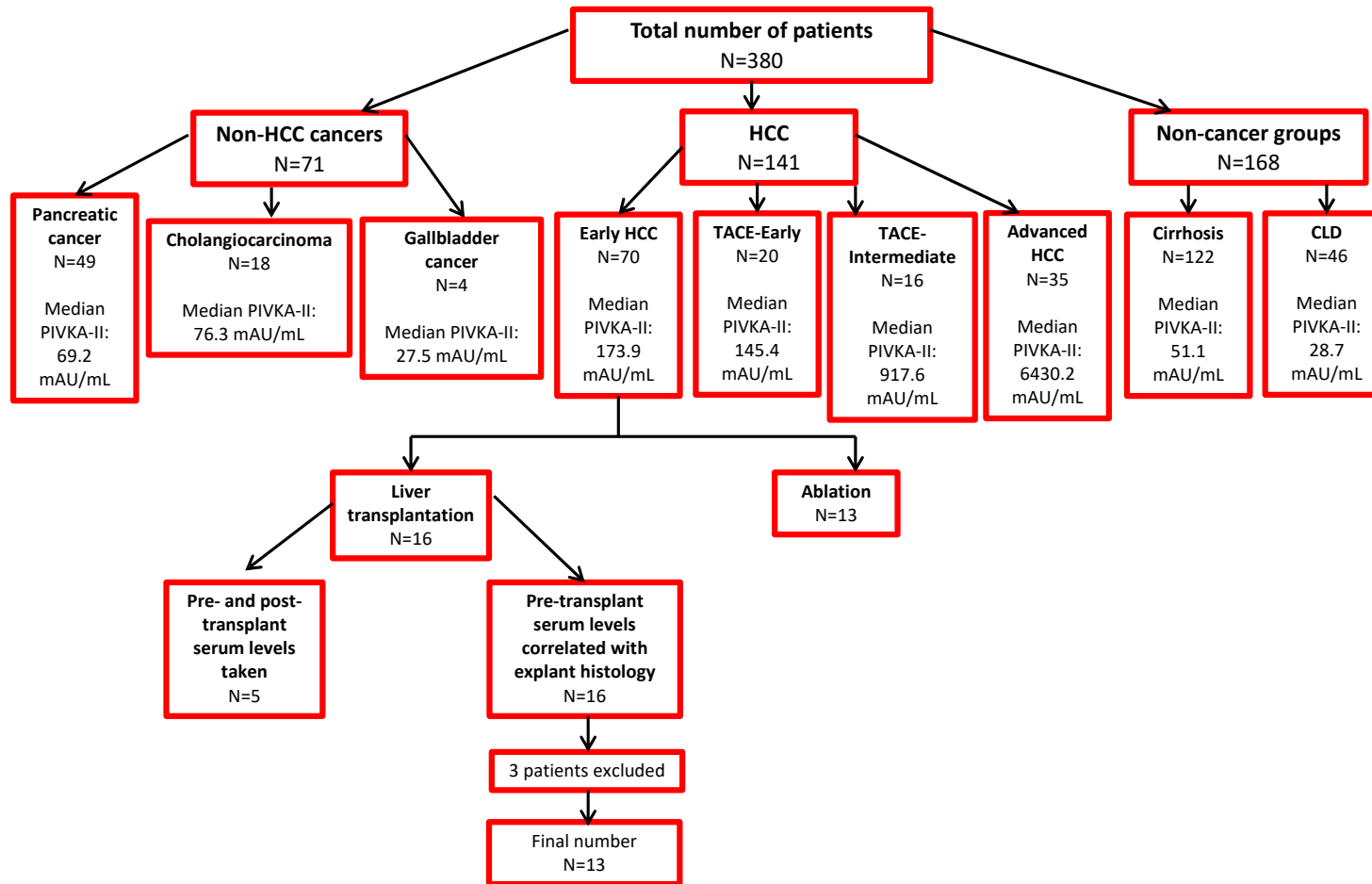
Figure 9b

Figure 9: Summary flow charts of recruitment into each study.

Figure 9a represents the patient groups recruited in VAP-1 in NETs study. Figure 9b represents the patient groups recruited into PIVKA-II in HCC study. VAP-1, vascular adhesion protein-1. CHD, carcinoid heart disease. sVAP-1, soluble VAP-1.

CHAPTER 2:

MATERIALS AND METHODS

2.1 The role of prothrombin induced by vitamin K absence-II in early hepatocellular carcinoma

2.1.1 Recruitment and sample collection

Ethical approval

Ethical approval was acquired from the National Research Ethics Service (NRES), Research Ethics Committee reference 06/Q2707/182. Written informed consent was obtained from all study participants.

Study participants for serum analysis

Consecutive patients with a diagnosis of early HCC included in the study were recruited prospectively between January 2016 and April 2018. Early HCC was defined by the MC: the presence of either a single lesion ≤5cm in size, or three lesions with a maximum diameter ≤3cm in size. Diagnosis of early HCC was made following either radiology investigations showing characteristic hallmarks or a liver biopsy.

Additionally, two reference cohorts were recruited over the same time period. The first cohort included patients with liver cirrhosis, as identified on radiological imaging. Patients with CLD (no features of cirrhosis radiologically or biochemically, or CLD diagnosed on biopsy) formed the second cohort. Additionally to the baseline serum samples taken, longitudinal measurements of PIVKA-II and AFP were taken at approximately three monthly intervals in patients with early HCC who underwent ablation therapy.

Patients receiving TACE treatment and Sorafenib were recruited by the oncology team, and the baseline serum PIVKA-II and AFP levels taken will be included in this study as comparison groups to patients with early HCC. A biobank of samples has also been used for non-HCC cancer type groups, and was collected by the oncology team.

Sample collection and analyser used

Blood was taken peripherally from all patients in gold-top tubes (containing serum separator clot activator), and centrifuged for 10 minutes. Serum was extracted, and aliquots stored at -80°C until analysis.

Tosoh Bioscience provided an immunoassay analyser which is validated for the measurements of PIVKA-II and AFP, and supplied all the reagents required to perform the analysis for the entire study. The Tosoh analyser AIA-900 is a two-step immunoenzymometric assay. The PIVKA-II analyte present in the test serum is bound to anti-PIVKA-II mouse monoclonal antibody (Ab), MU3, immobilised on the beads in the PIVKA cups. The beads are then washed to remove unbound materials, and are then incubated with the conjugate (enzyme-labelled anti-prothrombin rabbit polyclonal Ab). The beads are washed again to remove unbound conjugate and then incubated with a fluorogenic substrate (4-MUP). The enzyme labelled Ab changes the enzyme substrate that causes colouration to occur. PIVKA-II is calculated by measuring the absorbance of the coloured solution and comparing it with the reference calibrator. The amount of enzyme labelled Ab that binds to the beads is directly

proportional to the PIVKA-II concentration in test sample. Figure 10 summarises these reactions.
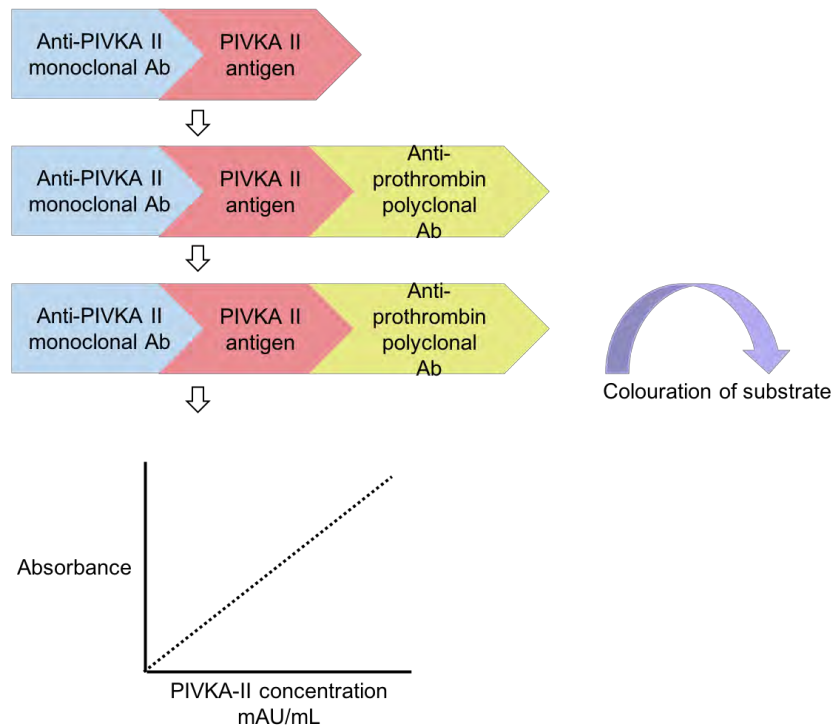
Figure 10: Summary of the TOSOH Analyser AIA-900 reactions. Ab, antibody.

Inclusion and exclusion criteria

To be included in this cross-sectional study, patients had to meet: i) the MC for early diagnosis of HCC; ii) radiological features to diagnose cirrhosis and iii) requirements to diagnose CLD.

Patients were excluded from this study if they were on anticoagulation, were pregnant or had co-existing malignancy.

Tissue sections for immunohistochemical staining

Immunohistochemical (IHC) staining of liver tissue, including HCC tissue, was also undertaken using Crystal Chem, Anti-PIVKA-II monoclonal antibody, clone number PIM 55 (stock concentration 11.3 milligrams /millilitres (mg/mL)). Various dilutions were used with a maximum dilution of 1/8000 (concentration used 0.0014 mg/mL) and both low pH and high pH antigen retrieval solutions were used. Casein concentrations were also increased up to 10X solution and addition of animal serum block was also performed. An ImmPRESS Excel Amplified peroxidase polymer staining kit was also used to enhance specificity for PIVKA-II.

Immunohistochemical staining method

Paraffin-embedded slides were firstly de-waxed by rinsing firstly three times with Xylene, three times with alcohol and twice with water. Each rinse was left in the pots for three minutes. 10mL of high or low pH antigen unmasking solution (Vector) was added to 1 litre of distilled water in a microwave pot. The low pH antigen solution is citrate-based with pH 6.0, and the high pH antigen solution is Tris-based with pH 9.0. This was then microwaved at high power for 10 minutes. After the slides had finished the final wash in water, they were loaded in a rack and microwaved at high power for 30 minutes and left to stand for 10 minutes. The slides were run in tap water to room temperature and placed in a smaller pot of water to cool. Following this, the slides were mounted in a cover slip and placed in a sequencer tray. The wells were filled with Tris buffered saline with 0.1% tween (TBST) and left for 5 minutes to allow the TBST to drain

through. 100 microlitres (μl) of hydrogen peroxidase blocking solution (Dako REAL) was then added to each well (or 2 drops of BLOXALL when the Excel amplified was used) and left for 10 – 20 minutes depending on the tissue type stained. After this time, the wells were re-filled with TBST to wash off the hydrogen peroxidase solution and left for 5 minutes. 100μl of 10X casein solution (various casein concentrations used for the PIVKA-II study) was then added to each well and left for 10 – 20 minutes depending on the tissue type stained. If animal serum blocking solution was used, this was left for 20 minutes. Following this, the primary antibody (Ab) was added to each well. The tray was covered and left to incubate for 1 hour at room temperature. The slides were then washed with TBST for 5 minutes. Following this, a polymer-based secondary antibody (Immpress Kit) was added and incubated for 30 minutes. When the Excel amplified kit was used, 2 drops of R.T.U. goat anti-mouse amplifier Ab was added after the wash for 15 minutes followed by a further wash with TBST for 5 minutes. With the Excel amplified kit, a horse anti-goat polymer-based secondary antibody was added and incubated for 30 minutes. Following the second incubation, two washes with TBST were done, each for 5 minutes. The wells were filled up again with TBST and the cover slip with the slide was pulled out and placed on a metal rack. A couple of drops of 3,3'-diaminobenzidine (DAB) was added to each slide and left for 5 minutes. Water was then poured over the slides and the excess water was drained off. Following this, 5-6 drops of filtered Mayer's haematoxylin was added and left for 30-40 seconds, and washed off by pouring water. The slides were then placed in warm water and the dehydration process then commenced. This involved

rinsing the slides three times in alcohol and then in Xylene three times. Cover glass slides were then placed on a piece of tissue paper and DPX mountant was put in the middle of each cover glass slide. The slides were taken out of the holder and placed on the DPX cover glass slide.

Visualisation of staining

The chromogenic stained tissue section images were taken using the Zeiss Axio Scan.Z1 slide scanner. Image analysis was performed using Zen Imaging Software.

2.1.2 Statistical analysis

Statistical analysis of data was performed using SPSS Statistics version 23 (*IBM Corp. Armonk, NY*). The distributions of continuous variables were assessed prior to analysis using graphical methods. Normally distributed factors were reported as means ± standard deviations (SDs), with medians and interquartile ranges (IQRs) used for non-normal factors. Categorical variables were stated as absolute values with percentages.

Comparisons between the three patient groups were then performed, using one-way analysis of variance (ANOVA) for normally distributed variables, Kruskal-Wallis tests for non-normal variables, and Fisher's exact tests for categorical variables. For the markers of interest, where the overall effect was significant by Kruskal-Wallis test, pairwise post-hoc comparisons were performed using Dunn's test. Comparisons of continuous variables between two

101

groups (e.g. HCC vs non-HCC) were performed using Mann-Whitney U tests. PIVKA-II and AFP levels were then compared across the different HCC stage groups using Jonckheere-Terpstra tests, to account for the fact that the HCC stages were ordinal. Relationships between PIVKA-II and a range of laboratory markers were assessed using Spearman's rank (rho) correlation coefficients. The abilities of PIVKA-II and AFP to differentiate between early HCC and both CLD and cirrhosis, and between early HCC and cirrhosis, were then assessed using receiver operating characteristic (ROC) curves. In order to further assess the relationship between PIVKA-II and the distribution of disease, patients were then divided into five groups, based on the quintiles of PIVKA-II, and the distribution of disease compared across each group.

A multivariable binary logistic regression model was then produced to assess whether PIVKA-II and AFP were significant independent predictors of early HCC. Hosmer-Lemeshow goodness of fit tests were produced for each variable separately, with $\log_2$-transformations applied where poor fit was detected. Predicted values were then produced from the model, and the predictive accuracy of the combination of PIVKA-II and AFP compared to that of the individual factors using ROC curves.

Median PIVKA-II/AFP levels were compared across various explant findings including the presence of vascular invasion, HCC differentiation and number of lesions. Mann-Whitney tests was used for comparison across two groups and Jonckheere-Terpstra tests for comparisons across ordinal factors. For

comparisons between non-HCC cancer types, Fisher's exact and Kruskal-Wallis tests were used for categorical and continuous variables, respectively.

Patients that had missing data for a variable were excluded from any analyses including that variable. For PIVKA-II/AFP values that were below the lower limit of detection for the assay, a value of 1 was assumed. Throughout the analysis, a critical p-value of $p < 0.05$ was used as a cut-off for statistical significance.

2.2 Assessing the role of vascular adhesion protein-1 in neuroendocrine tumours

2.2.1 Recruitment and sample collection

Ethical approval

Ethical approval for the Human Biomaterials Resource Centre (HBRC), University of Birmingham, generic tissue banking is NRES Committee North West – Haydock 15/NW/0079. Under this approval, the HBRC project approvals are HBRC 15 – 235 and HBRC 13 – 152. Written informed consent was obtained from all study participants.

Study participants for serum VAP-1 analysis

Consecutive patients with midgut NETs or CHD were recruited prospectively between October 2014 – August 2018. The pancreatic NET group were recruited prospectively between September 2016 – June 2018. Patients were recruited during NET clinic review. Baseline and subsequent longitudinal serum

samples of VAP-1 were taken within twelve months of the baseline sample in midgut NET patients having SSA treatment or undergoing surgery. Healthy volunteer samples were also used as a control group and were supplied by the University of Birmingham HBRC.

Blood samples were collected in red-top tubes (containing serum clot activator), spun, and serum extracted and stored in the University of Birmingham HBRC until analysis.

Tissue sections for immunohistochemical and immunofluorescence staining

The University of Birmingham HBRC have also provided us with surgically resected paraffin embedded tissue (4 micrometres sections) for immunohistochemical and immunofluorescence studies. This includes the CHD valves, midgut NET tissue, control valves and cardiac myxoma tissue. The control valves included both aortic and mitral degenerative disease.

Immunohistochemical staining method

The sections were stained as described previously but the Excel amplified kit was not used.

Haematoxylin and Eosin staining method

The midgut NET and CHD valve tissue were also stained with haematoxylin and eosin. This involved placing the paraffin-embedded slides in xylene three times

(2 minutes each time), three times in alcohol (2 minutes each time), twice in water (2 minutes each time), once in haematoxylin harris (PFM medical) for 4 minutes, once in water for 2 minutes, once in acid alcohol for 30 seconds, once in water for 2 minutes, once in Scott's Tap Water Substitute for 30 seconds, once in water for 2 minutes, once in Eosin for 1 minute, twice in water (2 minutes each time), three times in alcohol (2 minutes each time) and three times in xylene (2 minutes each time). The slides were then taken out of the holder and placed on the DPX cover glass slide and mounted using DPX.

Immunofluorescence staining method

The paraffin-embedded sections were initially stained following the same protocol as the immunohistochemical staining described earlier. After the slides had completed the de-waxing protocol, they were added to 1 litre of distilled water that contained 10mL of high or low pH antigen unmasking solution and microwaved at high power for 30 minutes and left to stand for 10 minutes. The slides were then run in tap water to room temperature and placed in a smaller pot of water to cool. Following this, the slides were mounted in a cover slip and placed in a sequencer tray. The wells were filled with phosphate-buffered saline with 0.1% tween (PBST) and left for 5 minutes to allow the PBST to drain through. 100μl of casein X2 solution and goat serum was then added to each well and left for 30 minutes. Following this, the primary antibody (Ab) was added to each well. The tray was covered and left to incubate for 1 hour. The slides were then washed with PBST for 5 minutes and a secondary fluorescent antibody (Thermofisher antibodies 1/500 dilution or VectoFluor Duet Double

Labeling Kit) was added and incubated for 30 minutes. Following the second incubation, two washes with PBST were done, each for 5 minutes. The slides were then removed from the sequencer tray and a frame was drawn around the tissue using an ImmEdge hydrophobic barrier pen. Thermofisher Hoerscht 33342 (dilution used 1/1000) was then applied and left on for 10 minutes. A further wash with PBST was performed for 5 minutes. Vector TrueVIEW Autofluorescence Quenching Kit (150μl of Vector TrueVIEW Reagent for each tissue section) was then applied for 5 minutes followed by a wash with PBST for another 5 minutes. Cover glass slides were then placed on a piece of tissue and mounting media in the Vector TrueVIEW Autofluorescnce Quenching kit was put in the middle of each cover glass slide. The slides were placed on the mountant cover glass slide.

Table 5 summarises the primary antibodies used for both staining methods in midgut NETs and cardiac tissue.

	Supplier	Clone number	Supplier code	Antigen Retrieval (All are Vector Labs)	Stock concentration	Used concentration for midgut NET tissue	Dilution for midgut NET tissue	Used concentration for cardiac tissue	Dilution for cardiac tissue
Chromogenic Staining									
VAP-1	R&D	393112		Tris-based	500 ug/mL	1.67 ug/mL	1/300	2.5 ug/mL	1/200
IMC IgG2b	Dako		X 0944	Tris-based	100 mg/L	1.67 ug/mL	1/60	2.5 ug/mL	1/40
Collagen I	Abcam		ab34710	Tris-based	1 mg/mL	5 ug/mL	1/200	5 ug/mL	1/200
IMC Rabbit IgG (Collagen I)	Dako		X 0903 pAb	Tris-based	1 mg/mL	5 ug/mL	1/200	5 ug/mL	1/200
Alpha-SMA	Sigma-Aldrich	1A4		Tris-based	2.3 mg/mL	0.5 ug/mL	1/5000	-	-
IMC IgG2a	Dako		X 0943	Tris-based	100 mg/L	0.5 ug/mL	1/200	-	-
CD45	Abcam		Ab10558 pAb	Citrate-based	1 mg/mL	2 ug/mL	1/500	2 ug/mL	1/500
IMC Rabbit IgG (CD45)	Dako		X 0903 pAb	Citrate-based	1 mg/mL	2 ug/mL	1/500	2 ug/mL	1/500
S100	Dako		IR504 pAb	Tris-based	Pre-dilute	-	-	Pre-dilute	Pre-dilute
CD34	Dako	QBEnd 10	IR632	Tris-based	Pre-dilute	-	-	Pre-dilute	Pre-dilute
CD31	Dako	JC70A		Tris-based	205 mg/L	-	-	2.05 ug/mL	1/100
IMC IgG1 (CD31)	Dako		X 0931	Tris-based	100 mg/L	-	-	2.05 ug/mL	1/50
Collagen III	Abcam		ab7778 pAb	Tris-based	1 mg/mL	-	-	5 ug/mL	1/200
IMC Rabbit IgG (Collagen III)	Dako		X 0903 pAb	Tris-based	1 mg/mL	-	-	5 ug/mL	1/200
Fluorescent Staining									
VAP-1	R&D	393112		Tris-based	500 ug/mL	2.5 ug/mL	1/200	2.5 ug/mL	1/200
IMC IgG2b	Dako		X 0944	Tris-based	100 mg/L	2.5 ug/mL	1/40	2.5 ug/mL	1/40
Collagen I	Abcam		ab34710	Tris-based	1 mg/mL	5 ug/mL	1/200	5 ug/mL	1/200
IMC Rabbit IgG (Collagen I)	Dako		X 0903 pAb	Tris-based	1 mg/mL	5 ug/mL	1/200	5 ug/mL	1/200
Alpha-SMA	Sigma-Aldrich	1A4		Tris-based	2.3 mg/mL	10 ug/mL	1/230	10 ug/mL	1/230
IMC IgG2a	Dako		X 0943	Tris-based	100 mg/L	10 ug/mL	1/10	10 ug/mL	1/10

Table 5: Summary of primary antibodies used for staining in midgut NET and cardiac tissue. IMC, isotype matched control. pAb, polyclonal antibody.

Visualisation of staining

The chromogenic stained tissue section images were taken using the Zeiss Axio Scan.Z1 slide scanner. The fluorescent stained tissue section images were taken using the Zeiss LSM 780 confocal microscope. Image analysis was performed using Zen Imaging Software.

Enzyme-linked immunosorbent assay (ELISA)

Serum aliquots were stored at -80°C until analysis. Measurement of soluble VAP-1 in patient serum was performed using the Human VAP-1 Quantikine ELISA kits (R&D, DVAP10). The human VAP-1 microplates were already coated with a monoclonal Ab specific for human VAP-1. To each well 100μl of assay diluent was added. The samples were prepared using a 70 or 80-fold dilution with the calibrator diluent. The human VAP-1 standard concentrations used were 50ng/mL, 25ng/mL, 12.5ng/mL, 6.25ng/mL, 3.13ng/mL, 1.56ng/mL, 0.781ng/mL and 0ng/mL. Both the standard concentrations and the samples were run in duplicates. Into each well, 50μl of human VAP-1 standard or sample were pipetted. The microplates were then covered with an adhesive strip and incubated for 2 hours at room temperature on a horizontal microplate shaker set at 500rpm. After the 2 hours incubation, each well was aspirated and washed with 400μl wash buffer for a total of four washes. After each wash, the plate was inverted and blotted against paper towels. Following the washes, 200μl of human VAP-1 conjugate (conjugated to horseradish peroxidase) was added to each well and the plate was covered with an adhesive strip and incubated for a further 2 hours on the microplate shaker. A total of four washes was again performed after the 2

hour incubation. 200μl of substrate solution was then added to each well and the plate was covered with an adhesive strip and incubated at room temperature for 30 minutes on the benchtop protected from light. 50μl of stop solution was then added after 30 minutes to each well. The colour in the wells changed from blue to yellow. The optical density of each well was determined within 30 minutes of adding the stop solution using a microplate reader set at 450nm and 540nm. The readings at 540nm were subtracted from the readings at 450nm to correct for optical imperfections in the plate. The standard curve used was the second order polynomial curve. The concentration of VAP-1 was then calculated and multiplied by the dilution factor of 70 or 80.

Inclusion and exclusion criteria

To be included in this study, patients had to have a diagnosis of midgut NET, CHD or pancreatic NET.

In the serum VAP-1 analysis, for the midgut NET patients who had a primary small bowel resection, there was evidence of recurrent disease when the sample was taken. No surgical resection was performed in the pancreatic NET group.

Patients were excluded from the serum VAP-1 analysis if they had active co-existing malignancy.

2.2.2 Image analysis

Once the tissue sections were uploaded using the slide scanner, the quantification of both VAP-1 and Collagen I were performed using Ilastik (version 1.3.0) and Fiji Image J (version 2.0.0-rc-66/1.52b). Using Ilastik, a group of sections from the midgut NET, control valves and the CHD cohorts were trained in order to recognise the antibody staining. A live update was performed to ensure the antibody staining was correctly identified. Once the training was complete, all the sections from each cohort were then inputted into Ilastik generating images that used the training performed to correctly identify the antibody staining in each section. Following this, an automated macro was inputted into Fiji Image J with the antibody staining set in the programme of the macro as '2'. The images generated by Ilastik were then analysed on Fiji Image J and the percentage area of antibody expression was calculated.

A highly experienced pathologist reviewed all the CHD and control valve stained sections to identify the exact location of the positive staining and also suggested additional stains to use to help further accurately identify the positive stained cells appearance, location within the valves using elastin and haematoxylin van gieson staining (EHVG), and assess the association of VAP-1 staining with other markers including S100 and CD34.

2.2.3 Statistical analysis

Statistical analysis of data was performed using SPSS Statistics version 23 (*IBM Corp. Armonk, NY*) and GraphPad software (Prism 7) version 7.0b.

A quantitative analysis was performed using the Mann-Whitney U test to assess the % area of VAP-1 expression in both the CHD and control valves. Continuous variables are reported as medians and IQRs, with comparisons between non-paired samples performed using Mann-Whitney U tests and the paired samples performed using Wilcoxon's test. Age is reported as mean ±SD with p-Values from independent samples t-tests. Categorical data is reported as N (%) with p-Values from Fisher's exact tests. Comparisons between more than two patient groups were performed using Kruskal-Wallis tests, with pairwise post-hoc comparisons performed using Dunn's test where significant differences were detected. Relationships between sVAP-1 and a range of clinical markers or findings were assessed using Spearman's correlation coefficients. Changes in carcinoid syndrome symptoms were compared using McNemar's test.

Throughout the analysis, a critical p-value of $p < 0.05$ was used as a cut-off for statistical significance.

CHAPTER 3:

THE ROLE OF PROTHROMBIN INDUCED BY VITAMIN K ABSENCE-II IN EARLY HEPATOCELLULAR CARCINOMA

3.1 Introduction and aims

3.1.1 Introduction

HCC distribution varies according to geographic location. In areas such as Eastern Asia and sub-Saharan Africa, the burden of HCC is highest due to a high prevalence of endemic HBV infection. In comparison with the global burden of disease, the UK has a low incidence of HCC.(298) However, the incidence of HCC is now rising in the UK.(4) The development of HCC in cirrhosis is not always associated with end-stage liver disease, and in fact does usually occur in the presence of adequate liver functional reserve.(299) Overall risk for developing HCC in patients with cirrhosis is dependent on various factors, including liver disease aetiology (highest in patients with HCV infection), location and ethnicity (highest in Asians) and cirrhosis stage (highest in those with hepatic decompensation).(300, 301) However, at present in a large number of cases, diagnosis is made in the advanced stages of disease, so curative treatment options are often limited.(302)

There is a demanding requirement for screening tests that can be used in the surveillance of HCC in at-risk patient groups to increase the number of cases diagnosed with early HCC so curative treatment options can be implemented and improve the overall life expectancy for patients. US imaging has limitations for use as a screening tool in HCC. The overall sensitivity of this radiological investigation is around 65-80%, and is lower in the early stages of disease where there are non-specific features seen and characteristics have not been well defined in the setting of cirrhosis and HCC surveillance.(303-306) Additionally, it is subjective

and increasing incidence of obesity in the West can also limit the sensitivity of US imaging.(53) Traditionally, AFP has been the marker used in HCC surveillance, but the EASL-EORTC guidelines suggest that AFP should no longer be monitored given the suboptimal sensitivity and specificity associated with this marker.(17)

PIVKA-II has emerged in Japanese guidelines as part of HCC surveillance in patients at high risk, and numerous studies in Asia have been performed looking at the value of this marker in HCC. Studies performed to date have shown variable efficacy of PIVKA-II as a single biomarker in diagnosing HCC. PIVKA-II does appear to be an attractive biomarker in European patient cohorts given that it has been shown to be elevated in early stage disease and in NASH associated HCC, whereas AFP is found to be high in viral hepatitis and advanced disease.(121) Studies (including those in the UK) involving the application of the GALAD model, which incorporates three serological markers (AFP, AFP-L3 and PIVKA-II), have shown that this improves the detection and diagnosis of HCC, including the detection of early HCC.(50, 306) PIVKA-II therefore does appear to have a role in the Western population.

The majority of studies already conducted evaluating the role of PIVKA-II in HCC have been largely performed in Asia, where liver disease aetiology differs from the UK, and viral hepatitis is the commonest disease aetiology in comparison to the UK, where alcoholic liver disease (ALD) and non-alcoholic fatty liver disease (NAFLD) are usually the causes of liver disease. PIVKA-II has been shown to perform better for viral aetiologies of cirrhosis and HCC compared to non-viral

aetiology.(307) Therefore it is important to assess this marker in the UK population to see if it could potentially be used as a screening test to provide early diagnosis of HCC early so that treatment can be offered and overall survival improved.

3.1.2 Aims

The overall aim of this study is to assess whether PIVKA-II could be a potential diagnostic biomarker in a cohort of UK patients with early HCC.

The aims of this study include:

a) Evaluating the role of PIVKA-II in diagnosing early HCC, compared to the traditional marker AFP, and as a combination of both biomarkers.

b) Assessing if levels of PIVKA-II are raised in non-HCC patients (including pancreatic cancer, cholangiocarcinoma and gallbladder cancer).

c) Assessing PIVKA-II levels in patients undergoing local ablative therapy and the ability of PIVKA-II to differentiate therapeutic responders from non-responders. If PIVKA-II accurately differentiates treatment responders from non-responders then it could potentially be used as a selection tool for patients suitable for early phase clinical trials i.e. immunotherapy.

d) Assessing if levels of PIVKA-II increase with disease progression of HCC.

3.2 Results

Immunohistochemistry analysis

HCC tissue was stained with an anti-PIVKA-II monoclonal Ab. Despite using increasing Ab dilutions (up to 1/8000 dilution), high casein solution concentrations (10X solution), addition of animal serum block and both low and high pH antigen retrieval solutions, background staining was present with positive PIVKA-II expression in normal liver, non-lesional liver tissue and HCC. No specific areas of PIVKA-II staining in HCC tissue was seen and granular staining was also present. Lower dilutions and use of the amplified kit increased the background staining, and positive staining was also evident in the fibrous septa as well as in the tumour and non-tumour parenchymal areas. **Figure 11.**

Normal liver 1/4000
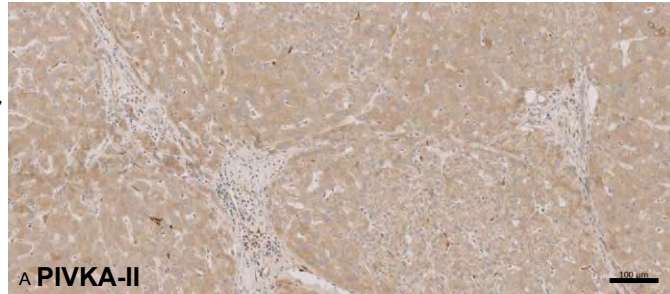
A PIVKA-II

HCC 1/800, amplified kit
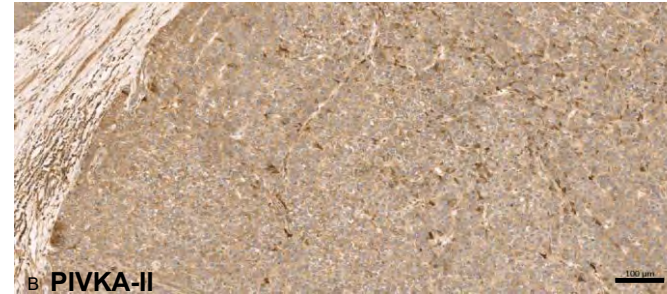
B PIVKA-II

HCC 1/8000, low pH antigen retrieval

C PIVKA-II

Non-lesional liver area to image C

D PIVKA-II

117
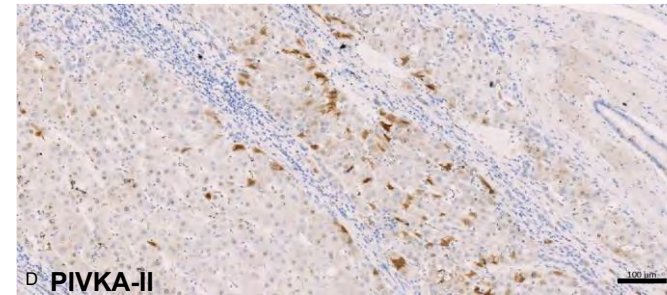
HCC 1/8000, high pH antigen retrieval solution, casein 10X
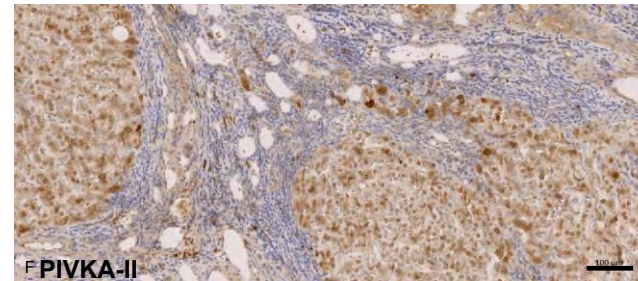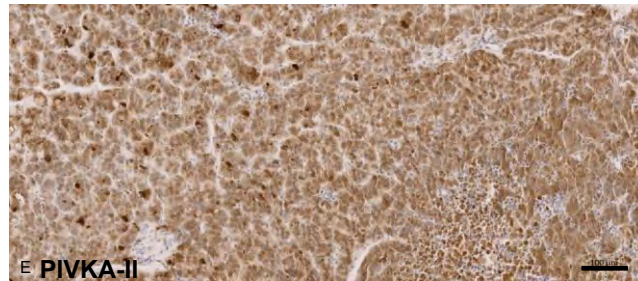
E PIVKA-II

F PIVKA-II

Non-lesional liver area to image E

Figure 11: Immunohistochemistry staining of PIVKA-II in normal liver and HCC sections. Scale bars 100 μm. Figure 11A represents normal liver tissue with positive PIVKA-II staining using a 1/4000 Ab dilution. Presence of background positive staining can be seen in Figure 11A with also darker areas present in the cytoplasm of the hepatocytes. Figure 11B represents HCC stained using a 1/800 Ab dilution and an amplified kit. A lot of background staining is present as well as positive lymphocyte and fibroblast staining seen in the fibrous septa. Figure 11C represents HCC tissue stained using a 1/8000 Ab dilution and a low pH antigen retrieval solution. In this image the presence of very non-specific positive staining can be seen. Figure 11D represents the non-lesional liver to the HCC tissue in Figure 11C and more positive staining is present here with the presence of granular staining as well as a checkerboard appearance. Figure 11E shows HCC tissue stained using a 1/8000 Ab dilution, high pH antigen retrieval solution and casein 10X solution. In this figure positive cytoplasmic and nuclear staining is present as well positive granular areas. This is similar to the staining seen in Figure 11F which represents the non-lesional liver area to the HCC tissue in Figure 11E, which additionally shows positive staining in the fibrous septa.

PIVKA-II and AFP with HCC stage

In total, 141 patients with HCC have been included. Early HCC was found in 70 patients, 20 patients were within the MC and underwent TACE treatment (termed TACE-early), 16 patients had TACE treatment and fell in the intermediate stage, BCLC stage B (termed TACE-intermediate), and 35 patients were within the advanced stage, BCLC stage C and received Sorafenib. Levels of PIVKA-II showed a significant increase with tumour stage (p<0.001) with medians of 173.9 mAU/mL (IQR: 47.2 – 515.7), 145.4 mAU/mL (IQR: 48.7 – 1224.0), 917.6 mAU/mL (IQR: 179.3 – 3802.1) and 6430.2 mAU/mL (IQR: 320.0 – 29306.4), respectively. Levels of AFP were also found to increase significantly with tumour stage (p=0.012), **Figure 12**.
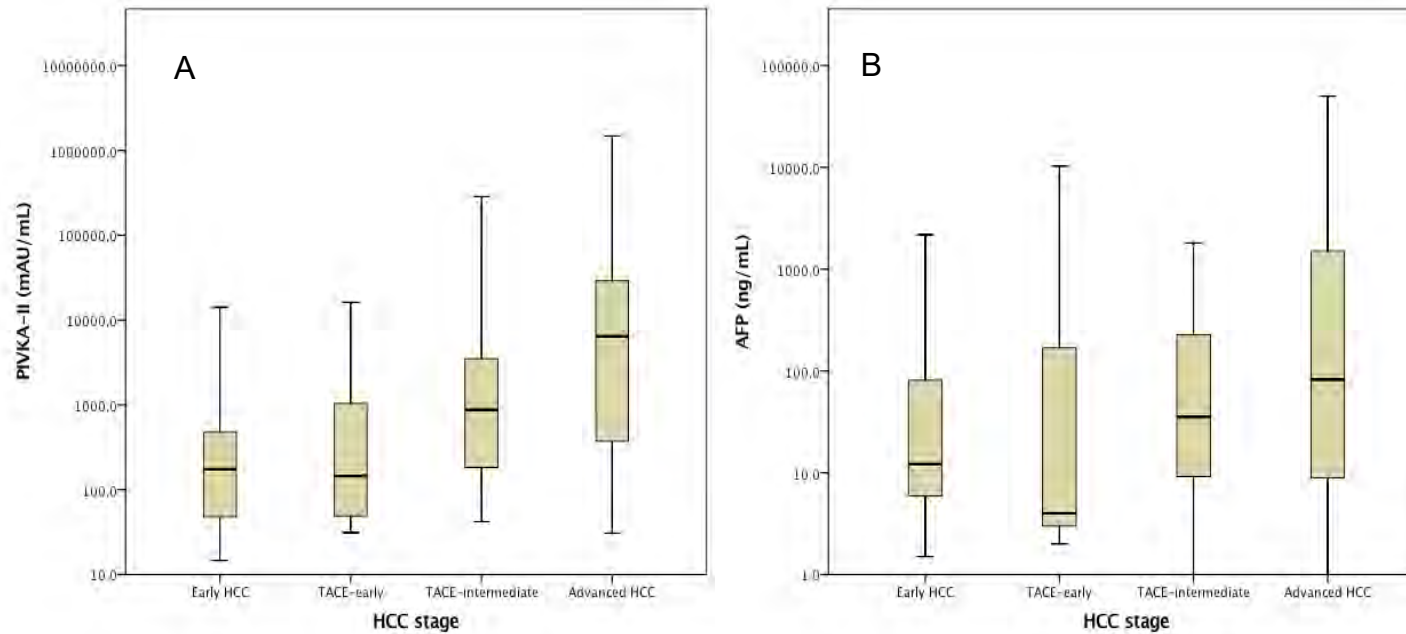
Figure 12: Medians of PIVKA-II and AFP with tumour stage. Medians of PIVKA-II (Figure 12A) and AFP (Figure 12B) across the four HCC groups (early HCC; n=70, TACE-early; n=20, TACE-intermediate; n=16, advanced HCC, n=35). A logarithmic$_{10}$ scale has been used for the PIVKA-II and AFP values. Jonckheere-Terpstra test performed and showed a significant difference across the groups (p<0.001 for PIVKA-II and p=0.012 for AFP). TACE, transarterial chemoembolisation.

Comparisons between non-HCC cancer types

Three cancer groups were included for analysis **(Table 6)**: pancreatic cancer (N=49), cholangiocarcinoma (N=18) and gallbladder cancer (N=4). PIVKA-II levels were found to differ significantly between the groups (p=0.034), being highest in cholangiocarcinoma 76.3 mAU/mL (IQR: 32.8 – 121.7), followed by pancreatic and gallbladder cancer, at 69.2 mAU/mL (IQR: 39.0 – 106.0) and 27.5 mAU/mL (IQR: 20.5 – 34.4) respectively. Post-hoc pairwise analysis found the difference in PIVKA-II between gallbladder and pancreatic cancer groups to be significant (p=0.028). No significant differences in AFP levels were detected between the groups, with medians ranging from 3.7 – 5.3 ng/mL (p=0.504).

Metastases were present in half of the pancreatic cancer group, and rates were not found to differ significantly across the three groups (p=0.661) In addition, there were no significant differences between the three groups in the rates of lymph node (LN) involvement (p=0.111) or vascular invasion (p=0.535).

Combining these three non-HCC groups as one and comparing it with the early HCC group, a significant difference in the median PIVKA-II and AFP level was found (p=0.004 and p<0.001 respectively).

Group	N	Metastases present	LN involved	Vascular invasion	PIVKA-II	AFP
Type of Cancer		p=0.661	p=0.111	p=0.535	**p=0.034**	p=0.504
Pancreatic	49	25 (51%)	12 (24%)	23 (47%)	69.2 (39.0 – 106.0)	3.7 (2.4 – 5.9)
Cholangiocarcinoma	18	8 (44%)	5 (28%)	6 (33%)	76.3 (32.8 – 121.7)	3.7 (2.5 – 7.2)
Gallbladder	4	1 (25%)	3 (75%)	1 (25%)	27.5 (20.5 – 34.4)	5.3 (3.5 – 7.3)

Table 6: Characteristics of three non-HCC cancer groups. Data are reported as N (%), with p-values from Fisher's exact tests, or as median (IQR), with p-values from Kruskal-Wallis tests, as applicable. Bold p-Values are significant at p<0.05. LN, lymph node. N, number.

Post-hoc test for PIVKA-II: Gallbladder cancer vs. Pancreatic cancer: p=0.028. Other two pairwise comparisons non-significant.

Patient characteristics

The total pool of patients in this study was 238: 70 with early HCC, 122 with cirrhosis and 46 with CLD. The cirrhosis and CLD groups served as reference groups for analysis. The majority of the CLD patients had an aetiology of NAFLD (67%), compared to <30% of the other groups. ALD was the most common aetiology in the cirrhosis group (51%), with only 4% of CLD patients having ALD. In the early HCC group, 33% had ALD, 23% NAFLD, and the remainder had other aetiologies.

Comparisons of baseline characteristics between the three disease groups are reported in **Table 7**. Of the continuous variables considered, only albumin and sodium were found to be normally distributed, hence values for the remainder were reported as medians and IQRs throughout. The three disease groups were found to have similar gender distributions (p=0.100), but significantly different ethnicity distributions (p<0.001), with higher proportions of non-Caucasian patients in the CLD group (24%) than in those with cirrhosis (4%) or early HCC (11%). Creatinine levels were not found to differ significantly between the three disease groups (p=0.352). However, significant differences in ALT, albumin, bilirubin, haemoglobin, platelets and INR (all p<0.001) as well as sodium (p=0.031) were detected. On post-hoc analysis of these factors, only ALT was found to differ significantly between the early HCC and cirrhosis groups, with medians of 33 vs. 24 units/litre (U/L) (p=0.002).

	N	CLD (N= 46)	Cirrhosis (N= 122)	Early HCC (N= 70)	p-Value
Demographics					
Age at Sample (Years)	238	50.9 ± 13.8	58.1 ± 10.2	61.8 ± 9.1	**<0.001**
Male	238	31 (67%)	76 (62%)	54 (77%)	0.100
Ethnicity	167				**<0.001**
Caucasian		26/34 (76%)	94/98 (96%)	31/35 (89%)	
Non-Caucasian		8/34 (24%)	4/98 (4%)	4/35 (11%)	
Laboratory tests					
ALT (U/L)	237	40 (26 – 61)	24 (19 – 34)	33 (23 – 49)	**<0.001**
Albumin (g/L)	237	49 ± 3	42 ± 6	42 ± 5	**<0.001**
Bilirubin (umol/L)	237	9 (6 – 13)	17 (10 – 37)	17 (11 – 24)	**<0.001**
Sodium (mmol/L)	237	141 ± 2	140 ± 3	140 ± 3	**0.031**
Creatinine (umol/L)	237	74 (65 – 93)	76 (63 – 88)	70 (64 – 85)	0.352
Haemoglobin (g/L)	238	147 ± 17	135 ± 22	141 ± 16	**<0.001**
Platelets (10^9/L)	238	224 (199 – 273)	115 (76 – 178)	102 (72 – 129)	**<0.001**
Prothrombin time (INR)	235	1.0 (1.0 – 1.1)	1.2 (1.1 – 1.4)	1.2 (1.1 – 1.2)	**<0.001**
Tumour markers					
AFP (ng/mL)	238	2.7 (1.9 – 4.1)	4.7 (3.0 – 6.9)	12.1 (5.9 – 80.8)	**<0.001**
PIVKA-II (mAU/mL)	238	28.7 (21.2 – 40.0)	51.1 (26.6 – 149.5)	173.9 (47.4 – 477.8)	**<0.001**

Table 7: Summary of patient demographics, laboratory tests and tumour markers across the three groups. The groups are early HCC (N=70), cirrhosis (N=122) and CLD (N=46). Micromole/litre (umol/L). Data are reported as N (%), with p-values from Fisher's exact tests; mean±SD, with p-Values from one-way ANOVA or median (IQR), with p-Values from Kruskal-Wallis tests, as applicable. Bold p-values are significant at p<0.05.

Dunn's Tests for tumour markers:

AFP: CLD vs cirrhosis (p=0.002), CLD vs early HCC (p<0.001) and cirrhosis vs early HCC (p<0.001)

PIVKA-II: CLD vs cirrhosis (p<0.001), CLD vs early HCC (p<0.001) and cirrhosis vs early HCC (p=0.001)

Performance of PIVKA-II and AFP as a diagnostic marker for early HCC

AFP and PIVKA-II values were found to follow skewed distributions, and so were analysed using a non-parametric approach. Both AFP and PIVKA-II were found to differ significantly across the three patient groups (both p<0.001, **Table 7**), with the median values showing progressive increases through the CLD, cirrhosis and early HCC cohorts. Post-hoc analyses found significant differences between every pair of patient groups for both AFP and PIVKA-II.

The discriminative abilities of the two markers were then assessed using a ROC curve analysis (**Figure 13**). Both AFP and PIVKA-II were found to be significantly predictive of early HCC vs. CLD or cirrhosis (both p<0.001). The predictive accuracy of AFP was found to be superior to that of PIVKA-II, with AUROCs of 0.845 (95% CI: 0.790 – 0.901) and 0.713 (95% CI: 0.641 – 0.784) respectively. A similar trend was also observed in using AFP and PIVKA-II for the prediction of HCC compared to cirrhosis, with AUROCs of 0.821 (95% CI: 0.758 – 0.884) and 0.663 (95% CI: 0.583 – 0.742) respectively.

A multivariable analysis was then produced, in order to consider the combined effect of the two biomarkers for the prediction of early HCC vs cirrhosis. A Hosmer-Lemeshow test showed reasonable model fit for AFP, but indicated significant poor fit for PIVKA-II. As such, the PIVKA-II values were $\log_2$-transformed, which improved the goodness of fit to acceptable levels.
The multivariable model found both biomarkers to be significant independent predictors of early HCC, with odds ratio of 1.15 (95% CI: 1.08 – 1.23, p<0.001)

for a unit increase in AFP, and 1.16 (95% CI: 1.01 – 1.34, p=0.039) for a two-fold increase in PIVKA-II. The predicted values were then generated from the model for each patient in the study, to give a combined value for the two biomarkers. The resulting values had an AUROC of 0.833 (95% CI: 0.773 – 0.894, p<0.001), indicating that the predictive accuracy of the combination of AFP and PIVKA-II was only a marginal improvement over that previously observed for AFP alone (AUROC=0.821, 95% CI: 0.758 – 0.884), **Table 8**.

(A) HCC vs CLD/cirrhosis

AFP AUROC 0.845 (95% CI: 0.790 – 0.901)
PIVKA-II AUROC 0.713 (95% CI: 0.641 – 0.784)

(B) HCC vs cirrhosis

AFP AUROC 0.821 (95% CI: 0.758 – 0.884)
PIVKA-II AUROC 0.663 (95% CI: 0.583 – 0.742)
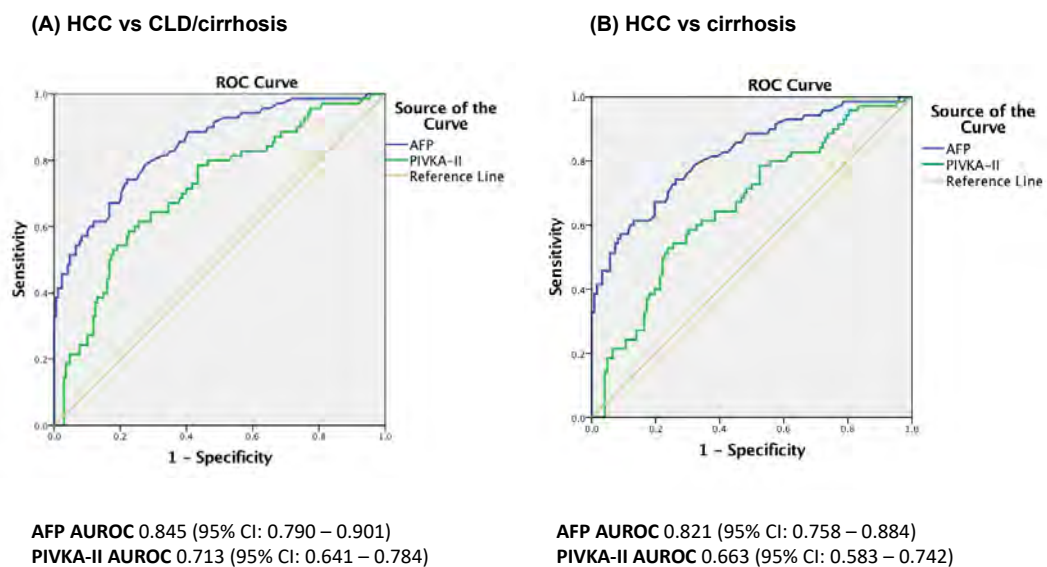
Figure 13: ROC curves for the diagnosis of early HCC vs. CLD/cirrhosis and vs. cirrhosis only. AUROC, area under the receiver operating characteristic curve.

	A) HCC vs. CLD/Cirrhosis		B) HCC vs. Cirrhosis	
Factor	AUROC (95% CI)	p-Value	AUROC (95% CI)	p-Value
PIVKA-II	0.713 (0.641 – 0.784)	**<0.001**	0.663 (0.583 – 0.742)	**<0.001**
AFP	0.845 (0.790 – 0.901)	**<0.001**	0.821 (0.758 – 0.884)	**<0.001**
AFP and PIVKA-II*	0.865 (0.815 – 0.915)	**<0.001**	0.833 (0.773 – 0.894)	**<0.001**

Table 8: Comparisons of ROC curves using individual markers and combining both markers. Bold p-Values are significant at p<0.05.*A combination of the two markers, based on the predicted values from a multivariable binary logistic regression model.

Cut-off levels of AFP and PIVKA-II

For the differentiation of early HCC from cirrhosis, the cut-off value for PIVKA-II with the greatest value of the Youden's J statistic was 155 mAU/mL, which returned a sensitivity of 53% and specificity of 76%. For AFP, a cut-off level of 8.5 ng/mL returned a sensitivity of 61% and specificity of 87%. When these two cut-offs were combined, of those with negative values for both AFP and PIVKA-II, 14% (13/95) had early HCC, compared to 82% (23/28) of patients with positive values for both markers. For 133 patients who had a negative AFP (≤8.5 ng/mL), 95 also had a negative PIVKA-II (≤155 mAU/mL), with 38 having a positive PIVKA-II. The rates of early HCC in these groups were 14% and 37% respectively, giving a sensitivity of 52% and specificity of 77%.

Distribution of disease groups by PIVKA-II

The relationship between PIVKA-II ranges and disease group (i.e. CLD, cirrhosis and early HCC) were then assessed in further detail. Patients were first divided into five groups based on PIVKA-II values, each made up of

approximately 20% of the cohort. The distribution of disease within each of these PIVKA-II groups was then calculated, and reported in **Table 9** and **Figure 14**.

The rate of early HCC was found to increase progressively across the groups, from 11% of those with PIVKA-II $\leq$ 24 mAU/mL, to 54% in those with PIVKA-II >293 mAU/mL, greater than a four-fold increase. No patients were seen to have CLD with the group with the highest PIVKA-II value (>293 mAU/mL).

PIVKA-II (mAU/mL)	CLD	Cirrhosis	Early HCC
≤24	15 (33%)	25 (56%)	5 (11%)
25 - 38	18 (36%)	23 (46%)	9 (18%)
39 - 72	11 (23%)	26 (54%)	11 (23%)
73 - 293	2 (4%)	26 (55%)	19 (40%)
>293	0 (0%)	22 (46%)	26 (54%)

Table 9: Distribution of disease based on PIVKA-II ranges. When the highest PIVKA-II level is applied, no patients are diagnosed with CLD. In the early HCC, the rates of diagnosis progressively increased across the PIVKA-II ranges, with a greater than four-fold increase from the lowest PIVKA-II level to the highest PIVKA-II level.
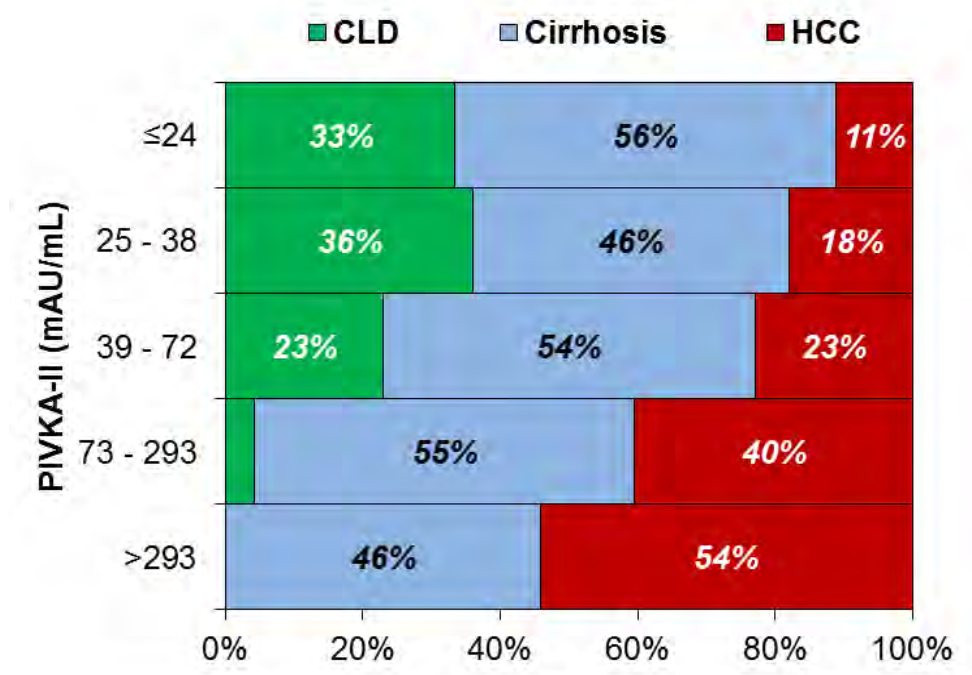
Figure 14: Graphical representation of the distribution of disease based on PIVKA-II ranges. PIVKA-II categories are based on the quintiles of the distribution.

Correlation between laboratory values with AFP and PIVKA-II

The associations between PIVKA-II and AFP with various laboratory variables were then assessed using Spearman's rho correlation coefficients. PIVKA-II showed a significant positive correlation with AFP. Significant positive correlations were found between PIVKA-II and bilirubin, INR and MELD score, with significant negative correlations with albumin, sodium and platelets identified. However, AFP showed significant correlations with fewer variables: significant negative correlations were found with albumin, sodium and platelets and no significant positive correlations were seen, **Table 10**.

	PIVKA-II		AFP	
	Rho	*p-Value*	*Rho*	*p-Value*
AFP	0.353	**<0.001**	-	-
ALT	-0.050	0.444	0.104	0.111
Albumin	-0.323	**<0.001**	-0.193	**0.003**
Bilirubin	0.256	**<0.001**	0.053	0.419
Sodium	-0.128	**0.050**	-0.132	**0.042**
Creatinine	-0.054	0.410	-0.038	0.559
Haemoglobin	-0.154	0.018	-0.043	0.511
Platelets	-0.273	**<0.001**	-0.224	**<0.001**
INR	0.342	**<0.001**	0.090	0.170
MELD score	0.289	**<0.001**	0.029	0.669

Table 10: Correlations between laboratory variables and PIVKA-II/AFP.
Data are reported as Spearman's rho correlation coefficients. Bold p-Values are significant at p<0.05. ALT, alanine transaminase. INR, international normalised ratio. MELD, model of end-stage liver disease.

AFP and PIVKA-II with size and number of lesions

Relationships between tumour-related factors (size and number of lesions) and both AFP and PIVKA-II were assessed within the early HCC subgroup (N=70), **Figure 15** and **Figure 16**. The size of lesions was split into three groups: < 20 millimetres (mm) (n=22), 20 – 29 mm (n=29) and ≥ 30 mm (n=19). AFP was not found to be significantly associated with the size of lesions (p=0.979) with median values of 12.4 ng/mL (IQR 6.6 – 114.7), 20.5 ng/mL (IQR 5.7 – 47.1) and 10.2 ng/mL (IQR 6.9 – 326.2) respectively. The number of lesions were divided into two groups: 1 lesion (n=55) and ≥ 2 lesions (n=15). AFP was also not significantly associated with the number of lesions (p=0.626), with median values of 11.4 ng/mL (IQR 5.9 – 70.7) and 23.9 ng/mL (IQR 5.8 – 124.6) respectively. PIVKA-II was not found to be significantly associated with the number of lesions (p=0.573), with median values of 191.2 mAU/mL (IQR 47.4 – 653.3) where there was 1 lesion present and 95.2 mAU/mL (IQR 46.7 – 367.2)

with ≥ 2 lesions. However, a significant correlation with the size of lesions was detected (rho: 0.348, p=0.003), with median PIVKA-II levels of 65.3 mAU/mL (IQR: 43.8 – 186.8), 211.2 mAU/mL (64.0 – 472.7) and 373.4 mAU/mL (48.6 – 3337.9) for lesions of < 20 mm, 20 – 29 mm and ≥ 30 mm, respectively.

A   **B**
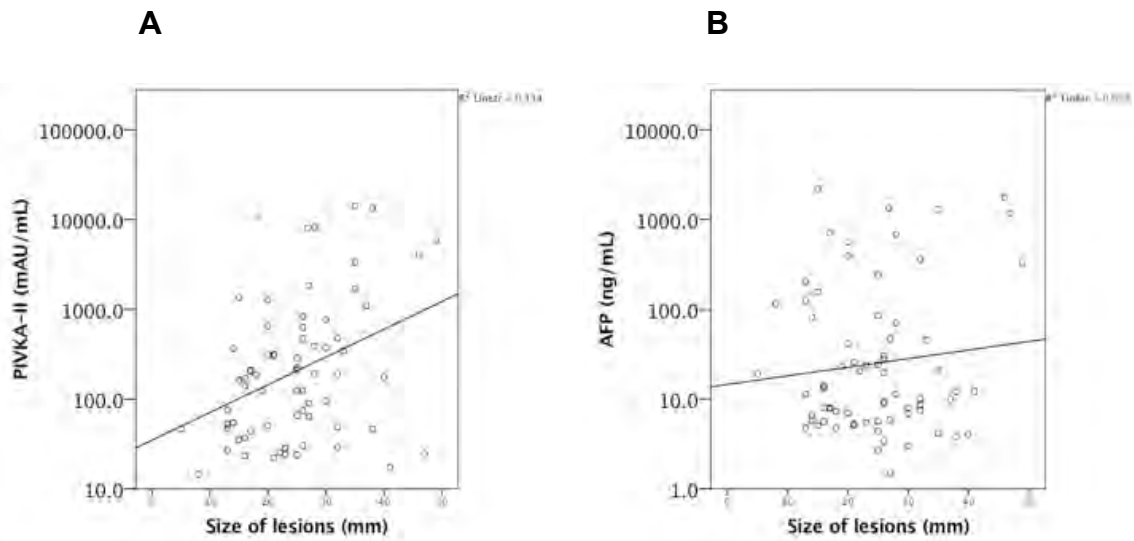
Figure 15: PIVKA-II and AFP correlating with lesion size. Median HCC size is 25 mm (IQR 17 – 30). Figure 15A shows a significant positive correlation with PIVKA-II and HCC size (Spearman's rho correlation co-efficient 0.348, p=0.003), whereas Figure 15B shows no significant correlation with AFP and HCC size (Spearman's rho correlation co-efficient 0.003, p=0.979). A logarithmic$_{10}$ scale has been used for both PIVKA-II and AFP values.
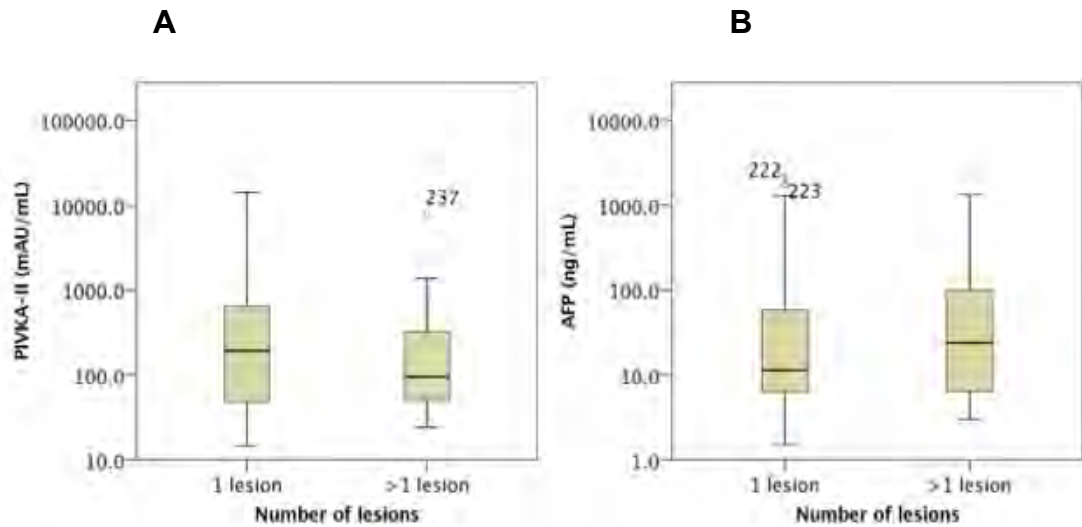
Figure 16: PIVKA-II and AFP correlating with the number of lesions.
Figure 16A shows a negative correlation with PIVKA-II and number of lesions (Spearman's rho correlation co-efficient -0.069, p=0.573) and Figure 16B shows a positive correlation with AFP and number of lesions (Spearman's rho correlation co-efficient 0.059, p=0.626). A logarithmic$_{10}$ scale has been used for both PIVKA-II and AFP values.

Changes in AFP and PIVKA-II post-transplant

In total, 5 patients underwent liver transplantation and had pre- and post-transplant AFP and PIVKA-II measurements taken with a median of 372 days (IQR 259 – 707) apart, **Table 11**. The median pre- and post-transplant AFP level was 5.8 ng/mL (IQR 3.4 – 27.9) and 8.5 ng/mL (IQR 3.7 – 11.5) respectively and showed no significant difference, (p=0.438). Although all 5 patients showed a reduction in PIVKA-II between the pre- and post-transplant measurements, resulting in the median from falling from 124.6 mAU/mL (IQR 95.2 – 472.7) to 38.2 mAU/mL (IQR 29.0 – 38.7), this change did not reach statistical significance (p=0.063), although this may be as a result of insufficient statistical power, due to the small sample size.

| | Median (IQR) | | Changes | | p-Value |
	Pre-Transplant	Post-Transplant	Decrease	Increase	
AFP (ng/mL)	5.8 (3.4 – 27.9)	8.5 (3.7 – 11.5)	3	2	0.438
PIVKA (mAU/mL)	124.6 (95.2 – 472.7)	38.2 (29.0 – 38.7)	5	0	0.063

Table 11: Changes in AFP and PIVKA-II post-transplant. Analysis is based on the N=5 transplant patients with pre- and post-transplant measurements recorded. The p-Values are from Wilcoxon's tests, and bold values are significant at p<0.05.

PIVKA-II and AFP correlating with explant histology

For early HCC, 16 patients underwent liver transplantation. The disease aetiology of liver disease was ALD (n=3), NAFLD (n=4), ALD/NAFLD (n=1), HBV (n=2), HCV (n=4), primary biliary cirrhosis (n=1) and PSC (n=1). No cancer was detected on explant histology in 2 patients, hence these were excluded from further analysis.

Table 12 shows the associations between tumour related factors and both AFP and PIVKA-II measurements. PIVKA-II was seen to be significantly higher in the presence of vascular invasion on explant histology (median 380.5 mAU/mL vs. 50.6 mAU/mL for yes vs. no, p=0.036), whereas no significant difference in AFP was detected (p=0.635). Neither PIVKA-II nor AFP showed a significant association with the number of lesions (p=0.364 and p=0.240) respectively. PIVKA-II was seen to increase significantly with poorer HCC differentiation (p=0.026), with a median of 50.6 mAU/mL vs. 2199.1 mAU/mL for well vs. poorly differentiated tumours.

	N	PIVKA-II (mAU/mL)	p-Value	AFP (ng/mL)	p-Value
Vascular Invasion			**0.036**		0.635
No	10	50.6 (28.7 – 205.6)		16.0 (5.8 – 202.8)	
Yes	4	380.5 (206.5 – 7343.5)		14.2 (3.8 – 26.0)	
Number of Lesions			0.364		0.240
1	9	205.6 (46.4 – 472.7)		8.0 (4.2 – 19.8)	
>1	5	54.8 (28.7 – 124.6)		24.1 (23.9 – 27.9)	
HCC Differentiation			**0.026**		0.198
Well	2	50.6 (46.4 – 54.8)		9.0 (5.8 – 12.1)	
Moderately	8	62.8 (28.0 – 165.1)		13.9 (4.3 – 25.9)	
Poorly	4	2199.1 (256.5 – 9162.1)		133.6 (14.2 – 1001.4)	

Table 12: AFP and PIVKA-II vs. explant findings in transplanted patients. Data are reported as medians (IQR), and p-Values are from Mann-Whitney tests for comparisons across two groups, or Jonckheere-Terpstra tests for three groups. Bold p-Values are significant at p<0.05.

AFP and PIVKA-II measurements in patients undergoing ablation treatment

A total of 13 patients underwent ablation treatment and had longitudinal measurements of AFP and PIVKA-II recorded. Baseline levels were recorded with a median of 35 days (range 19 – 112) days prior to ablation being performed. Levels were then measured in the post-ablation period until either recurrence or the end of follow up. A total of 31 measurements were performed during this period, with a median of 2 per patient (range: 1 – 6) over a median of 202 days of post-ablation follow up (range: 35 – 548). Four patients developed

recurrence during the study, at which point follow up ended, and no further

measurements of AFP or PIVKA-II were undertaken.

Longitudinal trends in both markers are shown graphically in **Figure 17a**. From

this, it appeared that those patients who developed recurrence tended to have

increasing PIVKA-II and AFP levels in the post-ablation period. In addition,

patients with recurrence also appeared to have higher PIVKA-II levels prior to

ablation. In order to assess the latter, patients were divided into groups based

on their PIVKA-II and AFP levels prior to ablation, using the median as a cut-off

value. Of those with pre-ablation PIVKA-II levels of less than 125 mAU/mL

(n=6), no patients developed recurrence during the follow-up period. However,

for those with PIVKA-II of 125 mAU/mL or more (n=7), a total of four developed

recurrence, giving a Kaplan-Meier estimated recurrence rate of 100% after 17

months of follow-up (**Figure 17b**). Despite this, no significant difference was

detected between the groups (p=0.097), likely as a result of small statistical

power resulting from the small sample size. A weaker association between pre-

ablation AFP levels and recurrence was detected, with Kaplan-Meier estimated

rates of 33% vs. 43% at one year for AFP < 9ng/mL (n=6) vs. 9+ ng/mL (n=7).
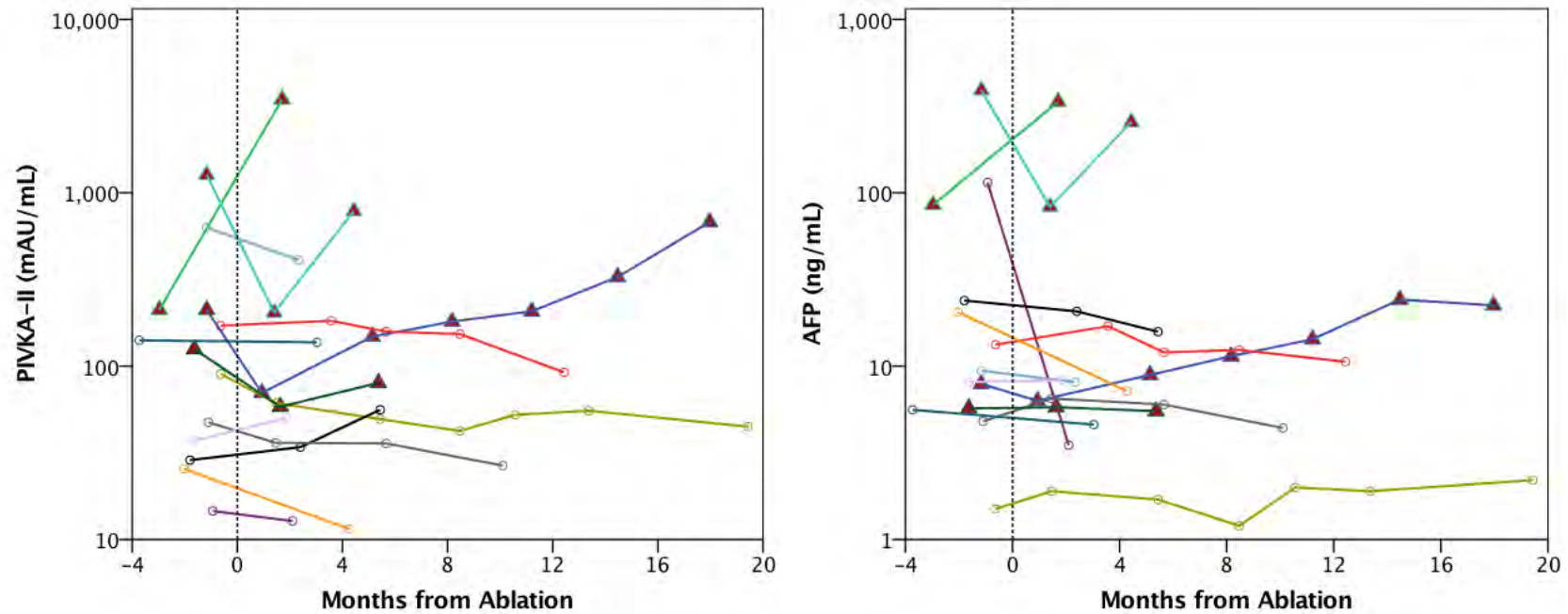
Figure 17a: Spider plots of longitudinal PIVKA-II and AFP levels. The broken line represents the timing of the ablation. Patients with red triangles are those where recurrence was diagnosed after the final measurement. The same colour coding for individual patients is used on both plots. A logarithmic$_{10}$ scale has been used for both PIVKA-II and AFP values.
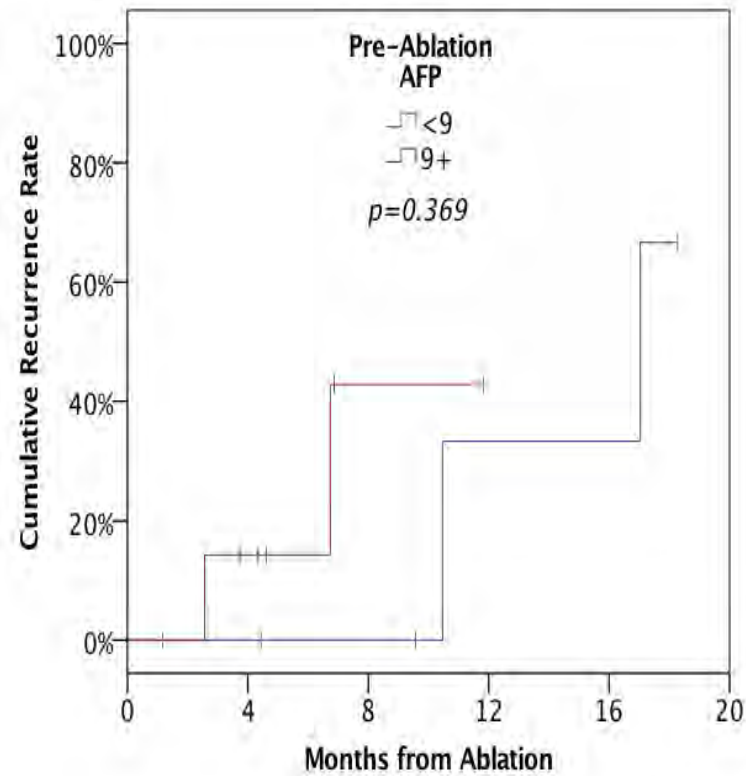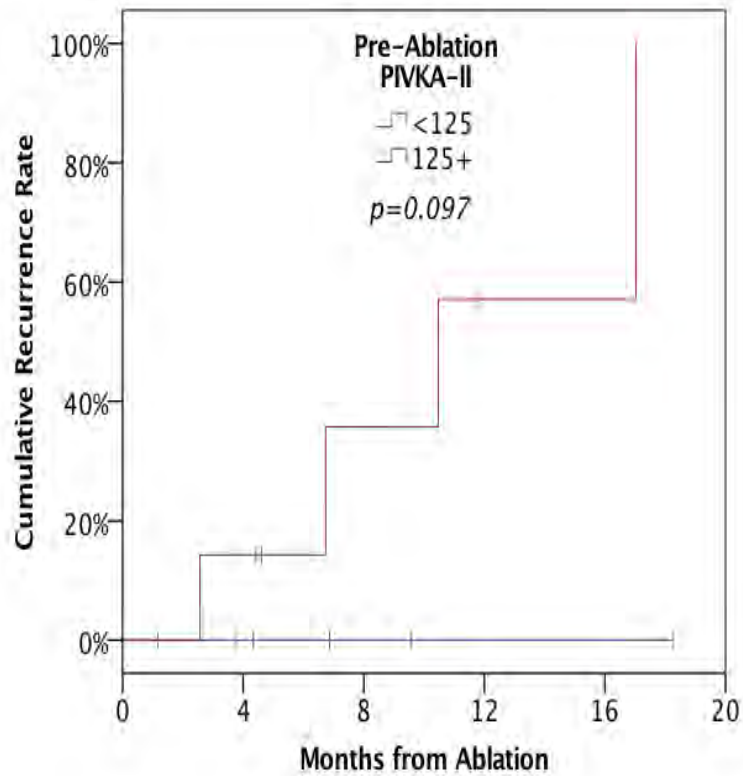
Figure 17b: Kaplan-Meier curves of recurrence by pre-ablation PIVKA-II and AFP levels. Pre-ablation levels were dichotomised based on the median levels. P-Values are from log-rank tests.

3.3 Discussion

Previous studies have shown positive PIVKA-II staining in the cytoplasm of HCC cells.(119, 135) An alternative anti-PIVKA-II Ab has been previously used in other studies which have described positive PIVKA-II staining (EIDIA Co. / Eisai Co., MU-3) (119, 132, 308, 309). Unfortunately on contacting the company the Ab was taken over by a different company (Sekisui) and was no longer available for research use and therefore I used the Ab from Crystal Chem. The IHC staining in this study did not show specific cytoplasmic staining in HCC cells and background staining was also present. Various factors were changed to improve the PIVKA-II staining in HCC tissue including increasing Ab dilution and increasing blocking steps and concentration of casein block, but this did not influence the PIVKA-II specific staining in HCC. Therefore, further staining analysis was not undertaken in this study.

This study aimed to assess the value of PIVKA-II in diagnosing early HCC and comparing this marker to the traditional marker used, AFP. Additionally, the efficacy of PIVKA-II as a treatment response marker following ablation therapy was explored. The results have shown that AFP is superior to PIVKA-II in diagnosing early HCC vs. cirrhosis. Both markers were found to be significant independent predictors of early HCC on multivariable analysis; however, the predictive accuracy of the combination of AFP with PIVKA-II was only marginally superior to that of AFP alone. Studies previously combining both markers have shown better performance than using

individual markers.(119-121, 126) Studies performed to date assessing the efficacy of PIVKA-II in diagnosing HCC have mainly been conducted in Asia, with fewer studies done in Europe. Studies performed in the western population have shown that PIVKA-II is a better marker in diagnosing early HCC, and the combination of both markers does improve the overall diagnostic accuracy.(119, 121) The main difference between this study and previous studies, including the study by Poté et al, is the cause of liver disease. The majority of other studies assessing the role of PIVKA-II have included patients with viral hepatitis, whereas the cause of liver disease in patients included in our study was predominantly either ALD or NAFLD. A possible explanation why PIVKA-II was not found to be a superior marker to AFP in diagnosing early HCC vs. cirrhosis, is that half of the cirrhosis cohort had underlying ALD, and it has been shown previously that serum PIVKA-II levels are higher in ALD than in patients with viral hepatitis.(310-312) A previous study using two different monoclonal antibodies to measure PIVKA-II (19B7 and MU-3), showed the presence of two separate PIVKA-II variants. The ratio of 19B7:MU-3 was significantly higher in ALD than in viral related liver disease or HCC, therefore suggesting the presence of a different PIVKA-II variant in ALD, and a different production pathway of PIVKA-II in ALD.(312) Another possible reason for serum PIVKA-II levels to be higher in patients with ALD, could be as a result of vitamin K deficiency, which has been shown to occur in patients with ALD.(313) The addition of vitamin K was found to inhibit PIVKA-II production in a dose-dependent manner, although there was no correlation seen between serum vitamin K

and PIVKA-II levels.(311) PIVKA-II has got a similar sensitivity to GP73 but poorer specificity in diagnosing early HCC (37), a poorer sensitivity but better specificity compared to OPN, and a poorer sensitivity compared to GP73 in diagnosing early HCC.(28, 39) In order to evaluate which marker(s) diagnose early HCC with the optimal sensitivity and specificity, comparisons between these markers with PIVKA-II, and also the combination of markers, by performing a multi-centre analysis is required, to validate and assess the sensitivity and specificity of the various markers.

Across the various HCC stages, the median PIVKA-II measurement was found to progressively increase with tumour stage (p<0.001), suggesting the possible role of PIVKA-II in determining stage of disease. From this cohort of patients, the cut-off for PIVKA-II in diagnosing early HCC was higher at 155 mAU/mL than cut-offs previously reported, yielding a sensitivity and specificity of 53% and 76% respectively. When the cut-off levels for both markers were used, the rate of early HCC was nearly six times more (82%) compared to both markers below the cut-off values (14%). In the subgroup of patients with a negative AFP (level below the cut-off value), PIVKA-II provided additional recognition of early HCC with a sensitivity of 52% and specificity of 77%. PIVKA-II levels found in the non-HCC cancer types were lower than the cut-off for diagnosing early HCC with the median PIVKA-II level greatest in the cholangiocarcinoma group. The median value of PIVKA-II was found to increase across the three groups (CLD, cirrhosis and early HCC). Interestingly, after PIVKA-II ranges were applied, no patients within the CLD group with the highest cut-off PIVKA-II value would be predicted to

have early HCC, and higher PIVKA-II values would increase the number of patients diagnosed with early HCC. The correlation of AFP and PIVKA-II with various laboratory variables found that PIVKA-II showed a significant correlation with variables that AFP did not, including bilirubin, INR and MELD score. Hence, this suggests that PIVKA-II is superior to AFP in assessing liver function which is an important factor when deciding on treatment.

Interestingly, the results showed that PIVKA-II has a significant positive correlation with tumour size, which surprisingly was not also seen with AFP ($p=0.003$ vs. $p=0.979$ respectively). This again is in keeping that PIVKA-II may be a superior marker in the advanced stages of HCC given that it has a better performance in larger tumours. Previous studies have also shown the role of PIVKA-II with BCLC stage and tumour size.(123, 124) The presence of MVI is a known prognostic indicator in patients with HCC who have undergone surgical resection and liver transplantation.(63, 314-316). In addition to MVI, tumour differentiation is another important prognostic factor in this group of patients.(317, 318) This study's results have shown that in the presence of MVI on explant histology, pre-transplant PIVKA-II serum levels were significantly higher ($p=0.034$), but this was not seen with AFP ($p=0.825$). PIVKA-II levels pre-transplant were found to be significantly higher in moderately- or poorly-differentiated HCC ($p=0.026$), and again this was not seen with AFP ($p=0.198$). Therefore, these results show that serum PIVKA-II levels are associated with the development of MVI suggesting that tumours secreting higher levels of PIVKA-II are of a more aggressive phenotype, which has previously been

shown and it has been reported that PIVKA-II levels are also associated

with the rate of tumour growth.(319) A study has previously shown that

PIVKA-II levels are an independent predictor for increased Ki-67

expression, thereby providing evidence for a positive correlation between

PIVKA-II levels and cellular proliferation rates.(122)

In the longitudinal data analysis following ablation treatment in early HCC,

those who developed recurrence tended to have higher AFP and PIVKA-II

levels that increased over time. The median values in the pre-ablation

period for PIVKA-II was 125 mAU/mL, and 9 ng/mL for AFP. Using these

cut-off levels, the Kaplan-Meier estimated recurrence rates were 100% vs.

0% in those with pre-ablation PIVKA-II of $\geq$125 vs. <125 mAU/mL after 17

months. The likely reason for this not reaching statistical significance

between these two groups is the small number of patients in the

longitudinal data analysis (p=0.097). However, the association between

recurrence and the pre-ablation AFP level was weaker. The Kaplan-Meier

estimated recurrence rates were 33% vs. 57% with AFP <9 ng/mL and $\geq$9

ng/mL respectively.

3.4 Conclusion

In conclusion, this study shows that AFP is superior to PIVKA-II in

diagnosing early HCC with only a marginal benefit when combining the

two markers. This challenges the current guidelines that recommend HCC

surveillance should not include AFP measurement. A likely reason for the

improved performance of AFP that is now seen, is the introduction of new anti-viral treatments that largely eliminates the previously false positive high AFP levels seen in active viral hepatitis. Pre-transplant PIVKA-II levels were significantly associated with the presence of MVI and in moderately- or poorly-differentiated HCC. PIVKA-II could therefore be a prognostic marker in HCC and may support patient stratification for therapy. Despite a small number in the longitudinal data analysis, PIVKA-II shows a promising role in the surveillance of recurrent HCC post-ablation. Incorporation of AFP-L3 with AFP and PIVKA-II measurements is an appealing area to study in various HCC centres in the UK to assess whether the combination of these three markers can further improve the diagnostic accuracy of early HCC.

CHAPTER 4:

SOLUBLE VAP-1 IN NEUROENDOCRINE TUMOURS

4.1 Introduction and aims

4.1.1 Introduction

NETs are known to be associated with desmoplasia and the development of fibrosis. Desmoplastic reactions that occur with midgut NETs can lead to serious complications including intestinal strictures and bowel obstruction. There are no biomarkers currently used in NET patients that allow the identification of possible fibrosis. Currently, when GI complications occur, there is no effective treatment other than surgery. For surgery to be performed, patients need to be at a certain level of physical fitness and additionally side effects post-surgery can also become problematic for the patient. Therefore surgery may not be suitable for some patients. CHD is a serious fibrotic complication that can occur with NETs and is associated with an increased mortality.(245) Once cardiac valvulopathy occurs, valve surgery is the only effective treatment available, which again requires the patient to have a certain level of fitness to undergo the operation. Some patients are asymptomatic and are not diagnosed until the disease is advanced, which may also limit treatment options. Therefore, identifying fibrosis early would allow a prompt diagnosis to be made which then enables treatment to be commenced in a timely manner with an aim to improve patients' quality of life and overall survival.

VAP-1 has been shown to play a vital role in promoting the onset of liver fibrosis in models of chronic liver injury as well as angiogenesis.(277) Increased levels of sVAP-1 have also been found in chronic liver disease.(277) Levels of sVAP-1 have been found to be lower in colorectal cancer (297) and levels have been

shown to be highest in early stage disease and decrease with disease

progression with lower levels predicting the presence of hepatic or lymph node

metastasis.(320) Similar findings have also been shown in gastric cancer with

sVAP-1 levels decreasing with disease progression.(321) In HCC, sVAP-1

levels have been shown to be significantly higher compared to cirrhosis (322).

Both an anti-VAP-1 monoclonal antibody and a small molecule inhibitor of VAP-

1 are already being studied in clinical trials (for liver disease and diabetic

retinopathy), and there is currently a high level of interest in the role of amine

oxidases such as VAP-1 in stromal biology.(323, 324)

Our preliminary data has shown that VAP-1 may also contribute to the fibrotic

complications in patients with NETs. Significantly elevated sVAP-1 levels have

been found in patients with NETs (median 562.5, IQR 438.8 – 697.3 ng/mL)

compared to the control group (median 256.0, IQR 212.0 – 308.0 ng/mL)

($p<0.0001$), and even higher sVAP-1 levels in in those with CHD (median 691.0,

IQR 684 – 854 ng/mL) compared to patients with NETs and no CHD (median

511, IQR 411.3 – 583.8 ng/mL) ($p<0.01$). However, given the low patient

numbers in the pilot study, further work was required to explore the role of

sVAP-1 in NETs given that no overall conclusion could be made from the

preliminary data due to a small sample cohort.

VAP-1 serum levels could be an effective stratification marker for patients with

NETs to predict outcomes and where to escalate therapy. More importantly

VAP-1 could be a new therapeutic target for NETs to prevent fibrotic complications and improve overall survival.

4.1.2 Aims

Preliminary data demonstrated increased concentrations of sVAP-1 in the peripheral blood of NET patients.

The aims of this section are to:

a)   Extend our cohort of patients in which we are measuring sVAP-1 and attempt to correlate the values we obtain with relevant clinical parameters.

b)   Compare sVAP-1 levels in the different NET cohorts and healthy volunteers. The NET cohorts included midgut NETs, pancreatic NETs (CHD is very rarely seen in pancreatic NETs so sVAP-1 are expected to be low) and CHD.

c)   Compare sVAP-1 levels pre- and post-treatment in midgut NETs.

4.2 Results

Soluble VAP-1 across all groups

In total, 99 patients have been included, consisting of 12 patients in the healthy control group, 20 patients with pancreatic NETs, 50 patients with midgut NETs and 17 patients with CHD. Circulating sVAP-1 levels differed significantly across the four groups ($p<0.001$), with median levels highest in the CHD group **(Figure 18)**. The median sVAP-1 (IQR) for the healthy controls, pancreatic NETs, midgut NETs and CHD were 740.4 ng/mL (IQR: 534.5 – 867.1), 979.4 ng/mL (IQR: 877.3 – 1620.0), 1005 ng/mL (IQR: 790.1 – 1148) and 1280 ng/mL (IQR: 961.2 – 1652.0) respectively.

From our own large NET and CHD centre's experience, CHD is very rarely seen in pancreatic NETs. Therefore a subgroup analysis was undertaken in which the pancreatic NET group was excluded, and the difference in sVAP-1 between the healthy controls, midgut NET and CHD groups was performed and remained significant ($p<0.001$, **Figure 19).** These results are in keeping with our pilot data which showed that sVAP-1 levels increased across the controls, midgut NET and CHD groups, differing from previous studies showing a decrease in sVAP-1 levels in tumour and in disease progression.(297, 320, 321)
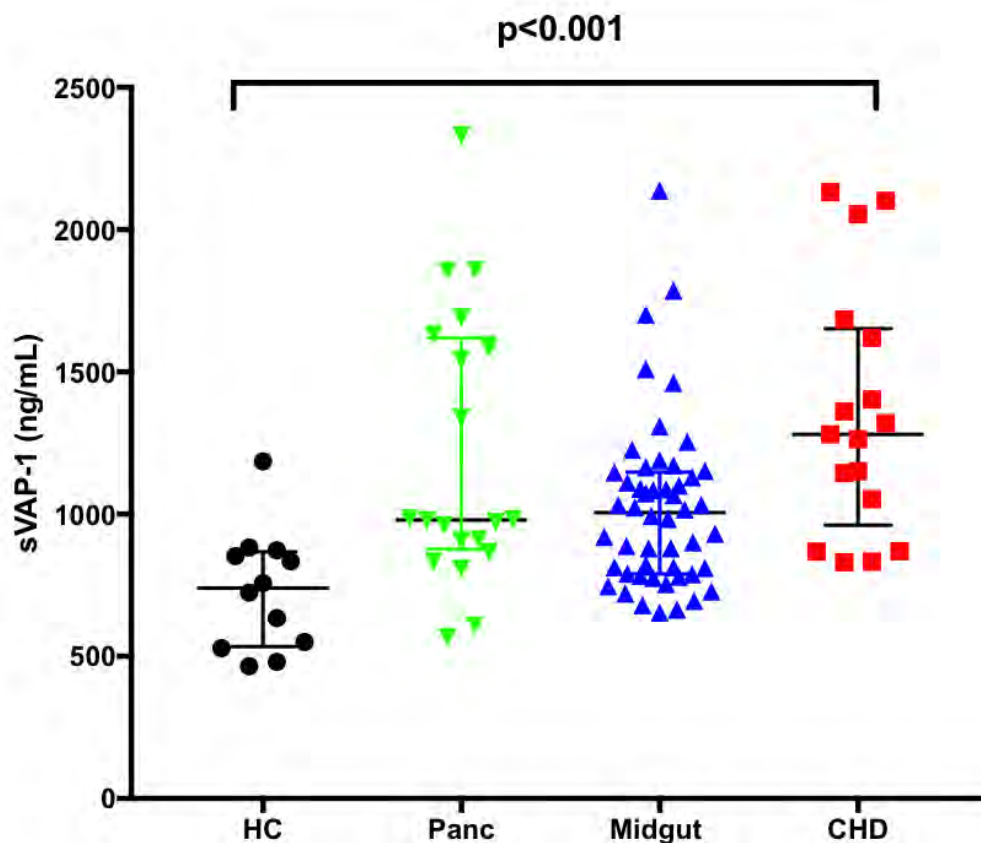
Figure 18: Levels of sVAP-1 shown across the healthy controls, pancreatic neuroendocrine tumour, midgut neuroendocrine tumour and CHD groups. A significant difference across the groups is seen, p<0.001. Post-hoc analysis showed a significant difference between the HC vs midgut NET group (p=0.032), HC vs pancreatic NET group (p=0.004), HC vs CHD group (p<0.001) and midgut NET vs CHD group (p=0.038). Post-hoc analysis showed both the pancreatic NET vs CHD group and pancreatic vs midgut NET groups had a p-Value of 1.000. HC, healthy controls. Panc, pancreatic.
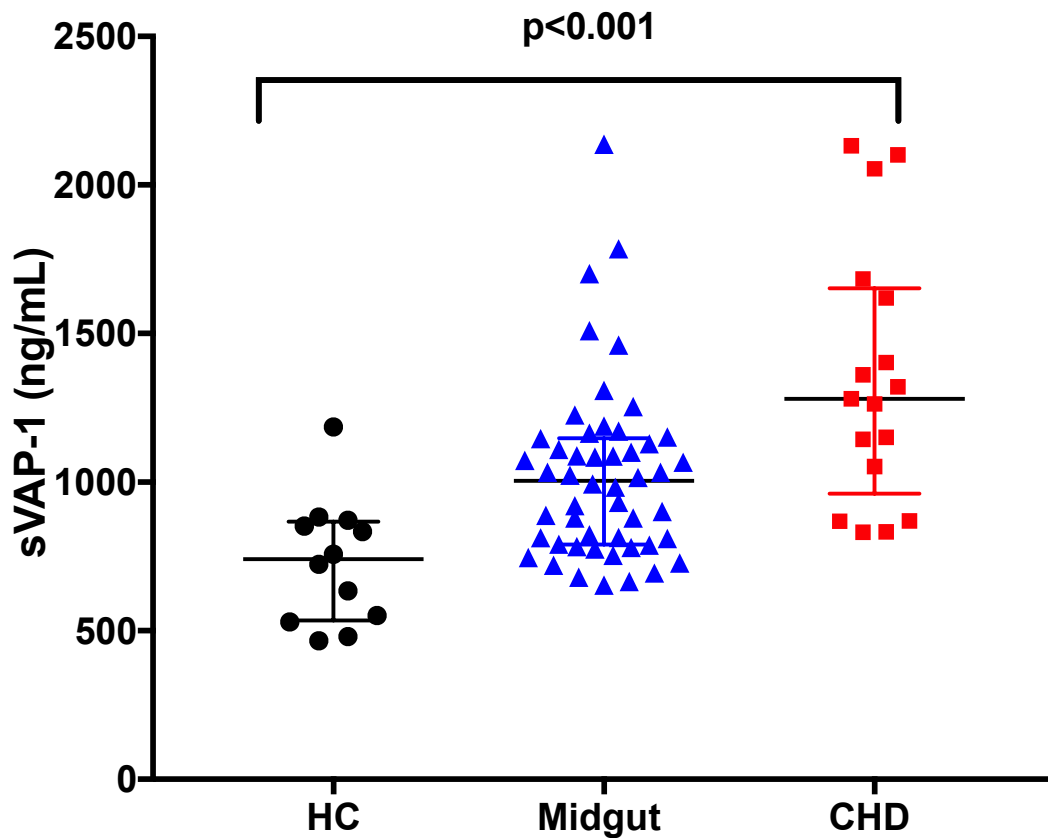
Figure 19: Levels of sVAP-1 shown across the healthy control, midgut neuroendocrine tumour and CHD groups. A significant difference, p<0.001, is observed. Post-hoc analysis demonstrated a significant difference between the HC vs midgut NET group (p=0.015), HC vs CHD group (p<0.001) and the midgut NET vs CHD groups (p=0.014).

Soluble VAP-1 levels and clinical variables

Various clinical variables were studied to assess their correlation with sVAP-1 levels. These included blood pressure, body mass index (BMI), HbA1c, gender, hypertension, cerebrovascular disease, ischaemic heart disease, hypercholesterolaemia (and being on a statin) and smoking. A previous study has shown significant correlations in women between sVAP-1 and BMI and triglycerides, and in men between sVAP-1 and diabetes, glucose and metabolic syndrome.(325) Out of the continuous variables correlated with sVAP-1, BMI

was found to be significantly negatively correlated with sVAP-1 (p=0.011), whilst

a significant positive correlation with HbA1c was detected (p=0.008), **Table 13.**

	Correlation with sVAP-1	
	rho	**p-Value**
Systolic BP (mmhg)	0.006	0.955
Diastolic BP (mmhg)	-0.060	0.582
BMI (kg/m^2)	-0.273	**0.011**
HbA1c (mmol/mol)	0.292	**0.008**

Table 13: Correlations between sVAP-1 and BP, BMI and HbA1c in the pancreatic neuroendocrine tumour, midgut neuroendocrine tumour and CHD groups. Data are reported as Spearman's rho correlation coefficients. Bold p-values are significant at p<0.05. BP, blood pressure. BMI, body mass index.

In patients where ethnicity was known (N=36), the majority were Caucasian

(97%). None of the categorical variables analysed were found to be significantly

associated with sVAP-1 levels. **Table 14.**

	Median (IQR) sVAP-1 (ng/mL)	p-Value
Gender		0.403
Male (N=51)	1016.1 (810.2 – 1308.4)	
Female (N=36)	1042.5 (874.4 – 1310.0)	
Hypertension		0.660
Yes (N=27)	1066.9 (780.1 – 1320.5)	
No (N= 60)	1019.8 (867.9 – 1267.1)	
Diabetes		0.084
Yes (N=15)	1189.2 (906.6 – 1631.2)	
No (N=72)	988.1 (818.0 – 1244.3)	
Cerebrovascular disease		0.675
Yes (N=6)	1010.5 (720.3 – 1461.7)	
No (N=81)	1023.6 (833.0 – 1280.4)	
Ischaemic heart disease		0.743
Yes (N=5)	1087.0 (920.3 – 1143.8)	
No (N=82)	1019.8 (831.1 – 1308.4)	
Hypercholesterolaemia		0.333
Yes (N=7)	833.0 (728.1 – 1189.2)	
No (N=80)	1028.1 (861.1 – 1314.4)	
On Statin		0.141
Yes (N=20)	1125.7 (905.1 – 1501.9)	
No (N=67)	982.6 (813.9 – 1280.4)	
Smoker		0.227
Yes (N=11)	931.2 (867.5 – 1339.7)	
No (N=34)	1019.4 (790.7 – 1320.5)	
Ex-smoker (N=12)	1147.4 (1034.2 – 1564.8)	

Table 14: Summary of categorical variables associated with sVAP-1 levels. Median and IQR of sVAP-1 shown, with p-Values derived from either Mann-Whitney U tests or Kruskal Whitney tests, as applicable.

Survival analysis

A survival analysis was performed in the pancreatic NET, midgut NET and CHD groups. Patients were split into three groups, based on the sVAP-1 tertiles. A trend towards higher mortality in higher sVAP-1 was observed, although this was not significant (p=0.153). **Figure 20.** These findings are similar to a study undertaken by our Birmingham group which showed that in patients with primary sclerosing cholangitis, higher sVAP-1 levels was significantly associated with the risk of liver transplantation or death (HR 2.02, 1.17 – 3.51, p=0.012).(291)
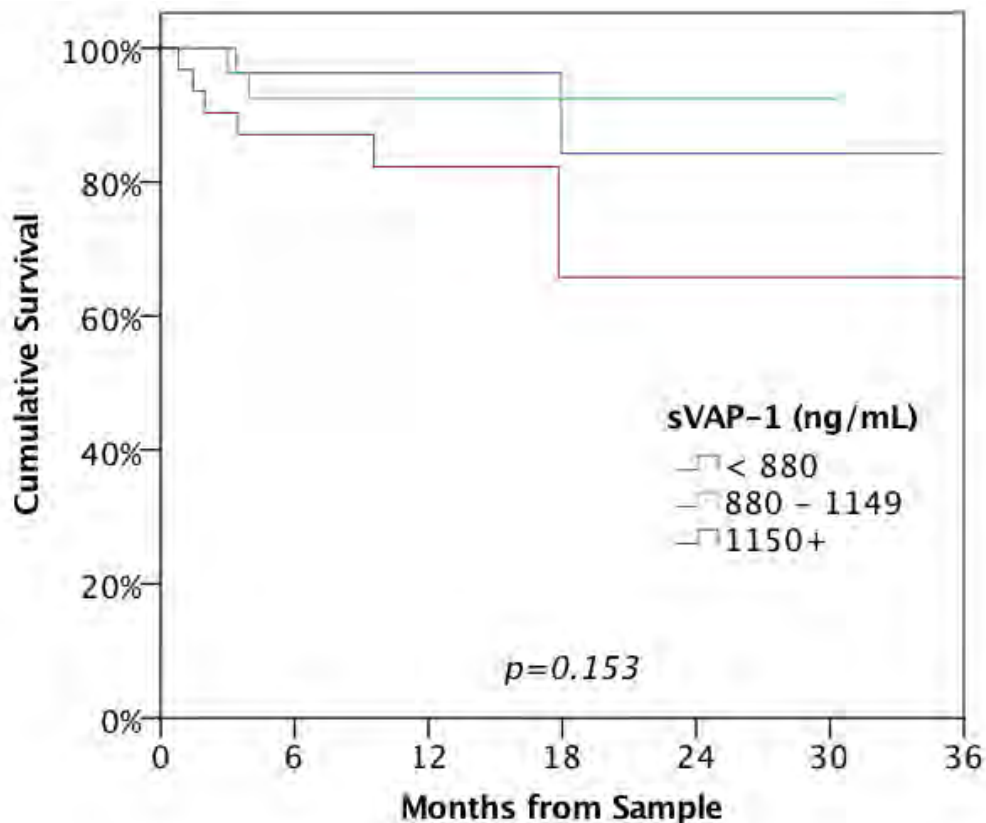
Figure 20: Kaplan Meier curve analysis based on sVAP-1 tertiles (<880, 880 – 1149 and 1150+ ng/mL).

Baseline characteristics of groups

Table 15 illustrates the baseline characteristics seen of patients in the midgut

NET and CHD groups. The pancreatic NETs have been analysed separately as

they are rarely associated with the development of CHD. A significant difference

was noted in the NT-proBNP level (p<0.001), with higher levels seen in the

CHD group than midgut NET, with medians of and 571 ng/L (IQR: 203 – 1691)

and 89 ng/L (IQR: 51 – 279) respectively. This significant difference is expected

given that NT-proBNP is released by the atria and ventricles in the heart in

response to wall stretch (265), and our results are also in keeping with previous

findings that showed significantly higher NT-proBNP levels in patients with CHD

compared with no CHD.(218) As expected, the presence of liver metastases

was found to be significantly higher in the CHD group, (p=0.028), whilst CHD

patients had a significantly lower rate of carcinoid symptoms than midgut NETs

(p=0.045). An explanation for the lower rate of carcinoid symptoms seen in

CHD compared with the midgut NET group is that prior to sample collection,

82% of patients in the CHD group were already on an SSA, compared to 6% of

the midgut NET group (p<0.001), therefore illustrating that their symptoms were

controlled by SSA treatment. The effect of surgical resection on sVAP-1 levels

was also analysed to assess whether resection and removal of the tumour

resulted in a reduction in sVAP-1 levels. Surgical resection was performed prior

to sample collection in 28% of patients in the midgut NET group and 12% of

patients in the CHD group (p=0.322). There was no significant difference

between the two groups regarding tumour grade (p=0.300) or CgA (p=0.148). In

the midgut NET group, the median sVAP-1 level in patients who had undergone

surgery pre-sample collection was 1024.3 ng/mL (IQR: 788.1 – 1128.9) and 925.8 ng/mL (800.5 – 1155.8) in those who had not undergone surgery pre-sample collection (p=0.856).

Patients from the midgut NET and CHD groups were then combined in order to analyse the NET patients as one group and increase the total cohort size, and associations between sVAP-1 levels and a range of factors were assessed. Levels of sVAP-1 were not found to differ significantly between those who had evidence of liver metastases and those who did not have evidence of liver metastases, p=0.745, with median levels of 1044.9 ng/mL (IQR: 813.9 – 1171.3) and 1052.4 ng/mL (IQR: 833.0 – 1262.6) respectively. In addition, no significant association between sVAP-1 and tumour grade was detected, with medians of 1052.4 ng/mL (IQR: 854.7 – 1171.3) seen in grade 1 and 1084 ng/mL (IQR: 993.7 – 1320.5) in grade 2, p=0.383.

	N	Midgut	CHD	p-Value
Demographics				
Age at sample (Years)	67	65.8 ± 11.5	68.2 ± 9.6	0.444
Male	67	32 (64%)	9 (53%)	0.565
Tumour features				
Grade	48			0.300
G1	31	25 (69%)	6 (50%)	
G2	17	11 (31%)	6 (50%)	
CgA (pmol/L)	62	206 (70 – 1062)	578 (160 – 3124)	0.148
24 hour urinary 5-HIAA (umol/24 hrs)	50	94.2 (29.9 – 174.9)	193.2 (90.05 – 788.1)	0.068
NT-proBNP (ng/L)	64	89 (51 – 279)	571 (203 – 1691)	**<0.001**
Liver metastases	67	33 (66%)	16 (94%)	**0.028**
Carcinoid symptoms	67	35 (70%)	7 (41%)	**0.045**
Facial flushing		22 (44%)	6 (35%)	0.581
Diarrhoea		20 (40%)	5 (29%)	0.565
Abdominal pain		17 (34%)	1 (6%)	**0.028**
Weight loss		16 (32%)	1 (6%)	**0.050**
Wheeze		-	-	-
Treatment pre-sample				
Had surgery for primary NET	67	14 (28%)	2 (12%)	0.322
On SSA	67	3 (6%)	14 (82%)	**<0.001**
Type of SSA	17			**0.029**
Sandostatin	11	-	11 (79%)	
Lanreotide	6	3 (100%)	3 (21%)	

Table 15: Summary of patient demographics, tumour features and treatment pre-sample across the midgut neuroendocrine tumour and CHD groups. The groups are midgut NET (N=50) and CHD (N=17). Data are reported as N (%), with p-values from Fisher's exact tests; mean±SD, with p-Values from independent samples t-tests, or median (IQR), with p-Values from Mann-Whitney U tests, as applicable. Bold p-values are significant at p<0.05. CgA, chromogranin A, 5-HIAA, 5-hydroxyindoleacetic acid. SSA, somatostatin analogue.

Correlation between sVAP-1 and tumour features

The associations between sVAP-1 with various tumour features, including CgA, 24 hour urinary 5-HIAA and NT-proBNP, were assessed in the combined midgut NET and CHD groups using Spearman's rho correlation coefficients. CgA and 24 hour urinary 5-HIAA are two biochemical tumour markers used in clinical practice in NETs, with the urinary 5-HIAA reflecting the hormone-secretion activity of the tumour and CgA reflecting tumour bulk. NT-proBNP is the biochemical marker used in CHD surveillance in NET patients. Positive correlations were seen between sVAP-1 and CgA, 24 hour urinary 5-HIAA and NT-proBNP, although none reached statistical significance. In the CHD group alone, positive correlations were found again between the three tumour features and sVAP-1, again not reaching statistical significance. **Tables 16a and 16b.** Statistical significance is likely not seen between sVAP-1 and the biochemical markers assessed given that the current markers used in clinical practice are not associated with the presence of fibrosis in NETs.

	N	sVAP-1 (ng/mL)	p-Value
CgA	62	0.149	0.247
24 hour urinary 5-HIAA	50	0.265	0.063
NT-proBNP	64	0.218	0.084

Table 16a: Correlations between sVAP-1 and CgA, 24 hour urinary 5-HIAA and NT-proBNP in both the midgut neuroendocrine tumour and CHD groups. Data are reported as Spearman's rho correlation co-efficients.

	N	sVAP-1 (ng/mL)	p-Value
CgA	16	0.406	0.119
24 hour urinary 5-HIAA	13	0.516	0.071
NT-proBNP	14	0.147	0.615

Table 16b: Correlations between sVAP-1 and CgA, 24 hour urinary 5-HIAA and NT-proBNP in the CHD group. Data are reported as Spearman's rho correlation co-efficients.

Longitudinal analysis of sVAP-1

A longitudinal analysis was performed to assess whether sVAP-1 could be a treatment response marker. Samples were taken in the midgut NET group prior to (termed first sample) and following treatment (termed second sample) with either surgery, SSA or both.

Due to time limitations in this project, a total of 23 patients were included in the analysis. At the time of first sample, 61% were male and the median age was 62 years (IQR: 53 – 70). Pre-first sample, 9 (39%) patients had undergone primary surgical resection and 1 (4%) patient was treated with SSA. Treatment was started after a median of 27 days (IQR: 0-70) following the first sample being taken, and 18 (78%) patients were started on SSA, 3 (13%) patients underwent surgery and 2 (9%) were followed up after having both treatments. The second sample was taken a median of 203 days (IQR: 56 – 260) following treatment, by which time 21 (91%) patients were on SSA. **Table 17.**

Factor	Statistic
Age at First Sample (Years)	62 (53 - 70)
Gender (Male)	14 (61%)
Grade	
1	14 (74%)
2	5 (26%)
Liver Metastases	16 (70%)
Surgery Pre-First Sample	9 (39%)
SSA Pre-First Sample	1 (4%)
Days First to Second Sample	231 (92 - 330)
First Sample to Treatment	27 (0 - 70)
Treatment to Second Sample	203 (56 - 260)
Treatment During Follow-up	
SSA	18 (78%)
Surgery	3 (13%)
Surgery + SSA	2 (9%)
On SSA by second sample	21 (91%)
Type of SSA	
Lanreotide	6 (29%)
Sandostatin	15 (71%)

Table 17: Summary of patient demographics in the longitudinal analysis in the midgut neuroendocrine tumour group. Data are reported as median (IQR), or as N (%), as applicable.

Levels of sVAP-1 were recorded at both sample timepoints for all patients included in this analysis. There was no significant change observed following treatment with medians of 1016 ng/mL (IQR: 812 – 1140) versus 1023 ng/mL (IQR: 927 – 1197) at the first and second sample taken respectively (p=0.501).

Figure 21. The changes in CgA, NT-proBNP and 24 hour urinary 5-HIAA were also assessed, but data were not recorded for all 23 patients, with the sample size ranging from N=8 – 15. There were no significant changes seen between the first and second samples for any of the three markers (p=0.092, p=0.497 and p=0.383, for CgA, NT-proBNP and 24 hour urinary 5-HIAA respectively).

Table 18.

Analyses were then performed to assess whether sVAP-1 levels differed based on whether or not patients had undergone surgery prior to the first sample (**Table 19**). This found no significant differences between the surgical and no surgical groups with respect to the first and second samples, or in the degree of change after treatment, with neither group having significant changes in sVAP-1 levels after surgery. A similar analysis was performed for those 20 patients who had imaging performed after the first sample was taken, to assess whether disease progression correlated with sVAP-1 levels (**Table 20**). None of these comparisons between the stable (N=15) and progressing (N=5) disease groups were found to be statistically significant.
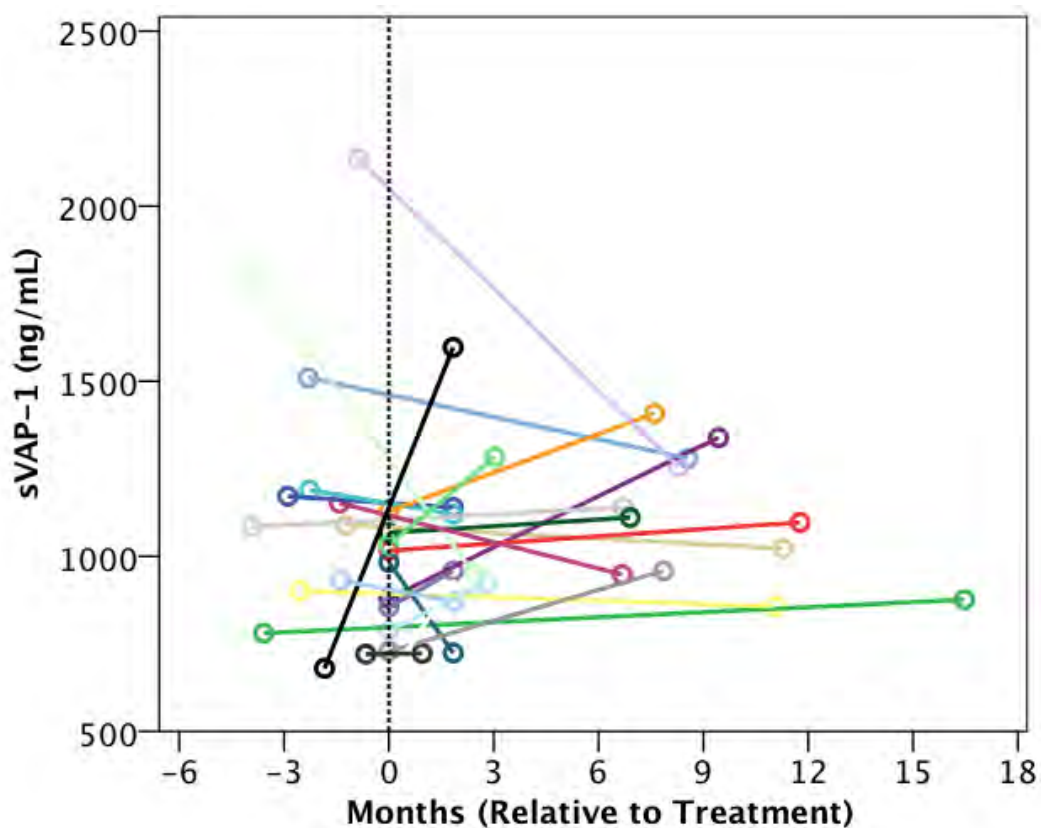
Figure 21: Changes in sVAP-1 levels between the first and second samples in the midgut neuroendocrine tumour group. Prior to treatment, the median sVAP-1 was 1016 ng/mL (IQR: 788 – 1152). This was not found to change significantly by the second sample following

treatment (p=0.501), with N=13 patients having an increase in VAP-1, and N=10 a reduction, resulting in a median of 1023 ng/mL (IQR: 921 – 1255). Each colour represents an individual patient.

Marker	N	Median IQR		N Patients with:		p-Value
		Sample 1	Sample 2	Reduction	Increase	
sVAP-1	23	1016 (821 - 1140)	1023 (927 - 1197)	10	13	0.501
5-HIAA*	8	107 (32 - 620)	37 (20 - 239)	6	2	0.383
CgA	12	170 (67 - 1403)	57 (41 - 259)	10	2	0.092
NT-proBNP	15	68 (51 - 131)	110 (43 - 165)	7	8	0.497

Table 18: Changes in sVAP-1, 24 hour urinary 5-HIAA, CgA and NT-proBNP between the first and second samples in the longitudinal analysis in the midgut neuroendocrine tumour group. Only patients with samples at both timepoints are included in the analysis. p-Values are from Wilcoxon's test. * represent 24 hour urinary 5-HIAA collection.

sVAP-1 (ng/mL)	Surgery Pre-First Sample		p-Value (Yes vs. No)**
	No (N=14)	Yes (N=9)	
First Sample	916 (728, 1171)	1033 (983, 1129)	0.557
Second Sample	990 (876, 1255)	1097 (948, 1120)	0.890
Change	-15 (-67, 230)	81 (-69, 133)	0.829
p-Value (First vs. Second)*	0.903	0.496	-

Table 19: Subgroup analyses for sVAP-1 by surgery in the longitudinal analysis in the midgut neuroendocrine tumour group. Data are reported as median (IQR). *Wilcoxon's tests comparing the first and second sample values within each subgroup. **Mann-Whitney tests, comparing values between those that did and did not undergo surgery before the first sample.

| sVAP-1 (ng/mL) | Disease on Imaging after First Sample | | p-Value (Stable vs. Progression)** |
	Stable (N=15)	Progression (N=5)	
First Sample	1067 (788, 1152)	880 (855, 1033)	0.672
Second Sample	952 (876, 1139)	1255 (958, 1284)	0.163
Change	-44 (-203, 133)	230 (104, 251)	0.349
p-Value (First vs. Second)*	0.978	0.625	-

Table 20: Subgroup analyses for sVAP-1 by imaging findings after the first sample in the longitudinal analysis in the midgut neuroendocrine tumour group. Data are reported as median (IQR). *Wilcoxon's tests comparing the first and second sample values within each subgroup. **Mann-Whitney tests, comparing values between those with stable versus progressive disease.

Carcinoid syndrome symptoms in longitudinal analysis

Changes in carcinoid syndrome symptoms were also assessed between the two samples taken. At the time of the first sample, 70% of patients displayed at least one carcinoid symptom, reducing significantly to 35% at the second sample (p=0.021, **Table 21**). All five individual symptoms were found to occur at a lower rate at the second sample, with the exception of wheeze, which had a rate of 0% at both times. However, a significant change was only noted in the rate of weight loss, falling from 22% to 0% (p<0.001).

Symptoms	First Sample	Second Sample	p-Value
Carcinoid Syndrome	16 (70%)	8 (35%)	**0.021**
Flushing	11 (48%)	6 (26%)	0.125
Diarrhoea	10 (43%)	3 (13%)	0.065
Abdominal Pain	9 (39%)	4 (17%)	0.180
Wheeze	0 (0%)	0 (0%)	-
Weight Loss	5 (22%)	0 (0%)	**<0.001**

Table 21: Changes in carcinoid syndrome symptoms between the first and second samples in the midgut neuroendocrine tumour longitudinal analysis. Data are reported as N (%), with p-values from McNemar's test. Bold p-values are significant at p<0.05.

Pancreatic NET analysis

Table 22 summarises the baseline characteristics in the pancreatic NET group. The mean age was 61.2 years and half the group were male. The median tumour size was 25.5mm (IQR: 18.8 – 47.8). Liver metastases was present in 7 (35%) patients and 5 (25%) patients experienced carcinoid symptoms. Three patients (15%) were on SSA pre-sample, all of whom were on Lanreotide Autogel.

	N	Pancreatic NET
Demographics		
Age at sample (Years)	20	61.4 ± 12.2
Male	20	10 (50%)
Tumour features		
Grade	18	
G1		8 (44%)
G2		10 (56%)
CgA (pmol/L)	20	43 (25 – 110)
24 hour urinary 5-HIAA (umol/24 hrs)	3	19.3 (7.0 – 33.5)
NT-proBNP (ng/L)	18	89 (42 – 135)
Liver metastases	20	7 (35%)
Size (mm)	18	25.5 (18.8 – 47.8)
Carcinoid symptoms	20	5 (25%)
Facial flushing		1 (5%)
Diarrhoea		1 (5%)
Abdominal pain		4 (20%)
Weight loss		1 (5%)
Wheeze		-
Treatment pre-sample		
On SSA	20	3 (15%)

Table 22: Summary of patient demographics, tumour features and treatment pre-sample in the pancreatic neuroendocrine tumour group. Data are reported as N (%), mean±SD, or median (IQR), as applicable.

Correlations between sVAP-1 levels and various factors were then assessed, none of which were found to be statistically significant, **Table 23.**

	N	sVAP-1 (ng/mL)	p-Value
CgA	20	-0.083	0.729
24 hour urinary 5-HIAA	3	0.500	0.667
NT-proBNP	18	0.157	0.533
Grade	18	-0.108	0.670
Size	18	-0.119	0.639
Liver metastases	20	0.027	0.909

Table 23: Correlations between sVAP-1 and CgA, 24 hour urinary 5-HIAA, NT-proBNP, tumour grade, tumour size and liver metastases in the pancreatic neuroendocrine tumour group. Data are reported as Spearman's rho correlation co-efficients.

Comparisons of markers across the midgut NET, pancreatic NET and CHD groups

Comparisons of CgA, NT-proBNP and 24 hour urinary 5-HIAA were performed across the pancreatic NET, midgut NET and CHD groups, using Kruskal-Wallis tests. A significant difference was seen across the three groups for all markers (CgA, $p<0.001$; NT-proBNP, $p<0.001$ and 24 hour urinary 5-HIAA, $p=0.013$). Post-hoc analyses using Dunn's multiple comparisons tests showed that a significant difference was present between the pancreatic NET and midgut NET groups ($p=0.002$), and the pancreatic NET and CHD groups ($p<0.001$) for CgA; the pancreatic NET and CHD groups ($p<0.001$), and the midgut NET and CHD groups ($p<0.001$) for NT-proBNP; and the pancreatic NET and CHD groups ($p=0.013$) for 24 hour urinary 5-HIAA. **Table 24.**

	Pancreatic	Midgut	CHD	p-Value
CgA (pmol/L)	43 (25 – 110)	206 (70 – 1062)	578 (160 – 3124)	**<0.001**
NT-proBNP (ng/L)	89 (42 – 135)	89 (51 – 279)	571 (203 – 1691)	**<0.001**
24 hour urinary 5-HIAA (umol/24 hrs)	19.3 (7.0 – 33.5)	94.2 (29.9 – 174.9)	193.2 (90.5 – 788.1)	**0.013**

Table 24: Comparisons of CgA, NT-proBNP and 24 hour urinary 5-HIAA across the pancreatic neuroendocrine tumour, midgut neuroendocrine tumour and CHD groups. Data reported as median (IQR), with p-Values from Kruskal Wallis tests. Bold p-values are significant at $p<0.05$. ***Dunn's Tests for tumour markers:*** CgA: pancreatic vs midgut, $p=0.002$, pancreatic vs CHD, $p<0.001$; NT-proBNP: pancreatic vs CHD ($p<0.001$), midgut vs CHD ($p<0.001$); 24 hour urinary 5-HIAA: pancreatic vs CHD, $p=0.013$.

Therefore, the sVAP-1 results in this chapter have shown that levels increase across the healthy controls, pancreatic NETs, midgut NETs and CHD groups with levels highest in CHD. Interestingly, there was no significant difference seen between sVAP-1 levels in pancreatic NETs vs. midgut NETs or CHD. No significant difference in sVAP-1 levels between the first and second samples in the midgut NET group was seen, similar to the results assessing changes in the current biochemical markers used in clinical practice (CgA, NT-proBNP and 24 hour urinary 5-HIAA) between the two samples.

4.3 Discussion

Despite NETs being slow-growing tumours, significant gastrointestinal and cardiac complications can occur related to intestinal, peritoneal and cardiac valve fibrosis, particularly in midgut NETs, which are the commonest site for tumour formation. Such complications are associated with significant morbidity and mortality, and at present there are no effective diagnostic markers or treatments targeted at diagnosing the fibrosis. Previous work has demonstrated that circulating sVAP-1 levels is higher in the presence of liver fibrosis with levels correlating with the degree of fibrosis present, as well as higher sVAP-1 levels are associated with a poorer liver transplant-free survival.(277, 291) Levels of sVAP-1 have been shown to be lower in colorectal cancer (297) and decrease with tumour progression in both colorectal and gastric cancer (320, 321), whereas sVAP-1 levels were found to be high in HCC.(322) By gaining a better understanding of sVAP-1 being associated with the development of scarring and fibrosis in NETs, patients could be stratified based on abundance of sVAP-1, in addition to offering the potential target for new treatments to cure or prevent fibrosis. A non-invasive method in screening for fibrosis in NETs is therefore paramount, so a diagnosis can be made and treatment instituted in a timely fashion.

The sVAP-1 analysis has shown results in keeping with the preliminary work previously carried out. A significant difference in sVAP-1 levels was observed across the healthy controls, midgut NETs, pancreatic NETs and CHD groups, with the highest levels seen in the CHD cohort. This reflects the degree of

fibrosis present in CHD resulting in right-sided valvular disease and heart failure. A Kaplan Meier curve for survival analysis across the midgut NET, pancreatic NET and CHD groups showed a trend that higher sVAP-1 levels are associated with poorer survival, although this was not statistically significant. This may not have reached statistical significance as the sample size was small and a longer duration of disease is required given that NETs are known to be generally slow-growing tumours. Previous work in Birmingham have shown that higher circulating VAP-1 levels are associated with a poorer liver transplant-free survival.(291) The source of sVAP-1 is not known in NETs, but one possible source could be from fibroblasts present in the fibrotic stroma and fibrotic area of the CHD valve.

After excluding the pancreatic NET group, comparisons across the three remaining groups (healthy controls, midgut NETs and CHD) found sVAP-1 levels were significantly different across the groups, again with levels seen highest in CHD. Post-hoc analysis demonstrated that the pairs exhibiting the significant change in sVAP-1 levels were healthy controls vs. midgut NETs (p=0.015), healthy controls vs. CHD (p<0.001) and midgut NETs vs CHD (p=0.014). In the midgut NET group, 70% of patients experienced carcinoid symptoms compared to 41% of CHD patients, p=0.045. Patients with CHD are likely to have liver metastases and develop carcinoid symptoms; however in these patient groups, over 80% of patients in the CHD cohort were already on a SSA injection at the time of sample collection compared to 6% of midgut NET patients, and therefore had controlled carcinoid symptoms.

The longitudinal analysis of sVAP-1 first and second samples showed variation in the changes seen between both samples, with 10 patients showing a reduction in the sVAP-1 levels and 13 patients having an increase in sVAP-1 levels following treatment, p=0.501. The markers currently used in clinical practice, CgA, NT-proBNP and 24 hour urinary 5-HIAA, also did not have a significant change in their measurements following treatment (p=0.092, p=0.497 and p=0.383 respectively). Serial measurements were not taken following treatment and the follow up sVAP-1 samples were taken at various timepoints (median of 203 days post-treatment, IQR: 56 – 260) for individual patients. Additionally, the half-life of circulating sVAP-1 is currently unknown, and therefore the optimal timepoint on when to measure the sVAP-1 level following treatment also remains unknown. In addition to the circulating form, future work could also assess the amine oxidase enzyme activity of VAP-1 in the different cohorts of patients. Having primary surgical resection prior to the first sample being taken did not influence the sVAP-1 levels, nor was there any significant change observed in sVAP-1 levels between the first and second samples. Similarly, no significant change was seen in sVAP-1 levels between patients who had stable disease or evidence of progression on imaging (p=0.349). A significant reduction in carcinoid symptoms was found following treatment (p=0.021). Therefore, the improvement seen in carcinoid symptoms did not correlate with the change in sVAP-1 levels between the first and second samples. Given that the half-life of VAP-1 is not known, future work should include analysing further sequential serum samples taken at more follow-up dates following treatment commencement including surgical resection in order

to assess any change seen in sVAP-1 more accurately. The current biomarkers used in clinical practice in NETs and CHD reflect the tumour bulk, functional status / hormone secretion and the presence of possible CHD. However, compared to VAP-1, none of these biomarkers indicate the presence of fibrosis which plays an important role in the complications, morbidity and mortality seen in NETs and CHD.

The pancreatic NET sVAP-1 levels were found to be significantly higher than the healthy controls (p=0.004), but were not significantly different to either the midgut NET or the CHD groups (p=1.000 for both comparisons). Comparing the median CgA, NT-proBNP and 24 hour urinary 5-HIAA across the pancreatic NETs, midgut NETs and CHD groups, the pancreatic NET group had the lowest values for CgA and 24 hour urinary 5-HIAA (p<0.001 and p=0.013, respectively). Therefore, sVAP-1 levels may be indicative of the degree of fibrosis present in pancreatic NETs, which is not the case with the current markers used in clinical practice. Further work to analyse this group further would require more patients to be included and then performing further statistical analysis using ROC curves or multivariate analysis to draw the comparisons between the various biochemical markers. This may be cost-effective as despite having high sVAP-1 levels in pancreatic NETs, the current tumour markers used in clinical practice are significantly lower in this group compared with the midgut NET and CHD groups. Therefore, fibrosis occurring in pancreatic NETs may be associated with complications, and treatment targeting VAP-1 may be beneficial in this group of patients as well.

4.4 Conclusion

In conclusion, the sVAP-1 levels seen in the groups analysed have shown that the levels are highest in the CHD group and levels are significantly higher in the pancreatic NET, midgut NET and CHD groups vs the healthy controls. Interestingly, the sVAP-1 levels seen in pancreatic NETs are higher than initially expected, suggesting an element of fibrosis occurring in the tumour stroma in pancreatic NETs, although the release of soluble VAP-1 from fibroblasts has yet to be demonstrated in this context. The levels of sVAP-1 were raised in both the pancreatic and midgut NETs, yet fibrotic complications mainly occur in midgut NETs. Most pancreatic NETs are characterised mainly by a hypervascular appearance with a less prominent fibrotic stroma.(326) However, previous studies have also shown a group of serotonin-expressing pancreatic NETs that are associated with a fibrous stroma.(327, 328) This group of tumours was found to differ from serotonin-positive ileal NETs in their histological pattern and had less positive staining for CDX2, possibly suggesting that pancreatic NETs are derived from a separate cell lineage compared to the enterochromaffin cell type seen in midgut NETs.(327, 328) This could also explain why sVAP-1 levels are increased in pancreatic NETs in this study as a fibrous stroma could be present in the pancreatic NETs. The 24 hour urinary 5-HIAA was normal in this study in the pancreatic NET group, but only 3 out of 20 patients had a result for this marker. The fibrotic pancreatic NETs are likely to have more benign biological characteristics compared to other fibrotic NETs (327), and this could explain why fibrotic complications, including CHD, is not commonly seen in pancreatic NETs. A positive significant correlation was found between HbA1c

and sVAP-1 levels. This is in keeping with previous work which have shown elevated sVAP-1 levels in hyperglycaemia and positive correlations with sVAP-1.(292, 295, 329) Survival analysis showed that higher sVAP-1 levels are associated with a poorer survival, although this was not statistically significant, likely due to the small sample size in this analysis. The longitudinal analysis did not show any significant changes in the sVAP-1 level between the first and second samples, which is likely to be multifactorial: serial measurements were not taken, and therefore the trend in sVAP-1 is not known after a particular timepoint following treatment; sample size is small and the circulating sVAP-1 half-life is currently not known. The changes in sVAP-1 did not correlate with the significant reduction in carcinoid symptoms seen following treatment, therefore suggesting the symptoms are hormone-related and not associated with the amount of fibrosis present.

Therefore, the overall findings show that the circulating form of sVAP-1 could be a possible biomarker used in screening for fibrosis in the NET patient cohorts and could be used as a stratification tool in patients as well. Further work is required to increase both patient numbers and samples for individual patients in the longitudinal analysis, as sVAP-1 may also have a role both as a prognostic marker as well as a treatment response marker.

CHAPTER 5:

IMMUNOHISTOCHEMICAL ANALYSIS OF MIDGUT NEUROENDOCRINE TUMOUR STROMA

5.1 Introduction and aims

5.1.1 Introduction

NETs are a slow-growing cancer and are associated with desmoplastic reactions, both local and distant to the tumour. Complications of fibrosis include the development of CHD and intestinal and peritoneal fibrosis.(196) Midgut NETs are associated with mesenteric fibrosis leading to intestinal oedema, ischaemia and obstruction causing significant morbidity in this group of patients.(330) Up to 50% of patients with a midgut NETs develop mesenteric fibrosis.(331) Mesenteric fibrosis is caused by an extensive desmoplastic reaction surrounding a mesenteric mass.(330) Surgery at present is the only treatment option that can be offered to patients with the fibrotic complication.(332) However, following post-surgical resection further complications can occur, these including malabsorption, short bowel syndrome and bile acid malabsorption.(194) In addition to resulting in significant morbidity, mesenteric fibrosis is also a poor prognostic factor relating to overall survival.(196, 198) There has been literature published describing possible factors of fibrosis development with treatments targeting these mediators.

Understanding of the tumour microenvironment is crucial given that this may influence tumour growth, tumour cell survival and facilitate metastases, therefore causing tumour progression.(333) It has been shown that the midgut NET stroma differs to other cancers with a predominant desmoplastic reaction occurring with limited leucocyte involvement.(330, 334) In addition to the tumour cells, fibroblasts are a major cellular component of tumour stroma. In cancer, these fibroblasts

(cancer-associated fibroblasts, CAFs) have a different phenotype and express α-SMA.(330) Unlike quiescent fibroblasts, CAFs have the potential to proliferate and form ECM and growth factors.(335) Midgut NETs express high levels of α-SMA in the fibroblast population present in the tumour stroma.(336) Kidd et al showed that cells from tumour stroma had the stellate appearance of CAFs and following stimulation with TGFβ1, led to upregulation of growth factor transcription, which highlights the possible role of CAFs in regulating fibrotic signalling in tumour stroma.(337) Leucocyte infiltration has been shown to be limited in NETs, with macrophages being the dominant leucocyte found, staining positive for TGFβ and platelet-derived growth factor, therefore acting as another mediator stimulating fibrosis.(334, 338) ECM remodelling and a change in the composition of the ECM has been found in both cancer and fibrotic conditions and inappropriate fibroblast activation seen in fibrotic conditions leads to increased collagen production.(339) Type I collagen and fibronectin are the main components found in tumour ECM (340) and only a limited understanding on the exact ECM composition in midgut NETs is currently known. It may be that the ECM composition may influence tumour function in midgut NETs by causing the tumour cells to release biochemical, including serotonin, and biomechanical signals, including adenosine triphosphate.(341) Kidd et al showed the collagen III expression surrounding CAFs in small bowel fibrosis.(337) The ECM also contain various proteoglycans, and transcription levels in these proteoglycans show changes in NETs during tumour progression, although their role in fibrosis development in midgut NETs remains unclear.(342)

Fibrotic complications of midgut NETs are therefore associated with significant morbidity and mortality, and at present, there are no effective diagnostic markers or treatments targeted at diagnosing the fibrosis. The application of non-invasive biomarkers could result in beneficial clinical implications. VAP-1 may have a significant role in NETs, given that the enzyme activity of VAP-1 is dependent on having amines as the substrate, and therefore either the amines secreted by the tumour, or breakdown products from monoamine oxidases or other amine oxidases, can stimulate certain cell populations to produce VAP-1. Therefore, VAP-1 could be a potential biomarker in diagnosing fibrosis, which could also be a treatment target in the future.

5.1.2 Aims

The overall aim is to understand the contribution of VAP-1 to the fibrosis that develops near and distal to the tumour which can lead to the onset of desmoplastic reactions.

The aim of this section is to:

a) Study the expression of VAP-1 in primary tumours from midgut NET primary and metastases.

b) Define the cell-specific expression of VAP-1 in the tumour microenvironment.

c) Correlate VAP-1 expression in the midgut NETs with the immune microenvironment.

5.2 Results

Tissue sections used

In total, 10 cases of midgut NETs with LN metastases were stained with various primary antibodies, in addition to 4 primary midgut NETs. **Figures 22** and **23** represent tissue sections stained with VAP-1 and collagen I, and the haematoxylin and eosin stained sections, respectively. **Figure 22** shows the presence of positive brown staining (representing VAP-1 and collagen I) in the peri-tumoural stroma surrounding the clusters of tumour cells. Collagen I was used as it is a known ECM marker. The positive staining of both markers is in a very similar distribution and can also be seen to be present lining adipocytes. Compared to collagen I, some VAP-1 positive staining can also be seen within the tumour cells. **Figure 23** shows the presence of clusters of NET cells and extracellular matrix with immune cell aggregates amongst the tumour cell areas.
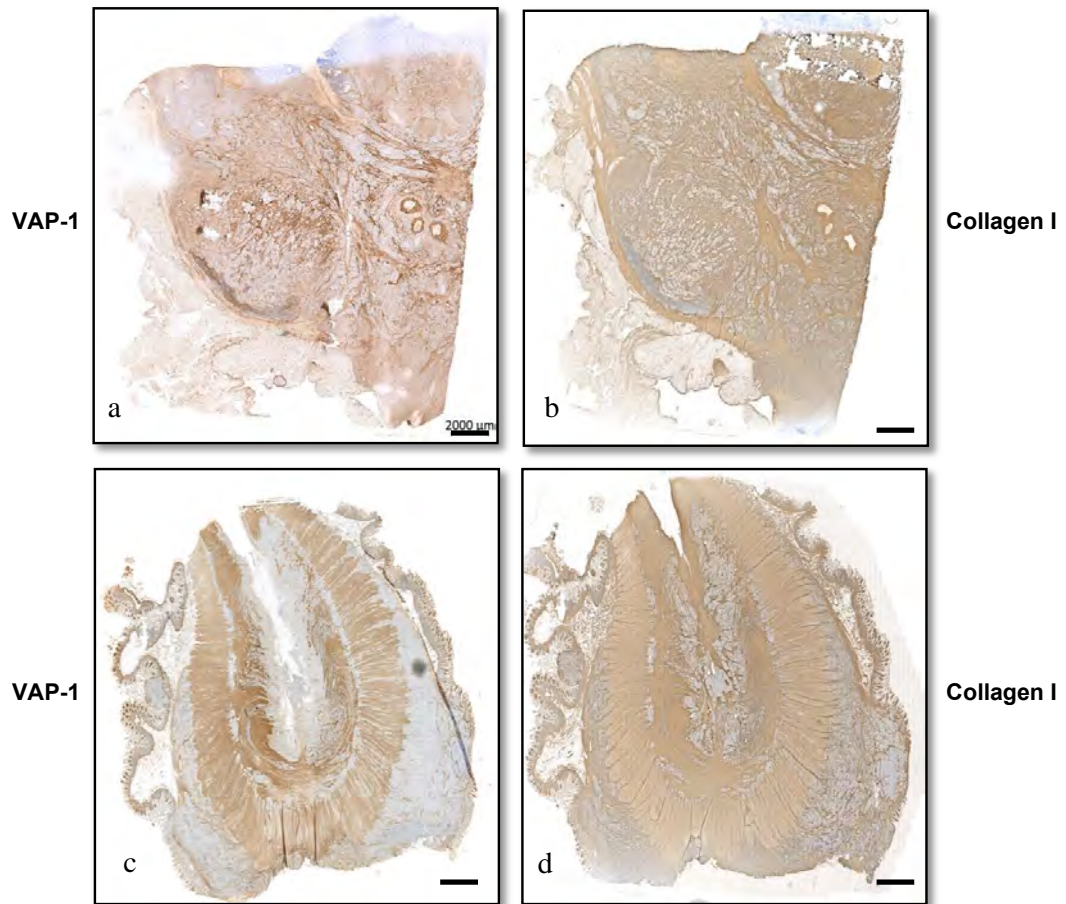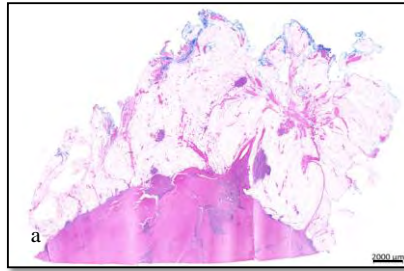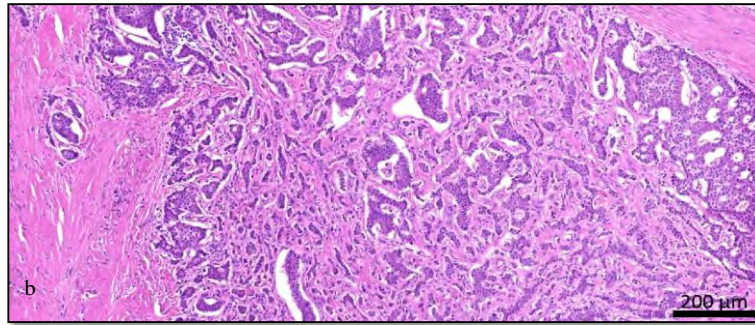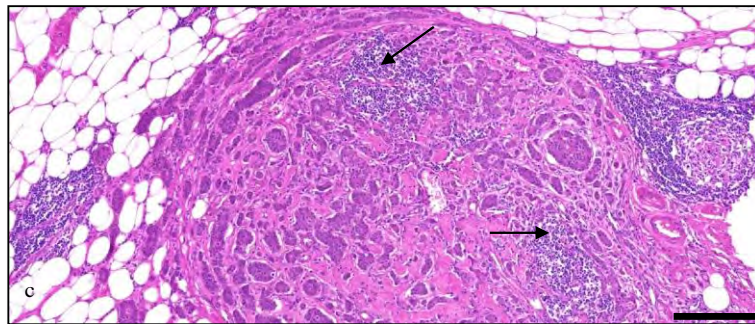
Figure 22: Representative images of paired whole midgut neuroendocrine tumour cases for VAP-1 staining and Collagen I staining. VAP-1 staining is shown in images a and c; collagen I staining is shown in images b and d; n=2. Objective 20X. Scale bars 2000 μm.

Whole midgut NET case: Haematoxylin and Eosin stain

Cropped area of whole midgut NET case

Cropped area of whole midgut NET case

Figure 23: Representative images of whole midgut neuroendocrine tumour case and cropped areas stained with haematoxylin and eosin. Whole midgut case is shown in image a, and cropped areas are shown in images b and c, n=1. Scale bar image a 2000 μm. Scale bars images b and c 200 μm. Haematoxylin and Eosin stain. Clusters of neuroendocrine tumour cells are seen in images b and c and extracellular matrix can be seen in image b. Immune cell aggregates can be seen in image c amongst the tumour cell areas (black arrows).

Threshold images

The VAP-1 and collagen I staining were analysed using Ilastik and Fiji Image J in order to establish the quantification of the % area of epitope expression. The threshold images represent the positive brown Ab staining on the images taken by Zen software and is seen as red on the images below. **Figure 24.**
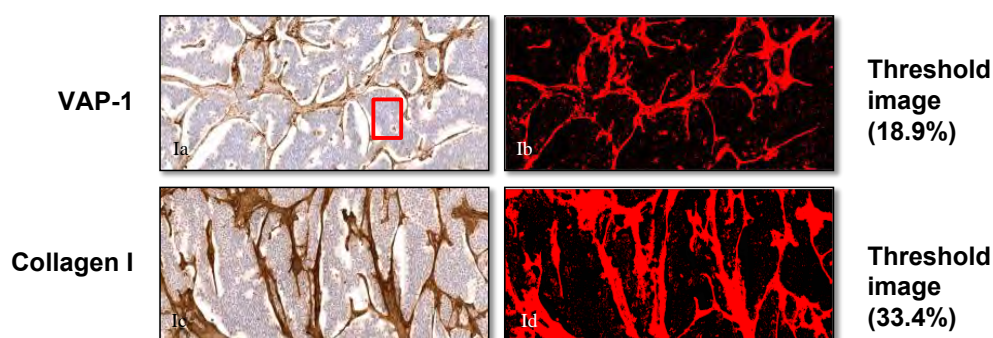

Figure 24: Representative images of cropped tumour areas of midgut neuroendocrine tumours with LN metastases stained with VAP-1 and Collagen I with matched threshold images. Image Ia represents VAP-1 staining and image Ic represents collagen I staining. Images Ib and Id represent the threshold images of Ia and Ic respectively, used for the quantification of % area of expression (staining shown as red); 18.9% and 33.4% respectively; n=1. Granules of VAP-1 (represented by a box in image Ia) within the tumour cells can be seen.

Percentage area of VAP-1 and Collagen I expression

Cropped tumour areas were taken to analyse the median (IQR) individual % area of VAP-1 and collagen I expression in all 14 midgut NET cases, **Figure 25**. Cropped areas were then taken to correlate median (IQR) VAP-1 expression with collagen I expression, **Table 25** and **Figure 26**. A positive correlation was found between VAP-1 and collagen I expression, although this was not significant (Spearman's rho correlation co-efficient 0.310, p=0.281). For whole

images used, a positive correlation was again seen between VAP-1 and

collagen I expression (Spearman's rho correlation co-efficient 0.064, p=0.829),

Table 26.

Median % expression (IQRs)	Case 1 (N=5)	Case 2 (N=3)	Case 3 (N=5)	Case 4 (N=5)	Case 5 (N=4)	Case 6 (N=4)	Case 7 (N=4)	Case 8 (N=5)	Case 9 (N=5)	Case 10 (N=5)	Case 11* (N=5)	Case 12* (N=5)	Case 13* (N=3)	Case 14* (N=5)
Collagen I	26.1 (23.7 – 32.1)	56.4 (53.5 – 79.8)	48.5 (28.7 – 65.2)	37.5 (29.9 – 44.0)	63.8 (45.5 – 80.5)	43.4 (20.8 – 57.7)	31.6 (25.2 – 66.2)	38.2 (31.9 – 40.9)	52.7 (43.6 – 60.1)	30.1 (25.2 – 35.0)	35.7 (32.9 – 42.1)	40.5 (36.3 – 48.3)	78.5 (50.9 – 87.1)	32.6 (21.9 – 53.5)
VAP-1	16.6 (15.3 – 23.3)	17.8 (7.2 – 26.0)	31.8 (15.0 – 36.0)	18.0 (15.1 – 22.7)	39.9 (20.3 – 48.0)	48.4 (31.8 – 63.2)	18.4 (17.0 – 20.9)	78.7 (65.7 – 88.1)	46.1 (10.4 – 53.0)	43.2 (36.4 – 48.5)	20.1 (9.9 – 24.2)	18.0 (11.0 – 19.7)	20.3 (9.0 – 35.4)	7.0 (5.5 – 17.0)

Table 25: Summary of the median % expression of Collagen I and VAP-1 in midgut NET cases with lymph node metastases and primary midgut NETs. * Represents the primary midgut NETs. Median values taken after cropped tumour areas of whole image performed, represented by 'N'.
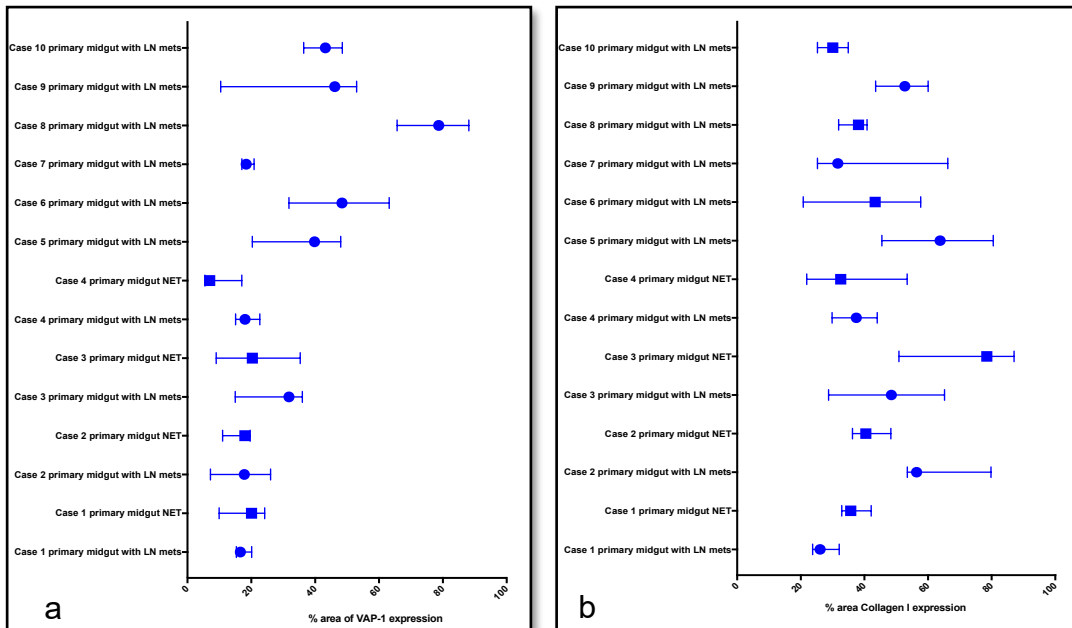
Figure 25: Graphs showing median values of % area of Vascular Adhesion Protein-1 and Collagen I expression. Graph a showing the median values of % area of VAP-1 expression for each case, shown as median values with IQRs of cropped tumour areas. Graph b showing the median values of % area of Collagen I expression for each case, shown as median values with IQRs of cropped tumour areas. Mets, metastases.
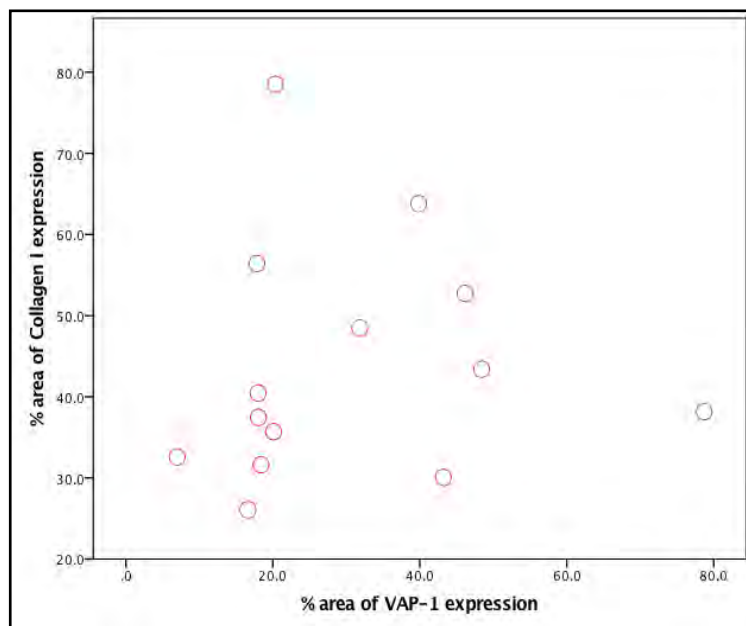

Figure 26: Scatter plot showing the median % area of VAP-1 expression against the % area of Collagen I expression for each case. Cropped tumour

areas of whole image used. Spearman's rho correlation co-efficient 0.310 (p=0.281). VAP-1, vascular adhesion protein-1.

	Collagen I	VAP-1	Spearman's Correlation Co-efficient	p-Value
Median	31.1	18.3	0.064	0.829
Percentile 25	26.8	15.9		
Percentile 75	33.0	23.8		

Table 26: Median values with IQRs of % area expression of whole images combined for Collagen I and VAP-1. Spearman's rho correlation co-efficient 0.064 (p=0.829).

Primary antibodies with isotype matched controls

Midgut NET tissue were individually stained with VAP-1, collagen I, α-SMA (fibroblasts marker) and CD45 (marker for leucocyte common antigen) , with their matched isotype matched control (IMC) for each primary Ab. VAP-1 expression can be seen in the peri-tumoral stroma, and a dense fibro-reticular network is present in these tumours with positive staining of collagen I and α-SMA in a very similar distribution. There is the presence of CD45 positive staining in these tumours as well, reflecting the presence of an immune component in the peri-tumoral stroma. **Figure 27.**
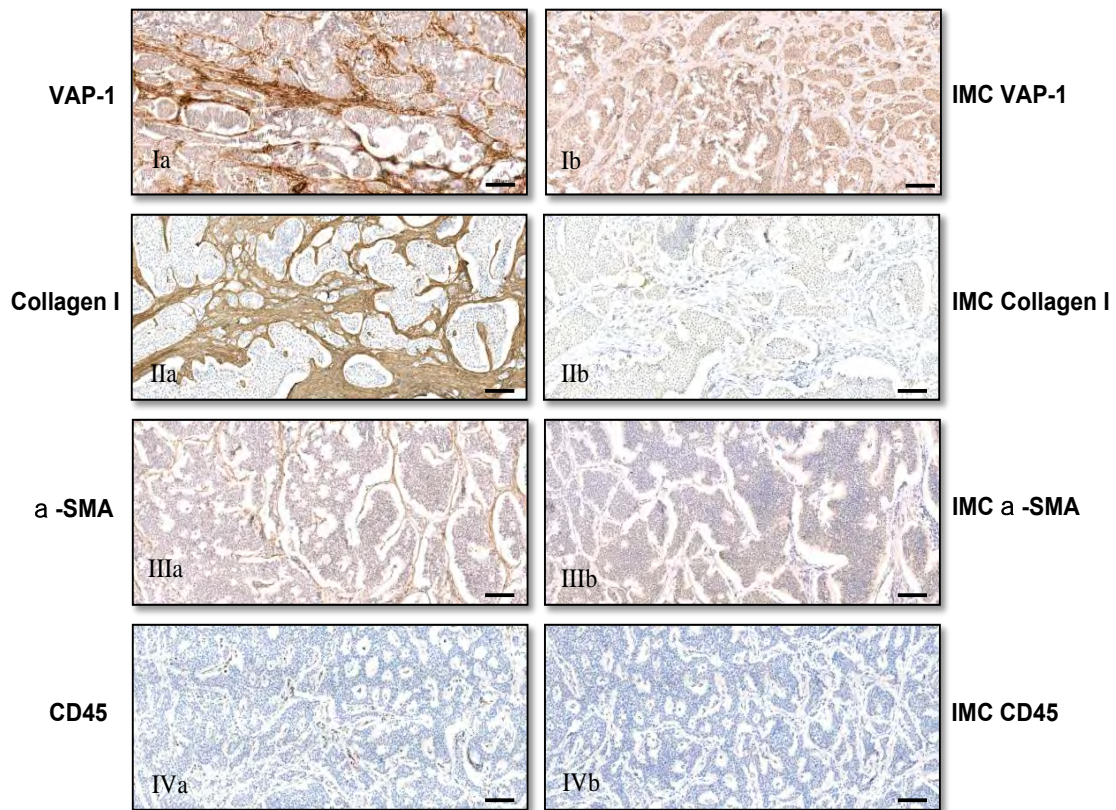
Figure 27: Representative images of cropped tumour areas of midgut neuroendocrine tumours with LN metastases stained with VAP-1, Collagen I, α-SMA, CD45 and matched IMC. Images Ia and Ib represents VAP-1 and IMC respectively; IIa and IIb represents Collagen I and IMC respectively; IIIa and IIIb represent α-SMA and IMC respectively; IVa and IVb represents CD45 and IMC respectively; n=3. Scale bars 100 μm. SMA, smooth muscle actin. IMC, isotype matched control.

VAP-1 positive staining

In addition to the positive VAP-1 staining seen in the peri-tumoral area in midgut NETs, VAP-1 is also present in the villous architecture, lamina propria layer and submucosal layer in the small bowel, as well as lining adipocytes. **Figure 28.** These findings are similar to our Birmingham group showing positive VAP-1 staining with a different primary antibody in the lamina propria and submucosal

layers of the colon (297), and to the study by Abella et al that showed positive VAP-1 expression using another primary antibody in the culture medium from adipocytes.(289)
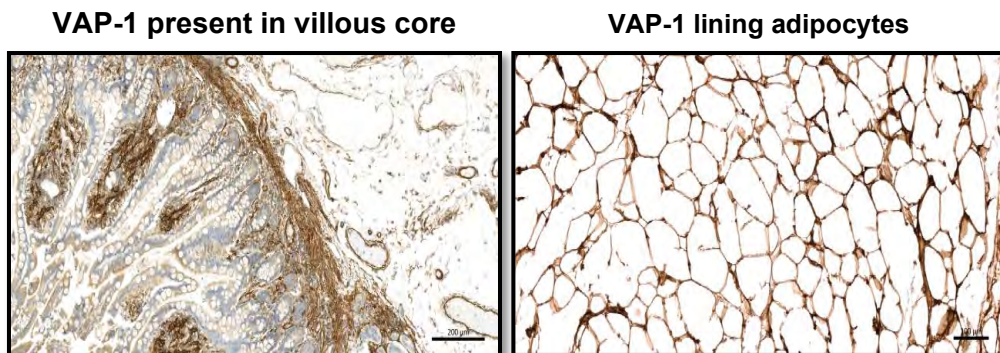
VAP-1 present in villous core   **VAP-1 lining adipocytes**

Figure 28: Representative images of cropped areas of midgut neuroendocrine tumours stained with VAP-1 in villous core and lining adipocytes. Image Ia shows VAP-1 staining present in the core of the villous architecture, the lamina propria layer and in the submuscosa layer. Image Ib shows the presence of abundant VAP-1 lining adipocytes. N=2. Scale bar as shown.

VAP-1 and α-SMA expression

The sections stained with both VAP-1 and α-SMA were then cropped to identify similar tumour areas stained with each marker. The distribution of VAP-1 and α-SMA staining appear to be in the same areas, with increased intensity of VAP-1 expression seen compared with α-SMA, indicating that midgut NETs are characterised by a dense stromal network. **Figure 29.** Given that NETs can cause fibrosis as a result of desmoplasia and VAP-1 is known to be associated with fibrosis, the findings of positive VAP-1 and α-SMA staining occurring in same areas was expected.
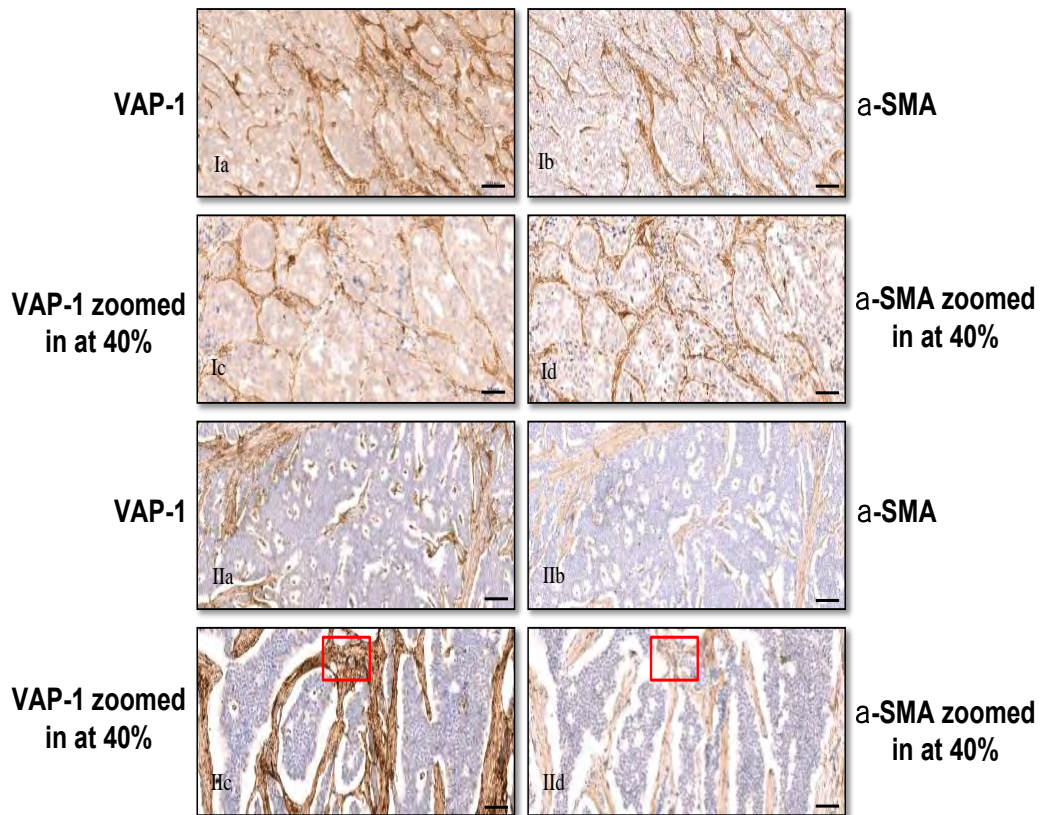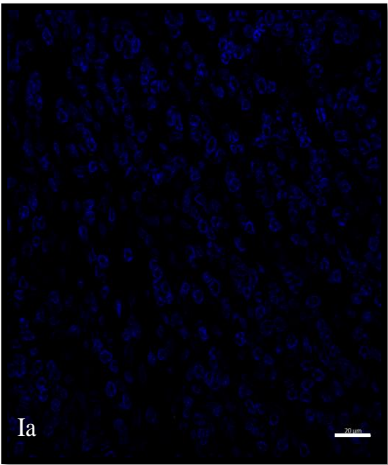
Figure 29: Representative images of cropped tumour areas of midgut neuroendocrine tumours with LN metastases stained with VAP-1 and α-SMA. Images Ia and IIa represent VAP-1 staining and images Ib and IIb represent α-SMA staining. Scale bars 100 μm. Images Ic and IIc represent VAP-1 staining zoomed in at 40% and images Id and IId represent α-SMA staining zoomed in at 40%. Scale bars 50 μm. There appears to be some areas where VAP-1 expression is seen more dense than α-SMA (red box in image IIc highlights this); n=2. Images I and II are separate cases.

Dual fluorescent staining in midgut NETs

Immunofluorescent staining was performed to allow visualisation of co-localisation using two markers together. Additionally, immunofluorescence enables more quantitative analysis given that an exact quantity of fluorescence is known per Ab and has a wider dynamic range. IHC staining is based on enzyme activity which increases variability and does not always represent the target concentration. Midgut NET tissue was dual stained with VAP-1 and collagen I, and VAP-1 and α-SMA. The cases show the presence of tumour cells surrounded by a dense stromal and collagen network, similar to the chromogenic staining performed. Co-localisation of both markers are seen as yellow in both VAP-1/collagen I and VAP-1/α-SMA, and individual areas of sole markers are also seen in the images below and VAP-1 can be seen lining the blood vessels. **Figures 30** and **31.**
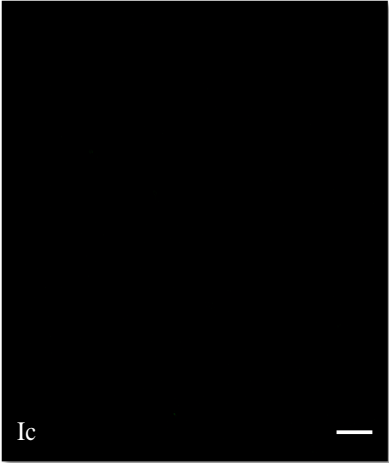
IMC VAP-1 and a-SMA. Hoerscht staining represents the nuclei (blue)
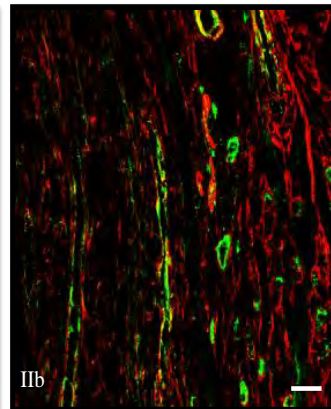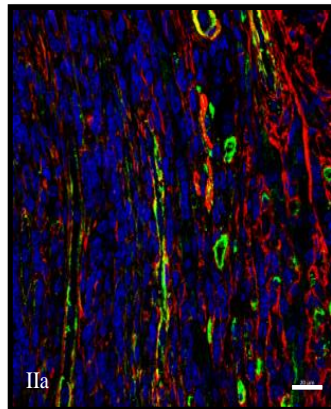
Ia

20 μm

IMC a-SMA

Ib

IMC VAP-1

Ic

VAP-1 (green) and a-SMA (red). Hoerscht staining represents the nuclei (blue)

IIa

VAP-1 (green) and a-SMA (red)

IIb

a-SMA (red)

IIc

VAP-1 (green)

IId

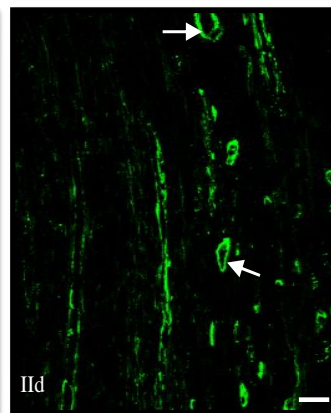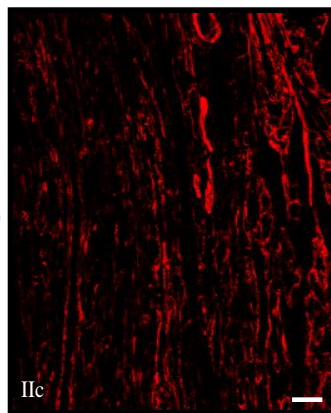**VAP-1 (green) and a-SMA (red). Hoerscht staining represents the nuclei (blue)**

VAP-1 (green) and a-SMA (red)

IIIa

20 µm

IIIb

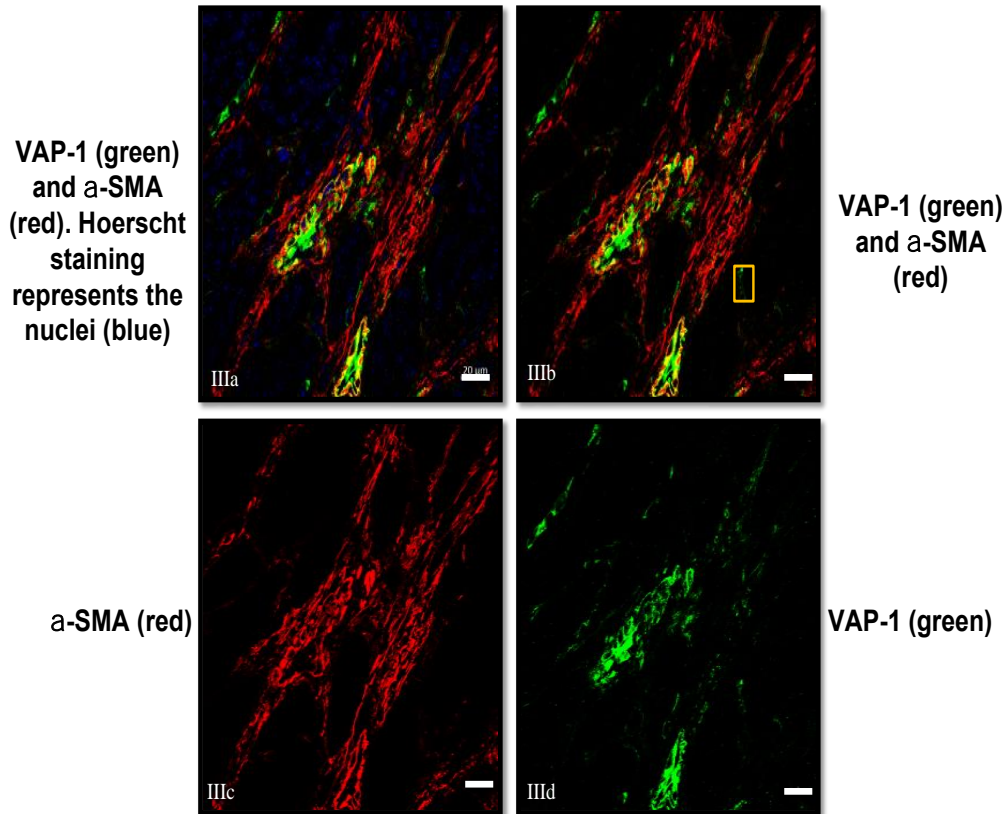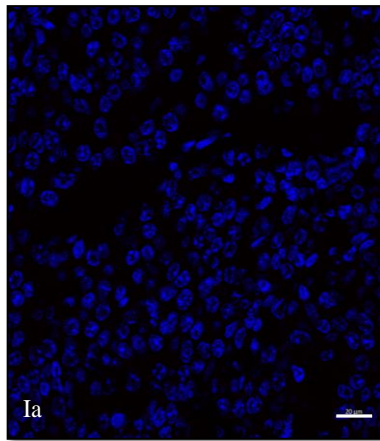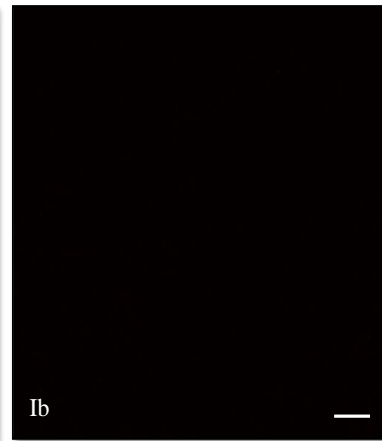**a-SMA (red)**

VAP-1 (green)

IIIc

IIId

Figure 30: Representative images of cropped tumour areas of midgut neuroendocrine tumours with LN metastases dual stained with VAP-1 and α-SMA. The blue staining (Hoerscht) illustrates the nuclei. The red staining indicates α-SMA, IgG2a Alexa Fluor wavelength 594. The green staining indicates VAP-1, IgG2b Alexa Fluor wavelength 488. Images Ia-c represent the matched IMC; Ia involves all three channels, Ib represents the red channel and Ic represents the green channel. Figures IIa-d and IIIa-d represent two different cases. Images IIa and IIIa show the presence of all three channels, IIb and IIIb show the presence of α-SMA and VAP-1, IIc and IIIc show the presence of α-SMA and IId and IIId show the presence of VAP-1; n=2. Scale bars 20 µm. Objective 20X. Co-localisation of the two markers can be seen as yellow in both cases, and the cases show the presence of tumour cells surrounded by a dense stromal network associated with VAP-1. Individual areas of α-SMA and VAP-1 can also be seen, with more VAP-1 staining seen lining blood vessels in image II (white arrow). Certain areas of VAP-1 expression can also be seen with no α-SMA expression (represented as a box in image III).
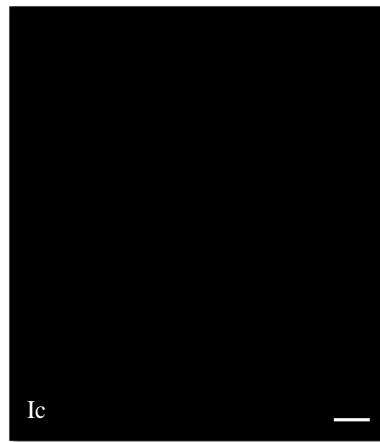
IMC VAP-1 and collagen I. Hoerscht staining represents the nuclei (blue)
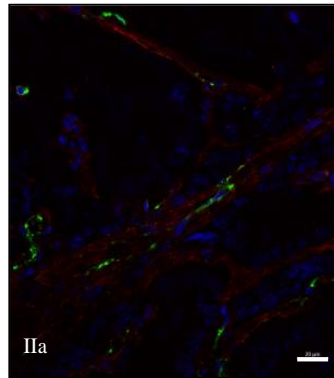
Ia

IMC collagen I

Ib

IMC VAP-1

Ic

VAP-1 (green) and collagen I (red). Hoerscht staining represents the nuclei (blue)

VAP-1 (green) and collagen I (red)
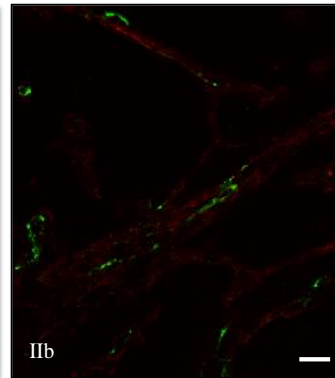
Collagen I (red)

VAP-1 (green)

IIa   IIb   IIc   IId
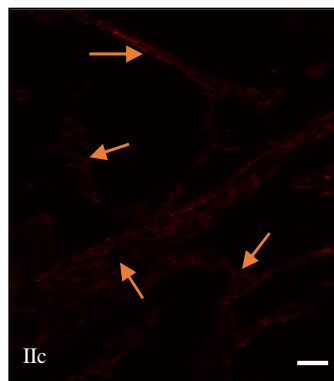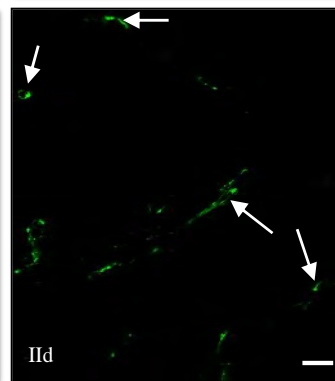
Figure 31: Representative images of cropped tumour areas of midgut neuroendocrine tumours with LN metastases dual stained with VAP-1 and Collagen I. The blue staining (Hoerscht) illustrates the nuclei. The red staining indicates collagen I, VectaFluor Duet Dylight 594. The green staining indicates VAP-1, VectaFluor Duet Dylight 488. Images Ia-c represent the matched IMC; Ia involves all three channels, Ib represents the red channel and Ic represents the green channel. Figures IIa-d and IIIa-d represent two different cases. Images IIa and IIIa show the presence of all three channels, IIb and IIIb show the presence of collagen I and VAP-1, IIc and IIIc show the presence of collagen I and IId and IIId show the presence of VAP-1; n=2. Scale bars 20 μm. Objective 20X. Co-localisation of the two markers can be seen as yellow in images IIIa-b, and both cases show the presence of tumour cells surrounded by a dense collagen network associated with VAP-1. Individual areas of collagen I (orange arrow) and VAP-1 (white arrow) can also be seen. Certain areas of VAP-1 expression can also be seen with no collagen I expression.

Immune cell recruitment

The immune microenvironment in midgut NETs has not been widely studied. CD45 was used to assess the presence of leucocyte infiltration in midgut NETs. An immune cell infiltrate is present surrounding the tumour cell clusters, similar to the VAP-1 staining. **Figure 32.** Previous work has highlighted that VAP-1 drives the immune cell infiltrate and this could explain the findings shown here where positive CD45 staining is seen in similar areas where VAP-1 resides due to leucocyte transmigration.

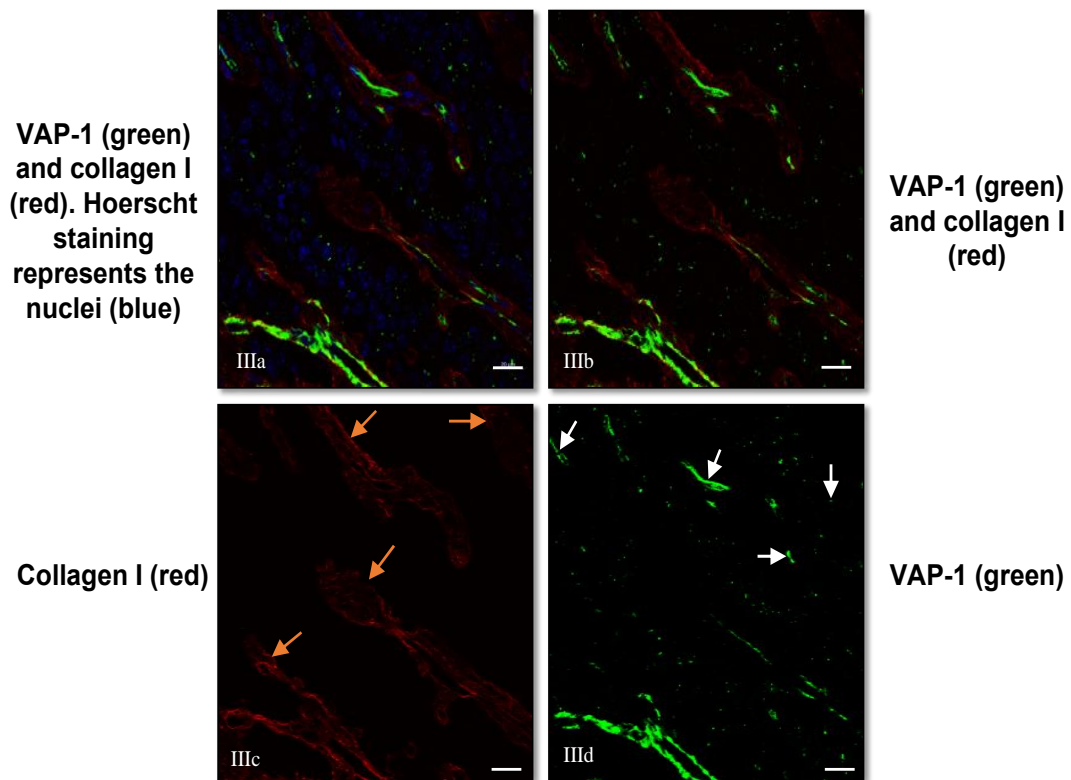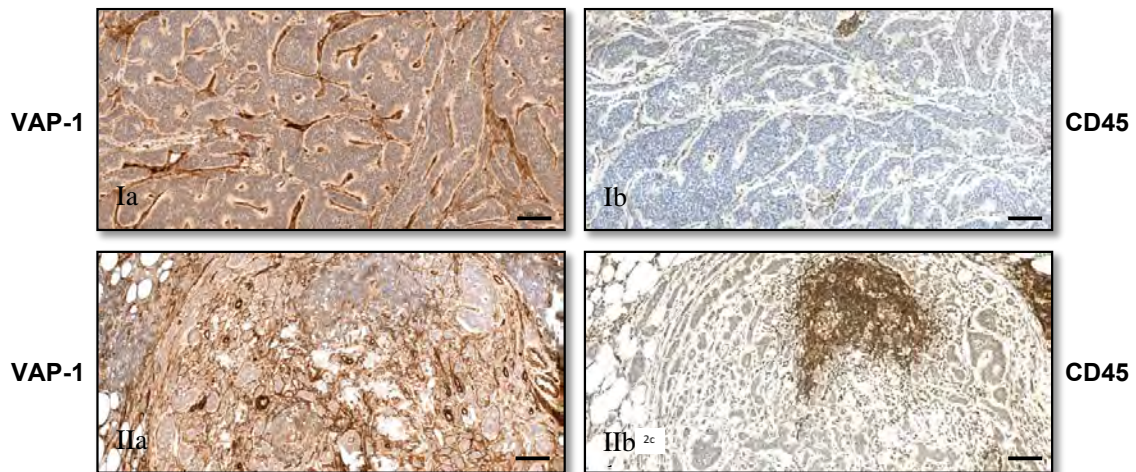**Figure 32: Representative images of cropped tumour areas of midgut neuroendocrine tumours with LN metastases stained with VAP-1 and CD45.** Images Ia and IIa represent VAP-1 staining and images Ib and IIb represent CD45 staining; n=2. Scale bars 100 μm. The images show an immune cell infiltrate surrounding the tumour areas similar to the VAP-1 staining. Image IIb shows a highly infiltrated immune cell area present in between the clusters of neuroendocrine tumour cells.

5.3 Discussion

Despite NETs generally being slow-growing tumours, they are associated with considerable complications as a result of desmoplasia. Midgut NETs are associated with mesenteric fibrosis, which in turn can lead to ischaemia and small bowel obstruction, which is a significant cause of morbidity in these patients.(330) At present, surgery remains the only treatment option when patients develop mesenteric fibrotic complications. Further side effects and consequences following surgery can also have an impact on patients' quality of life, including short bowel syndrome and malabsorption.(194, 332)

The Birmingham group have identified VAP-1 as a potential marker of fibrosis and therefore I investigated the expression of this protein in NETs. VAP-1 expression was found in the peritumoral stroma and the villous architecture, and was also seen to line blood vessels and adipocytes. NET cells abundantly express proangiogenic molecules, thereby enhancing the recruitment and proliferation of endothelial cell precursors leading to angiogenesis.(343) The VAP-1 positive endothelial cells present in the tumour, could also be driving this process secondary to the oxidase activity of VAP-1, and the production of hydrogen peroxide, which in turn may regulate the process of angiogenesis.(344) Granules of VAP-1 within the tumour cells were seen, possibly indicating that VAP-1 may also be released by these cells and then adhere to the underlying matrix.

A positive correlation was seen between VAP-1 and collagen I, although this was not statistically significant, suggesting that the clusters of tumour cells are

surrounded by a dense ECM. Alpha-SMA expression was also found in the

peritumoral area, supporting previous findings of high levels of α-SMA

production in the fibroblast population in tumour stroma.(336) These findings

are in keeping with previous work undertaken in Birmingham which have shown

that VAP-1 promotes the expression of profibrotic genes, including, COL1A1,

and therefore increased production of collagen I (277) and that either absence

or inhibition of VAP-1 in mouse models protected the liver from steatohepatitis

and hepatic fibrogenesis with a reduction in SMA and COL1A1 gene

expression.(345) Dual staining using VAP-1/α-SMA and VAP-1/collagen I did

show some evidence of co-localisation of both markers and the presence of

tumour cells being surrounded by a dense stromal and collagen network

associated with VAP-1. Weston et al also showed that VAP-1 is expressed in α-

SMA stromal cells in liver cirrhosis.(277) Therefore it is likely that NET

associated fibroblasts express VAP-1 and that both tumour and stroma may

contribute to the pool of circulating VAP-1.

This is the first description of VAP-1 in the tumour microenvironment in NETs.

Interestingly it has been shown that midgut NETs may have evidence of

chromosomal gain in chromosome 17q (346), and the AOC3 gene is located on

chromosome 17q.(347) Therefore, given that there is evidence of chromosomal

gain in midgut NETs, increased production of VAP-1 may take place. Previous

studies reporting on the NET microenvironment have shown that there is

predominantly a desmoplastic reaction mainly composed of CAFs expressing α-

SMA and limited leucocyte infiltration. Studies have shown that through their

secretion of factors including serotonin, TGF-β and platelet derived growth factor, NET cells can stimulate the activation and proliferation of fibroblasts.(343) Previous work has shown that CD8+ lymphocytes, T regulatory cells and programmed death ligand 1 expressed on tumour cells / tumour infiltrating cells are present in midgut NETs.(348, 349) Impaired cytolytic activity of natural killer cells has also observed in gastroenteropancreatic NETs.(350) Results in this chapter have shown an immune cell infiltrate surrounding the tumour areas similar to the VAP-1 staining. This could represent the VAP-1 driving the immune cell infiltrate to areas where VAP-1 resides by the rolling, adhesion and transmigration steps of leucocyte transmigration. This therefore suggests that, in addition to the fibrotic composition of midgut NETs, an inflammatory component may also be present in the tumour microenvironment of midgut NETs. Additionally, liver myofibroblasts are known to control recruitment and positioning of lymphocytes (351), and VAP-1 may play a similar role in controlling the entry and retention of these immune cell populations through its adhesive function or enzymatic activity. Given the previous findings a high population of CAFs present in the tumour stroma, VAP-1 may be expressed on activated fibroblasts given the similar distribution of α-SMA and VAP-1 seen in the staining. On the dual fluorescent staining, individual areas of VAP-1, α-SMA and collagen I were seen, where there was no co-localisation present, possibly suggesting two reasons: firstly, individual cell types are producing each marker separately and are also present in the tumour microenvironment, and secondly, where there are certain areas of solely VAP-1 expression, this could be as a result of circulating sVAP-1 adhering to the

stromal matrix. There may also be other markers that VAP-1 could be related to that have not been assessed in this study. These include markers of CAFs including, fibroblast activation protein, desmin and vimentin.(352, 353) Additionally, collagen III fibres and connective tissue growth factor have been found to be abundantly expressed in small bowel NETs (336, 337, 343) and therefore assessing the association between these markers and VAP-1 should also be considered in future work.

In this chapter, the presence of VAP-1 has been shown in the tumour stroma of midgut NETs, and is associated with a dense fibrotic network, with the presence of immune cell infiltration. CHD is a major fibrotic complication of NETs which is associated with major morbidity and mortality. Understanding the microenvironment present in this fibrotic complication would potentially allow targeted treatment to be given. Levels of sVAP-1 have already been shown in this thesis to be significantly raised in CHD. The tissue expression of VAP-1 also needs to be studied in CHD, to assess whether VAP-1 may also have a similar expression in CHD valves, given that it is a known fibrotic site occurring in NETs.

5.4 Conclusion

In conclusion, the immunohistochemical and immunofluorescent staining has shown the presence of VAP-1 in the peritumoral stroma of midgut NETs. A dense fibro-reticular network is present in these tumours, illustrating the fibrotic nature of this cancer. An inflammatory component can also be identified in

these tumours with the leucocyte recruitment possibly being driven by the presence of VAP-1.

Surgery at present is the only treatment that can be offered to patients who develop mesenteric fibrosis as a result of the midgut NET. VAP-1 as a treatment target could be an alternative treatment option offered in these patients who develop fibrotic complications without the associated risk of post-surgical adverse effects that can occur.

CHAPTER 6:

IMMUNOHISTOCHEMICAL ANALYSIS OF CARCINOID HEART DISEASE VALVES

6.1 Introduction and aims

6.1.1 Introduction

In patients with CS, CHD still remains a major negative prognostic factor with valve surgery currently being the only effective treatment. Despite valve replacement being the mainstay of treatment in CHD, a high mortality rate is present post-operatively.(354) CHD usually affects the right- and left -sided valves in 85% and 15% of cases respectively.(355) Transthoracic echocardiography is usually able to identify CHD in the advanced stages, yet the identification and diagnosis of early stage disease remains a challenge.(356) Current clinical practice for surveillance of CHD includes NT-proBNP measurement and an echocardiogram if the NT-proBNP is above the normal level, or an echocardiogram is directly performed based on examination findings or patients' symptoms. The urinary 5-HIAA is well known to be significantly higher in CHD compared with NET patients without this cardiac complication.(357)

The exact pathogenesis involved in CHD is not fully understood. The exposure of high levels of serotonin and other vasoactive mediators are thought to be factors involved in CHD development.(355) 5-HT receptors play an important role in the development of CHD. Following activation of these receptors, mitogenesis of fibroblasts and smooth muscle cells takes place, as does up-regulation of TGF-β1.(213) Fibrous-like plaques then get deposited, usually on the right-sided valves, leading to heart failure.(243)

Another factor that may play a role in the pathogenesis and development of CHD is VAP-1, given its association with fibrosis. As well as being a diagnostic marker, VAP-1 could also be a treatment target. This would therefore enable earlier recognition and diagnosis of CHD being made, and treatment can then be offered at an appropriate time, thereby improving overall morbidity and mortality in this group of patients.

6.1.2 Aims

The aim is to understand the contribution of VAP-1 to the fibrosis that develops in CHD valves. This will be correlated with the expression of ECM proteins, angiogenesis markers and cellular populations (such as fibroblasts):

The aim of this section is to:

    a) Study the expression of VAP-1 in CHD valves and define the cell specific expression of VAP-1 and correlate with the immune microenvironment.

6.3 Results

In total 33 CHD valves, 6 control valves and 4 myxoma tissue sections were used. The disease aetiology in the control valves used included calcific aortic stenosis, acute aortic dissection, aortic and mitral fibrotic valves and aortic medial cystic degeneration. These control valves were chosen as the underlying disease either only affected the aortic root and not the valve, with no valve fibrosis involved, or valve fibrosis was present but not expected to be to the same extent as seen in CHD valves.

Comparisons between the CHD and control valves were initially performed, in relation to VAP-1 expression, and haematoxylin and eosin staining in both valve types. Following this, a quantitative analysis was performed to assess the VAP-1 expression in the CHD valves and control valves to determine if a significant difference in expression of VAP-1 is present between both valves. The next aim was to analyse the distribution of VAP-1 in CHD valves by undertaking a comprehensive study of the stroma seen in CHD valves using collagen I and III and α-SMA. These markers were used as it is known that the carcinoid plaque deposits are comprised of myofibroblasts, smooth muscle cells and ECM. Additionally, CD31 and CD45 staining were undertaken in both valve types to assess the possible presence of neovascularisation and an immune cell infiltration, and determine if these processes are related to VAP-1 expression. The expression of VAP-1 was also compared in different areas of the carcinoid plaque, to assess if expression increases with increasing fibrosis in the plaque.

CHD express increased levels of VAP-1 compared to control valves

Figure 33 represents the haematoxylin- and eosin-stained sections of CHD and control valves. A cluster of immune cells are seen in the CHD valve both in the underlying valve as well as in the carcinoid plaque found superior to the valve.

Figure 34 represents whole-image tissue sections stained with VAP-1 and the matched IMC in a CHD valve and control valve.
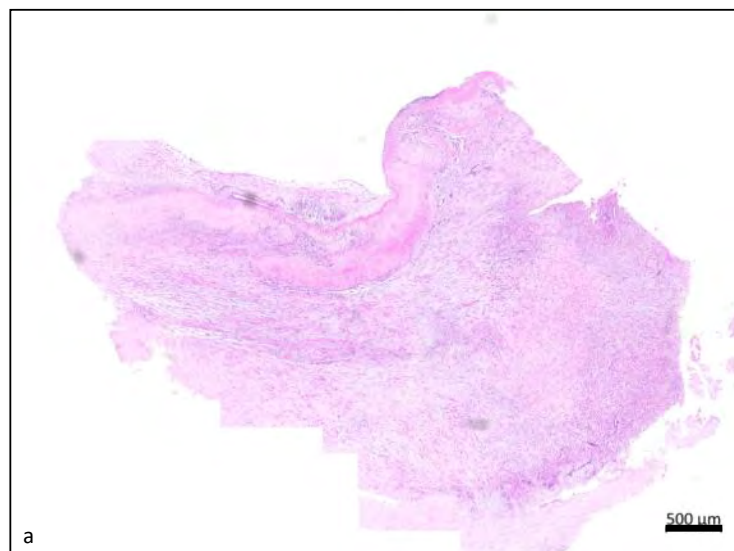
CHD.
Haematoxylin and Eosin stain
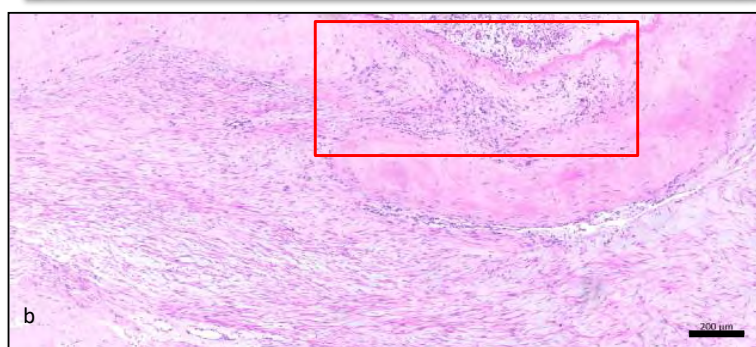
Cropped area of image a
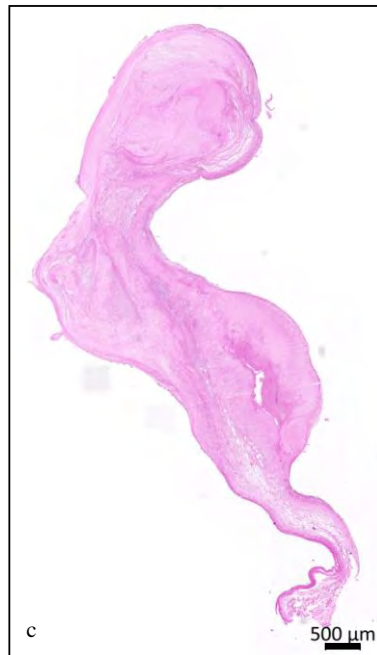
Control.
Haematoxylin
and Eosin
stain

c

500 μm
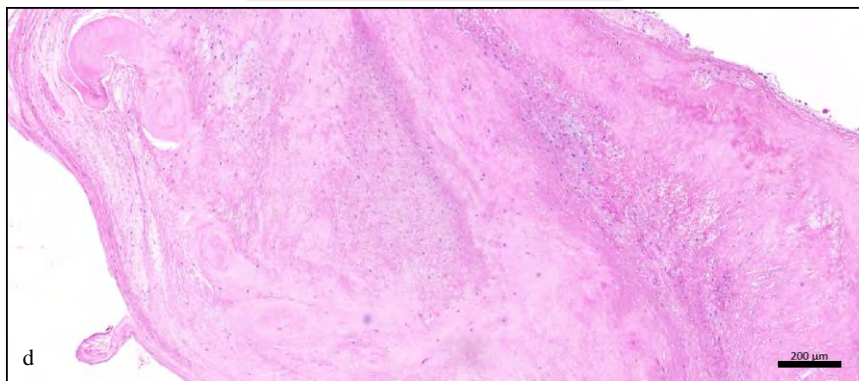
Cropped area
of image c

d

200 μm

Figure 33: Representative images of a carcinoid heart disease case with a cropped area, and a control valve case with a cropped area stained with haematoxylin and eosin. CHD case shown in image a, cropped area in image b, control valve case in image c and cropped control valve area in image d. Scale bars as illustrated; n=2. A cluster of immune cells can be seen in image b (highlighted by red box) present in the underlying valve and also in the plaque area superior to the valve.
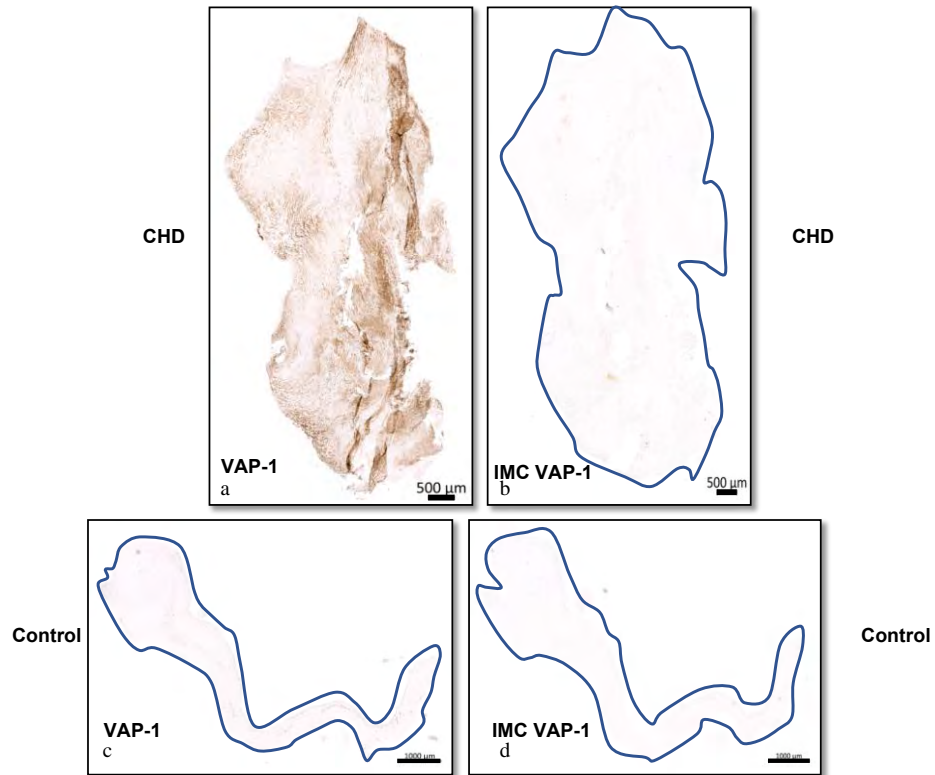
Figure 34: Representative images of a whole carcinoid heart disease case and a control valve case for VAP-1 staining with paired IMC. CHD case is shown in image a, control valve case is shown in image c with their paired IMC in images b and d respectively. N=2. Objective 20X. Scale bars as illustrated.

The VAP-1 stained CHD and control valves were analysed using Ilastik and Fiji Image J in order to establish the quantification of the % area of VAP-1 expression. The threshold images below are seen in red and represent the positive brown Ab staining on the images taken by Zen software. **Figure 35.**

Threshold image
Ia

CHD
Ib
VAP-1
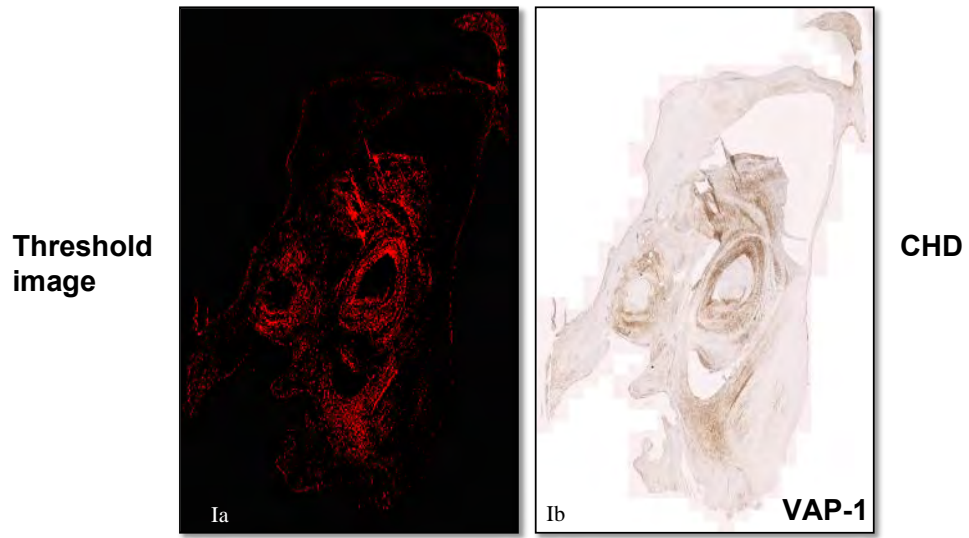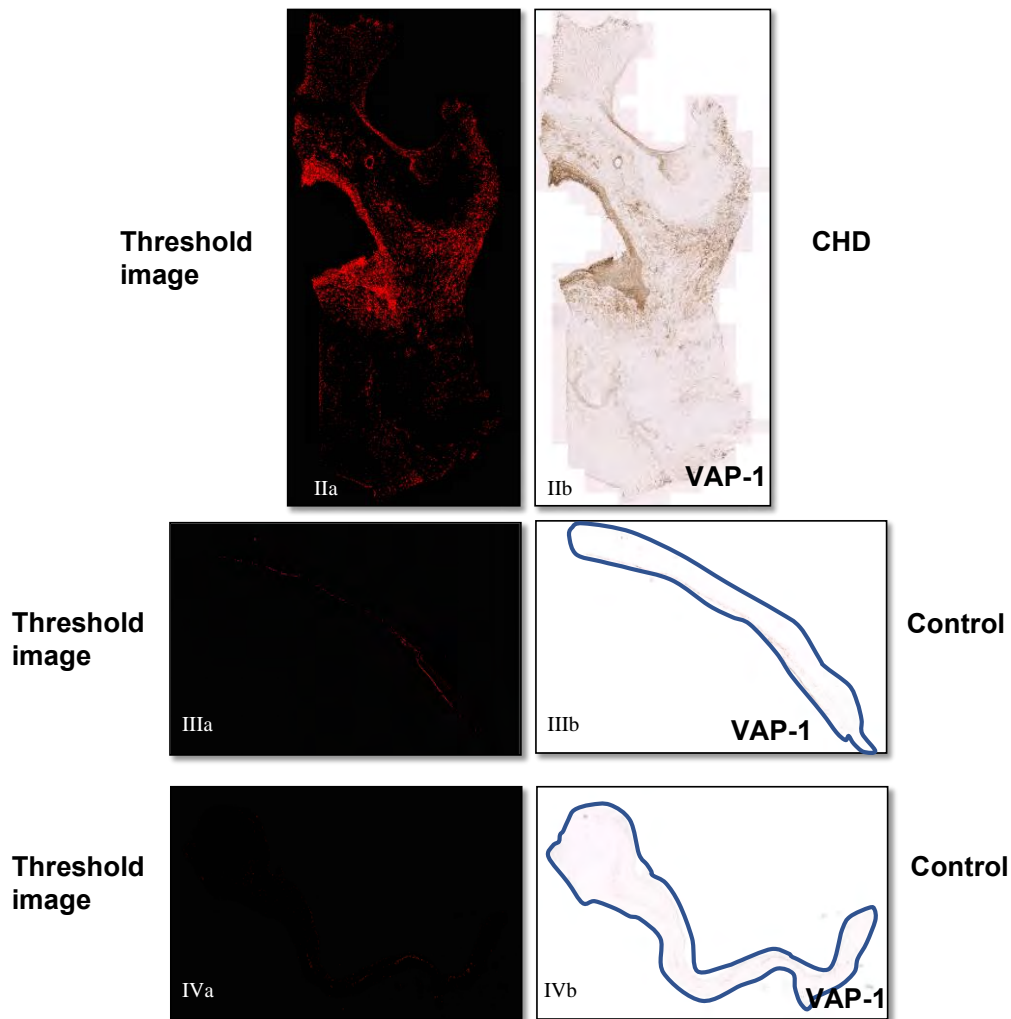
Figure 35: Representative images of whole CHD and control valves stained with VAP-1 with matched threshold images. Images Ib and IIb represent VAP-1 staining in CHD valves and images IIIb and IVb represent VAP-1 staining in control valves. Images Ia and IIa represent the threshold images of Ib and IIb respectively, used for the quantification of % area of VAP-1 expression (staining shown as red); 3.4% and 5.4% respectively. Images IIIa and IVa represent the threshold images of IIIb and IVb respectively, used for the quantification of % area of VAP-1 expression (staining shown as red); 0.3% and 0.1% respectively. N=4.

The % area of VAP-1 expression was quantified in both the CHD and control valves. **Table 27, Table 28, Figure 36**. The median % area of VAP-1 expression values for CHD and control valves were 1.40% (IQR 0.80 – 2.15) versus 0.15%

(IQR 0.10 – 0.23) respectively, and this was found to be significant (p<0.001),

Figure 37.

% area VAP-1 expression	Case 1 (N=4)	Case 2 (N=3)	Case 3 (N=3)	Case 4 (N=2)	Case 5 (N=3)	Case 6 (N=6)
25% percentile	0.1	0.1	0.1	0.1	0.1	0.1
Median	0.2	0.1	0.3	0.1	0.1	0.2
75% percentile	0.4	0.2	0.3	0.2	0.1	0.4

Table 27: Summary of the median % area VAP-1 expression in the whole images of six control valve cases with the IQRs.

VAP-1, Vascular Adhesion Protein-1. N, number of values taken for each case.

% area VAP-1 expression	25% percentile	Median	75% percentile
Case 1 (N=2)	2.9	3.4	3.9
Case 2 (N=3)	2.3	2.7	10.3
Case 3 (N=5)	1.4	1.6	1.9
Case 4 (N=4)	0.8	2.1	2.7
Case 5 (N=4)	0.6	0.8	2.1
Case 6 (N=9)	0.9	1.1	2.3
Case 7 (N=7)	4.2	5.4	6.5
Case 8 (N=12)	3.2	4.5	5.9
Case 9 (N=3)	0.6	0.7	3.7
Case 10 (N=4)	1.2	1.5	5.5
Case 11 (N=16)	1.5	2.7	4.4
Case 12 (N=8)	0.8	2.2	4.0
Case 13 (N=4)	0.8	1.7	2.7
Case 14 (N=4)	1.9	2.7	3.6
Case 15 (N=7)	0.5	1.0	1.4
Case 16 (N=5)	1.2	1.8	7.2
Case 17 (N=3)	0.8	1.1	1.4
Case 18 (N=1)	0.6	0.6	0.6
Case 19 (N=3)	0.3	0.4	1.2
Case 20 (N=2)	0.6	0.8	0.9
Case 21 (N=4)	0.4	0.5	1.3
Case 22 (N=3)	0.4	0.5	0.6
Case 23 (N=13)	0.4	1.5	2.0
Case 24 (N=4)	1.1	1.5	2.4
Case 25 (N=3)	0.4	0.5	1.5
Case 26 (N=1)	2.2	2.2	2.2
Case 27 (N=2)	0.7	1.1	1.5
Case 28 (N=2)	0.8	0.9	1.0
Case 29 (N=7)	0.9	1.0	1.5
Case 30 (N=8)	0.7	1.2	2.3
Case 31 (N=3)	0.6	0.8	1.0
Case 32 (N=3)	1.3	1.7	2.4
Case 33 (N=4)	1.2	1.4	2.2

Table 28: Summary of the median % area VAP-1 expression in the whole images of thirty-three CHD valve cases with the IQRs. VAP-1, Vascular Adhesion Protein-1. N= number of values taken for each case.
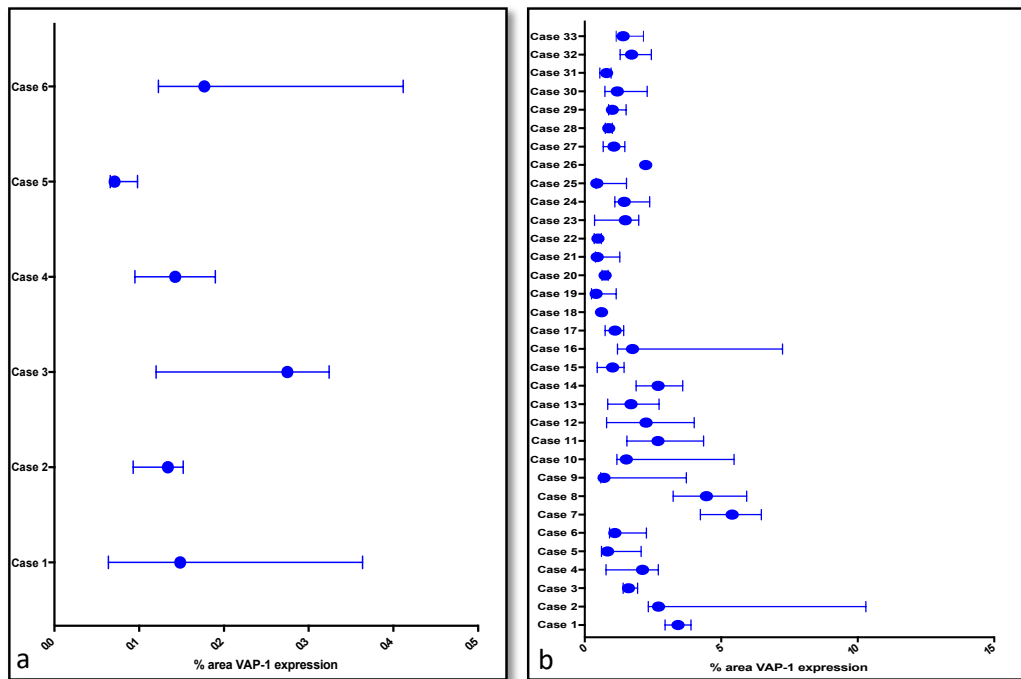
Figure 36. Graphs showing the median values of % area of VAP-1 expression in control valves and CHD valves. Graph a shows the median values of % area of VAP-1 expression for each control valve case, shown as median values with IQRs of whole images. Graph b shows the median values of % area of VAP-1 expression for each CHD case, shown as median values with IQRs of whole images. Please note differences in the x-axis scale between the two cohorts. VAP-1, vascular adhesion protein-1. CHD, carcinoid heart disease.

212
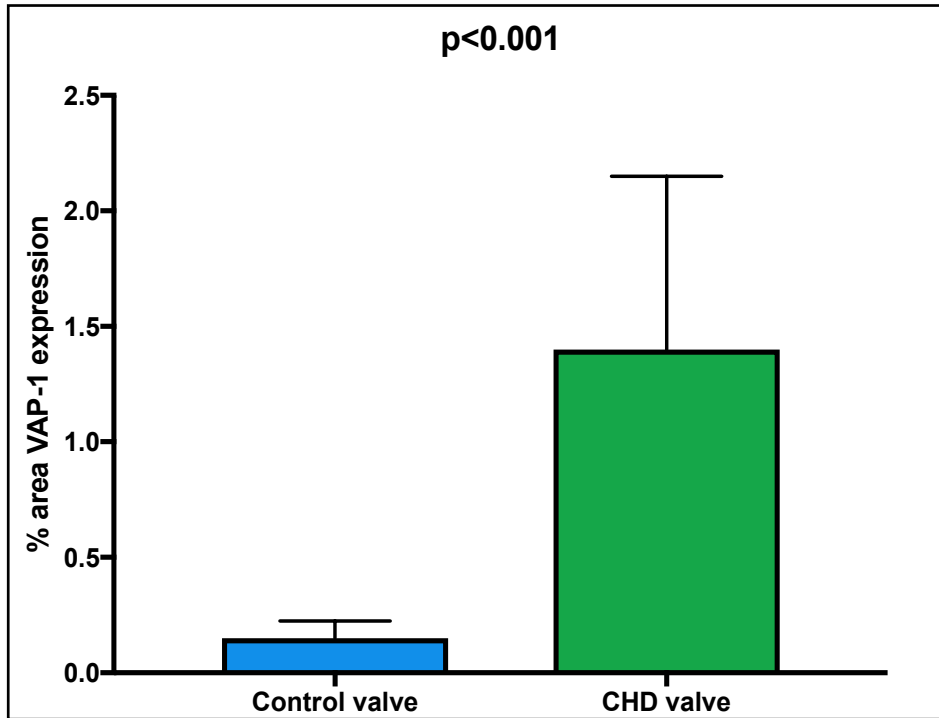
Figure 37. Graph showing the median with IQR % area of VAP-1 expression between the CHD and control valve groups. A significant difference is seen between the two groups (p<0.001).

The CHD and control valve sections were reviewed by a pathologist with extensive experience in identifying valvular diseases and understanding the valve anatomy. IHC staining of VAP-1 in CHD valves shows evidence of VAP-1 expression in the carcinoid plaque as well as in the atrial/ventricular and fibrous valve layers, **Figure 38**. VAP-1 expression is also present lining the vasculature both in the carcinoid plaque as well as in the underlying valve, **Figure 39**.
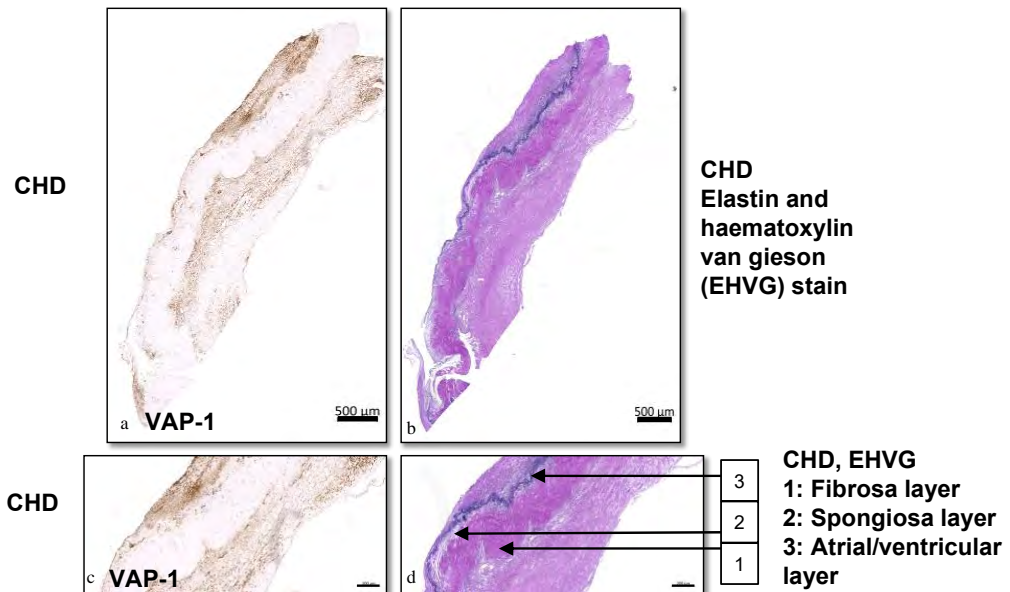
Figure 38: Representative images of a CHD case with VAP-1 staining and matched EHVG staining. VAP-1 staining shown in images a and c, and matched EHVG staining shown in images b and d. The three valve layers are arrowed in image d (1= fibrosa layer, 2= spongiosa layer, 3= atrial / ventricular layer). Carcinoid plaque is evident on the atrial/ventricular surface and also on the fibrous surface. N=1. Scale bars as illustrated. EHVG, Elastin and Haematoxylin Van Gieson.

CHD

Ia **VAP-1**
200 μm
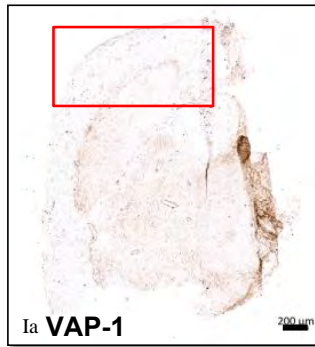
**CHD
Elastin and
haematoxylin
van gieson
stain**

Ib
500 μm

**Cropped area
of image Ia
highlighted
by the red
box**

Ic **VAP-1**
100 μm

**Different
case of CHD**

II **VAP-1**
100 μm

Different case of CHD

III VAP-1
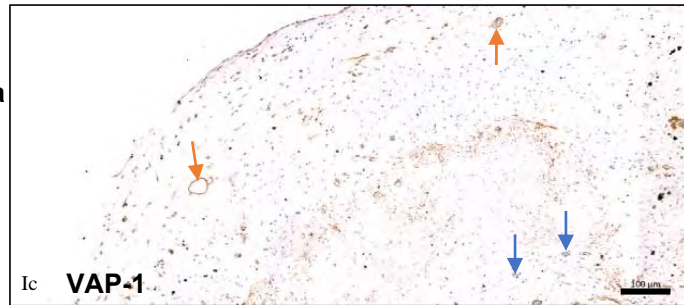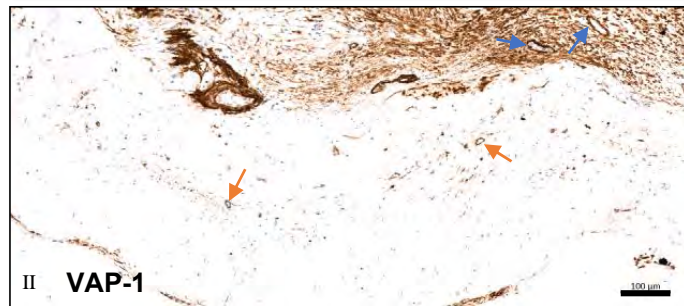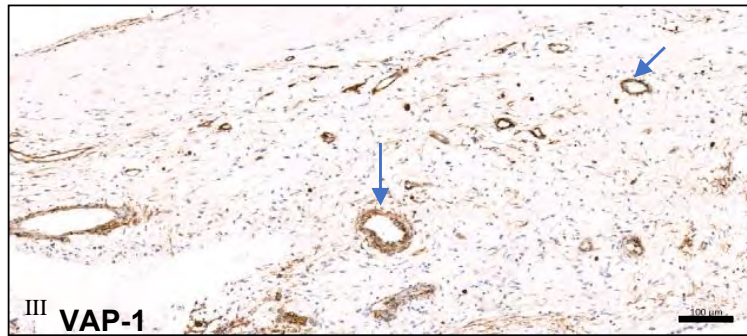
Figure 39: Representative images of CHD cases with VAP-1 staining.
VAP-1 staining seen in images Ia, Ic, II and III. Image Ib represents the matched EHVG staining for image Ia. Image Ic is the cropped area highlighted by the red box in image Ia and images II and III represent different CHD cases. VAP-1 can be seen lining vasculature both in the carcinoid plaque (blue arrow in images Ic, II and III) as well as in the underlying valve (orange arrow in images Ic and II); n=3. Scale bars as illustrated.

The vascular areas seen within the underlying valve in the above figure could be a result of hypoxia secondary to valve injury leading to neovascularisation or may occur as a granulation repair response driven by VAP-1 present in the carcinoid plaque.

VAP-1 expression was seen to vary according to the CHD valve area. There was no VAP-1 expression seen in the chords of the CHD valve, with increasing VAP-1 expression seen in the myxoid area (a myxoid stroma rich in proteoglycans), collagen area and elastin area of the valve respectively. **Figure 40**. This reflects that VAP-1 is expressed in different degrees of fibrosis, where fibrosis is most mature in the elastin area, and the absence of fibrosis in the chords of the valve. The cells staining positive in the myxoid, collagen and elastin areas do display a

stellate appearance. In the myxoid and collagen areas, VAP-1 expression is confined to the cells, whereas there is positive staining both in the cells as well as in the interstitium with increasing maturity in the elastin areas of the plaque.
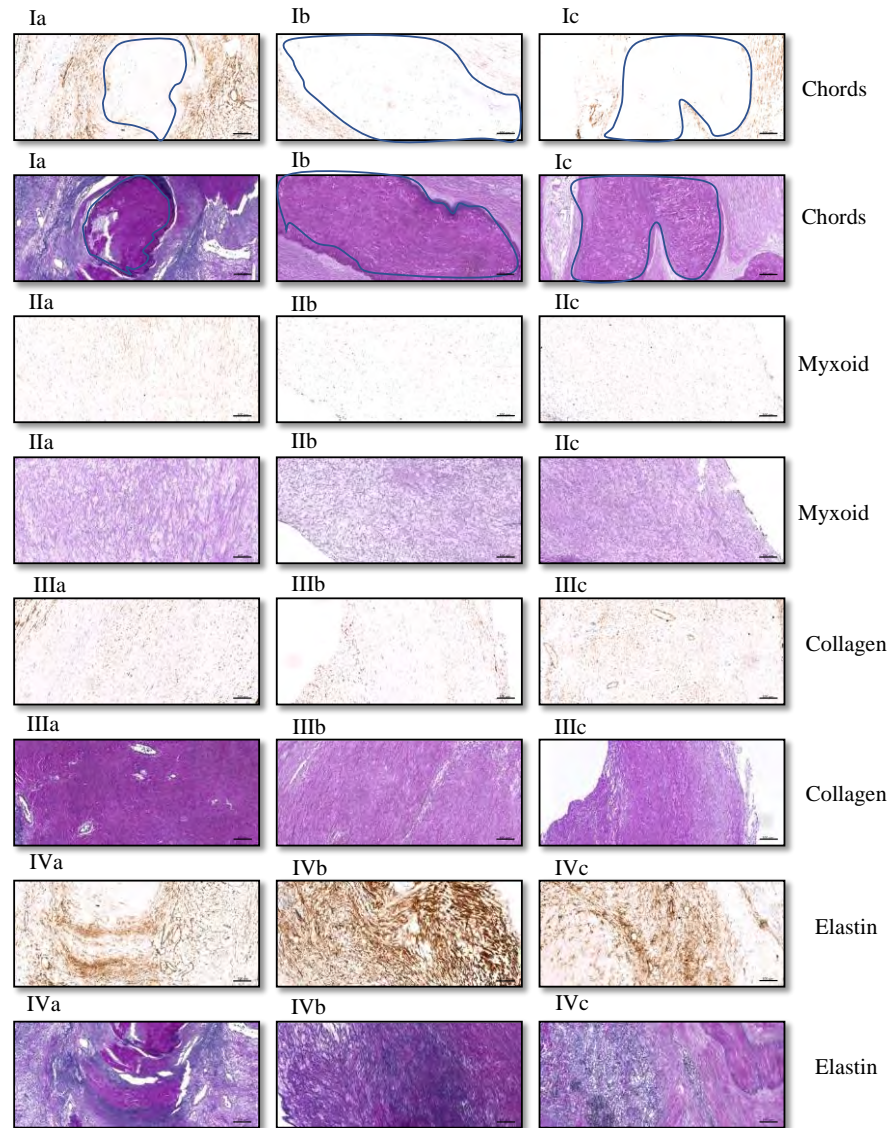
Figure 40: Representative images of CHD cases with VAP-1 staining and matched EHVG staining through the different fibrotic areas of the CHD plaque. Images Ia-c represent the chords (n=3) where no VAP-1 expression is seen. Images IIa-c represent the myxoid area (n=3), images IIIa-c the collagen area (n=3) and IVa-c the elastin area (n=3) of the plaque. Increasing VAP-1 expression can be seen reflecting maturity of fibrosis within the plaque. The chords are outlined in images a-c, with overlying plaque. Scale bars 100 μm

Collagen I and collagen III in CHD and control valves

Increased expression of collagen I and collagen III was seen in both the CHD and control valves, but with greater expression in the CHD valves. Collagen I was detected in both the cells producing collagen I and also in the surrounding stroma, whereas collagen III stained more selectively. The staining of collagen I was greater in the CHD valves compared to the control valves, **Figures 41** and **42**.

Figure 41: Representative images of a CHD case and control valve case stained with Collagen I and IMC. Image Ia represents collagen I staining in a CHD case with the IMC shown in image Ib. Image IIa represents collagen I staining in a control valve case with the IMC shown in image IIb. N=2. Scale bars 200 μm.

Figure 42: Representative images of matched CHD cases and matched control valve cases stained with Collagen I and VAP-1. The top two rows are both CHD cases and the bottom two rows are control valve cases. Matched cases have been used for collagen I and VAP-1. In all cases, collagen I expression can be seen in cells producing collagen I but also in the stroma surrounding the cells. Higher intensity of collagen I expression can be seen in the CHD cases compared with the control valve cases. N=4. Scale bars 200 μm.

Collagen III can be seen to stain more selectively compared with collagen I with staining present in the cells producing collagen III and not in the surrounding stroma, **Figures 43** and **44**. Collagen III has similar staining to VAP-1 expression seen in the CHD cases. Like collagen I, more intense collagen III staining was seen in the CHD cases compared with the control valve cases.

Figure 43: Representative images of a CHD case and control valve case stained with Collagen III and IMC. Image Ia represents collagen III staining in a CHD valve with the IMC shown in image Ib. Image IIa represents collagen III staining in a control valve case with the IMC shown in image IIb. N=2. Scale bars 200 μm.

Figure 44: Representative images of matched CHD cases and matched control valve cases stained with Collagen III and VAP-1. The top two rows are both CHD cases and the bottom two rows are control valve cases. Matched cases have been used for collagen III and VAP-1. Collagen III can be seen to stain more selectively compared with collagen I, with staining present in the cells producing collagen III and not in the surrounding stroma. Collagen III has similar staining to VAP-1 expression seen in the CHD cases. Less intense collagen III expression can be seen in the control valve images compared with the CHD cases as well as compared with the collagen I expression seen in control valves. N=4. Scale bars 200 μm.

CD45, CD31 and CD34 in CHD and control valves

CD45 positive staining was present in both the CHD and control valves. There did not appear to be increased CD45 staining in the CHD group compared with the control valve group. **Figures 45** and **46**.
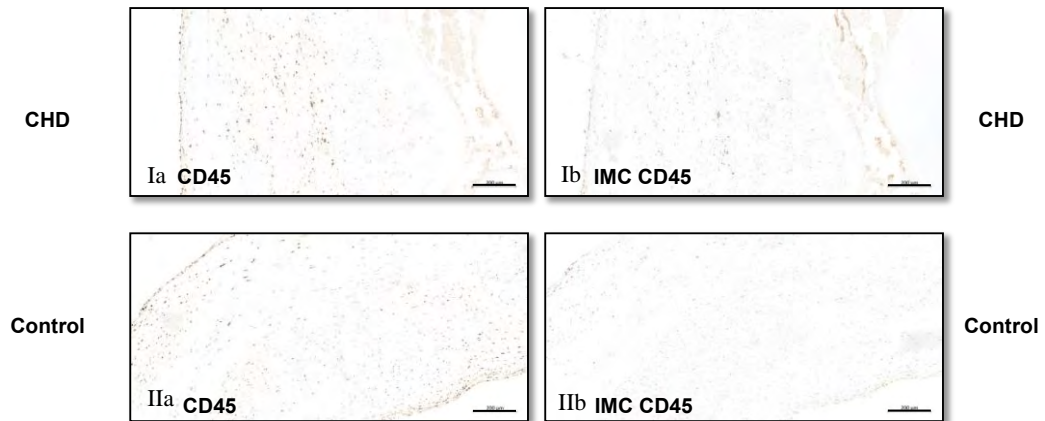
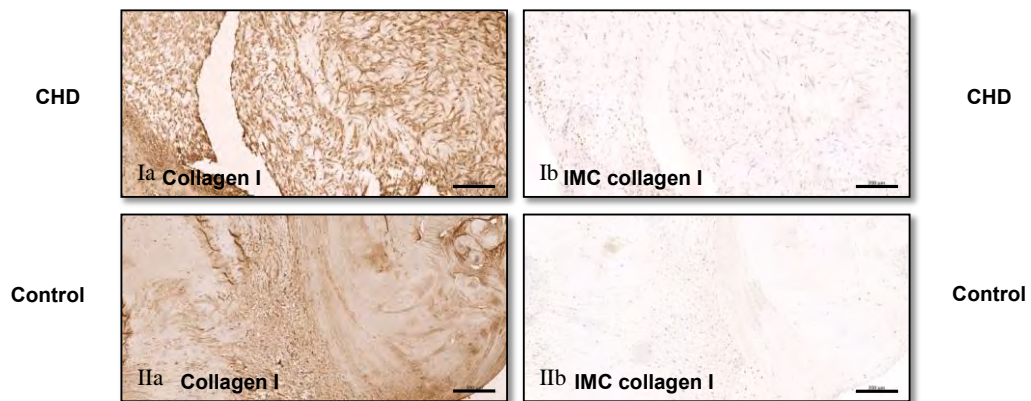**Figure 45: Representative images of a CHD case and a control valve case stained with CD45 and IMC.** Image Ia represents CD45 staining in a CHD valve with the IMC shown in image Ib. Image IIa represents CD45 staining in a control valve case with the IMC shown in image IIb. N=2. Scale bars 200 μm.
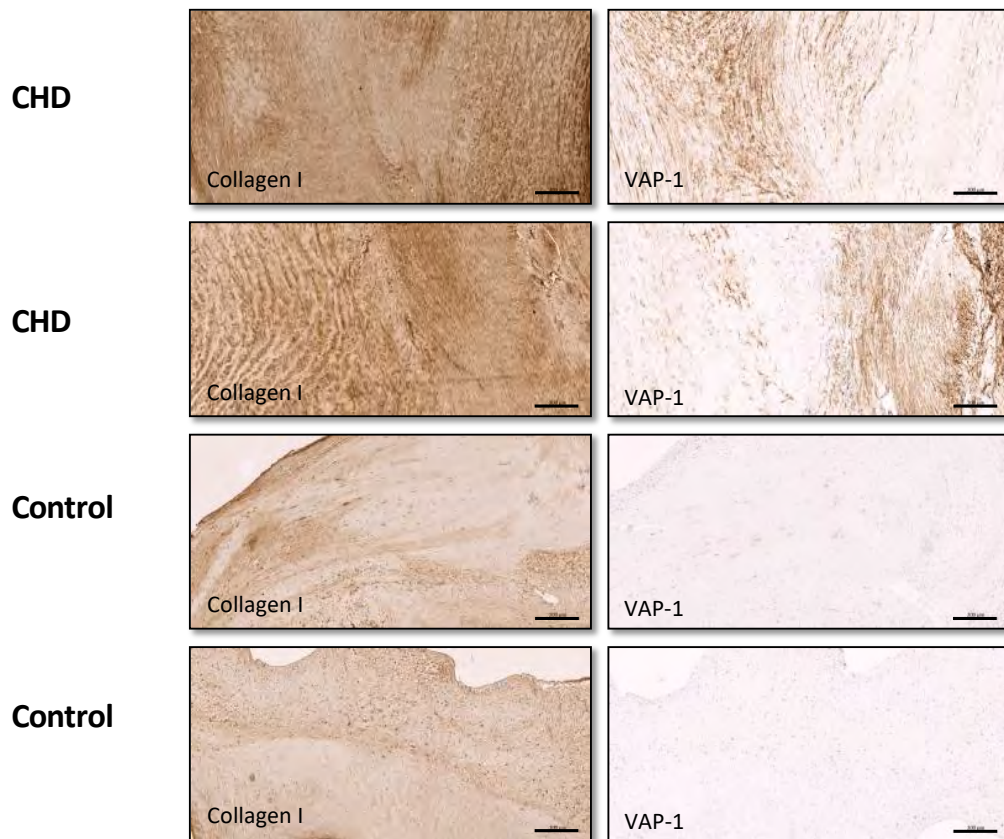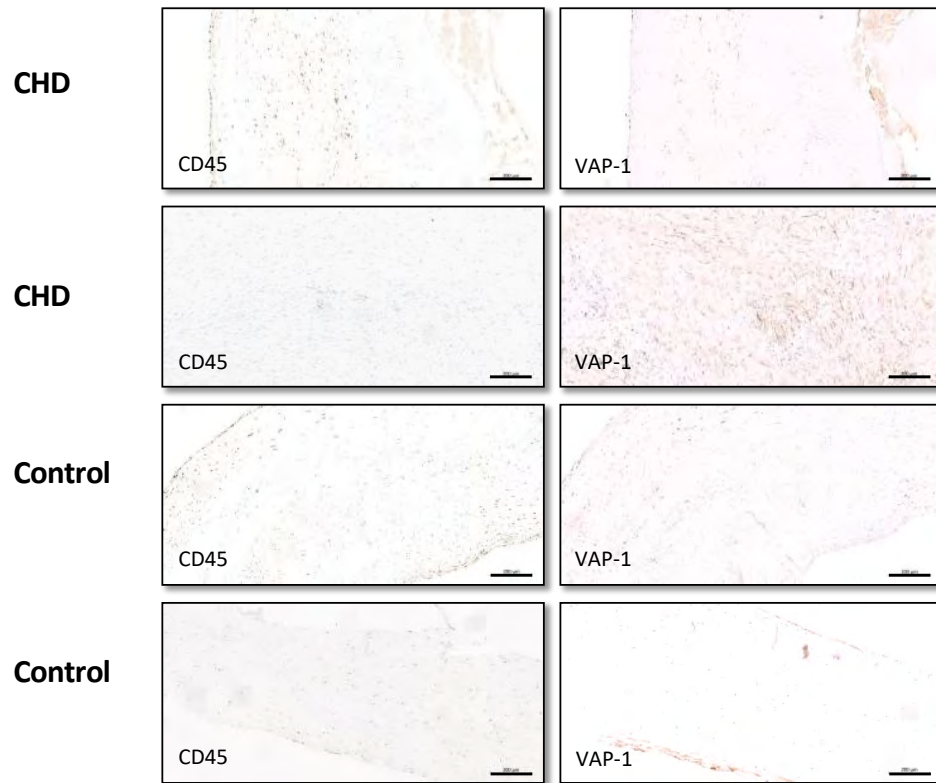
Figure 46: Representative images of matched CHD cases and matched control valve cases stained with CD45 and VAP-1 . The top two rows are both CHD cases and the bottom two rows are control valve cases. Matched cases have been used for CD45 and VAP-1. CD45 staining is present in both CHD valves and control valves. The staining of CD45 appears to be in similar areas to the positive VAP-1 staining present. N=4. Scale bars 200 μm.

CD31 positive vessels were noted in the CHD valves, with very low expression in the control valves, highlighting a potential role for VAP-1 in the development of valvular neovascularisation, **Figures 47** and **48**.
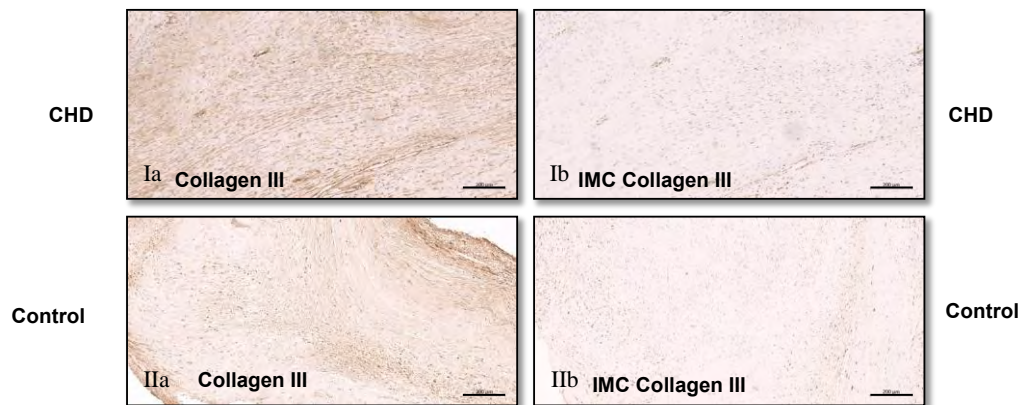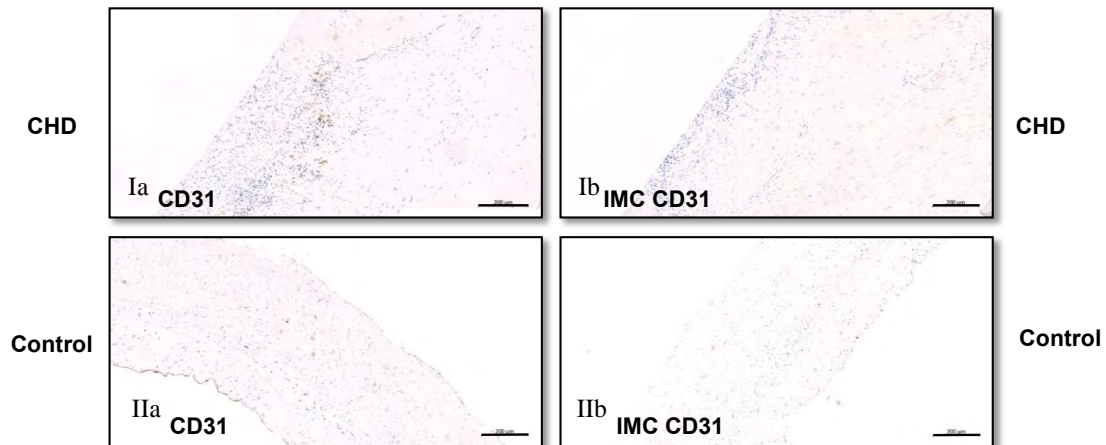

Figure 47: Representative images of a CHD case and control valve case stained with CD31 and IMC. Image Ia represents CD31 staining in a CHD valve with the IMC shown in image Ib. Image IIa represents CD31 staining in a control valve case with the IMC shown in image IIb. N=2. Scale bars 200 μm.
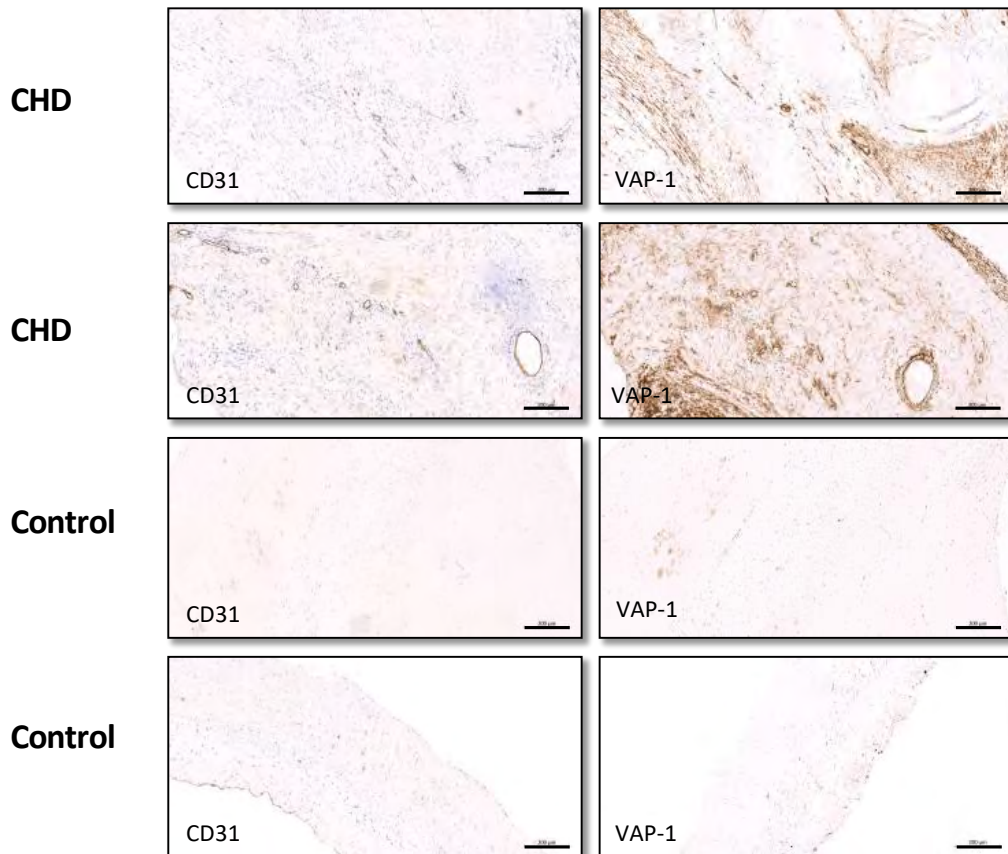
Figure 48: Representative images of matched CHD cases and matched control valve cases stained with CD31 and VAP-1. The top two rows are both CHD cases and the bottom two rows are control valve cases. Matched cases have been used for CD31 and VAP-1. CD31 expression can be seen in the CHD valves but not in the control valves illustrating the neovascularisation present in CHD. N=4. Scale bars 200 μm.

CD34 positive staining is present in both valve types. The staining can be seen lining vasculature. Given that CD34 is a progenitor cell marker, the positive staining seen in the control valves in addition to the non-vascular areas in the CHD valves could represent the differentiating cells present. **Figure 49**.
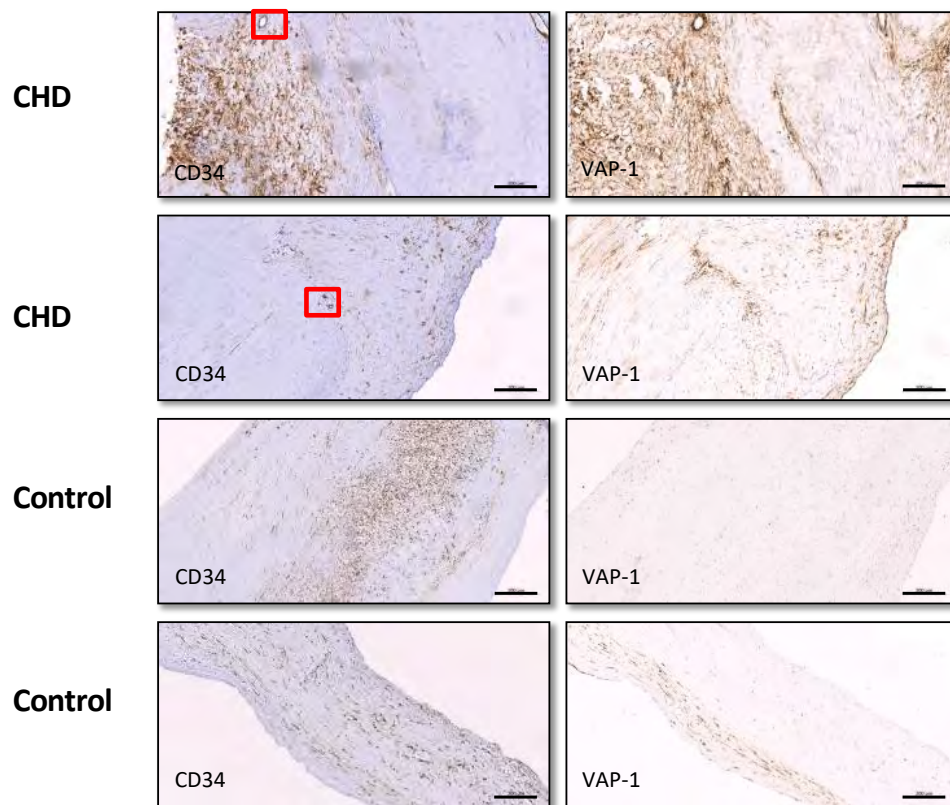
Figure 49: Representative images of matched CHD cases and matched control valve cases stained with CD34 and VAP-1. The top two rows are both CHD cases and the bottom two rows are control valve cases. Matched cases have been used for CD34 and VAP-1. CD34 staining can be seen in both valve types. CD34 staining can be seen lining vasculature (highlighted by red boxes in CHD images). N=4. Scale bars 200 μm.

Dual fluorescent staining in CHD valves

CHD valve tissue was dual stained with VAP-1 and α-SMA, **Figure 50** and

VAP-1 and collagen III, **Figure 51**. The staining shows the presence of a dense

stromal and collagen network in the CHD valves. Co-localisation of both

markers is seen as yellow in both VAP-1/collagen III and VAP-1/α-SMA, and

individual areas of each marker are also seen in the images. Compared to the

chromogenic staining, positive collagen III staining appears to be present more

in the surrounding stroma than the cells producing collagen III and there does

appear to be a greater collagenous deposition than VAP-1 expression.
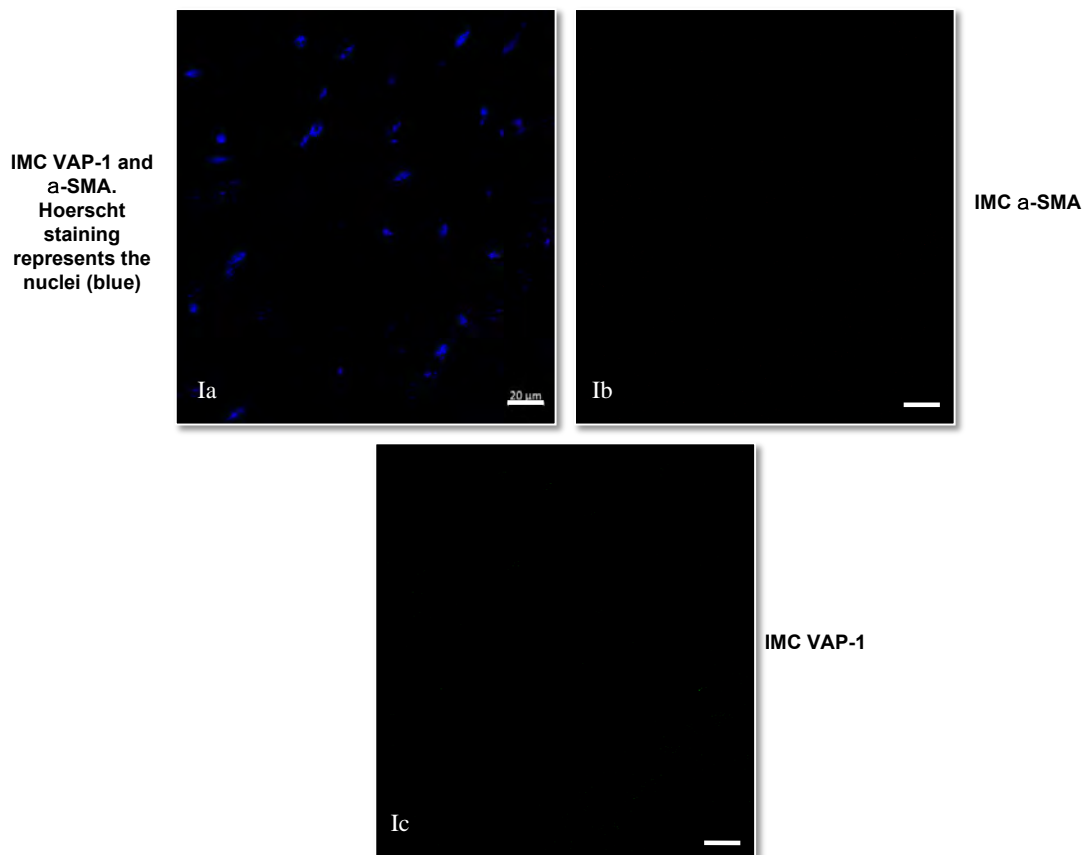
IMC VAP-1 and a-SMA. Hoerscht staining represents the nuclei (blue)

Ia   20 µm

IMC a-SMA

Ib

IMC VAP-1

Ic

VAP-1 (green) and a-SMA (red). Hoerscht staining represents the nuclei (blue)
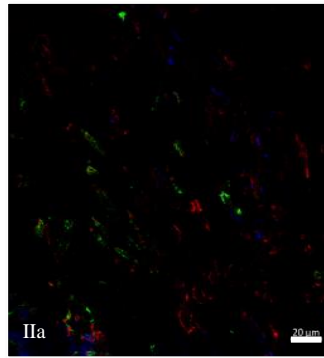
VAP-1 (green) and a-SMA (red)

a-SMA (red)

VAP-1 (green)

VAP-1 (green) and α-SMA (red). Hoerscht staining represents the nuclei (blue)

IIIa

VAP-1 (green) and α-SMA (red)

IIIb

α-SMA (red)

IIIc

VAP-1 (green)

IIId
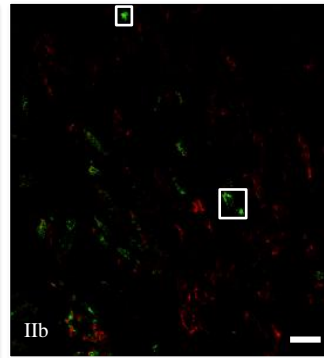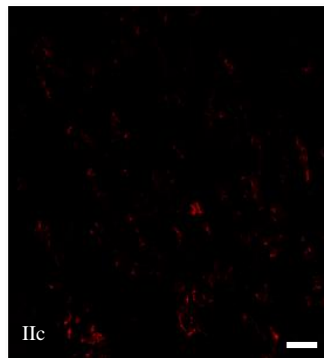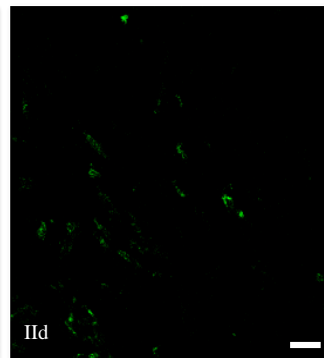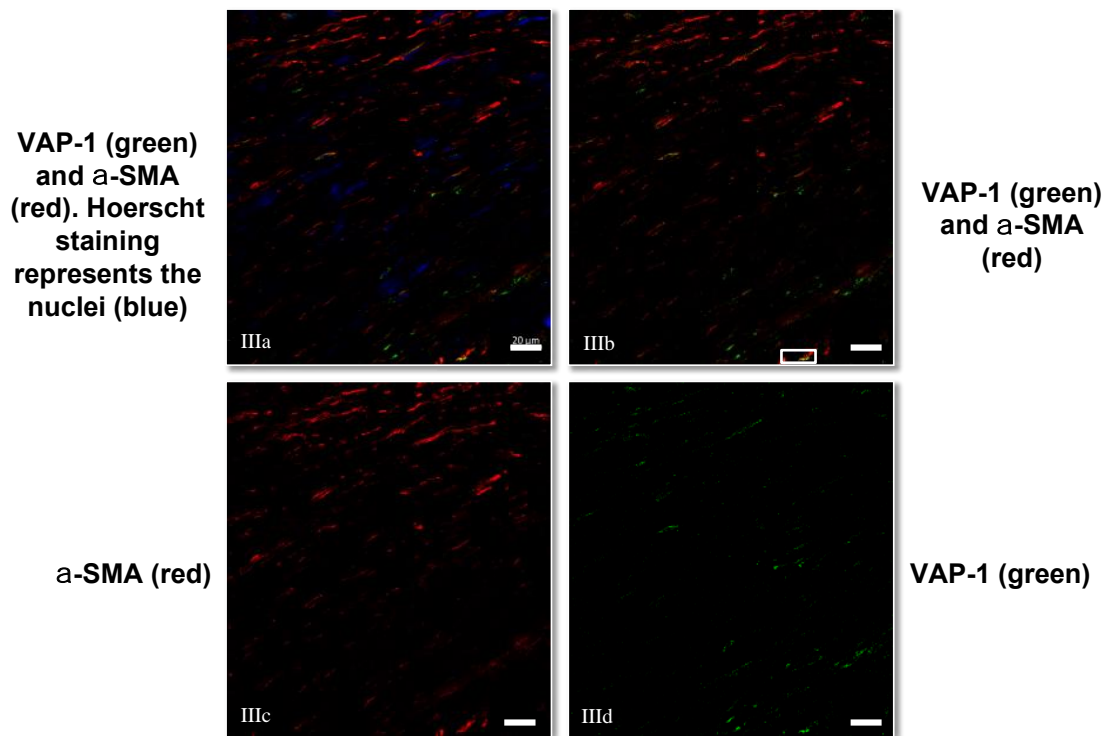
Figure 50: Representative images of CHD cases dual stained with VAP-1 and α-SMA. The blue staining (Hoerscht) illustrates the nuclei. The red staining indicates α-SMA, IgG2a Alexa Fluor wavelength 594. The green staining indicates VAP-1, IgG2b Alexa Fluor wavelength 488. Images Ia-c represent the matched IMC; Ia involves all three channels, Ib represents the red channel and Ic represents the green channel. Figures IIa-d and IIIa-d represent two different cases. Images IIa and IIIa show the presence of all three channels, IIb and IIIb show the presence of α-SMA and VAP-1, IIc and IIIc show the presence of α-SMA and IId and IIId show the presence of VAP-1. N=2. Scale bars 20 μm. Co-localisation of the two markers can be seen as yellow in image IIIb (white box), and the cases show the presence of valve cells surrounded by a dense stromal network associated with VAP-1. Individual areas of α-SMA and VAP-1 can also be seen. This therefore highlights that cells producing both VAP-1 and α-SMA are present in these valves, but individual cell types produce each marker independently too. Certain areas of VAP-1 expression can also be seen with no α-SMA expression (represented as a white box in image IIb).

IMC VAP-1 and collagen I. Hoerscht staining represents the nuclei (blue)

Ia

20 μm

Ib

IMC collagen III

Ic
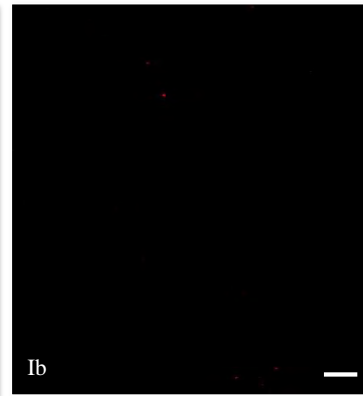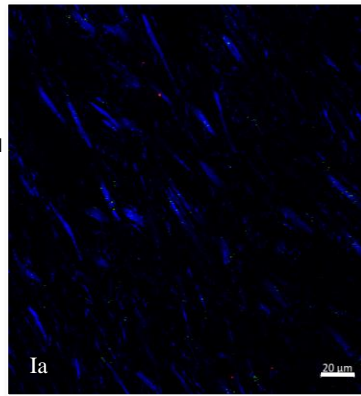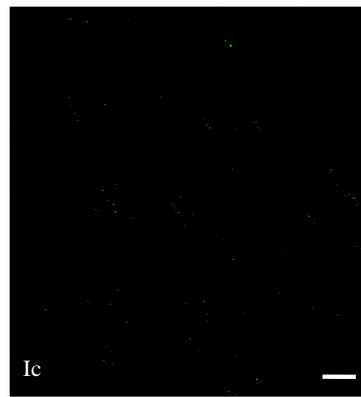
IMC VAP-1

VAP-1 (green) and collagen III (red). Hoerscht staining represents the nuclei (blue)
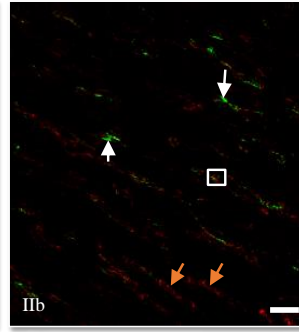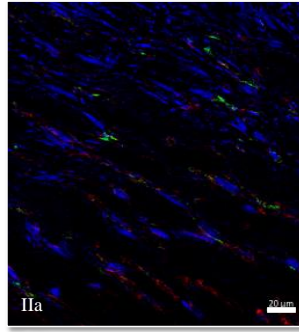
VAP-1 (green) and collagen III (red)

Collagen III (red)

VAP-1 (green)

VAP-1 (green) and collagen III (red). Hoerscht staining represents the nuclei (blue)

Collagen III (red)

VAP-1 (green) and collagen III (red)
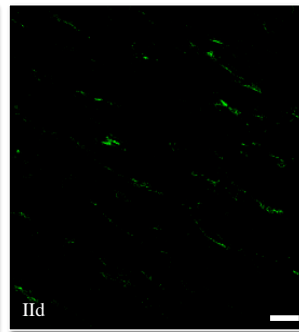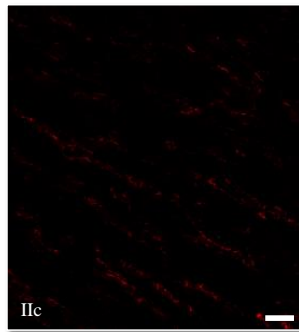
VAP-1 (green)
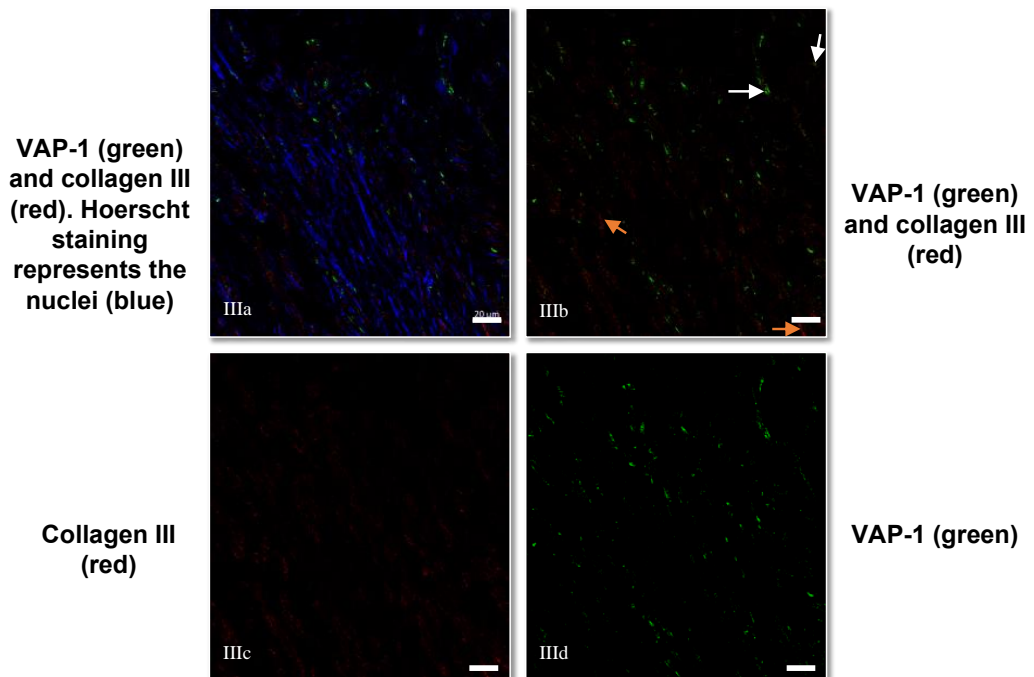
Figure 51: Representative images of CHD cases dual stained with VAP-1 and Collagen III. The blue staining (Hoerscht) illustrates the nuclei. The red staining indicates collagen III, VectaFluor Duet Dylight 594. The green staining indicates VAP-1, VectaFluor Duet Dylight 488. Images Ia-c represent the matched IMC; Ia involves all three channels, Ib represents the red channel and Ic represents the green channel. Figures IIa-d and IIIa-d represent two different cases. Images IIa and IIIa show the presence of all three channels, IIb and IIIb show the presence of collagen III and VAP-1, IIc and IIIc show the presence of collagen III and IId and IIId show the presence of VAP-1. N=2. Scale bars 20 μm. Co-localisation of the two markers can be seen as yellow in image IIb (white box), and the cases show the presence of valve cells surrounded by a dense collagen network associated with VAP-1. Individual areas of collagen III (orange arrow) and VAP-1 (white arrow) can also be seen. Certain areas of VAP-1 expression can also be seen with no collagen III expression.

S100 and VAP-1 in CHD and control valves and myxoma tissue

After reviewing the tissue sections with our pathologist, the overlap with cardiac myxomas was suggested. Cardiac myxomas are a benign tumour of the heart, and represent nearly half of all benign cardiac tumours, with an incidence of 0.03%.(358, 359) Around 75% of these tumours occur in the left atrium and are composed of fibrous and gelatinous areas. The myxoma cells are stellate, with the myxoma stroma composed of proteoglycans, elastin and collagen.(359) The cells producing VAP-1 appeared to display a stellate appearance, **Figure 52**.
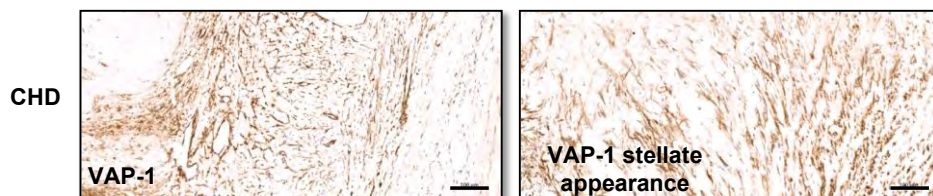
Figure 52: Representative images of CHD valves stained with VAP-1 with the cells producing VAP-1 have a stellate appearance. N=2. Scale bars 100 μm.

The presence of stellate cells in CHD in a myxoid background was found to be similar to the myxoma cells seen in cardiac myxomas, and therefore myxoma tissue was also stained to see if a similar cell type is present in both diseases. One of the cell markers known to be positive in cardiac myxomas is S100 (359, 360), which also has a stellate appearance, **Figure 53**. S100 is regulated by calcium binding and is capable of actively participating in processes involved in cellular proliferation, tumour angiogenesis and metastasis and immune evasion.(361)

233

Figure 53: Representative images of myxoma valves with S100 staining. Images I and II are separate cases. Images Ib and IIb are zoomed in areas of images Ia and IIa respectively. Cells producing S100 have a stellate appearance (black arrow in image Ib). Haemosiderin can also be seen which are golden in colour and granular in appearance (red box in image Ib). N=2. Scale bars as illustrated.

Myxoma tissue were also stained with VAP-1. VAP-1 expression was present in the myxoma tissue and some cells producing S100 did appear to be similar to the cells producing VAP-1, **Figure 54**.
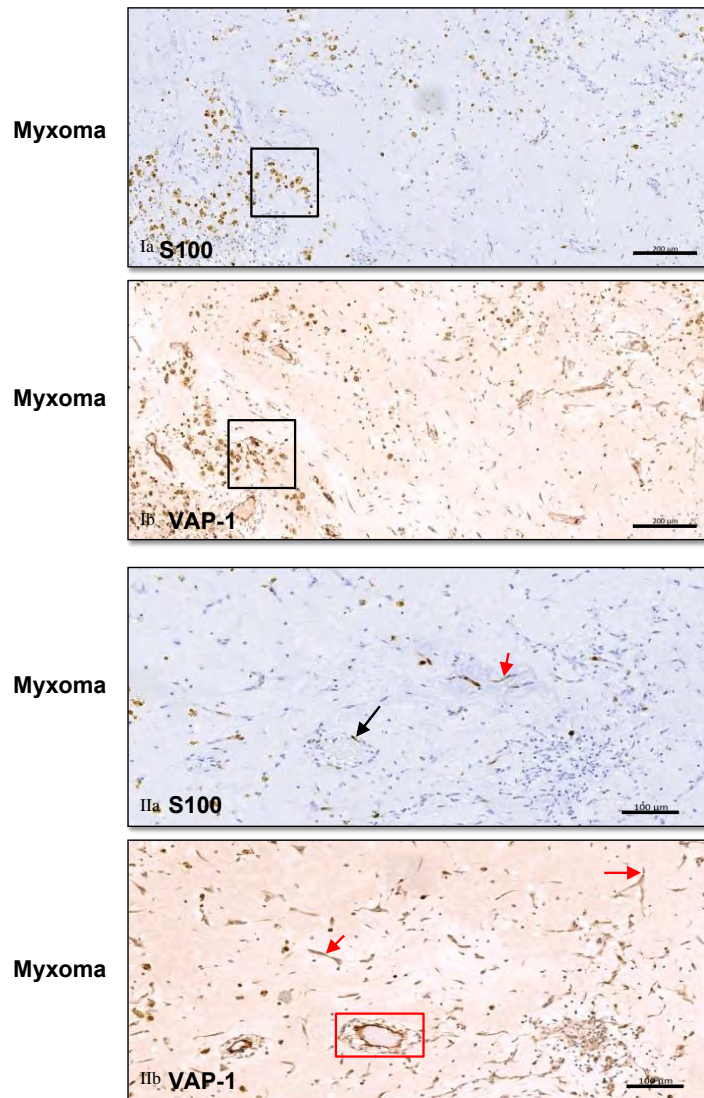
Figure 54: Representative images of matched myxoma cases with S100 and VAP-1 staining. Images Ia and IIa illustrate S100 staining and images Ib and IIb are matched cases of VAP-1 staining. Some myxoma cells producing S100 do appear to be similar to the cells producing VAP-1 (shown in black boxes). VAP-1 expression can be seen in myxoma tumour tissue as well. Image IIa shows the presence of myxoma cells around a vessel (black arrow). The stellate cell appearance can be clearly seen in Images IIa and IIb (red arrows). VAP-1 can again be seen lining the vasculature in image IIb (red box). In all images more VAP-1 positive cells can be seen compared to S100 positive cells. Scale bars as illustrated.

CHD and control valves were both stained with S100. In CHD, the cells producing S100 also have a stellate appearance. S100 positive cells are also seen in the control valves. **Figure 55**.

CHD

IIa **S100**

200 µm

CHD

IIb **VAP-1**

200 µm
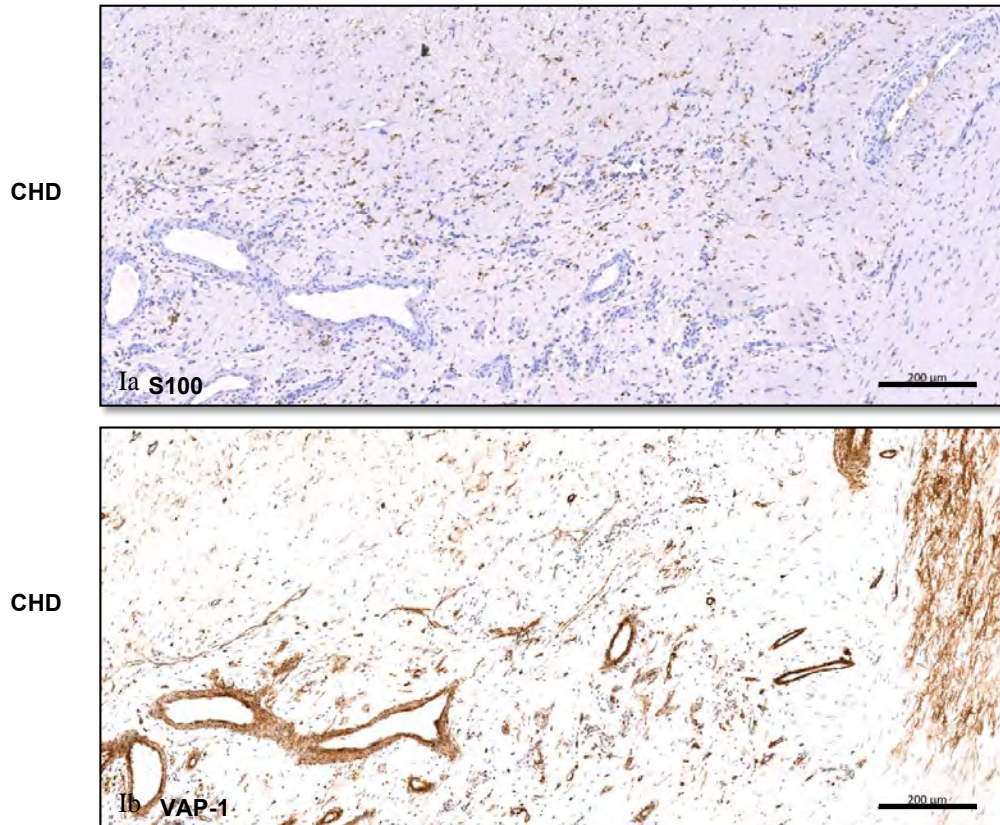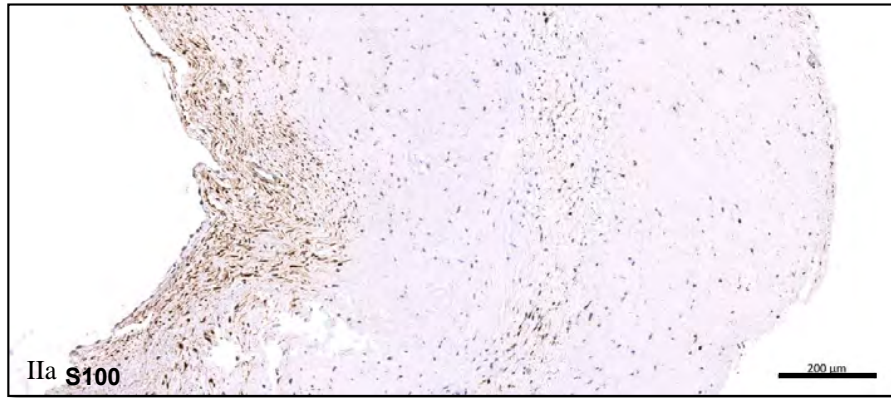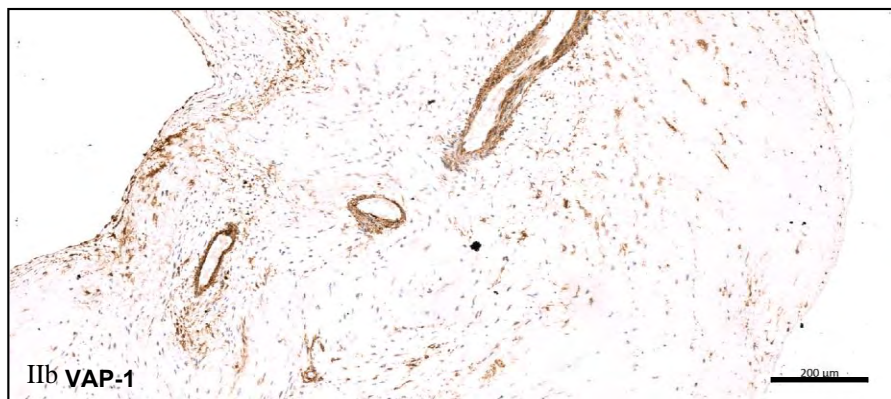
Zoomed in area of image IIa

IIc **S100**

100 µm

Control

IIIa **S100**

200 um

Control

IIIb **VAP-1**

200 um
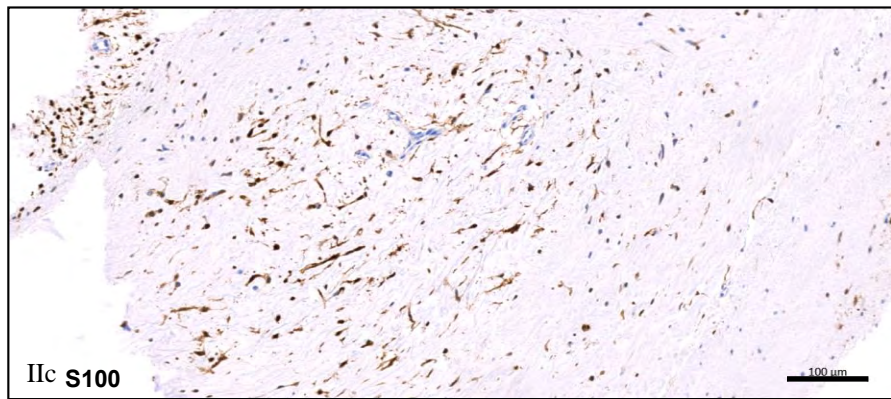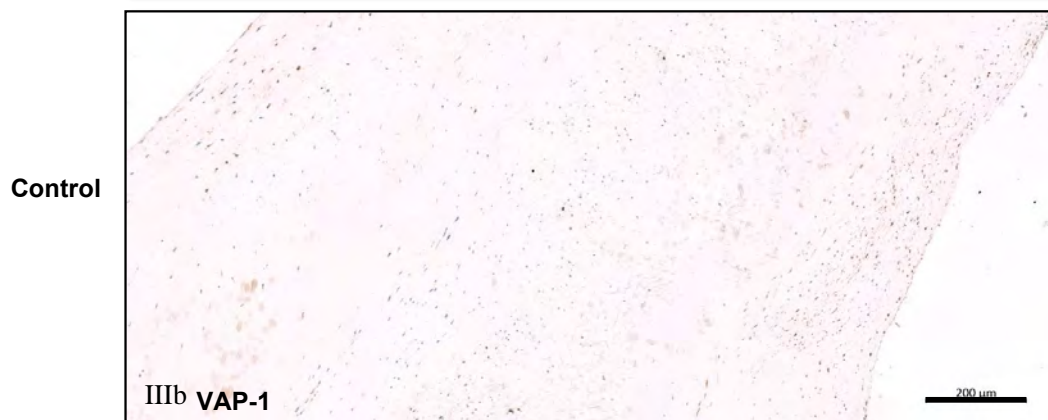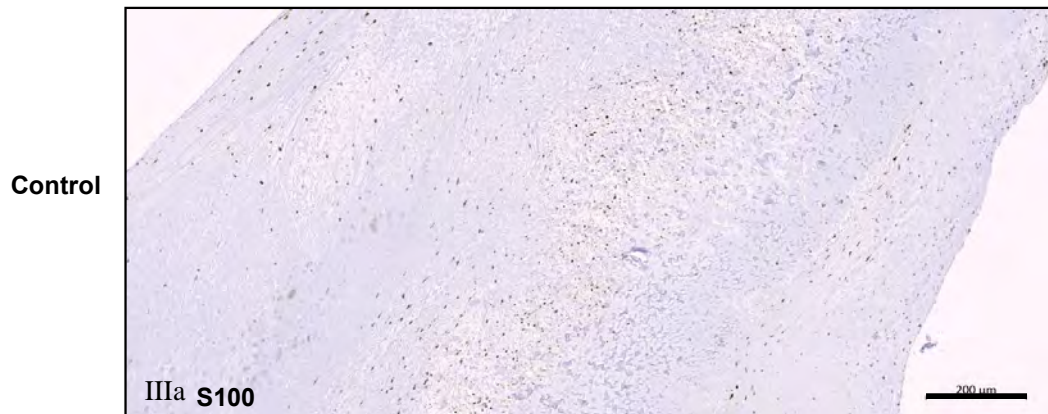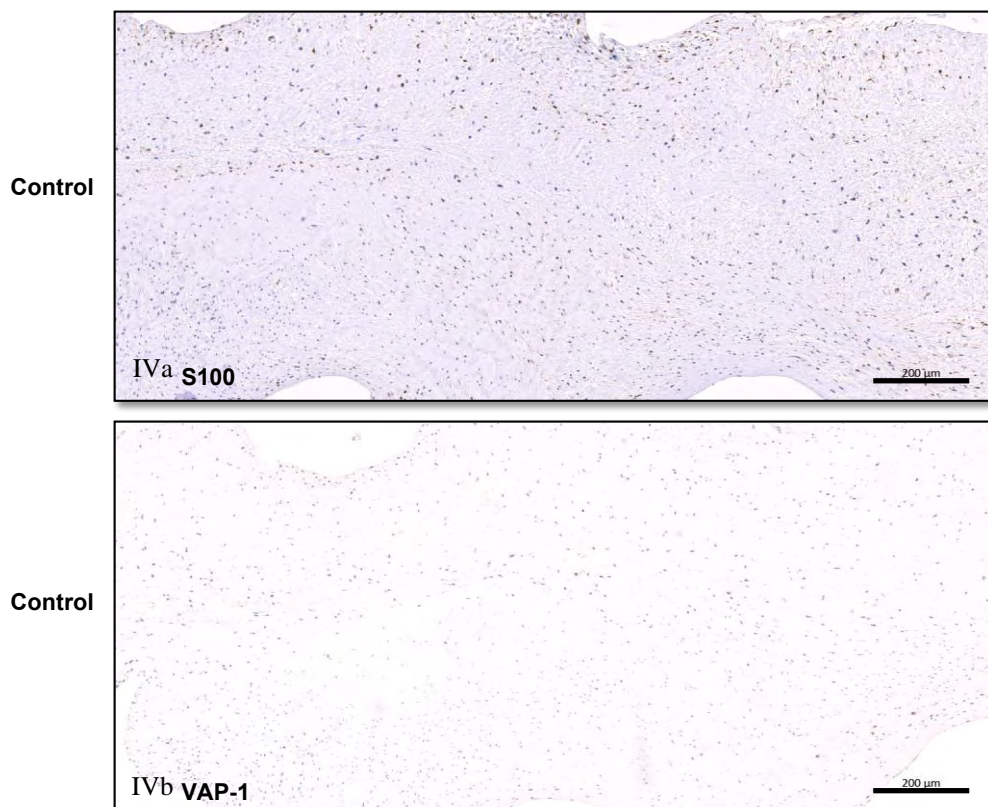
Figure 55: Representative images of CHD and control valve cases with S100 and VAP-1 staining. Images I and II are CHD cases and images III and IV are control valve cases. Images Ia, IIa, IIIa and IVa illustrate S100 staining and images Ib, IIb, IIIb and IVb show paired VAP-1 staining. Image IIc is a zoomed in area of S100 staining which shows the cells producing S100 in CHD also display a stellate appearance. S100 positive cells are also present in the control valves. N=4. Scale bars as illustrated.

Therefore, in summary this chapter shows a significantly increased VAP-1 tissue expression in CHD valves compared with control valves. A dense stromal and collagen network is present in the valves with co-localisation of VAP-1/collagen III and VAP-1//α-SMA seen in some areas. There is increased VAP-1 expression seen with older ECM in the carcinoid plaque and neovascularisation can be seen in the CHD valves but not in the control valves, possibly highlighting the angiogenesis role of VAP-1 in CHD.

6.4 Discussion

CHD is a serious complication associated with NETs and can lead to significant morbidity and mortality. Some patients may be asymptomatic and therefore making the diagnosis of CHD can be delayed where treatment options are then limited. Currently, the only definitive treatment for CHD is valve surgery which can only be performed if the patient is fit enough to undergo a major operation.

A significant difference in the VAP-1 expression was seen in the CHD cohort compared to the control valve cohort. VAP-1 expression was present in both the carcinoid plaque as well as in the atrial/ventricular and fibrous valve layers. A reason for the increased VAP-1 expression seen in CHD could be that expression of VAP-1 is driven by an increase in circulating amines. Either the amines themselves or the breakdown products from monoamine oxidases (or other amine oxidases) can stimulate certain cell populations to produce VAP-1, and subsequent autocrine and paracrine activities perpetuate expression of the protein. I would hypothesis therefore that in the control valves the circulating levels of amines are below a certain threshold that is required to trigger the expression of VAP-1 by these cells.

VAP-1 lined the vasculature both in the carcinoid plaque as well as in the underlying valve. The vascular areas seen within the underlying valve could be a result of hypoxia secondary to valve injury leading to neovascularisation, or may occur as a granulation repair response driven by VAP-1 present in the carcinoid plaque.

VAP-1 expression varied according to the CHD valve area. There was no VAP-1 expression seen in the chords of the CHD valve, with increasing VAP-1 expression evident with increasing degrees of fibrosis as revealed by EHVG staining. Increasing expression was seen in the myxoid area, collagen area and elastin area of the valve where fibrosis is most mature in the elastin area. The carcinoid plaque may contribute to a change in the nutrients, vascular supply and oxygenation to the plaque which then leads to development of the myxoid layer, and as the fibrosis matures, the collagen and the elastin layer then form. A scoring system for VAP-1 expression could be proposed, reflecting expression present in chords, myxoid, collagen and elastin area respectively.

Collagen I and collagen III were expressed in both the CHD and control valve groups. Collagen III stained more selectively than collagen I, with collagen I expression seen in both the cells producing collagen I as well as in the stroma surrounding the cells, whereas collagen III was seen in the cells producing it and not in the surrounding stroma. The positive staining seen in the control valves is probably because the control valves are not completely normal valves and therefore will have some pathology associated with them. CD45 positive staining was present in the CHD and control valves, and VAP-1 may have a role in the immune cell recruitment seen. In the control valves, the positive staining could be explained by the underlying valve injury that has occurred with the activation of VICs. Positive CD31 staining was seen in the CHD valves but not in the control valves, and this could be attributable to the angiogenesis role of VAP-1 leading to neovascularisation.

Another reason for the fibrosis and inflammatory cell recruitment seen in CHD could be that the products released by VAP-1 including hydrogen peroxide lead to further valvular damage which then results in the activation of VICs to enable valvular remodelling and repair. In the diseased CHD valves, the VICs stay in a continuous activated state leading to fibrosis, calcification and inflammation.

The dual fluorescent staining showed that VAP-1 was associated with a dense stromal and collagen network in the CHD group. Co-localisation of both VAP-1/collagen III and VAP-1/α-SMA were present but with reduced expression compared to the individual areas of α-SMA or collagen III and VAP-1 seen. This highlights that cells producing both VAP-1 and either collagen III or α-SMA are possibly present in these valves, but individual cell types also produce each marker independently. Certain areas of VAP-1 expression was present with no α-SMA / collagen III expression, which could suggest circulating soluble VAP-1 adhering to the carcinoid plaque and underlying valve matrix. Therefore more advanced techniques such as single cell RNA sequencing or laser capture microdissection may allow us to identify different stromal cell populations within these tissues, e.g. VAP-1+α-SMA- or VAP-1-α-SMA+, which have discrete functions.

The cell type producing VAP-1 displays a stellate appearance. This is also seen in cardiac myxomas where single stellate cells are embedded in a myxoid stroma.(362) S100 is a marker that has been shown to be positive in this cardiac tumour.(363) The cells producing S100 in CHD also displayed a stellate

appearance. S100 positive cells were also present in the control valves, which is not surprising given that S100 is a marker for one cell type of the valvular pVICs which is a source for activated valve interstitial cells following valvular injury.(253) Interestingly, the myxoma tissue also stained positive for VAP-1, and therefore could also be a potential treatment target in this group of patients.

6.5 Conclusion

CHD valves are associated with a dense collagen and stroma network with strong VAP-1 expression and the development of neovascularisation. VAP-1 may be a key driver of the cardiac fibrotic complication seen in NETs. Treatment options for CHD are limited at present, and diagnosis may be delayed if patients are asymptomatic or current biochemical markers used in clinical practice are normal. VAP-1 can therefore be utilised in various ways for CHD: it can be tagged with imaging, including both functional and anatomic imaging to diagnose the degree of fibrosis present, and it can also be used as a potential treatment target. Additionally, it can have a non-invasive role in the measurement of serum VAP-1 levels in this group which can then lead on to further investigations, diagnosis and treatment in a timely manner. This would therefore enable patients with CHD to have an additional treatment offered, which could potentially be given to those unsuitable for cardiac surgery, with an overall aim of improving their quality of life and overall survival.

CHAPTER 7: CONCLUSIONS AND FUTURE WORK

7.1 Overview

At present there can be a delay in diagnosing cancer at an early stage and detecting complications associated with the underlying tumour. This can then lead to limited treatment options available to patients once the cancer or associated complications have progressed to a certain stage or when the patient is physically not well enough to undergo invasive treatment, thereby increasing their morbidity and mortality.

Accurate biomarkers that assist clinicians in identifying and diagnosing early cancer correctly are ideal and beneficial. The prompt identification of complications associated with cancer is also necessary. Early cancer diagnosis and the recognition of the presence of complications associated with the underlying cancer both allow further investigations to be performed, with more treatment options available and the early commencement of treatment which in turn will improve patients' overall quality of life and survival.

7.2. Summary of principal findings

7.2.1 PIVKA-II in early HCC

PIVKA-II has been widely studied mainly in Asia and has been incorporated into the Japanese guidelines as part of HCC surveillance in their at-risk groups.(364) However, there is limited published data in Europe looking at the role of PIVKA-II in diagnosing early HCC. No studies in the UK have yet directly compared the role of PIVKA-II in diagnosing early HCC with AFP and evaluating which marker has a better sensitivity and specificity. Two scores (GALAD and BALAD-2) evaluated

in the UK have been shown to optimise the sensitivity and specificity in diagnosing HCC as well as showing a clear differentiation in the four different BALAD-2 score categories in the UK median survival.(48, 306) However, PIVKA-II's association with prognosis and the response of PIVKA-II with ablation treatment remain unknown.

In the data shown in chapter 3, PIVKA-II was not found to be superior to AFP in diagnosing early HCC and the combination of both markers was only marginally superior to AFP alone. These findings differ from previous studies where PIVKA-II was found to be a better marker in diagnosing early HCC compared to AFP,(98, 119), and the combination of both makers has a better performance in diagnosing HCC including in the early stages.(121, 365) Previous studies have shown similar results to these findings where AFP is superior to PIVKA-II in diagnosing early HCC.(22, 120) PIVKA-II was found to be superior in advanced stages of disease and showed a better performance in larger tumours, in keeping with previous studies.(130, 131) On explant histology, pre-transplant PIVKA-II levels were found to be significantly higher in the presence of MVI and in moderately- or poorly-differentiated HCC, which was not seen with AFP. Previous studies have also shown similar results with increased PIVKA-II levels seen in MVI, in moderately- or poorly-differentiated HCC, and has also been found to independently predict the presence of MVI.(122, 123) In this longitudinal analysis where samples were taken pre- and post-ablation, results showed that those who developed recurrence tended to have higher AFP and PIVKA-II levels that increased over time. There was a 100% vs 0% estimated recurrence rate in those with a pre-ablation PIVKA-II of $\geq$125 mAU/mL vs <125 mAU/mL. However, a weaker

association was seen with the pre-ablation AFP and estimated recurrence rate. Therefore, these findings do raise the need to consider whether AFP should be incorporated back into clinical guidelines in the surveillance of HCC in patients with cirrhosis. A meta-analysis published in 2018 found that in HCC patients treated with ablation and had elevated PIVKA-II levels, this was significantly associated with a poorer overall survival and recurrence-free survival.(139) A Japanese group showed that the cumulative survival rate, recurrence-free survival rates and staying within the MC were significantly lower in patients treated with ablation who had a PIVKA-II ≥100 mAU/mL compared to a PIVKA-II <100 mAU/mL.(141)

Compared to other biomarkers that have been studied, the sensitivity of PIVKA-II was found to be superior in this study compared to previous study findings of the sensitivity of AFP-L3 in diagnosing early HCC, but similar to GPC3.(11, 37) OPN, GP73 and molecular biomarkers were found to have a higher sensitivity in diagnosing early HCC compared to PIVKA-II.(28, 39, 44) A higher specificity in diagnosing early HCC was seen with a AFP-L3, GPC3 and molecular biomarkers compared to PIVKA-II.(22, 37, 44)

PIVKA-II could be a prognostic marker in HCC and may support patient stratification for therapy, in particular when a decision for ablation vs transplantation is being considered. PIVKA-II does also show a promising role in the surveillance of recurrent HCC post-ablation. A multi-centre analysis would validate PIVKA-II in patient cohorts in the UK. Additionally, assessing the use of the GALAD score and comparing this to individual markers would be beneficial in the UK to determine which method has the greatest sensitivity and specificity in

diagnosing early HCC. Increasing numbers in the longitudinal analysis and across various UK centres would also help to evaluate the role of PIVKA-II in the UK as a surveillance marker of developing recurrent HCC post-ablation, thereby enabling patient stratification for therapy.

7.2.2 VAP-1 in NETs

Despite NETs being generally slow-growing tumours, they can be associated with significant GI and cardiac valve pathology related to the underlying fibrosis.(196) This can then lead to complications that include intestinal obstruction and bowel ischaemia / infarction, CHD and heart failure. When GI complications occur, surgery is the only effective treatment. However, patients need to be fit enough to undergo surgery, and side-effects following surgery may also be problematic. CHD is the major cause of mortality and morbidity in patients with NETs and valve surgery is the only treatment that can be offered to patients and again, the patient has to be physically fit enough to have the operation.(213, 245) CHD can be asymptomatic, leading to a delayed diagnosis when the disease is at an advanced stage and treatment options are limited. Current biomarkers that are used in NETs are primarily used for monitoring of cancer, treatment response and to help determine overall prognosis. These include CgA, CgB, 5-HIAA and NT-proBNP. Higher levels of CgA correlate with tumour bulk (202) and 5-HIAA represents the hormone secretion by the tumour with elevated levels likely to be present in CS.(204, 210) NT-proBNP is a marker used to screen for CHD.(216) However, at present, there are no biomarkers that may indicate the presence of fibrosis which

will allow further investigations to be performed and treatment to be commenced at an earlier opportunity.

Circulating sVAP-1 have been shown to be higher in chronic liver disease, with levels correlating with the degree of fibrosis present.(277) Increased levels have also been found to be associated with a poorer liver transplant-free survival (either death or liver transplant).(291) There are trials that are targeting VAP-1 in their treatment, by either using a monoclonal antibody or a small molecule inhibitor of VAP-1.(323, 324)

I have therefore assessed the role of VAP-1 in NETs and CHD both as a circulating form as well as the tissue expression of this molecule, to see whether this marker could be associated with the presence of fibrosis seen in NETs.

7.2.2.1 The role of circulating sVAP-1 in NETs

The data in chapter 4 has shown significantly higher levels of sVAP-1 in pancreatic NETs, midgut NETs and CHD vs healthy controls. Analysing the midgut NET, CHD and healthy control groups alone, a significant difference in sVAP-1 levels was found between the midgut NET vs healthy controls, CHD vs healthy controls and midgut NET vs CHD. Interestingly the pancreatic NETs only showed a significant difference in sVAP-1 levels compared to the healthy controls and there was no significant difference in levels between the pancreatic NETs vs midgut NETs, nor the pancreatic NETs vs CHD groups. Despite the presence of CHD in pancreatic NETs being uncommon, circulating sVAP-1 levels did not differ significantly between both groups. Analysing the midgut NET and CHD groups

together, neither the presence of liver metastases, nor having surgery pre-sample collection influenced sVAP-1 levels. These findings differ from previous studies which have shown levels of sVAP-1 in other malignancies including colorectal cancer decreasing with disease progression.(297, 320) However, there have been similar findings with raised sVAP-1 seen in HCC.(322)

The longitudinal analysis demonstrated no significant change in sVAP-1 post-treatment, similar to the markers currently used in clinical practice. Similarly, no significant differences were seen in sVAP-1 levels in patients who underwent surgery prior to the first sample being taken compared to those who did not undergo surgery. Despite these results, a significant reduction was observed in the carcinoid syndrome symptoms experienced. Therefore, this highlights that sVAP-1 levels do not resemble the carcinoid symptoms experienced, and the symptoms improve after treatment when a reduction in hormone levels is the likely factor for this, whereas the underlying fibrous stroma is not affected by the treatment. Another possible reason is that the half-life of the circulating sVAP-1 levels is currently not known, and therefore serial measurements are required at the same timepoints for each patient in order to further assess the role of circulating sVAP-1.

Overall across the three disease groups, significant correlations were found between sVAP-1 and BMI (significant negative correlation), and sVAP-1 and HbA1c (significant positive correlation). Various studies have shown different correlations between sVAP-1 and BMI. A previous study has shown similar results with BMI correlating indirectly with sVAP-1 levels in women.(325) However,

another study showed no correlation between sVAP-1 levels and BMI (366), whereas a different study showed a direct correlation between sVAP-1 levels and morbid obesity in non-diabetics.(367) A study has shown that sVAP-1 levels are increased in type 1 diabetics, and that the elevated glucose levels did not increase sVAP-1 levels, but instead, circulating insulin concentrations indirectly correlate with sVAP-1 levels.(368) Increased levels of sVAP-1 are also thought to be a response to hyperglycaemia (369) and, through the SSAO activity of VAP-1 regulates glucose homeostasis by increasing glucose uptake and glucose transporter-4 expression.(370)

Circulating sVAP-1 levels could be an effective stratification marker for patients with NETs to predict outcomes and where to escalate therapy. Multi-centre evaluation of sVAP-1 levels within the UK and internationally would be important to validate this not only as a biomarker but also as a prognostic marker. My work has helped us collaborate with another large NET centre in Manchester, and we will also be receiving serum samples from their cohort of patients for sVAP-1 analysis. Immunohistochemistry analysis of pancreatic NETs is required to assess in further detail the tumour microenvironment and analyse the presence of fibrosis seen in this group.

7.2.2.2 Tissue expression of VAP-1 in NETs

Knowledge of the tumour microenvironment is important to gain an understanding of potential mechanisms occurring in the tumour stroma that may lead to tumour growth, survival and metastases.(333) Previous findings have

shown that there is predominantly a desmoplastic reaction with limited leucocyte presence in midgut NETs, therefore differing to other cancer microenvironments.(330) Limited knowledge is known on the exact ECM composition in midgut NETs but these tumours are known to highly express α-SMA in the tumour stroma.(336)

In CHD, the exact pathogenesis leading to this fibrotic complication is not fully understood. Exposure of high levels of serotonin and other vasoactive substances are thought to be involved in the pathogenesis and development of CHD.(355)

Tissue expression of VAP-1 was analysed in both midgut NETs and CHD with the data shown in chapters 5 and 6. In summary, the presence of VAP-1 is seen associated with a dense stromal and collagen network in both midgut NETs and CHD. An immune cell involvement can be appreciated with positive CD45 cells in a similar area to the presence of VAP-1. However, this is an observational finding and a previous study has shown the adhesive function of VAP-1 which drives the immune cell infiltration.(277) A similar underlying mechanism may also be present in midgut NETs. Staining midgut NET tissue sections with α-SMA and VAP-1 showed that the fibroblasts were in a very similar distribution to VAP-1, therefore suggesting that a similar cell type produces both markers. This is in keeping with previous findings of increased expression of α-SMA in the tumour stroma of midgut NETs.(336) Additionally, liver myofibroblasts have been shown to control both lymphocyte recruitment and positioning (351), and VAP-1 may have a similar role in controlling the entry

and retention of immune cell populations via either its adhesive function or enzymatic activity. Co-localisation of both VAP-1 and α-SMA, and VAP-1 and collagen I/III in both midgut NETs and CHD was present but with very low expression compared to areas of individual markers seen. Areas without overlap may be due to the presence of sVAP-1 associating with additional undefined cell types, and cells that have secreted VAP-1 into the media or downregulated VAP-1 protein production. Further studies using confocal microscopy with z-stack images and a broader cell marker panel are required to determine the extent of co-localisation. VAP-1 was seen in the ECM evident in midgut NETs, which may be the circulating sVAP-1 adhering to this area. Significantly higher tissue expression of VAP-1 was noted in the CHD valves compared to the control valves. Interestingly, increasing VAP-1 expression was seen through increasing fibrotic areas of the CHD plaque. This could be incorporated into a scoring system to help grade the severity of fibrosis in CHD.

The fibrosis and inflammatory cell recruitment seen in CHD could also be a result of the products released through the enzymatic activity of VAP-1 including hydrogen peroxide leading to further valvular damage, with resulting activation of VICs in response to valvular injury.(253) Positive CD31 staining was found in the CHD valves but not in the control valves. This could be the result of the angiogenesis role of VAP-1 resulting in neovascularisation which may be seen in tumour.(371) In order to confirm these possible explanations the mechanistic role of VAP-1 in CHD needs to be performed in future work. The cell type producing VAP-1 in CHD displayed a very similar appearance to the myxoma cells seen in cardiac myxomas.(362) To assess this further, S100 staining was

performed in both control and CHD valves, with positive staining seen in both groups. The cells producing S100 did appear to have a stellate appearance similar to VAP-1. Myxoma tissue was also stained with VAP-1 with positive expression seen, therefore suggesting VAP-1 could also be a future treatment target in cardiac myxomas.

Therefore, the tissue expression analysis of VAP-1 has shown that this molecule may play a role in the fibrosis seen in midgut NETs and may be involved in the pathogenesis and development of CHD. A previous study has suggested that there are discrete populations of fibroblasts that may be activated by different factors (296) and VAP-1 positive fibroblasts also expression the transcription factor NKX2-3, and therefore, this may also be a similar reason for the VAP-1 expression seen in NETs and CHD with expression being driven by certain mediators or the tumour ECM. In CHD, VAP-1 may also be a receptor to the high levels of circulating amines that then drives the fibrotic process and activates the VICs present in cardiac valves, accentuating the production of a fibrous stroma and a rich ECM seen in CHD. The association of VAP-1 and ECM in other tumours and fibrous tissue has not been fully explored and sVAP-1 may be trapped either on or in the ECM and then influence the immune and other cells function. Future trials comparing using a VAP-1 antibody vs. an enzyme inhibitor would be worthwhile looking into. The VAP-1 antibody solely blocks the VAP-1 receptor and the adhesive function of VAP-1 and does not have any effect on blocking the catalysis of small molecule amines. Therefore by comparing both the antibody with the enzyme inhibitor will allow us to understand if it is only the adhesive

function which is required to drive the fibrotic process or immune cell recruitment or if the enzyme function of VAP-1 is also necessary for this to take place.

7.3 Study limitations and study strengths

In this thesis, the biggest limitation for both projects are the low numbers of study participants for serum analysis, particularly in the longitudinal analyses. Additionally, in the longitudinal analyses, exact time-points for sample collections have not been taken for each patient with either a variable number of follow-up samples being taken or just one measurement post-treatment analysed. Therefore the timing and number of follow-up samples for all patients have not been consistent in either project. Serum samples taken for both projects were only from one centre. Having a multi-centre participation would not only increase patient numbers in both studies, but would also validate VAP-1 as a potential biomarker in NETs and CHD.

A limitation in the VAP-1 project is that the circulating sVAP-1 samples were not matched to the tissue sections analysed, and therefore no direct correlation between circulating sVAP-1 and tissue VAP-1 expression could be done. With the tissue sections stained in both the midgut NETs and CHD groups, no clinical information on the patients was known, and therefore correlating tissue expression of VAP-1 with demographics and various clinical factors could not be done. Additionally, the enzymatic function of VAP-1 is not known in these samples nor the levels of circulating amines present which may be driving the pathogenesis and expression of VAP-1. The findings of the tissue VAP-1

expression in NETs and CHD in this thesis are purely observational findings, and therefore do not suggest the underlying mechanistic role of VAP-1 in this group of tumours nor in CHD.

There are a number of strengths in both studies. Firstly, for both projects, this is the first time PIVKA-II has been analysed in the UK and compared it to AFP as a potential marker for diagnosing early HCC as well as a treatment response marker following ablation. Similarly, for the first time, the role of VAP-1 in NETs and CHD has been assessed both as tissue expression and also as a circulating form. Another strength of the PIVKA-II project is that pre-transplant serum PIVKA-II levels were matched with explant histology for all patients, and therefore allowed prognostic factors to be assessed according to serum PIVKA-II levels. In the VAP-1 project, the Queen Elizabeth Hospital Birmingham is one of the largest CHD centres, which allowed a good size CHD cohort to be recruited into the study.

7.4 Suggested future work

The PIVKA-II data presented in this thesis is very interesting and the suitability of PIVKA-II as a potential surveillance marker for recurrent HCC post-ablation is promising. Expanding numbers overall and having a multi-centre analysis would greatly strengthen the analysis of PIVKA-II in the UK. Further assessment in comparing PIVKA-II to other biomarkers discussed earlier (AFP-L3, GPC3, OPN, GP73, nucleic acids and miRNAs), in addition to the combination of biomarkers, is required in different centres in the UK to establish the optimal biomarker(s) required to diagnose early HCC. Additionally, comparing individual markers to the

GALAD score would allow us to evaluate which combination or marker(s) is the optimal way to diagnose early HCC in at-risk patients to enable an early diagnosis to be made so potentially curative treatment can be offered.

The role of VAP-1 in NETs and CHD shown in this thesis are observational findings. Evaluating the mechanistic role of VAP-1 in pre-clinical models would allow us to understand the pathways and mechanisms involved in the pathogenesis of fibrosis and development of CHD. Increasing numbers of study participants from various NET specialist centres would allow us to validate VAP-1 as a biomarker and a prognostic marker in NETs and CHD, and collaborations with The Christie Hospital are already underway. Additionally, at present NT-proBNP is the most effective biomarker used to screen for CHD.(218) Comparisons between sVAP-1 and NT-proBNP would be interesting to see which of these two markers is the best way to detect and diagnose CHD. Using reagents that target VAP-1 could be conjugated with either anatomic or functional imaging, which could both diagnose the presence of fibrosis and be used as treatment target in patients. VAP-1 has been shown to be expressed under normal conditions in vascular endothelial cells, adipocytes and smooth muscle cells.(371) Therefore targeting VAP-1 in NETs or CHD, may also affect VAP-1 expressed in non-target cells and have detrimental effects on normal tissue homeostasis. The precise role of VAP-1 in the modulation of ECM is not entirely known, and if VAP-1 is associated with the deposition and/or maturation of elastin, blocking VAP-1 may also disrupt the development of ECM components potentially leading to adverse events. It is known that genetic knockout of lysyl oxidase, a related amine oxidase that contributes to cross-linking of collagens and elastin (372) in mice

leads to perinatal death from weakening of the arterial walls.(373, 374) Therefore, a similar effect may also occur in humans by blocking VAP-1 if the timing and dosing is not chosen carefully. The circulating soluble form of VAP-1 may also have an undescribed beneficial role in human biology, and by removing this protein pool from the circulation may lead to increased potential for systemic inflammatory responses. A previous study has shown that using conjugated siglec-9 (lymphocytic ligand to VAP-1) with ^{68}Ga-DOTA imaging showed positive uptake in areas of tumour and inflammation.(284) Finally, plans are underway to enable a scoring system of fibrosis in NETs using radiological imaging which could then be matched to circulating sVAP-1 levels to enable an earlier recognition of fibrosis present, so treatment can then be offered at an appropriate time, thereby improving overall morbidity and mortality in this group of patients.

References

1.   Henry NL, Hayes DF. Cancer biomarkers. Mol Oncol. 2012;6(2):140-6.

2.   National Cancer Institute Dictionary of Cancer Terms [Available from: https://www.cancer.gov/publications/dictionaries/cancer-terms?expand=B.

3.   Ghouri YA, Mian I, Rowe JH. Review of hepatocellular carcinoma: Epidemiology, etiology, and carcinogenesis. J Carcinog. 2017;16:1.

4.   Liver Cancer Statistics [Available from: https://www.cancerresearchuk.org/health-professional/cancer-statistics/statistics-by-cancer-type/liver-cancer#heading-One.

5.   Zhang DY, Friedman SL. Fibrosis-dependent mechanisms of hepatocarcinogenesis. Hepatology. 2012;56(2):769-75.

6.   Seitz HK, Stickel F. Risk factors and mechanisms of hepatocarcinogenesis with special emphasis on alcohol and oxidative stress. Biol Chem. 2006;387(4):349-60.

7.   O'Rourke JM, Sagar VM, Shah T, Shetty S. Carcinogenesis on the background of liver fibrosis: Implications for the management of hepatocellular cancer. World J Gastroenterol. 2018;24(39):4436-47.

8.   Llovet JM, Zucman-Rossi J, Pikarsky E, Sangro B, Schwartz M, Sherman M, et al. Hepatocellular carcinoma. Nat Rev Dis Primers. 2016;2:16018.

9.   Yu DC, Chen J, Ding YT. Hypoxic and highly angiogenic non-tumor tissues surrounding hepatocellular carcinoma: the 'niche' of endothelial progenitor cells. Int J Mol Sci. 2010;11(8):2901-9.

10.   Seki E, Schnabl B. Role of innate immunity and the microbiota in liver fibrosis: crosstalk between the liver and gut. J Physiol. 2012;590(3):447-58.

11.   Tsuchiya N, Sawada Y, Endo I, Saito K, Uemura Y, Nakatsura T. Biomarkers for the early diagnosis of hepatocellular carcinoma. World J Gastroenterol. 2015;21(37):10573-83.

12.   Siegel RL, Miller KD, Jemal A. Cancer Statistics, 2017. CA Cancer J Clin. 2017;67(1):7-30.

13.   Soriano A, Varona A, Gianchandani R, Moneva ME, Arranz J, Gonzalez A, et al. Selection of patients with hepatocellular carcinoma for liver transplantation: Past and future. World J Hepatol. 2016;8(1):58-68.

14.   Kokudo N, Hasegawa K, Akahane M, Igaki H, Izumi N, Ichida T, et al. Evidence-based Clinical Practice Guidelines for Hepatocellular Carcinoma: The Japan Society of Hepatology 2013 update (3rd JSH-HCC Guidelines). Hepatol Res. 2015;45(2).

15.   Lim TS, Kim DY, Han KH, Kim HS, Shin SH, Jung KS, et al. Combined use of AFP, PIVKA-II, and AFP-L3 as tumor markers enhances diagnostic accuracy for hepatocellular carcinoma in cirrhotic patients. Scand J Gastroenterol. 2016;51(3):344-53.

16.   Bruix J, Sherman M, American Association for the Study of Liver D. Management of hepatocellular carcinoma: an update. Hepatology. 2011;53(3):1020-2.

17.   European Association For The Study Of The L, European Organisation For R, Treatment Of C. EASL-EORTC clinical practice guidelines: management of hepatocellular carcinoma. J Hepatol. 2012;56(4):908-43.

18.   Lou J, Zhang L, Lv S, Zhang C, Jiang S. Biomarkers for Hepatocellular Carcinoma. Biomark Cancer. 2017;9:1-9.

19.   Wan HG, Xu H, Gu YM, Wang H, Xu W, Zu MH. Comparison osteopontin vs AFP for the diagnosis of HCC: a meta-analysis. Clin Res Hepatol Gastroenterol. 2014;38(6):706-14.

20. Tangkijvanich P, Anukulkarnkusol N, Suwangool P, Lertmaharit S, Hanvivatvong O, Kullavanijaya P, et al. Clinical characteristics and prognosis of hepatocellular carcinoma: analysis based on serum alpha-fetoprotein levels. J Clin Gastroenterol. 2000;31(4):302-8.

21. Soresi M, Magliarisi C, Campagna P, Leto G, Bonfissuto G, Riili A, et al. Usefulness of alpha-fetoprotein in the diagnosis of hepatocellular carcinoma. Anticancer Res. 2003;23(2C):1747-53.

22. Marrero JA, Feng Z, Wang Y, Nguyen MH, Befeler AS, Roberts LR, et al. Alpha-fetoprotein, des-gamma carboxyprothrombin, and lectin-bound alpha-fetoprotein in early hepatocellular carcinoma. Gastroenterology. 2009;137(1):110-8.

23. Bai DS, Zhang C, Chen P, Jin SJ, Jiang GQ. The prognostic correlation of AFP level at diagnosis with pathological grade, progression, and survival of patients with hepatocellular carcinoma. Sci Rep. 2017;7(1):12870.

24. Tzartzeva K, Obi J, Rich NE, Parikh ND, Marrero JA, Yopp A, et al. Surveillance Imaging and Alpha Fetoprotein for Early Detection of Hepatocellular Carcinoma in Patients With Cirrhosis: A Meta-analysis. Gastroenterology. 2018;154(6):1706-18 e1.

25. Taketa K, Okada S, Win N, Hlaing NK, Wind KM. Evaluation of tumor markers for the detection of hepatocellular carcinoma in Yangon General Hospital, Myanmar. Acta Med Okayama. 2002;56(6):317-20.

26. Sung YK, Hwang SY, Park MK, Farooq M, Han IS, Bae HI, et al. Glypican-3 is overexpressed in human hepatocellular carcinoma. Cancer Sci. 2003;94(3):259-62.

27. Hippo Y, Watanabe K, Watanabe A, Midorikawa Y, Yamamoto S, Ihara S, et al. Identification of soluble NH2-terminal fragment of glypican-3 as a serological marker for early-stage hepatocellular carcinoma. Cancer Res. 2004;64(7):2418-23.

28. Marrero JA, Romano PR, Nikolaeva O, Steel L, Mehta A, Fimmel CJ, et al. GP73, a resident Golgi glycoprotein, is a novel serum marker for hepatocellular carcinoma. J Hepatol. 2005;43(6):1007-12.

29. Muramatsu T. Midkine and pleiotrophin: two related proteins involved in development, survival, inflammation and tumorigenesis. J Biochem. 2002;132(3):359-71.

30. Zhu WW, Guo JJ, Guo L, Jia HL, Zhu M, Zhang JB, et al. Evaluation of midkine as a diagnostic serum biomarker in hepatocellular carcinoma. Clin Cancer Res. 2013;19(14):3944-54.

31. Fouad SA, Mohamed NA, Fawzy MW, Moustafa DA. Plasma Osteopontin Level in Chronic Liver Disease and Hepatocellular Carcinoma. Hepat Mon. 2015;15(9):e30753.

32. Zhang H, Yao M, Wu W, Qiu L, Sai W, Yang J, et al. Up-regulation of annexin A2 expression predicates advanced clinicopathological features and poor prognosis in hepatocellular carcinoma. Tumour Biol. 2015;36(12):9373-83.

33. Mao Y, Yang H, Xu H, Lu X, Sang X, Du S, et al. Golgi protein 73 (GOLPH2) is a valuable serum marker for hepatocellular carcinoma. Gut. 2010;59(12):1687-93.

34. Giannelli G, Fransvea E, Trerotoli P, Beaugrand M, Marinosci F, Lupo L, et al. Clinical validation of combined serological biomarkers for improved hepatocellular carcinoma diagnosis in 961 patients. Clin Chim Acta. 2007;383(1-2):147-52.

35. Hussein MM, Ibrahim AA, Abdella HM, Montasser IF, Hassan MI. Evaluation of serum squamous cell carcinoma antigen as a novel biomarker for diagnosis of hepatocellular carcinoma in Egyptian patients. Indian J Cancer. 2008;45(4):167-72.

36.   Witjes CD, van Aalten SM, Steyerberg EW, Borsboom GJ, de Man RA, Verhoef C, et al. Recently introduced biomarkers for screening of hepatocellular carcinoma: a systematic review and meta-analysis. Hepatol Int. 2013;7(1):59-64.

37.   Jia X, Liu J, Gao Y, Huang Y, Du Z. Diagnosis accuracy of serum glypican-3 in patients with hepatocellular carcinoma: a systematic review with meta-analysis. Arch Med Res. 2014;45(7):580-8.

38.   Shevde LA, Das S, Clark DW, Samant RS. Osteopontin: an effector and an effect of tumor metastasis. Curr Mol Med. 2010;10(1):71-81.

39.   Shang S, Plymoth A, Ge S, Feng Z, Rosen HR, Sangrajrang S, et al. Identification of osteopontin as a novel marker for early hepatocellular carcinoma. Hepatology. 2012;55(2):483-90.

40.   Abu El Makarem MA, Abdel-Aleem A, Ali A, Saber R, Shatat M, Rahem DA, et al. Diagnostic significance of plasma osteopontin in hepatitis C virus-related hepatocellular carcinoma. Ann Hepatol. 2011;10(3):296-305.

41.   Kladney RD, Cui X, Bulla GA, Brunt EM, Fimmel CJ. Expression of GP73, a resident Golgi membrane protein, in viral and nonviral liver disease. Hepatology. 2002;35(6):1431-40.

42.   Hu JS, Wu DW, Liang S, Miao XY. GP73, a resident Golgi glycoprotein, is sensibility and specificity for hepatocellular carcinoma of diagnosis in a hepatitis B-endemic Asian population. Med Oncol. 2010;27(2):339-45.

43.   Villanueva A, Minguez B, Forner A, Reig M, Llovet JM. Hepatocellular carcinoma: novel molecular approaches for diagnosis, prognosis, and therapy. Annu Rev Med. 2010;61:317-28.

44.   Shi M, Chen MS, Sekar K, Tan CK, Ooi LL, Hui KM. A blood-based three-gene signature for the non-invasive detection of early human hepatocellular carcinoma. Eur J Cancer. 2014;50(5):928-36.

45.   Wang J, Sen S. MicroRNA functional network in pancreatic cancer: from biology to biomarkers of disease. J Biosci. 2011;36(3):481-91.

46.   Liu AM, Yao TJ, Wang W, Wong KF, Lee NP, Fan ST, et al. Circulating miR-15b and miR-130b in serum as potential markers for detecting hepatocellular carcinoma: a retrospective cohort study. BMJ Open. 2012;2(2):e000825.

47.   Berhane S, Toyoda H, Tada T, Kumada T, Kagebayashi C, Satomura S, et al. Role of the GALAD and BALAD-2 Serologic Models in Diagnosis of Hepatocellular Carcinoma and Prediction of Survival in Patients. Clin Gastroenterol Hepatol. 2016;14(6):875-86 e6.

48.   Johnson PJ. The BALAD-2 and GALAD Biomarker Models for Hepatocellular Carcinoma. Gastroenterol Hepatol (N Y). 2017;13(4):231-3.

49.   Toyoda H, Kumada T, Osaki Y, Oka H, Urano F, Kudo M, et al. Staging hepatocellular carcinoma by a novel scoring system (BALAD score) based on serum markers. Clin Gastroenterol Hepatol. 2006;4(12):1528-36.

50.   Best J, Bilgi H, Heider D, Schotten C, Manka P, Bedreli S, et al. The GALAD scoring algorithm based on AFP, AFP-L3, and DCP significantly improves detection of BCLC early stage hepatocellular carcinoma. Z Gastroenterol. 2016;54(12):1296-305.

51.   Kudo M. Review of 4th Single Topic Conference on HCC. Hepatocellular carcinoma: International consensus and controversies. Hepatol Res. 2007;37 Suppl 2:S83-7.

52.   Trinchet JC, Chaffaut C, Bourcier V, Degos F, Henrion J, Fontaine H, et al. Ultrasonographic surveillance of hepatocellular carcinoma in cirrhosis: a randomized trial comparing 3- and 6-month periodicities. Hepatology. 2011;54(6):1987-97.

53.   Singal A, Volk ML, Waljee A, Salgia R, Higgins P, Rogers MA, et al. Meta-analysis: surveillance with ultrasound for early-stage hepatocellular carcinoma in patients with cirrhosis. Aliment Pharmacol Ther. 2009;30(1):37-47.

54.   Andersson KL, Salomon JA, Goldie SJ, Chung RT. Cost effectiveness of alternative surveillance strategies for hepatocellular carcinoma in patients with cirrhosis. Clin Gastroenterol Hepatol. 2008;6(12):1418-24.

55.   Bruix J, Sherman M, Practice Guidelines Committee AAftSoLD. Management of hepatocellular carcinoma. Hepatology. 2005;42(5):1208-36.

56.   Roskams T, Kojiro M. Pathology of early hepatocellular carcinoma: conventional and molecular diagnosis. Semin Liver Dis. 2010;30(1):17-25.

57.   Forner A, Vilana R, Ayuso C, Bianchi L, Sole M, Ayuso JR, et al. Diagnosis of hepatic nodules 20 mm or smaller in cirrhosis: Prospective validation of the noninvasive diagnostic criteria for hepatocellular carcinoma. Hepatology. 2008;47(1):97-104.

58.   Silva MA, Hegab B, Hyde C, Guo B, Buckels JA, Mirza DF. Needle track seeding following biopsy of liver lesions in the diagnosis of hepatocellular cancer: a systematic review and meta-analysis. Gut. 2008;57(11):1592-6.

59.   Di Tommaso L, Franchi G, Park YN, Fiamengo B, Destro A, Morenghi E, et al. Diagnostic value of HSP70, glypican 3, and glutamine synthetase in hepatocellular nodules in cirrhosis. Hepatology. 2007;45(3):725-34.

60.   Di Tommaso L, Destro A, Seok JY, Balladore E, Terracciano L, Sangiovanni A, et al. The application of markers (HSP70 GPC3 and GS) in liver biopsies is useful for detection of hepatocellular carcinoma. J Hepatol. 2009;50(4):746-54.

61.   Tremosini S, Forner, A, Boix L, Rimola J, Rodriguez de Lope C, Reig, M, et al. . Biopsy diagnosis of hepatocellular carcinoma <2 cm: prosepective validation of glypican 3, heat-shock protein 70, and glutamine synthetase staining in fine needle biopsy samples. ILCA book of abstracts. 2011.

62.   International Consensus Group for Hepatocellular NeoplasiaThe International Consensus Group for Hepatocellular N. Pathologic diagnosis of early hepatocellular carcinoma: a report of the international consensus group for hepatocellular neoplasia. Hepatology. 2009;49(2):658-64.

63.   Lauwers GY, Terris B, Balis UJ, Batts KP, Regimbeau JM, Chang Y, et al. Prognostic histologic indicators of curatively resected hepatocellular carcinomas: a multi-institutional analysis of 425 patients with definition of a histologic prognostic index. Am J Surg Pathol. 2002;26(1):25-34.

64.   Selcuk H. Prognostic Factors and Staging Systems in Hepatocellular Carcinoma. Exp Clin Transplant. 2017;15(Suppl 2):45-9.

65.   Llovet JM, Burroughs A, Bruix J. Hepatocellular carcinoma. Lancet. 2003;362(9399):1907-17.

66.   D'Amico G, Garcia-Tsao G, Pagliaro L. Natural history and prognostic indicators of survival in cirrhosis: a systematic review of 118 studies. J Hepatol. 2006;44(1):217-31.

67.   Takayama T, Makuuchi M, Hirohashi S, Sakamoto M, Yamamoto J, Shimada K, et al. Early hepatocellular carcinoma as an entity with a high rate of surgical cure. Hepatology. 1998;28(5):1241-6.

68.   Livraghi T, Meloni F, Di Stasi M, Rolle E, Solbiati L, Tinelli C, et al. Sustained complete response and complications rates after radiofrequency ablation of very early hepatocellular carcinoma in cirrhosis: Is resection still the treatment of choice? Hepatology. 2008;47(1):82-9.

69.   Llovet JM, Fuster J, Bruix J. Intention-to-treat analysis of surgical treatment for early hepatocellular carcinoma: resection versus transplantation. Hepatology. 1999;30(6):1434-40.

70.   Llovet JM, Bruix J. Systematic review of randomized trials for unresectable hepatocellular carcinoma: Chemoembolization improves survival. Hepatology. 2003;37(2):429-42.

71.   Llovet JM, Ricci S, Mazzaferro V, Hilgard P, Gane E, Blanc JF, et al. Sorafenib in advanced hepatocellular carcinoma. N Engl J Med. 2008;359(4):378-90.

72.   Llovet JM, Bru C, Bruix J. Prognosis of hepatocellular carcinoma: the BCLC staging classification. Semin Liver Dis. 1999;19(3):329-38.

73.   Mazzaferro V, Regalia E, Doci R, Andreola S, Pulvirenti A, Bozzetti F, et al. Liver transplantation for the treatment of small hepatocellular carcinomas in patients with cirrhosis. N Engl J Med. 1996;334(11):693-9.

74.   Barbara L, Benzi G, Gaiani S, Fusconi F, Zironi G, Siringo S, et al. Natural history of small untreated hepatocellular carcinoma in cirrhosis: a multivariate analysis of prognostic factors of tumor growth rate and patient survival. Hepatology. 1992;16(1):132-7.

75.   Elshamy M, Aucejo F, Menon KV, Eghtesad B. Hepatocellular carcinoma beyond Milan criteria: Management and transplant selection criteria. World J Hepatol. 2016;8(21):874-80.

76.   Gosalia AJ, Martin P, Jones PD. Advances and Future Directions in the Treatment of Hepatocellular Carcinoma. Gastroenterol Hepatol (N Y). 2017;13(7):398-410.

77.   Mazzaferro V, Bhoori S, Sposito C, Bongini M, Langer M, Miceli R, et al. Milan criteria in liver transplantation for hepatocellular carcinoma: an evidence-based analysis of 15 years of experience. Liver Transpl. 2011;17 Suppl 2:S44-57.

78.   Zalewska K. Liver Transplantation: Selection Criteria and Recipient Registration. 2/5/2017.

79.   Duvoux C, Roudot-Thoraval F, Decaens T, Pessione F, Badran H, Piardi T, et al. Liver transplantation for hepatocellular carcinoma: a model including alpha-fetoprotein improves the performance of Milan criteria. Gastroenterology. 2012;143(4):986-94 e3; quiz e14-5.

80.   White SA, Manas DM, Farid SG, Prasad KR. Optimal treatment for hepatocellular carcinoma in the cirrhotic liver. Ann R Coll Surg Engl. 2009;91(7):545-50.

81.   Parikh ND, Waljee AK, Singal AG. Downstaging hepatocellular carcinoma: A systematic review and pooled analysis. Liver Transpl. 2015;21(9):1142-52.

82.   Duffy JP, Vardanian A, Benjamin E, Watson M, Farmer DG, Ghobrial RM, et al. Liver transplantation criteria for hepatocellular carcinoma should be expanded: a 22-year experience with 467 patients at UCLA. Ann Surg. 2007;246(3):502-9; discussion 9-11.

83.   NHS Blood and Transplant LAG. Liver transplantation for hepatocellular carcinoma in the UK - report from a national consensus meeting (Birmingham January 2014). 2014.

84.   Lencioni R, Llovet JM. Modified RECIST (mRECIST) assessment for hepatocellular carcinoma. Semin Liver Dis. 2010;30(1):52-60.

85. NHS Blood and Transplant ODaTD, Liver Advisory Group. Update on the HCC down-staging service evaluation. 2018.

86. Gordon-Weeks AN, Snaith A, Petrinic T, Friend PJ, Burls A, Silva MA. Systematic review of outcome of downstaging hepatocellular cancer before liver transplantation in patients outside the Milan criteria. Br J Surg. 2011;98(9):1201-8.

87. Liebman HA, Furie BC, Tong MJ, Blanchard RA, Lo KJ, Lee SD, et al. Des-gamma-carboxy (abnormal) prothrombin as a serum marker of primary hepatocellular carcinoma. N Engl J Med. 1984;310(22):1427-31.

88. Xing H, Yan C, Cheng L, Wang N, Dai S, Yuan J, et al. Clinical application of protein induced by vitamin K antagonist-II as a biomarker in hepatocellular carcinoma. Tumour Biol. 2016.

89. Stenflo J. Vitamin K and the biosynthesis of prothrombin. II. Structural comparison of normal and dicoumarol-induced bovine prothrombin. J Biol Chem. 1972;247(24):8167-75.

90. Stenflo J, Ganrot PO. Vitamin K and the biosynthesis of prothrombin. I. Identification and purification of a dicoumarol-induced abnormal prothrombin from bovine plasma. J Biol Chem. 1972;247(24):8160-6.

91. Stenflo J, Fernlund P, Egan W, Roepstorff P. Vitamin K dependent modifications of glutamic acid residues in prothrombin. Proc Natl Acad Sci U S A. 1974;71(7):2730-3.

92. Fernlund P, Stenflo J, Roepstorff P, Thomsen J. Vitamin K and the biosynthesis of prothrombin. V. Gamma-carboxyglutamic acids, the vitamin K-dependent structures in prothrombin. J Biol Chem. 1975;250(15):6125-33.

93. Morris HR, Dell A. Mass-spectrometric identification and sequence location of the ten residues of the new amino acid (gamma-Carboxyglutamic acid) in the N-terminal region of prothrombin. Biochem J. 1976;153(3):663-79.

94. Chapter 10: vitamin K [Available from: http://www.fao.org/docrep/004/y2809e/y2809e0g.htm.

95. Jinghe X, Mizuta T, Ozaki I. Vitamin K and hepatocellular carcinoma: The basic and clinic. World J Clin Cases. 2015;3(9):757-64.

96. Uotila L. Chapter 49 Vitamin K: Metabolic functions, mechanism of action, and human requirements 1997 [965-84]. Available from: https://www.sciencedirect.com/science/article/pii/S1569258297801109.

97. Naraki T, Kohno N, Saito H, Fujimoto Y, Ohhira M, Morita T, et al. gamma-Carboxyglutamic acid content of hepatocellular carcinoma-associated des-gamma-carboxy prothrombin. Biochim Biophys Acta. 2002;1586(3):287-98.

98. Zakhary NI, Khodeer SM, Shafik HE, Abdel Malak CA. Impact of PIVKA-II in diagnosis of hepatocellular carcinoma. J Adv Res. 2013;4(6):539-46.

99. Kinukawa H, Shirakawa T, Yoshimura T. Epitope characterization of an anti-PIVKA-II antibody and evaluation of a fully automated chemiluminescent immunoassay for PIVKA-II. Clin Biochem. 2015;48(16-17):1120-5.

100. Liebman HA. Isolation and characterization of a hepatoma-associated abnormal (des-gamma-carboxy)prothrombin. Cancer Res. 1989;49(23):6493-7.

101. Yamagata H, Nakanishi T, Furukawa M, Okuda H, Obata H. Levels of vitamin K, immunoreactive prothrombin, des-gamma-carboxy prothrombin and gamma-glutamyl carboxylase activity in hepatocellular carcinoma tissue. J Gastroenterol Hepatol. 1995;10(1):8-13.

102. Miyakawa T, Kajiwara Y, Shirahata A, Okamoto K, Itoh H, Ohsato K. Vitamin K contents in liver tissue of hepatocellular carcinoma patients. Jpn J Cancer Res. 2000;91(1):68-74.

103. Bardelli A, Longati P, Williams TA, Benvenuti S, Comoglio PM. A peptide representing the carboxyl-terminal tail of the met receptor inhibits kinase activity and invasive growth. J Biol Chem. 1999;274(41):29274-81.

104. Ponzetto C, Bardelli A, Zhen Z, Maina F, dalla Zonca P, Giordano S, et al. A multifunctional docking site mediates signaling and transformation by the hepatocyte growth factor/scatter factor receptor family. Cell. 1994;77(2):261-71.

105. Ferracini R, Longati P, Naldini L, Vigna E, Comoglio PM. Identification of the major autophosphorylation site of the Met/hepatocyte growth factor receptor tyrosine kinase. J Biol Chem. 1991;266(29):19558-64.

106. Hu CT, Wu JR, Cheng CC, Wu WS. The Therapeutic Targeting of HGF/c-Met Signaling in Hepatocellular Carcinoma: Alternative Approaches. Cancers (Basel). 2017;9(6).

107. Kim KH, Kim H. Progress of antibody-based inhibitors of the HGF-cMET axis in cancer therapy. Exp Mol Med. 2017;49(3):e307.

108. Suzuki M, Shiraha H, Fujikawa T, Takaoka N, Ueda N, Nakanishi Y, et al. Des-gamma-carboxy prothrombin is a potential autologous growth factor for hepatocellular carcinoma. J Biol Chem. 2005;280(8):6409-15.

109. Zhang YS, Chu JH, Cui SX, Song ZY, Qu XJ. Des-gamma-carboxy prothrombin (DCP) as a potential autologous growth factor for the development of hepatocellular carcinoma. Cell Physiol Biochem. 2014;34(3):903-15.

110. Inagaki Y, Qi F, Gao J, Qu X, Hasegawa K, Sugawara Y, et al. Effect of c-Met inhibitor SU11274 on hepatocellular carcinoma cell growth. Biosci Trends. 2011;5(2):52-6.

111. Morimoto Y, Nouso K, Wada N, Takeuchi Y, Kinugasa H, Miyahara K, et al. Involvement of platelets in extrahepatic metastasis of hepatocellular carcinoma. Hepatol Res. 2014;44(14):E353-9.

112. Yue P, Gao ZH, Xue X, Cui SX, Zhao CR, Yuan Y, et al. Des-gamma-carboxyl prothrombin induces matrix metalloproteinase activity in hepatocellular carcinoma cells by involving the ERK1/2 MAPK signalling pathway. Eur J Cancer. 2011;47(7):1115-24.

113. Muto J, Shirabe K, Sugimachi K, Maehara Y. Review of angiogenesis in hepatocellular carcinoma. Hepatol Res. 2015;45(1):1-9.

114. Wang YH, Dong YY, Wang WM, Xie XY, Wang ZM, Chen RX, et al. Vascular endothelial cells facilitated HCC invasion and metastasis through the Akt and NF-kappaB pathways induced by paracrine cytokines. J Exp Clin Cancer Res. 2013;32(1):51.

115. Cui SX, Yu XF, Qu XJ. Roles and Signaling Pathways of Des-gamma-Carboxyprothrombin in the Progression of Hepatocellular Carcinoma. Cancer Invest. 2016;34(9):459-64.

116. Matsubara M, Shiraha H, Kataoka J, Iwamuro M, Horiguchi S, Nishina S, et al. Des-gamma-carboxyl prothrombin is associated with tumor angiogenesis in hepatocellular carcinoma. J Gastroenterol Hepatol. 2012;27(10):1602-8.

117. Fujikawa T, Shiraha H, Ueda N, Takaoka N, Nakanishi Y, Matsuo N, et al. Des-gamma-carboxyl prothrombin-promoted vascular endothelial cell proliferation and migration. J Biol Chem. 2007;282(12):8741-8.

118. Servier [Available from: http://www.servier.co.uk.

119. Pote N, Cauchy F, Albuquerque M, Voitot H, Belghiti J, Castera L, et al. Performance of PIVKA-II for early hepatocellular carcinoma diagnosis and prediction of microvascular invasion. J Hepatol. 2015;62(4):848-54.

120. Chen H, Zhang Y, Li S, Li N, Chen Y, Zhang B, et al. Direct comparison of five serum biomarkers in early diagnosis of hepatocellular carcinoma. Cancer Manag Res. 2018;10:1947-58.

121. Ertle JM, Heider D, Wichert M, Keller B, Kueper R, Hilgard P, et al. A combination of alpha-fetoprotein and des-gamma-carboxy prothrombin is superior in detection of hepatocellular carcinoma. Digestion. 2013;87(2):121-31.

122. Ma XL, Zhu J, Wu J, Tian L, Gao YY, Zhang CY, et al. Significance of PIVKA-II levels for predicting microvascular invasion and tumor cell proliferation in Chinese patients with hepatitis B virus-associated hepatocellular carcinoma. Oncol Lett. 2018;15(6):8396-404.

123. Wang X, Zhang W, Liu Y, Gong W, Sun P, Kong X, et al. Diagnostic value of prothrombin induced by the absence of vitamin K or antagonist-II (PIVKA-II) for early stage HBV related hepatocellular carcinoma. Infect Agent Cancer. 2017;12:47.

124. Wu J, Xiang Z, Bai L, He L, Tan L, Hu M, et al. Diagnostic value of serum PIVKA-II levels for BCLC early hepatocellular carcinoma and correlation with HBV DNA. Cancer Biomark. 2018.

125. Viggiani V, Palombi S, Gennarini G, D'Ettorre G, De Vito C, Angeloni A, et al. Protein induced by vitamin K absence or antagonist-II (PIVKA-II) specifically increased in Italian hepatocellular carcinoma patients. Scand J Gastroenterol. 2016;51(10):1257-62.

126. Caviglia GP, Ribaldone DG, Abate ML, Ciancio A, Pellicano R, Smedile A, et al. Performance of protein induced by vitamin K absence or antagonist-II assessed by chemiluminescence enzyme immunoassay for hepatocellular carcinoma detection: a meta-analysis. Scand J Gastroenterol. 2018:1-7.

127. Choi JY, Jung SW, Kim HY, Kim M, Kim Y, Kim DG, et al. Diagnostic value of AFP-L3 and PIVKA-II in hepatocellular carcinoma according to total-AFP. World J Gastroenterol. 2013;19(3):339-46.

128. Park SJ, Jang JY, Jeong SW, Cho YK, Lee SH, Kim SG, et al. Usefulness of AFP, AFP-L3, and PIVKA-II, and their combinations in diagnosing hepatocellular carcinoma. Medicine (Baltimore). 2017;96(11):e5811.

129. Choi J, Kim GA, Han S, Lee W, Chun S, Lim YS. Longitudinal Assessment of Three Serum Biomarkers to Detect Very Early Stage Hepatocellular Carcinoma. Hepatology. 2018.

130. Durazo FA, Blatt LM, Corey WG, Lin JH, Han S, Saab S, et al. Des-gamma-carboxyprothrombin, alpha-fetoprotein and AFP-L3 in patients with chronic hepatitis, cirrhosis and hepatocellular carcinoma. J Gastroenterol Hepatol. 2008;23(10):1541-8.

131. Yu R, Tan Z, Xiang X, Dan Y, Deng G. Effectiveness of PIVKA-II in the detection of hepatocellular carcinoma based on real-world clinical data. BMC Cancer. 2017;17(1):608.

132. Inagaki Y, Xu HL, Hasegawa K, Aoki T, Beck Y, Sugawara Y, et al. Des-gamma-carboxyprothrombin in patients with hepatocellular carcinoma and liver cirrhosis. J Dig Dis. 2011;12(6):481-8.

133. Tamano M, Sugaya H, Oguma M, Iijima M, Yoneda M, Murohisa T, et al. Serum and tissue PIVKA-II expression reflect the biological malignant potential of small hepatocellular carcinoma. Hepatol Res. 2002;22(4):261-9.

134.   Tang W, Kokudo N, Sugawara Y, Guo Q, Imamura H, Sano K, et al. Des-gamma-carboxyprothrombin expression in cancer and/or non-cancer liver tissues: association with survival of patients with resectable hepatocellular carcinoma. Oncol Rep. 2005;13(1):25-30.

135.   Miskad UA, Yano Y, Nakaji M, Kishi S, Itoh H, Kim SR, et al. Histological study of PIVKA-II expression in hepatocellular carcinoma and adenomatous hyperplasia. Pathol Int. 2001;51(12):916-22.

136.   Borie F, Bouvier AM, Herrero A, Faivre J, Launoy G, Delafosse P, et al. Treatment and prognosis of hepatocellular carcinoma: a population based study in France. J Surg Oncol. 2008;98(7):505-9.

137.   Ebara M, Okabe S, Kita K, Sugiura N, Fukuda H, Yoshikawa M, et al. Percutaneous ethanol injection for small hepatocellular carcinoma: therapeutic efficacy based on 20-year observation. J Hepatol. 2005;43(3):458-64.

138.   Huang GT, Lee PH, Tsang YM, Lai MY, Yang PM, Hu RH, et al. Percutaneous ethanol injection versus surgical resection for the treatment of small hepatocellular carcinoma: a prospective study. Ann Surg. 2005;242(1):36-42.

139.   Zhang D, Liu Z, Yin X, Qi X, Lu B, Liu Y, et al. Prognostic value of PIVKA-II in hepatocellular carcinoma patients receiving curative ablation: A systematic review and meta-analysis. Int J Biol Markers. 2018:1724600818760234.

140.   Shiina S, Tateishi R, Arano T, Uchino K, Enooku K, Nakagawa H, et al. Radiofrequency ablation for hepatocellular carcinoma: 10-year outcome and prognostic factors. Am J Gastroenterol. 2012;107(4):569-77; quiz 78.

141.   Takahashi S, Kudo M, Chung H, Inoue T, Ishikawa E, Kitai S, et al. PIVKA-II is the best prognostic predictor in patients with hepatocellular carcinoma after radiofrequency ablation therapy. Oncology. 2008;75 Suppl 1:91-8.

142.   Ramage JK, Ahmed A, Ardill J, Bax N, Breen DJ, Caplin ME, et al. Guidelines for the management of gastroenteropancreatic neuroendocrine (including carcinoid) tumours (NETs). Gut. 2012;61(1):6-32.

143.   Xavier S, Rosa B, Cotter J. Small bowel neuroendocrine tumors: From pathophysiology to clinical approach. World J Gastrointest Pathophysiol. 2016;7(1):117-24.

144.   Jernman J, Valimaki MJ, Louhimo J, Haglund C, Arola J. The novel WHO 2010 classification for gastrointestinal neuroendocrine tumours correlates well with the metastatic potential of rectal neuroendocrine tumours. Neuroendocrinology. 2012;95(4):317-24.

145.   Williams ED, Sandler M. The classification of carcinoid tum ours. Lancet. 1963;1(7275):238-9.

146.   Duh QY, Hybarger CP, Geist R, Gamsu G, Goodman PC, Gooding GA, et al. Carcinoids associated with multiple endocrine neoplasia syndromes. Am J Surg. 1987;154(1):142-8.

147.   Griffiths DF, Williams GT, Williams ED. Duodenal carcinoid tumours, phaeochromocytoma and neurofibromatosis: islet cell tumour, phaeochromocytoma and the von Hippel-Lindau complex: two distinctive neuroendocrine syndromes. Q J Med. 1987;64(245):769-82.

148.   Tamura K, Nishimori I, Ito T, Yamasaki I, Igarashi H, Shuin T. Diagnosis and management of pancreatic neuroendocrine tumor in von Hippel-Lindau disease. World J Gastroenterol. 2010;16(36):4515-8.

149.   Debas HT, Mulvihill SJ. Neuroendocrine gut neoplasms. Important lessons from uncommon tumors. Arch Surg. 1994;129(9):965-71; discussion 71-2.

150.   Kytola S, Nord B, Elder EE, Carling T, Kjellman M, Cedermark B, et al. Alterations of the SDHD gene locus in midgut carcinoids, Merkel cell carcinomas, pheochromocytomas, and abdominal paragangliomas. Genes Chromosomes Cancer. 2002;34(3):325-32.

151.   Reichlin S. Secretion of somatostatin and its physiologic function. J Lab Clin Med. 1987;109(3):320-6.

152.   Barnett P. Somatostatin and somatostatin receptor physiology. Endocrine. 2003;20(3):255-64.

153.   Patel YC. Somatostatin and its receptor family. Front Neuroendocrinol. 1999;20(3):157-98.

154.   Kunz PL. Carcinoid and neuroendocrine tumors: building on success. J Clin Oncol. 2015;33(16):1855-63.

155.   Longnecker SM. Somatostatin and octreotide: literature review and description of therapeutic activity in pancreatic neoplasia. Drug Intell Clin Pharm. 1988;22(2):99-106.

156.   Papotti M, Bongiovanni M, Volante M, Allia E, Landolfi S, Helboe L, et al. Expression of somatostatin receptor types 1-5 in 81 cases of gastrointestinal and pancreatic endocrine tumors. A correlative immunohistochemical and reverse-transcriptase polymerase chain reaction analysis. Virchows Arch. 2002;440(5):461-75.

157.   Reubi JC, Waser B, Schaer JC, Laissue JA. Somatostatin receptor sst1-sst5 expression in normal and neoplastic human tissues using receptor autoradiography with subtype-selective ligands. Eur J Nucl Med. 2001;28(7):836-46.

158.   Banck MS, Kanwar R, Kulkarni AA, Boora GK, Metge F, Kipp BR, et al. The genomic landscape of small intestine neuroendocrine tumors. J Clin Invest. 2013;123(6):2502-8.

159.   Francis JM, Kiezun A, Ramos AH, Serra S, Pedamallu CS, Qian ZR, et al. Somatic mutation of CDKN1B in small intestine neuroendocrine tumors. Nat Genet. 2013;45(12):1483-6.

160.   Scarpa A, Chang DK, Nones K, Corbo V, Patch AM, Bailey P, et al. Whole-genome landscape of pancreatic neuroendocrine tumours. Nature. 2017;543(7643):65-71.

161.   England PH. Incidence and survival in neuroendocrine tumours and neuroendocrine carcinomas (NETs / NECs) in England, 2013 - 2014. 2016 [Available from: http://www.ukinets.org/2016/10/public-health-england-publishes-net-data/.

162.   Sagar VM, Elshafie M, Shah T. Making the Diagnosis of Neuroendocrine Tumour Disease. In: Cross T, Palmer DH, editors. Liver Cancers From Mechanisms to Management. 1 ed: Springer; 2019. p. 245-58.

163.   Kulke MH, Siu LL, Tepper JE, Fisher G, Jaffe D, Haller DG, et al. Future directions in the treatment of neuroendocrine tumors: consensus report of the National Cancer Institute Neuroendocrine Tumor clinical trials planning meeting. J Clin Oncol. 2011;29(7):934-43.

164.   Kim SJ, Kim JW, Han SW, Oh DY, Lee SH, Kim DW, et al. Biological characteristics and treatment outcomes of metastatic or recurrent neuroendocrine tumors: tumor grade and metastatic site are important for treatment strategy. BMC Cancer. 2010;10:448.

165.   Pape UF, Jann H, Muller-Nordhorn J, Bockelbrink A, Berndt U, Willich SN, et al. Prognostic relevance of a novel TNM classification system for upper gastroenteropancreatic neuroendocrine tumors. Cancer. 2008;113(2):256-65.

166.   Kim JY, Hong SM, Ro JY. Recent updates on grading and classification of neuroendocrine tumors. Ann Diagn Pathol. 2017;29:11-6.

167.   Oberg K, Castellano D. Current knowledge on diagnosis and staging of neuroendocrine tumors. Cancer Metastasis Rev. 2011;30 Suppl 1:3-7.

168.   Scoazec JY, Couvelard A, Reseau T. [Classification of pancreatic neuroendocrine tumours: Changes made in the 2017 WHO classification of tumours of endocrine organs and perspectives for the future]. Ann Pathol. 2017;37(6):444-56.

169.   Travis WD, Brambilla E, Nicholson AG, Yatabe Y, Austin JHM, Beasley MB, et al. The 2015 World Health Organization Classification of Lung Tumors: Impact of Genetic, Clinical and Radiologic Advances Since the 2004 Classification. J Thorac Oncol. 2015;10(9):1243-60.

170.   Caplin ME, Baudin E, Ferolla P, Filosso P, Garcia-Yuste M, Lim E, et al. Pulmonary neuroendocrine (carcinoid) tumors: European Neuroendocrine Tumor Society expert consensus and recommendations for best practice for typical and atypical pulmonary carcinoids. Ann Oncol. 2015;26(8):1604-20.

171.   Zandee WT, Kamp K, van Adrichem RC, Feelders RA, de Herder WW. Effect of hormone secretory syndromes on neuroendocrine tumor prognosis. Endocr Relat Cancer. 2017;24(7):R261-R74.

172.   Kaltsas GA, Besser GM, Grossman AB. The diagnosis and medical management of advanced neuroendocrine tumors. Endocr Rev. 2004;25(3):458-511.

173.   Gut P, Waligorska-Stachura J, Czarnywojtek A, Sawicka-Gutaj N, Baczyk M, Ziemnicka K, et al. Management of the hormonal syndrome of neuroendocrine tumors. Arch Med Sci. 2017;13(3):515-24.

174.   Papaxoinis G, Syrigos K, Saif MW. New concepts in the treatment strategy of neuroendocrine tumors: the role of biotherapy. Discov Med. 2016;21(117):381-9.

175.   Farley HA, Pommier RF. Surgical Treatment of Small Bowel Neuroendocrine Tumors. Hematol Oncol Clin North Am. 2016;30(1):49-61.

176.   Grozinsky-Glasberg S, Grossman AB, Gross DJ. Carcinoid Heart Disease: From Pathophysiology to Treatment--'Something in the Way It Moves'. Neuroendocrinology. 2015;101(4):263-73.

177.   Grozinsky-Glasberg S, Shimon I, Korbonits M, Grossman AB. Somatostatin analogues in the control of neuroendocrine tumours: efficacy and mechanisms. Endocr Relat Cancer. 2008;15(3):701-20.

178.   Page IH. Serotonin (5-hydroxytryptamine). Physiol Rev. 1954;34(3):563-88.

179.   Thorson A, Biorck G, Bjorkman G, Waldenstrom J. Malignant carcinoid of the small intestine with metastases to the liver, valvular disease of the right side of the heart (pulmonary stenosis and tricuspid regurgitation without septal defects), peripheral vasomotor symptoms, bronchoconstriction, and an unusual type of cyanosis; a clinical and pathologic syndrome. Am Heart J. 1954;47(5):795-817.

180.   Pavel M, O'Toole D, Costa F, Capdevila J, Gross D, Kianmanesh R, et al. ENETS Consensus Guidelines Update for the Management of Distant Metastatic Disease of Intestinal, Pancreatic, Bronchial Neuroendocrine Neoplasms (NEN) and NEN of Unknown Primary Site. Neuroendocrinology. 2016;103(2):172-85.

181.   Modlin IM, Pavel M, Kidd M, Gustafsson BI. Review article: somatostatin analogues in the treatment of gastroenteropancreatic neuroendocrine (carcinoid) tumours. Aliment Pharmacol Ther. 2010;31(2):169-88.

182.   Rinke A, Muller HH, Schade-Brittinger C, Klose KJ, Barth P, Wied M, et al. Placebo-controlled, double-blind, prospective, randomized study on the effect of

octreotide LAR in the control of tumor growth in patients with metastatic neuroendocrine midgut tumors: a report from the PROMID Study Group. J Clin Oncol. 2009;27(28):4656-63.

183.   Caplin ME, Pavel M, Cwikla JB, Phan AT, Raderer M, Sedlackova E, et al. Lanreotide in metastatic enteropancreatic neuroendocrine tumors. N Engl J Med. 2014;371(3):224-33.

184.   Lamarca A, Barriuso J, McNamara MG, Hubner RA, Valle JW. Telotristat ethyl: a new option for the management of carcinoid syndrome. Expert Opin Pharmacother. 2016;17(18):2487-98.

185.   Bodei L, Cwikla JB, Kidd M, Modlin IM. The role of peptide receptor radionuclide therapy in advanced/metastatic thoracic neuroendocrine tumors. J Thorac Dis. 2017;9(Suppl 15):S1511-S23.

186.   Strosberg J, El-Haddad G, Wolin E, Hendifar A, Yao J, Chasen B, et al. Phase 3 Trial of (177)Lu-Dotatate for Midgut Neuroendocrine Tumors. N Engl J Med. 2017;376(2):125-35.

187.   Pavel ME, Hainsworth JD, Baudin E, Peeters M, Horsch D, Winkler RE, et al. Everolimus plus octreotide long-acting repeatable for the treatment of advanced neuroendocrine tumours associated with carcinoid syndrome (RADIANT-2): a randomised, placebo-controlled, phase 3 study. Lancet. 2011;378(9808):2005-12.

188.   Yao JC, Fazio N, Singh S, Buzzoni R, Carnaghi C, Wolin E, et al. Everolimus for the treatment of advanced, non-functional neuroendocrine tumours of the lung or gastrointestinal tract (RADIANT-4): a randomised, placebo-controlled, phase 3 study. Lancet. 2016;387(10022):968-77.

189.   Liu E, Marincola P, Oberg K. Everolimus in the treatment of patients with advanced pancreatic neuroendocrine tumors: latest findings and interpretations. Therap Adv Gastroenterol. 2013;6(5):412-9.

190.   Delle Fave G, O'Toole D, Sundin A, Taal B, Ferolla P, Ramage JK, et al. ENETS Consensus Guidelines Update for Gastroduodenal Neuroendocrine Neoplasms. Neuroendocrinology. 2016;103(2):119-24.

191.   Li TT, Qiu F, Qian ZR, Wan J, Qi XK, Wu BY. Classification, clinicopathologic features and treatment of gastric neuroendocrine tumors. World J Gastroenterol. 2014;20(1):118-25.

192.   Hoffmann KM, Furukawa M, Jensen RT. Duodenal neuroendocrine tumors: Classification, functional syndromes, diagnosis and medical treatment. Best Pract Res Clin Gastroenterol. 2005;19(5):675-97.

193.   Cacciapuoti F, Agrusta M, Chiorazzo G, Midolla A, Agrusta F, Cacciapuoti F. Carcinoid Heart Disease: A Rare Cause of Right Ventricular Dysfunction Evaluation by Transthoracic 2D, Doppler and 3-D Echocardiography. J Cardiovasc Ultrasound. 2011;19(2):99-101.

194.   Sagar VM, Cooper SC, Johnson J, Shetty S, Shah T. Gastrointestinal manifestations of neuroendocrine tumours: their investigation and management. Postgrad Med J. 2017;93(1102):494-7.

195.   Bhattacharyya S, Burke M, Caplin ME, Davar J. Utility of 3D transoesophageal echocardiography for the assessment of tricuspid and pulmonary valves in carcinoid heart disease. Eur J Echocardiogr. 2011;12(1):E4.

196.   Laskaratos FM, Rombouts K, Caplin M, Toumpanakis C, Thirlwell C, Mandair D. Neuroendocrine tumors and fibrosis: An unsolved mystery? Cancer. 2017;123(24):4770-90.

197. Druce MR, Bharwani N, Akker SA, Drake WM, Rockall A, Grossman AB. Intra-abdominal fibrosis in a recent cohort of patients with neuroendocrine ('carcinoid') tumours of the small bowel. QJM. 2010;103(3):177-85.

198. Daskalakis K, Karakatsanis A, Stalberg P, Norlen O, Hellman P. Clinical signs of fibrosis in small intestinal neuroendocrine tumours. Br J Surg. 2017;104(1):69-75.

199. Makridis C, Ekbom A, Bring J, Rastad J, Juhlin C, Oberg K, et al. Survival and daily physical activity in patients treated for advanced midgut carcinoid tumors. Surgery. 1997;122(6):1075-82.

200. Klimstra DS. Pathology reporting of neuroendocrine tumors: essential elements for accurate diagnosis, classification, and staging. Semin Oncol. 2013;40(1):23-36.

201. Klimstra DS, Beltran H, Lilenbaum R, Bergsland E. The spectrum of neuroendocrine tumors: histologic classification, unique features and areas of overlap. Am Soc Clin Oncol Educ Book. 2015:92-103.

202. Oberg K, Modlin IM, De Herder W, Pavel M, Klimstra D, Frilling A, et al. Consensus on biomarkers for neuroendocrine tumour disease. Lancet Oncol. 2015;16(9):e435-e46.

203. Deftos LJ. Chromogranin A: its role in endocrine function and as an endocrine and neuroendocrine tumor marker. Endocr Rev. 1991;12(2):181-7.

204. Oberg K, Couvelard A, Delle Fave G, Gross D, Grossman A, Jensen RT, et al. ENETS Consensus Guidelines for Standard of Care in Neuroendocrine Tumours: Biochemical Markers. Neuroendocrinology. 2017;105(3):201-11.

205. Baudin E, Gigliotti A, Ducreux M, Ropers J, Comoy E, Sabourin JC, et al. Neuron-specific enolase and chromogranin A as markers of neuroendocrine tumours. Br J Cancer. 1998;78(8):1102-7.

206. Modlin IM, Gustafsson BI, Moss SF, Pavel M, Tsolakis AV, Kidd M. Chromogranin A--biological function and clinical utility in neuro endocrine tumor disease. Ann Surg Oncol. 2010;17(9):2427-43.

207. Sanduleanu S, De Bruine A, Stridsberg M, Jonkers D, Biemond I, Hameeteman W, et al. Serum chromogranin A as a screening test for gastric enterochromaffin-like cell hyperplasia during acid-suppressive therapy. Eur J Clin Invest. 2001;31(9):802-11.

208. Razzore P AG. Circulating neuroendocrine tumors biomarkers. Why? When? How? Suggestions for clinical practice from guidelines and consensus. J Cancer Metasta Treat. 2016;2:348-56.

209. O'Toole D, Grossman A, Gross D, Delle Fave G, Barkmanova J, O'Connor J, et al. ENETS Consensus Guidelines for the Standards of Care in Neuroendocrine Tumors: biochemical markers. Neuroendocrinology. 2009;90(2):194-202.

210. Meijer WG, Kema IP, Volmer M, Willemse PH, de Vries EG. Discriminating capacity of indole markers in the diagnosis of carcinoid tumors. Clin Chem. 2000;46(10):1588-96.

211. Feldman JM. Urinary serotonin in the diagnosis of carcinoid tumors. Clin Chem. 1986;32(5):840-4.

212. Feldman JM, O'Dorisio TM. Role of neuropeptides and serotonin in the diagnosis of carcinoid tumors. Am J Med. 1986;81(6B):41-8.

213. Davar J, Connolly HM, Caplin ME, Pavel M, Zacks J, Bhattacharyya S, et al. Diagnosing and Managing Carcinoid Heart Disease in Patients With Neuroendocrine Tumors: An Expert Statement. J Am Coll Cardiol. 2017;69(10):1288-304.

214. Tellez MR, Mamikunian G, O'Dorisio TM, Vinik AI, Woltering EA. A single fasting plasma 5-HIAA value correlates with 24-hour urinary 5-HIAA values and other biomarkers in midgut neuroendocrine tumors (NETs). Pancreas. 2013;42(3):405-10.

215. Bay M, Kirk V, Parner J, Hassager C, Nielsen H, Krogsgaard K, et al. NT-proBNP: a new diagnostic screening tool to differentiate between patients with normal and reduced left ventricular systolic function. Heart. 2003;89(2):150-4.

216. Korse CM, Taal BG, de Groot CA, Bakker RH, Bonfrer JM. Chromogranin-A and N-terminal pro-brain natriuretic peptide: an excellent pair of biomarkers for diagnostics in patients with neuroendocrine tumor. J Clin Oncol. 2009;27(26):4293-9.

217. Sabatasso S, Vaucher P, Augsburger M, Donze N, Mangin P, Michaud K. Sensitivity and specificity of NT-proBNP to detect heart failure at post mortem examination. Int J Legal Med. 2011;125(6):849-56.

218. Bhattacharyya S, Toumpanakis C, Caplin ME, Davar J. Usefulness of N-terminal pro-brain natriuretic peptide as a biomarker of the presence of carcinoid heart disease. Am J Cardiol. 2008;102(7):938-42.

219. Basuroy R, Srirajaskanthan R, Ramage JK. Neuroendocrine Tumors. Gastroenterol Clin North Am. 2016;45(3):487-507.

220. Thoeni RF, Mueller-Lisse UG, Chan R, Do NK, Shyn PB. Detection of small, functional islet cell tumors in the pancreas: selection of MR imaging sequences for optimal sensitivity. Radiology. 2000;214(2):483-90.

221. Owen NJ, Sohaib SA, Peppercorn PD, Monson JP, Grossman AB, Besser GM, et al. MRI of pancreatic neuroendocrine tumours. Br J Radiol. 2001;74(886):968-73.

222. Reubi JC. Somatostatin and other Peptide receptors as tools for tumor diagnosis and treatment. Neuroendocrinology. 2004;80 Suppl 1:51-6.

223. Kwekkeboom DJ, Krenning EP, Scheidhauer K, Lewington V, Lebtahi R, Grossman A, et al. ENETS Consensus Guidelines for the Standards of Care in Neuroendocrine Tumors: somatostatin receptor imaging with (111)In-pentetreotide. Neuroendocrinology. 2009;90(2):184-9.

224. Lu SJ, Gnanasegaran G, Buscombe J, Navalkissoor S. Single photon emission computed tomography/computed tomography in the evaluation of neuroendocrine tumours: a review of the literature. Nucl Med Commun. 2013;34(2):98-107.

225. Maxwell JE, Howe JR. Imaging in neuroendocrine tumors: an update for the clinician. Int J Endocr Oncol. 2015;2(2):159-68.

226. Bural GG, Muthukrishnan A, Oborski MJ, Mountz JM. Improved Benefit of SPECT/CT Compared to SPECT Alone for the Accurate Localization of Endocrine and Neuroendocrine Tumors. Mol Imaging Radionucl Ther. 2012;21(3):91-6.

227. Krausz Y, Keidar Z, Kogan I, Even-Sapir E, Bar-Shalom R, Engel A, et al. SPECT/CT hybrid imaging with 111In-pentetreotide in assessment of neuroendocrine tumours. Clin Endocrinol (Oxf). 2003;59(5):565-73.

228. Dromain C, de Baere T, Lumbroso J, Caillet H, Laplanche A, Boige V, et al. Detection of liver metastases from endocrine tumors: a prospective comparison of somatostatin receptor scintigraphy, computed tomography, and magnetic resonance imaging. J Clin Oncol. 2005;23(1):70-8.

229. Chiti A, Fanti S, Savelli G, Romeo A, Bellanova B, Rodari M, et al. Comparison of somatostatin receptor imaging, computed tomography and ultrasound in the clinical management of neuroendocrine gastro-entero-pancreatic tumours. Eur J Nucl Med. 1998;25(10):1396-403.

230. Dahdaleh FS, Lorenzen A, Rajput M, Carr JC, Liao J, Menda Y, et al. The value of preoperative imaging in small bowel neuroendocrine tumors. Ann Surg Oncol. 2013;20(6):1912-7.

231. Shi W, Johnston CF, Buchanan KD, Ferguson WR, Laird JD, Crothers JG, et al. Localization of neuroendocrine tumours with [111In] DTPA-octreotide scintigraphy (Octreoscan): a comparative study with CT and MR imaging. QJM. 1998;91(4):295-301.

232. Balon HR, Brown TL, Goldsmith SJ, Silberstein EB, Krenning EP, Lang O, et al. The SNM practice guideline for somatostatin receptor scintigraphy 2.0. J Nucl Med Technol. 2011;39(4):317-24.

233. Gabriel M, Decristoforo C, Kendler D, Dobrozemsky G, Heute D, Uprimny C, et al. 68Ga-DOTA-Tyr3-octreotide PET in neuroendocrine tumors: comparison with somatostatin receptor scintigraphy and CT. J Nucl Med. 2007;48(4):508-18.

234. Sundin A. Radiological and nuclear medicine imaging of gastroenteropancreatic neuroendocrine tumours. Best Pract Res Clin Gastroenterol. 2012;26(6):803-18.

235. Ambrosini V, Campana D, Tomassetti P, Fanti S. (6)(8)Ga-labelled peptides for diagnosis of gastroenteropancreatic NET. Eur J Nucl Med Mol Imaging. 2012;39 Suppl 1:S52-60.

236. Ambrosini V, Campana D, Bodei L, Nanni C, Castellucci P, Allegri V, et al. 68Ga-DOTANOC PET/CT clinical impact in patients with neuroendocrine tumors. J Nucl Med. 2010;51(5):669-73.

237. Vallabhajosula S, Nikolopoulou A. Radioiodinated metaiodobenzylguanidine (MIBG): radiochemistry, biology, and pharmacology. Semin Nucl Med. 2011;41(5):324-33.

238. Raja A, Leung K, Stamm M, Girgis S, Low G. Multimodality imaging findings of pheochromocytoma with associated clinical and biochemical features in 53 patients with histologically confirmed tumors. AJR Am J Roentgenol. 2013;201(4):825-33.

239. Lumachi F, Tregnaghi A, Zucchetta P, Cristina Marzola M, Cecchin D, Grassetto G, et al. Sensitivity and positive predictive value of CT, MRI and 123I-MIBG scintigraphy in localizing pheochromocytomas: a prospective study. Nucl Med Commun. 2006;27(7):583-7.

240. Ezziddin S, Logvinski T, Yong-Hing C, Ahmadzadehfar H, Fischer HP, Palmedo H, et al. Factors predicting tracer uptake in somatostatin receptor and MIBG scintigraphy of metastatic gastroenteropancreatic neuroendocrine tumors. J Nucl Med. 2006;47(2):223-33.

241. Sundin A, Eriksson B, Bergstrom M, Langstrom B, Oberg K, Orlefors H. PET in the diagnosis of neuroendocrine tumors. Ann N Y Acad Sci. 2004;1014:246-57.

242. Pasquali C, Rubello D, Sperti C, Gasparoni P, Liessi G, Chierichetti F, et al. Neuroendocrine tumor imaging: can 18F-fluorodeoxyglucose positron emission tomography detect tumors with poor prognosis and aggressive behavior? World J Surg. 1998;22(6):588-92.

243. Hayes AR, Davar J, Caplin ME. Carcinoid Heart Disease: A Review. Endocrinol Metab Clin North Am. 2018;47(3):671-82.

244. Bhattacharyya S, Toumpanakis C, Caplin ME, Davar J. Analysis of 150 patients with carcinoid syndrome seen in a single year at one institution in the first decade of the twenty-first century. Am J Cardiol. 2008;101(3):378-81.

245. Fox DJ, Khattar RS. Carcinoid heart disease: presentation, diagnosis, and management. Heart. 2004;90(10):1224-8.

246.   Pellikka PA, Tajik AJ, Khandheria BK, Seward JB, Callahan JA, Pitot HC, et al. Carcinoid heart disease. Clinical and echocardiographic spectrum in 74 patients. Circulation. 1993;87(4):1188-96.

247.   Bhattacharyya S, Toumpanakis C, Burke M, Taylor AM, Caplin ME, Davar J. Features of carcinoid heart disease identified by 2- and 3-dimensional echocardiography and cardiac MRI. Circ Cardiovasc Imaging. 2010;3(1):103-11.

248.   Connolly HM, Nishimura RA, Smith HC, Pellikka PA, Mullany CJ, Kvols LK. Outcome of cardiac surgery for carcinoid heart disease. J Am Coll Cardiol. 1995;25(2):410-6.

249.   Dobson R, Burgess MI, Valle JW, Pritchard DM, Vora J, Wong C, et al. Serial surveillance of carcinoid heart disease: factors associated with echocardiographic progression and mortality. Br J Cancer. 2014;111(9):1703-9.

250.   Moller JE, Pellikka PA, Bernheim AM, Schaff HV, Rubin J, Connolly HM. Prognosis of carcinoid heart disease: analysis of 200 cases over two decades. Circulation. 2005;112(21):3320-7.

251.   Askew JW, Connolly HM. Carcinoid valve disease. Curr Treat Options Cardiovasc Med. 2013;15(5):544-55.

252.   Mulholland DL, Gotlieb AI. Cell biology of valvular interstitial cells. Can J Cardiol. 1996;12(3):231-6.

253.   Liu AC, Joag VR, Gotlieb AI. The emerging role of valve interstitial cell phenotypes in regulating heart valve pathobiology. Am J Pathol. 2007;171(5):1407-18.

254.   Helske S, Kupari M, Lindstedt KA, Kovanen PT. Aortic valve stenosis: an active atheroinflammatory process. Curr Opin Lipidol. 2007;18(5):483-91.

255.   Rutkovskiy A, Malashicheva A, Sullivan G, Bogdanova M, Kostareva A, Stenslokken KO, et al. Valve Interstitial Cells: The Key to Understanding the Pathophysiology of Heart Valve Calcification. J Am Heart Assoc. 2017;6(9).

256.   Durbin AD, Gotlieb AI. Advances towards understanding heart valve response to injury. Cardiovasc Pathol. 2002;11(2):69-77.

257.   Armstrong EJ, Bischoff J. Heart valve development: endothelial cell signaling and differentiation. Circ Res. 2004;95(5):459-70.

258.   Paranya G, Vineberg S, Dvorin E, Kaushal S, Roth SJ, Rabkin E, et al. Aortic valve endothelial cells undergo transforming growth factor-beta-mediated and non-transforming growth factor-beta-mediated transdifferentiation in vitro. Am J Pathol. 2001;159(4):1335-43.

259.   Paruchuri S, Yang JH, Aikawa E, Melero-Martin JM, Khan ZA, Loukogeorgakis S, et al. Human pulmonary valve progenitor cells exhibit endothelial/mesenchymal plasticity in response to vascular endothelial growth factor-A and transforming growth factor-beta2. Circ Res. 2006;99(8):861-9.

260.   Yoder MC, Mead LE, Prater D, Krier TR, Mroueh KN, Li F, et al. Redefining endothelial progenitor cells via clonal analysis and hematopoietic stem/progenitor cell principals. Blood. 2007;109(5):1801-9.

261.   Tamura K, Jones M, Yamada I, Ferrans VJ. Wound healing in the mitral valve. J Heart Valve Dis. 2000;9(1):53-63.

262.   Desmouliere A, Badid C, Bochaton-Piallat ML, Gabbiani G. Apoptosis during wound healing, fibrocontractive diseases and vascular wall injury. Int J Biochem Cell Biol. 1997;29(1):19-30.

263. Rajamannan NM, Caplice N, Anthikad F, Sebo TJ, Orszulak TA, Edwards WD, et al. Cell proliferation in carcinoid valve disease: a mechanism for serotonin effects. J Heart Valve Dis. 2001;10(6):827-31.

264. Elangbam CS, Job LE, Zadrozny LM, Barton JC, Yoon LW, Gates LD, et al. 5-hydroxytryptamine (5HT)-induced valvulopathy: compositional valvular alterations are associated with 5HT2B receptor and 5HT transporter transcript changes in Sprague-Dawley rats. Exp Toxicol Pathol. 2008;60(4-5):253-62.

265. Bhattacharyya S, Davar J, Dreyfus G, Caplin ME. Carcinoid heart disease. Circulation. 2007;116(24):2860-5.

266. Schweizer W, Gloor F, Von B, Dubach UC. Carcinoid Heart Disease with Left-Sided Lesions. Circulation. 1964;29:253-7.

267. Zuetenhorst JM, Bonfrer JM, Korse CM, Bakker R, van Tinteren H, Taal BG. Carcinoid heart disease: the role of urinary 5-hydroxyindoleacetic acid excretion and plasma levels of atrial natriuretic peptide, transforming growth factor-beta and fibroblast growth factor. Cancer. 2003;97(7):1609-15.

268. Denney WD, Kemp WE, Jr., Anthony LB, Oates JA, Byrd BF, 3rd. Echocardiographic and biochemical evaluation of the development and progression of carcinoid heart disease. J Am Coll Cardiol. 1998;32(4):1017-22.

269. Moller JE, Connolly HM, Rubin J, Seward JB, Modesto K, Pellikka PA. Factors associated with progression of carcinoid heart disease. N Engl J Med. 2003;348(11):1005-15.

270. Bhattacharyya S, Toumpanakis C, Chilkunda D, Caplin ME, Davar J. Risk factors for the development and progression of carcinoid heart disease. Am J Cardiol. 2011;107(8):1221-6.

271. Salmi M, Jalkanen S. VAP-1: an adhesin and an enzyme. Trends Immunol. 2001;22(4):211-6.

272. Jalkanen S, Salmi M. Cell surface monoamine oxidases: enzymes in search of a function. EMBO J. 2001;20(15):3893-901.

273. Salmi M, Jalkanen S. Human vascular adhesion protein 1 (VAP-1) is a unique sialoglycoprotein that mediates carbohydrate-dependent binding of lymphocytes to endothelial cells. J Exp Med. 1996;183(2):569-79.

274. Salmi M, Jalkanen S. Vascular Adhesion Protein-1: A Cell Surface Amine Oxidase in Translation. Antioxid Redox Signal. 2017.

275. Salmi M, Jalkanen S. A 90-kilodalton endothelial cell molecule mediating lymphocyte binding in humans. Science. 1992;257(5075):1407-9.

276. Kurkijarvi R, Adams DH, Leino R, Mottonen T, Jalkanen S, Salmi M. Circulating form of human vascular adhesion protein-1 (VAP-1): increased serum levels in inflammatory liver diseases. J Immunol. 1998;161(3):1549-57.

277. Weston CJ, Shepherd EL, Claridge LC, Rantakari P, Curbishley SM, Tomlinson JW, et al. Vascular adhesion protein-1 promotes liver inflammation and drives hepatic fibrosis. J Clin Invest. 2015;125(2):501-20.

278. Lalor PF, Sun PJ, Weston CJ, Martin-Santos A, Wakelam MJ, Adams DH. Activation of vascular adhesion protein-1 on liver endothelium results in an NF-kappaB-dependent increase in lymphocyte adhesion. Hepatology. 2007;45(2):465-74.

279. Jalkanen S, Karikoski M, Mercier N, Koskinen K, Henttinen T, Elima K, et al. The oxidase activity of vascular adhesion protein-1 (VAP-1) induces endothelial E- and P-selectins and leukocyte binding. Blood. 2007;110(6):1864-70.

280. Noonan T, Lukas S, Peet GW, Pelletier J, Panzenbeck M, Hanidu A, et al. The oxidase activity of vascular adhesion protein-1 (VAP-1) is essential for function. Am J Clin Exp Immunol. 2013;2(2):172-85.

281. Koskinen K, Vainio PJ, Smith DJ, Pihlavisto M, Yla-Herttuala S, Jalkanen S, et al. Granulocyte transmigration through the endothelium is regulated by the oxidase activity of vascular adhesion protein-1 (VAP-1). Blood. 2004;103(9):3388-95.

282. Tohka S, Laukkanen M, Jalkanen S, Salmi M. Vascular adhesion protein 1 (VAP-1) functions as a molecular brake during granulocyte rolling and mediates recruitment in vivo. FASEB J. 2001;15(2):373-82.

283. Kivi E, Elima K, Aalto K, Nymalm Y, Auvinen K, Koivunen E, et al. Human Siglec-10 can bind to vascular adhesion protein-1 and serves as its substrate. Blood. 2009;114(26):5385-92.

284. Aalto K, Autio A, Kiss EA, Elima K, Nymalm Y, Veres TZ, et al. Siglec-9 is a novel leukocyte ligand for vascular adhesion protein-1 and can be used in PET imaging of inflammation and cancer. Blood. 2011;118(13):3725-33.

285. Maula SM, Salminen T, Kaitaniemi S, Nymalm Y, Smith DJ, Jalkanen S. Carbohydrates located on the top of the "cap" contribute to the adhesive and enzymatic functions of vascular adhesion protein-1. Eur J Immunol. 2005;35(9):2718-27.

286. Zorzano A, Abella A, Marti L, Carpene C, Palacin M, Testar X. Semicarbazide-sensitive amine oxidase activity exerts insulin-like effects on glucose metabolism and insulin-signaling pathways in adipose cells. Biochim Biophys Acta. 2003;1647(1-2):3-9.

287. Weston CJ, Adams DH. Hepatic consequences of vascular adhesion protein-1 expression. J Neural Transm (Vienna). 2011;118(7):1055-64.

288. Kurkijarvi R, Yegutkin GG, Gunson BK, Jalkanen S, Salmi M, Adams DH. Circulating soluble vascular adhesion protein 1 accounts for the increased serum monoamine oxidase activity in chronic liver disease. Gastroenterology. 2000;119(4):1096-103.

289. Abella A, Garcia-Vicente S, Viguerie N, Ros-Baro A, Camps M, Palacin M, et al. Adipocytes release a soluble form of VAP-1/SSAO by a metalloprotease-dependent process and in a regulated manner. Diabetologia. 2004;47(3):429-38.

290. Stolen CM, Yegutkin GG, Kurkijarvi R, Bono P, Alitalo K, Jalkanen S. Origins of serum semicarbazide-sensitive amine oxidase. Circ Res. 2004;95(1):50-7.

291. Trivedi PJ, Tickle J, Vesterhus MN, Eddowes PJ, Bruns T, Vainio J, et al. Vascular adhesion protein-1 is elevated in primary sclerosing cholangitis, is predictive of clinical outcome and facilitates recruitment of gut-tropic lymphocytes to liver in a substrate-dependent manner. Gut. 2018;67(6):1135-45.

292. Meszaros Z, Szombathy T, Raimondi L, Karadi I, Romics L, Magyar K. Elevated serum semicarbazide-sensitive amine oxidase activity in non-insulin-dependent diabetes mellitus: correlation with body mass index and serum triglyceride. Metabolism. 1999;48(1):113-7.

293. Karadi I, Meszaros Z, Csanyi A, Szombathy T, Hosszufalusi N, Romics L, et al. Serum semicarbazide-sensitive amine oxidase (SSAO) activity is an independent marker of carotid atherosclerosis. Clin Chim Acta. 2002;323(1-2):139-46.

294. Boomsma F, van Veldhuisen DJ, de Kam PJ, Man in't Veld AJ, Mosterd A, Lie KI, et al. Plasma semicarbazide-sensitive amine oxidase is elevated in patients with congestive heart failure. Cardiovasc Res. 1997;33(2):387-91.

295.   Li HY, Wei JN, Lin MS, Smith DJ, Vainio J, Lin CH, et al. Serum vascular adhesion protein-1 is increased in acute and chronic hyperglycemia. Clin Chim Acta. 2009;404(2):149-53.

296.   Hsia LT, Ashley N, Ouaret D, Wang LM, Wilding J, Bodmer WF. Myofibroblasts are distinguished from activated skin fibroblasts by the expression of AOC3 and other associated markers. Proc Natl Acad Sci U S A. 2016;113(15):E2162-71.

297.   Ward ST, Weston CJ, Shepherd EL, Hejmadi R, Ismail T, Adams DH. Evaluation of serum and tissue levels of VAP-1 in colorectal cancer. BMC Cancer. 2016;16:154.

298.   Mittal S, El-Serag HB. Epidemiology of hepatocellular carcinoma: consider the population. J Clin Gastroenterol. 2013;47 Suppl:S2-6.

299.   Colombo M, de Franchis R, Del Ninno E, Sangiovanni A, De Fazio C, Tommasini M, et al. Hepatocellular carcinoma in Italian patients with cirrhosis. N Engl J Med. 1991;325(10):675-80.

300.   El-Serag HB. Epidemiology of viral hepatitis and hepatocellular carcinoma. Gastroenterology. 2012;142(6):1264-73 e1.

301.   Fattovich G, Stroffolini T, Zagni I, Donato F. Hepatocellular carcinoma in cirrhosis: incidence and risk factors. Gastroenterology. 2004;127(5 Suppl 1):S35-50.

302.   Tayob N, Lok AS, Do KA, Feng Z. Improved Detection of Hepatocellular Carcinoma by Using a Longitudinal Alpha-Fetoprotein Screening Algorithm. Clin Gastroenterol Hepatol. 2016;14(3):469-75 e2.

303.   Pateron D, Ganne N, Trinchet JC, Aurousseau MH, Mal F, Meicler C, et al. Prospective study of screening for hepatocellular carcinoma in Caucasian patients with cirrhosis. J Hepatol. 1994;20(1):65-71.

304.   Rizzi PM, Kane PA, Ryder SD, Ramage JK, Gane E, Tan KC, et al. Accuracy of radiology in detection of hepatocellular carcinoma before liver transplantation. Gastroenterology. 1994;107(5):1425-9.

305.   Yu NC, Chaudhari V, Raman SS, Lassman C, Tong MJ, Busuttil RW, et al. CT and MRI improve detection of hepatocellular carcinoma, compared with ultrasound alone, in patients with cirrhosis. Clin Gastroenterol Hepatol. 2011;9(2):161-7.

306.   Johnson PJ, Pirrie SJ, Cox TF, Berhane S, Teng M, Palmer D, et al. The detection of hepatocellular carcinoma using a prospectively developed and validated model based on serological biomarkers. Cancer Epidemiol Biomarkers Prev. 2014;23(1):144-53.

307.   Sengupta S, Parikh ND. Biomarker development for hepatocellular carcinoma early detection: current and future perspectives. Hepat Oncol. 2017;4(4):111-22.

308.   Sumi A, Akiba J, Ogasawara S, Nakayama M, Nomura Y, Yasumoto M, et al. Des-gamma-carboxyprothrombin (DCP) and NX-DCP expressions and their relationship with clinicopathological features in hepatocellular carcinoma. PLoS One. 2015;10(3):e0118452.

309.   Tamano M, Sugaya H, Oguma M, Murohisa T, Tomita Y, Matsumura A, et al. Immunolocalisation of PIVKA-II in paraffin-embedded specimens of hepatocellular carcinoma. Liver. 1999;19(5):406-10.

310.   Kang KH, Kim JH, Kang SH, Lee BJ, Seo YS, Yim HJ, et al. The influence of alcoholic liver disease on serum PIVKA-II levels in patients without hepatocellular carcinoma. Gut Liver. 2015;9(2):224-30.

311.   Sakizono K, Oita T, Eto M, Bito S, Takegawa H, Kasakura S. [Studies on the mechanism of elevation of serum PIVKA-II levels in alcoholic liver cirrhosis]. Rinsho Byori. 2002;50(3):289-95.

312. Ohhira M, Saito H, Suzuki Y, Naraki T, Sakurai S, Ohtake T, et al. A variant of des-gamma-carboxy prothrombin was increased in alcoholic liver disease without hepatocellular carcinoma. Alcohol Clin Exp Res. 2001;25(6 Suppl):46S-50S.

313. Iber FL, Shamszad M, Miller PA, Jacob R. Vitamin K deficiency in chronic alcoholic males. Alcohol Clin Exp Res. 1986;10(6):679-81.

314. Shah SA, Cleary SP, Wei AC, Yang I, Taylor BR, Hemming AW, et al. Recurrence after liver resection for hepatocellular carcinoma: risk factors, treatment, and outcomes. Surgery. 2007;141(3):330-9.

315. Pommergaard HC, Rostved AA, Adam R, Thygesen LC, Salizzoni M, Gomez Bravo MA, et al. Vascular invasion and survival after liver transplantation for hepatocellular carcinoma: a study from the European Liver Transplant Registry. HPB (Oxford). 2018;20(8):768-75.

316. Mazzaferro V, Llovet JM, Miceli R, Bhoori S, Schiavo M, Mariani L, et al. Predicting survival after liver transplantation in patients with hepatocellular carcinoma beyond the Milan criteria: a retrospective, exploratory analysis. Lancet Oncol. 2009;10(1):35-43.

317. Tamura S, Kato T, Berho M, Misiakos EP, O'Brien C, Reddy KR, et al. Impact of histological grade of hepatocellular carcinoma on the outcome of liver transplantation. Arch Surg. 2001;136(1):25-30; discussion 1.

318. Yip VS, Gomez D, Tan CY, Staettner S, Terlizzo M, Fenwick S, et al. Tumour size and differentiation predict survival after liver resection for hepatocellular carcinoma arising from non-cirrhotic and non-fibrotic liver: a case-controlled study. Int J Surg. 2013;11(10):1078-82.

319. Cuccurullo V, Di Stasio GD, Mazzarella G, Cascini GL. Microvascular Invasion in HCC: The Molecular Imaging Perspective. Contrast Media Mol Imaging. 2018;2018:9487938.

320. Toiyama Y, Miki C, Inoue Y, Kawamoto A, Kusunoki M. Circulating form of human vascular adhesion protein-1 (VAP-1): decreased serum levels in progression of colorectal cancer and predictive marker of lymphatic and hepatic metastasis. J Surg Oncol. 2009;99(6):368-72.

321. Yasuda H, Toiyama Y, Ohi M, Mohri Y, Miki C, Kusunoki M. Serum soluble vascular adhesion protein-1 is a valuable prognostic marker in gastric cancer. J Surg Oncol. 2011;103(7):695-9.

322. Kemik O, Sumer A, Kemik AS, Itik V, Dulger AC, Purisa S, et al. Human vascular adhesion protein-1 (VAP-1): serum levels for hepatocellular carcinoma in non-alcoholic and alcoholic fatty liver disease. World J Surg Oncol. 2010;8:83.

323. Arndtz K, Corrigan M, Rowe A, Kirkham A, Barton D, Fox RP, et al. Investigating the safety and activity of the use of BTT1023 (Timolumab), in the treatment of patients with primary sclerosing cholangitis (BUTEO): A single-arm, two-stage, open-label, multi-centre, phase II clinical trial protocol. BMJ Open. 2017;7(6):e015081.

324. A Study That Tests BI 1467335 in Patients With Diabetic Eye Disease (Diabetic Retinopathy). It Looks at the Way BI 1467335 is Taken up, the Effects it Has, and How Well it is Tolerated. (ROBIN) 2017 [Available from: https://clinicaltrials.gov/ct2/show/NCT03238963.

325. Aalto K, Maksimow M, Juonala M, Viikari J, Jula A, Kahonen M, et al. Soluble vascular adhesion protein-1 correlates with cardiovascular risk factors and early atherosclerotic manifestations. Arterioscler Thromb Vasc Biol. 2012;32(2):523-32.

326.   Capelli P, Martignoni G, Pedica F, Falconi M, Antonello D, Malpeli G, et al. Endocrine neoplasms of the pancreas: pathologic and genetic features. Arch Pathol Lab Med. 2009;133(3):350-64.

327.   McCall CM, Shi C, Klein AP, Konukiewitz B, Edil BH, Ellison TA, et al. Serotonin expression in pancreatic neuroendocrine tumors correlates with a trabecular histologic pattern and large duct involvement. Hum Pathol. 2012;43(8):1169-76.

328.   La Rosa S, Franzi F, Albarello L, Schmitt A, Bernasconi B, Tibiletti MG, et al. Serotonin-producing enterochromaffin cell tumors of the pancreas: clinicopathologic study of 15 cases and comparison with intestinal enterochromaffin cell tumors. Pancreas. 2011;40(6):883-95.

329.   Kuo CH, Wei JN, Yang CY, Ou HY, Wu HT, Fan KC, et al. Serum vascular adhesion protein-1 is up-regulated in hyperglycemia and is associated with incident diabetes negatively. Int J Obes (Lond). 2018.

330.   Blazevic A, Hofland J, Hofland LJ, Feelders RA, de Herder WW. Small intestinal neuroendocrine tumours and fibrosis: an entangled conundrum. Endocr Relat Cancer. 2018;25(3):R115-R30.

331.   Rodriguez Laval V, Pavel M, Steffen IG, Baur AD, Dilz LM, Fischer C, et al. Mesenteric Fibrosis in Midgut Neuroendocrine Tumors: Functionality and Radiological Features. Neuroendocrinology. 2018;106(2):139-47.

332.   Niederle B, Pape UF, Costa F, Gross D, Kelestimur F, Knigge U, et al. ENETS Consensus Guidelines Update for Neuroendocrine Neoplasms of the Jejunum and Ileum. Neuroendocrinology. 2016;103(2):125-38.

333.   Schuppan D, Somasundaram R, Dieterich W, Ehnis T, Bauer M. The extracellular matrix in cellular proliferation and differentiation. Ann N Y Acad Sci. 1994;733:87-102.

334.   Funa K, Papanicolaou V, Juhlin C, Rastad J, Akerstrom G, Heldin CH, et al. Expression of platelet-derived growth factor beta-receptors on stromal tissue cells in human carcinoid tumors. Cancer Res. 1990;50(3):748-53.

335.   Kalluri R. The biology and function of fibroblasts in cancer. Nat Rev Cancer. 2016;16(9):582-98.

336.   Cunningham JL, Tsolakis AV, Jacobson A, Janson ET. Connective tissue growth factor expression in endocrine tumors is associated with high stromal expression of alpha-smooth muscle actin. Eur J Endocrinol. 2010;163(4):691-7.

337.   Kidd M, Modlin I, Shapiro M, Camp R, Mane S, Usinger W, et al. CTGF, intestinal stellate cells and carcinoid fibrogenesis. World J Gastroenterol. 2007;13(39):5208-16.

338.   Chaudhry A, Papanicolaou V, Oberg K, Heldin CH, Funa K. Expression of platelet-derived growth factor and its receptors in neuroendocrine tumors of the digestive system. Cancer Res. 1992;52(4):1006-12.

339.   Cox TR, Erler JT. Remodeling and homeostasis of the extracellular matrix: implications for fibrotic diseases and cancer. Dis Model Mech. 2011;4(2):165-78.

340.   Provenzano PP, Eliceiri KW, Campbell JM, Inman DR, White JG, Keely PJ. Collagen reorganization at the tumor-stromal interface facilitates local invasion. BMC Med. 2006;4(1):38.

341.   Linan-Rico A, Ochoa-Cortes F, Beyder A, Soghomonyan S, Zuleta-Alarcon A, Coppola V, et al. Mechanosensory Signaling in Enterochromaffin Cells and 5-HT Release: Potential Implications for Gut Inflammation. Front Neurosci. 2016;10:564.

342.   Garcia-Suarez O, Garcia B, Fernandez-Vega I, Astudillo A, Quiros LM. Neuroendocrine tumors show altered expression of chondroitin sulfate, glypican 1,

glypican 5, and syndecan 2 depending on their differentiation grade. Front Oncol. 2014;4:15.

343. Cives M, Pelle E, Quaresmini D, Rizzo FM, Tucci M, Silvestris F. The Tumor Microenvironment in Neuroendocrine Tumors: Biology and Therapeutic Implications. Neuroendocrinology. 2019.

344. Marttila-Ichihara F, Auvinen K, Elima K, Jalkanen S, Salmi M. Vascular adhesion protein-1 enhances tumor growth by supporting recruitment of Gr-1+CD11b+ myeloid cells into tumors. Cancer Res. 2009;69(19):7875-83.

345. Claridge LC, Weston CJ, Haughton EL, Westerlund N, Lalor PF, Smith DJ, et al. P46 Vascular adhesion protein-1 promotes inflammation and fibrogenesis in murine steatohepatitis. Gut 2010;59:A29.

346. Tonnies H, Toliat MR, Ramel C, Pape UF, Neitzel H, Berger W, et al. Analysis of sporadic neuroendocrine tumours of the enteropancreatic system by comparative genomic hybridisation. Gut. 2001;48(4):536-41.

347. Pannecoeck R, Serruys D, Benmeridja L, Delanghe JR, van Geel N, Speeckaert R, et al. Vascular adhesion protein-1: Role in human pathology and application as a biomarker. Crit Rev Clin Lab Sci. 2015;52(6):284-300.

348. Lamarca A, Nonaka D, Breitwieser W, Ashton G, Barriuso J, McNamara MG, et al. PD-L1 expression and presence of TILs in small intestinal neuroendocrine tumours. Oncotarget. 2018;9(19):14922-38.

349. Vikman S, Sommaggio R, De La Torre M, Oberg K, Essand M, Giandomenico V, et al. Midgut carcinoid patients display increased numbers of regulatory T cells in peripheral blood with infiltration into tumor tissue. Acta Oncol. 2009;48(3):391-400.

350. Aparicio-Pages MN, Verspaget HW, Pena AS, Jansen JB, Lamers CB. Natural killer cell activity in patients with neuroendocrine tumours of the gastrointestinal tract; relation with circulating gastrointestinal hormones. Neuropeptides. 1991;20(1):1-7.

351. Holt AP, Haughton EL, Lalor PF, Filer A, Buckley CD, Adams DH. Liver myofibroblasts regulate infiltration and positioning of lymphocytes in human liver. Gastroenterology. 2009;136(2):705-14.

352. Brennen WN, Isaacs JT, Denmeade SR. Rationale behind targeting fibroblast activation protein-expressing carcinoma-associated fibroblasts as a novel chemotherapeutic strategy. Mol Cancer Ther. 2012;11(2):257-66.

353. Shiga K, Hara M, Nagasaki T, Sato T, Takahashi H, Takeyama H. Cancer-Associated Fibroblasts: Their Characteristics and Their Roles in Tumor Growth. Cancers (Basel). 2015;7(4):2443-58.

354. Mortelmans P, Herregods MC, Rega F, Timmermans P. The path to surgery in carcinoid heart disease: a retrospective study and a multidisciplinary proposal of a new algorithm. Acta Cardiol. 2018:1-8.

355. Lee SY, Li S, Sian K, Mejia R. Metastatic small bowel neuroendocrine tumour and carcinoid heart disease with aortic valve involvement-a rare occurrence. J Thorac Dis. 2018;10(2):E103-E7.

356. Bertin N, Favretto S, Pelizzo F, Mos L, Pertoldi F, Vriz O. Carcinoid Heart Disease: Starting From Heart Failure. J Investig Med High Impact Case Rep. 2017;5(2):2324709617713511.

357. Robiolio PA, Rigolin VH, Wilson JS, Harrison JK, Sanders LL, Bashore TM, et al. Carcinoid heart disease. Correlation of high serotonin levels with valvular abnormalities detected by cardiac catheterization and echocardiography. Circulation. 1995;92(4):790-5.

358. Reynen K. Cardiac myxomas. N Engl J Med. 1995;333(24):1610-7.
359. Di Vito A, Mignogna C, Donato G. The mysterious pathways of cardiac myxomas: a review of histogenesis, pathogenesis and pathology. Histopathology. 2015;66(3):321-32.
360. Singhal P, Luk A, Rao V, Butany J. Molecular basis of cardiac myxomas. Int J Mol Sci. 2014;15(1):1315-37.
361. Bresnick AR, Weber DJ, Zimmer DB. S100 proteins in cancer. Nat Rev Cancer. 2015;15(2):96-109.
362. Krikler DM, Rode J, Davies MJ, Woolf N, Moss E. Atrial myxoma: a tumour in search of its origins. Br Heart J. 1992;67(1):89-91.
363. Pucci A, Gagliardotto P, Zanini C, Pansini S, di Summa M, Mollo F. Histopathologic and clinical characterization of cardiac myxoma: review of 53 cases from a single institution. Am Heart J. 2000;140(1):134-8.
364. Kudo M. Clinical Practice Guidelines for Hepatocellular Carcinoma Differ between Japan, United States, and Europe. Liver Cancer. 2015;4:85-95.
365. Huang S, Jiang F, Wang Y, Yu Y, Ren S, Wang X, et al. Diagnostic performance of tumor markers AFP and PIVKA-II in Chinese hepatocellular carcinoma patients. Tumour Biol. 2017;39(6):1010428317705763.
366. Gurecka R, Koborova I, Csongova M, Sebek J, Sebekova K. Correlation among soluble receptors for advanced glycation end-products, soluble vascular adhesion protein-1/semicarbazide-sensitive amine oxidase (sVAP-1) and cardiometabolic risk markers in apparently healthy adolescents: a cross-sectional study. Glycoconj J. 2016;33(4):599-606.
367. Weiss HG, Klocker J, Labeck B, Nehoda H, Aigner F, Klingler A, et al. Plasma amine oxidase: a postulated cardiovascular risk factor in nondiabetic obese patients. Metabolism. 2003;52(6):688-92.
368. Salmi M, Stolen C, Jousilahti P, Yegutkin GG, Tapanainen P, Janatuinen T, et al. Insulin-regulated increase of soluble vascular adhesion protein-1 in diabetes. Am J Pathol. 2002;161(6):2255-62.
369. Kuo CH, Wei JN, Yang CY, Ou HY, Wu HT, Fan KC, et al. Serum vascular adhesion protein-1 is up-regulated in hyperglycemia and is associated with incident diabetes negatively. Int J Obes (Lond). 2019;43(3):512-22.
370. Karim S, Liaskou E, Fear J, Garg A, Reynolds G, Claridge L, et al. Dysregulated hepatic expression of glucose transporters in chronic disease: contribution of semicarbazide-sensitive amine oxidase to hepatic glucose uptake. Am J Physiol Gastrointest Liver Physiol. 2014;307(12):G1180-90.
371. Salmi M, Jalkanen S. Vascular Adhesion Protein-1: A Cell Surface Amine Oxidase in Translation. Antioxid Redox Signal. 2019;30(3):314-32.
372. Maki JM, Sormunen R, Lippo S, Kaarteenaho-Wiik R, Soininen R, Myllyharju J. Lysyl oxidase is essential for normal development and function of the respiratory system and for the integrity of elastic and collagen fibers in various tissues. Am J Pathol. 2005;167(4):927-36.
373. Maki JM, Rasanen J, Tikkanen H, Sormunen R, Makikallio K, Kivirikko KI, et al. Inactivation of the lysyl oxidase gene Lox leads to aortic aneurysms, cardiovascular dysfunction, and perinatal death in mice. Circulation. 2002;106(19):2503-9.
374. Hornstra IK, Birge S, Starcher B, Bailey AJ, Mecham RP, Shapiro SD. Lysyl oxidase is required for vascular and diaphragmatic development in mice. J Biol Chem. 2003;278(16):14387-93.